UMI University Microfilms International

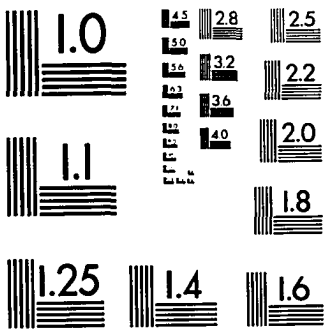

MICROCOPY RESOLUTION TEST CHART
NATIONAL BUREAU OF STANDARDS
STANDARD REFERENCE MATERIAL 1010a
(ANSI and ISO TEST CHART No. 2)

University Microfilms Inc.
300 N. Zeeb Road, Ann Arbor, MI 48106

Downloaded from SHAREOK. Persistent Handle URL: https://hdl.handle.net/11244/5359

INFORMATION TO USERS

This reproduction was made from a copy of a manuscript sent to us for publication and microfilming. While the most advanced technology has been used to photograph and reproduce this manuscript, the quality of the reproduction is heavily dependent upon the quality of the material submitted. Pages in any manuscript may have indistinct print. In all cases the best available copy has been filmed.

The following explanation of techniques is provided to help clarify notations which may appear on this reproduction.

1. Manuscripts may not always be complete. When it is not possible to obtain missing pages, a note appears to indicate this.

2. When copyrighted materials are removed from the manuscript, a note appears to indicate this.

3. Oversize materials (maps, drawings, and charts) are photographed by sectioning the original, beginning at the upper left hand corner and continuing from left to right in equal sections with small overlaps. Each oversize page is also filmed as one exposure and is available, for an additional charge, as a standard 35mm slide or in black and white paper format.*

4. Most photographs reproduce acceptably on positive microfilm or microfiche but lack clarity on xerographic copies made from the microfilm. For an additional charge, all photographs are available in black and white standard 35mm slide format.*

***For more information about black and white slides or enlarged paper reproductions, please contact the Dissertations Customer Services Department.**

UMI University Microfilms International

8601140

Ashrafzadeh, Ahmad Reza

A DUAL-PULSED DOPPLER ULTRASOUND AND ITS APPLICATIONS IN DETERMINING TURBULENT BLOOD FLOW CHARACTERISTICS

The University of Oklahoma PH.D. 1985

University
Microfilms
International 300 N. Zeeb Road, Ann Arbor, MI 48106

Copyright 1985

by

Ashrafzadeh, Ahmad Reza

All Rights Reserved

PLEASE NOTE:

In all cases this material has been filmed in the best possible way from the available copy. Problems encountered with this document have been identified here with a check mark ✓.

1. Glossy photographs or pages _____
2. Colored illustrations, paper or print _____
3. Photographs with dark background _____
4. Illustrations are poor copy _____
5. Pages with black marks, not original copy ✓
6. Print shows through as there is text on both sides of page _____
7. Indistinct, broken or small print on several pages _____
8. Print exceeds margin requirements _____
9. Tightly bound copy with print lost in spine _____
10. Computer printout pages with indistinct print ✓
11. Page(s) _____ lacking when material received, and not available from school or author.
12. Page(s) _____ seem to be missing in numbering only as text follows.
13. Two pages numbered _____. Text follows.
14. Curling and wrinkled pages _____
15. Dissertation contains pages with print at a slant, filmed as received _____
16. Other _____

_____

_____

University
Microfilms
International

THE UNIVERSITY OF OKLAHOMA

GRADUATE COLLEGE

A DUAL TRANSDUCER PULSED-DOPPLER ULTRASOUND AND ITS APPLICATIONS IN DETERMINING TURBULENT BLOOD FLOW CHARACTERISTICS

A DISSERTATION

SUBMITTED TO THE GRADUATE FACULTY

in partial fulfillment of the requirements for the degree of

DOCTOR OF PHILOSOPHY

By

AHMAD R. ASHRAFZADEH

Norman, Oklahoma

1985

A DUAL-TRANSDUCER PULSED DOPPLER ULTRASOUND AND ITS APPLICATIONS IN DETERMINING TURBULENT BLOOD FLOW CHARACTERISTICS

A DISSERTATION

APPROVED FOR THE SCHOOL OF ELECTRICAL ENGINEERING AND COMPUTER SCIENCE

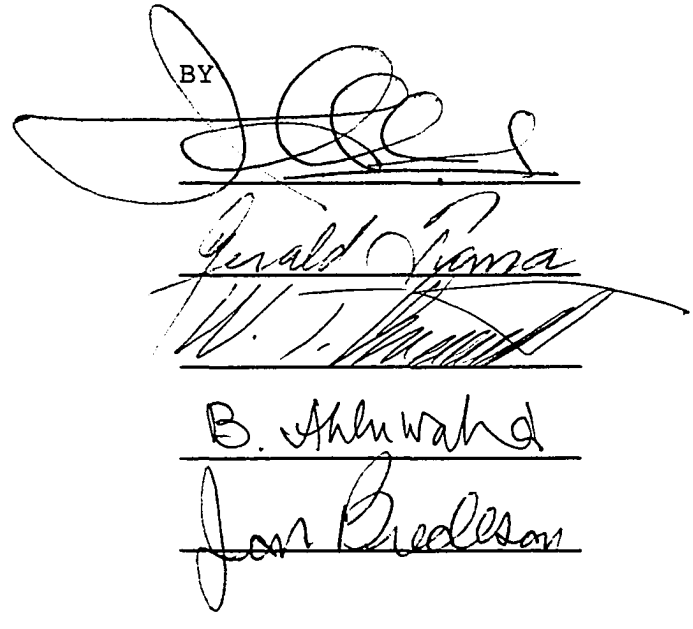

©Copyright by Ahmad Reza Ashrafzadeh 1985
All Rights Reserved

Dedicated to the memory of my father,

Javad Ashrafzadeh

ACKNOWLEDGMENTS

The author is indebted to his advisor, Dr. J. Cheung, for his inspiration, guidance, and constant encouragement during the course of this study.

The author would like to express his sincere thanks to his Dissertation Committee members, Dr. B. Ahluwalia, Dr. J. Bredeson, Dr. W. Cronenwett, and Dr. G. Tuma, for their valuable time and advice rendered.

The author would also like to thank Dr. K. Dormer for his guidance and for accomplishing experimental surgery which provided the basic data for these conclusions. Further, the author wishes to thank Dr. T. Bedford for his assistance in setting up the in-vitro experiments.

A special thanks goes to Ms. Betty Sudduth for her excellent typing of the manuscript.

Most of all, the author thanks the members of his family, especially his wife, Mimi, his mother, Masih Zaman, and his loving daughter, Aria Naz, for their patience and understanding during the period of this study. Special thanks also go to his brothers and sisters: Hamid Reza, Mohammad Reza, Afsaneh, Pari, Hoori, Amir Mohammad and to his brother- and sisters-in-low Mohammad Reza, Vajihe, Susan, and to his cousin, Masoud.

The author gratefully acknowledges the time and help which was provided by Mr. Raymond Schlecht in transferring data from the O.U. Health Sciences Center to the main campus, in addition to Mr. Hammack in the Engineering Library.

ABSTRACT

The quantitative capability of Single Transducer Pulsed-Doppler Ultrasound (STP-DU) in clinical practice is limited by the effects of acoustics, tissue, and system parameters, as well as its inability to obtain precise measurement of the Doppler angle, which in most cases must be estimated. In this study, a practical approximation for the backscattering of a damped sine wave by a volume of randomly distributed scattered particles has been developed. The approximation has been applied to the measurement of a volumetric backscattered cross section, taking into account most of the parameters involved in the process. A dual transducer pulsed-Doppler ultrasound (DTP-DU) has then been introduced for direct calculation of the Doppler angle and for accurate determination of blood flow velocities. A comparison was also made between STP-DU and DTP-DU models. The components of the blood flow velocities are used to obtain the blood flow characteristics such as volume rate and shear stress, and to express a relationship between blood flow characteristics and pathological changes, such as stenosis.

Experimental results based on theoretical investigations are presented. The dual transducer model was

constructed and has been used to obtain the information needed to verify the theoretical work. The results indicate that the new transducer model increases dramatically the accuracy of measuring the blood velocity and thereby improves our ability to characterize the blood flow patterns which are valuable for research and diagnostic purposes.

TABLE OF CONTENTS

Page

ACKNOWLEDGMENTS iii

ABSTRACT iv

LIST OF TABLES ix

LIST OF FIGURES x

CHAPTER

I. INTRODUCTION 1

1.1 The Doppler Principle 2

1.1.1 The Continuous Wave Doppler Ultrasound 3
1.1.2 The Pulsed-Doppler Ultrasound . . . 4

1.1.2.1 Pulsed-Doppler Ultrasound Limitations 7

1.2 Clinical Applications of Ultrasonic Doppler Technique 9
1.3 Blood Flow Patterns 13
1.4 Goals of the Study 15
1.5 Flow Chart 16

II. LITERATURE REVIEW 18

2.1 Theoretical Investigations 19

2.1.1 Processing the Doppler Signal . . . 19
2.1.2 Determining the Doppler Angle . . . 24
2.1.3 Fluid Dynamics Aspect of Blood Flow 26

2.2 Experimental Investigations 32

2.2.1 In-Vitro Experimental Investigations 32
2.2.2 In-Vivo Experimental Investigations 36

CHAPTER Page

III. THE THEORETICAL INVESTIGATIONS 46

3.1 Scattering of Ultrasound by Blood 46
3.2 Transducer Modeling 62

3.2.1 Theoretical Investigations 64
3.2.2 Theoretical Comparison of Doppler Models 70

3.2.2.1 One Dimensional Analysis 70
3.2.2.2 Two Dimensional Analysis 71

3.3 Relationship Between Velocity Components and Turbulent Blood Flow Characteristics . . 92

IV. EXPERIMENTAL PROCEDURE 104

4.1 Experimental Model 104

4.1.1 The Variable Pulsatile Pump 105
4.1.2 The Dual Transducer Model 105
4.1.3 The Bidirectional Pulsed-Doppler Ultrasound Machine with Two Channels 107
4.1.4 The Chart Recorder 108
4.1.5 The Communication Unit 109
4.1.6 The Analog-to-Digital Converter . . 109
4.1.7 The Digital Computer 110

V. EXPERIMENTAL RESULTS 111

5.1 Parameters Calculation 112

5.1.1 Doppler Angle 112
5.1.2 Velocity 112
5.1.3 Blood Flow Volume Rate 112
5.1.4 Shear Stress 113

5.2 In-Vivo Experiment 113

5.2.1 Experimental Results 114

5.2.1.1 Normal Heartbeats (180 bpm) 114

5.2.1.1a Range a (1/6 of diameter) . 114
5.2.1.1b Range b (1/3 of diameter) . 118
5.2.1.1c Range c (1/2 of diameter) . 118

CHAPTER Page

5.2.1.2 Reduced Heartbeat (150 bpm) 121
5.2.1.3 Increased Heartbeat (190 bpm) 126

5.3 In-Vitro Experiments 130

5.3.1 Calculation of the Velocity, Volume Rate in the Femoral Artery . 130
5.3.2 Calculation of Volume Rate From the Velocity Profile (femoral artery) 137
5.3.3 Determination of Statistical Parameters of Flow Volume Rate (carotid artery) 146
5.3.4 Determining the Turbulent Flow Characteristics (carotid artery) . . 156
5.3.5 Determining the Degree of Stenosis Using Turbulent Flow Characteristics (carotid artery) 171

VI. SUMMARY 197

REFERENCES 200

APPENDIX A Some of the Numerical Results of Experiment 5.3.3 211

APPENDIX B Description of the 5453-c Ultrasound Machine. 218

APPENDIX C Some of the Operation Software 225

LIST OF TABLES

TABLE		Page
3.1	Numerical Values for Normalized Percentage of Error and Rate of Change in the Velocity for both STP-DU and DTP-DU Models	82
5.1	The Doppler Angle, Flow Velocity and Flow Volume Rate for normal condition of the Heart	117
5.2	The Doppler Angle, Flow Velocity and Flow Volume Rate for Reduced Heartbeats (150 bpm)	126
5.3	The Doppler Angle, Flow Velocity and Flow Volume Rate for Increased Heartbeats (190 bpm)	129
5.4	The Doppler Angle, Measured and Calculated Volume Rate at Different Ranges for Normal Femoral Artery	134
5.5	The Doppler Angle, Measured and Calculated Volume Rate at Different Ranges and for Different degrees of Stenosis for the Femoral Artery	134
5.6	The Doppler Angle, Blood Flow Volume Rate and Normalized Velocity Error for the Normal Femoral Artery	145
5.7	The Doppler Angle, Blood Flow Volume Rate and Normalized Velocity Error for Stenotic (33 percent to 35 percent) Femoral Artery	145
5.8	The Doppler Angle, Measured Volume Rate, Mean Value of Calculated Volume Rate and Standard Deviation of Calculated Volume Rate	154

LIST OF ILLUSTRATIONS

FIGURE		Page
1.1	A continuous wave Doppler ultrasound system	5
1.2	A pulsed Doppler ultrasound system	7
2.1	Doppler insonation of the blood	20
2.2	An example of a Doppler signal	20
2.3	The power spectrum of a Doppler signal in CW	22
2.4	The common femoral artery	39
3.1	A two-sidedly damped sinusoidal waveform, curve (c)	48
3.2	Scattering of the ultrasound signal by red cell	49
3.3	Illustration of the ensemble $P_k(t_e)$	57
3.4	A typical configuration for a dual transducer model	66
3.5	The percentage of normalized velocity error for single transducer pulsed Doppler ultrasound model	72
3.6	Discrepancy between actual and measured flow for single transducer pulsed Doppler ultrasound model	73
3.7	The percentage of normalized velocity error for dual transducer pulsed Doppler ultrasound model	77
3.8	The percentage of normalized velocity error for dual transducer pulsed Doppler ultrasound model for fixed values of ξ	78
3.9	Discrepancy between actual and measured flow for dual transducer pulsed-Doppler ultrasound model	80

Figure Page

3.10 Discrepancy between actual and measured flow for dual transducer pulsed Doppler ultrasound model for fixed values of θ 81

3.11 The percentage of velocity error for STP-DU and DTP-DU models (special case α = 90°, θ = 45°) 86

3.12 Percentage of velocity error for STP-DU and DTP-DU models (special case α = 90°, θ = 55°). . 87

3.13 Discrepancy between actual and measured flow for STP-DU and DTP-DU models (special case α = 90°, θ = 45°) 88

3.14 Discrepancy between actual and measured flow for STP-DU and DTP-DU models (special case α = 90°, θ = 45°) 89

3.15 Percentage of velocity error for STP-DU model for different values of α and for θ = 90° 90

3.16 Percentage of velocity error for DTP-DU model for different values of α and for θ = 90° 91

3.17 An example of pulsatile turbulent flow 95

3.18 Turbulent velocity components
a) phase average of the velocity
b) fluctuation velocity 95

3.19 A geometric presentation of stenosis in the artery 101

4.1 Illustration of experimental setup 106

5.1 The Doppler signals recorded from normal common carotid artery at range a 115

5.2 The Doppler signals recorded from stenotic (25 percent to 35 percent) common carotid artery at range a 116

Figure | Page

5.3 The Doppler signals recorded from stenotic (45 percent to 55 percent) common carotid artery at range a 116

5.4 The Doppler signals recorded from occluded (85 percent to 95 percent) common carotid artery at range a 116

5.5 The Doppler signals recorded from normal common carotid artery at range b 119

5.6 The Doppler signals recorded from stenotic (25 percent to 35 percent) common carotid artery at range b 119

5.7 The Doppler signals recorded from stenotic (45 percent to 55 percent) common carotid artery at range b 120

5.8 The Doppler signals recorded from normal common carotid artery at range c 122

5.9 The Doppler signals recorded from stenotic (25 percent to 35 percent) common carotid artery at range c 122

5.10 The Doppler signals recorded from stenotic (45 percent to 55 percent) common carotid artery at range c 123

5.11 The Doppler signals recorded from normal common carotid artery at the center (heartbeats = 150 bpm) 124

5.12 The Doppler signals recorded from stenotic (25 percent to 35 percent) common carotid artery at the center (heartbeats = 150 bpm) 124

5.13 The Doppler signals recorded from stenotic (45 percent to 55 percent) common carotid artery at the center (heartbeats = 150 bpm) 125

Figure Page

5.14 The Doppler signals recorded from stenotic (85 percent to 95 percent) common carotid artery at the center (heartbeats = 150 bpm) . 125

5.15 The Doppler signals recorded from normal common carotid artery at the center (heartbeats = 190 bpm) 127

5.16 The Doppler signals recorded from stenotic (25 percent to 35 percent) common carotid artery at the center (heartbeats = 190 bpm) . 127

5.17 The Doppler signals recorded from stenotic (45 percent to 55 percent) common carotid artery at the center (heartbeats = 190 bpm) . 128

5.18 The Doppler signals recorded from normal femoral artery for Q_m = 94 ml/min. 132

5.19 The Doppler signals recorded from normal femoral artery for Q_m = 85 ml/min. 132

5.20 The Doppler signals recorded from normal femoral artery for Q_m = 95 ml/min. 133

5.21 The Doppler signals recorded from normal femoral artery for Q_m = 108 ml/min 133

5.22 The Doppler signals recorded from stenotic (33 percent) femoral artery at 1/3 range (Q_m = 40 ml/min) 134

5.23 The Doppler signals recorded from stenotic (33 percent) femoral artery at 2/3 range (Q_m = 41 ml/min) 134

5.24 The doppler signals recorded from stenotic (33 percent) femoral artery at 1/2 range (Q_m = 41 ml/min 135

5.25 The Doppler signals recorded from stenotic (50 percent) femoral artery at 1/3 range (Q_m = 17 ml/min) 135

Figure Page

5.26 The Doppler signals recorded from normal femoral artery at a range close to the near wall (1st range) 139

5.27 The Doppler signals recorded from normal femoral artery (2nd range) 139

5.28 The Doppler signals recorded from normal femoral artery (3rd range) 140

5.29 The Doppler signals recorded from normal femoral artery at the center 140

5.30 The Doppler signals recorded from normal femoral artery (6th range) 141

5.31 The Doppler signals recorded from normal femoral artery (7th range) 141

5.32 The Doppler signals recorded from normal femoral artery at a point close to far wall (8th range) 142

5.33 a) The velocity profile for normal femoral artery 144

b) The velocity profile for stenotic (33 percent to 35 percent) femoral artery . . 144

5.34 The Doppler signals recorded from normal carotid artery for Q_m = 23.5 ml/min (test C) . . 148

5.35 The Doppler signals recorded from normal carotid artery for Q_m = 35 ml/min (test J) . . . 148

5.36 The Doppler signals recorded from normal carotid artery for Q_m = 58 ml/min (test N). . . . 149

5.37 The Doppler signals recorded from normal carotid artery for Q_m = 59 ml/min (test H). . . . 149

5.38 The Doppler signals recorded from normal carotid artery for Q_m = 62.5 ml/min (test P). . . 150

5.39 The Doppler signals recorded from normal carotid artery for Q_m = 65 ml/min (test R) . . . 150

Figure		Page
5.40	The Doppler signals recorded from normal carotid artery for Q_m = 83.75 ml/min (test E) . .	151
5.41	The Doppler signals recorded from normal carotid artery for Q_m = 86 ml/min (test D) . . .	151
5.42	The Doppler signals recorded from normal carotid artery for Q_m = 93.75 ml/min (test C) . .	152
5.43	The Doppler signals recorded from normal carotid artery for Q_m = 95.5 ml/min (test I) . .	152
5.44	The mean and standard deviation of calculated volume rate versus measured volume rate	155
5.45	Turbulent producing orifice	156
5.46	The velocity profile recorded from normal carotid artery in turbulent flow	158
5.47	An example of Doppler signals recorded from normal carotid artery in turbulent flow	158
5.48	The velocity profile recorded from stenotic (25 percent) carotid artery in turbulent flow	160
5.49	An example of Doppler signals recorded from stenotic (25 percent) carotid artery in turbulent flow	160
5.50	The velocity profile recorded from stenotic (50 percent) carotid artery in turbulent flow	161
5.51	An example of Doppler signals recorded from stenotic (50 percent) common carotid artery in turbulent flow	161
5.52	The velocity profile recorded from stenotic (75 percent) carotid artery in turbulent core	162

Figure Page

5.53 An example of Doppler signals recorded from stenotic (75 percent) artery in turbulent flow 162

5.54 The velocity, phase average velocity and fluctuation velocity for normal carotid artery in turbulent flow 163

5.55 The velocity, phase average of the velocity and fluctuation velocity for stenotic (25 percent) carotid artery in turbulent flow . . 164

5.56 The velocity, phase average of the velocity and fluctuation velocity for stenotic (50 percent) carotid artery in turbulent flow . . 165

5.57 The velocity, phase average of the velocity and fluctuation velocity for stenotic (75 percent) carotid artery in turbulent flow . . 166

5.58 The shear stress and time average of shear stress for normal carotid artery 167

5.59 The shear stress and time average of shear stress for stenotic (25 percent) carotid artery 168

5.60 The shear stress and time average of shear stress for stenotic (50 percent) carotid artery 169

5.61 The shear stress and time average of shear stress for stenotic (75 percent) carotid artery 170

5.62 The velocity profile recorded from normal carotid artery in turbulent flow 173

5.63 The velocity profile recorded from stenotic (25 percent) carotid artery in turbulent flow 173

5.64 The velocity profile recorded from stenotic (33 percent) carotid artery in turbulent flow 174

Figure Page

5.65 The velocity profile recorded from stenotic (50 percent) carotid artery in turbulent flow 174

5.66 The Doppler signals recorded from the near wall of the normal carotid artery 175

5.67 The Doppler signals recorded from the center of the normal carotid artery 175

5.68 The Doppler signals recorded from the near wall of the stenotic (25 percent) carotid artery 176

5.69 The Doppler signals recorded from the center of the stenotic (25 percent) carotid artery . 176

5.70 The Doppler signals recorded from the far wall of the stenotic (25 percent) carotid artery 177

5.71 The Doppler signals recorded from the near wall of the stenotic (33 percent) carotid artery 177

5.72 The Doppler signals recorded from the center of the stenotic (33 percent) carotid artery . 178

5.73 The Doppler signals recorded from the far wall of the stenotic (33 percent) carotid artery 178

5.74 The Doppler signals recorded from the near wall of the stenotic (50 percent) carotid artery 179

5.75 The Doppler signals recorded from the center of the stenotic (50 percent) carotid artery . . 179

5.76 The Doppler signals recorded from the far wall of the stenotic (50 percent) carotid artery 180

5.77 The velocity and phase average of the velocity for normal carotid artery 182

Figure		Page
5.78	The velocity and phase average of the velocity for stenotic (25 percent) carotid artery	183
5.79	The velocity and phase average of the velocity for stenotic (33 percent) carotid artery	184
5.80	The velocity and phase average of the velocity for stenotic (50 percent) carotid artery	185
5.81	The fluctuation component of the velocity for the normal carotid artery	186
5.82	The fluctuation component of the velocity for stenotic (25 percent) carotid artery . .	187
5.83	The fluctuation component of the velocity for stenotic (33 percent) carotid artery . .	188
5.84	The fluctuation component of the velocity for stenotic (50 percent) carotid artery . .	189
5.85	The power spectrum of the shear stress for the normal carotid artery	190
5.86	The power spectrum of the shear stress for stenotic (25 percent) carotid artery	191
5.87	The power spectrum of the shear stress for stenotic (33 percent) carotid artery	192
5.88	The power spectrum of the shear stress for stenotic (50 percent) carotid artery	193

A DUAL TRANSDUCER PULSED-DOPPLER ULTRASOUND AND ITS APPLICATIONS IN DETERMINING TURBULENT BLOOD FLOW CHARACTERISTICS

CHAPTER I

INTRODUCTION

Ultrasonic Doppler instruments are now used in many research centers and hospitals as part of the assessment of patients with arterial diseases. These instruments, which utilize Doppler frequency shift on a beam of ultrasound scattered from the erythrocytes to determine blood velocity, have many advantages: 1) they are noninvasive and thus may be used in screening procedures and serial studies, 2) they provide haemodynamic rather than anatomical information (although imaging machines based on the Doppler principle are now being built, and 3) the basic machines such as the one used in this study are inexpensive.

The ability of ultrasonic Doppler instruments to measure blood flow velocity is of great importance in the field of medicine. Blood flow characteristics, which are related to pathological parameters inside the artery, are largely functions of the blood flow velocity. Therefore, accurate measurement of the velocity can enhance the diagnostic ability of ultrasonic Doppler instruments. In this study, we developed a transducer model that improves dramatically

the measurement of the velocity. In this chapter, we discuss the Doppler principle, the application of ultrasonic Doppler instruments in medicine, blood flow patterns, the goal of this study, and flow chart of this study.

1.1 The Doppler Principle

One of the most significant contributions to medical technology in recent years has been the development of the Doppler ultrasound. Doppler ultrasound development is based on the Doppler radar design, therefore, limitations in Doppler radar such as velocity-range ambiguity and velocity-range resolution are applicable here as well. The Doppler ultrasound is used in the study of moving structures within the body, and is based on the analysis of the Doppler shifted frequency signal.

The apparent change in frequency when relative motion occurs between a source of sound and the observer is called "the Doppler effect." The Doppler effect happens because of the propagation velocity of sound in any homogeneous material [1] - [3]. Thus, if a sound source (S) is moving at a constant velocity toward the observer (R), the time between two successive peaks of compression is reduced, resulting in a higher frequency. On the other hand, if the source (S) is moving away from the observer, the time between two successive compressions is increased, resulting in a lower frequency. Fortunately, it makes no difference whether the

sound coming from a moving object is generated by the object or is an echo reflected from the object. The design, based on the Doppler effect is called the ultrasound Doppler flowmeter. In this device, the ultrasound source (transducer) is stationary, and echoes are reflected from moving biological structures such as red cells in the blood. If the source and detector are at the same location (as in Doppler ultrasound instruments), the object acts first as a moving detector as it receives the ultrasound wave, and then as a moving source as it reflects the signal. As a result, the ultrasound signal received by the detector exhibits a frequency shift of

$$\Delta f = 2 \cdot f_0 \cdot v_R / c \qquad (1.1)$$

Equation (1.5) is held only if the ultrasound beam is parallel to the direction of the motion of the object. In more general cases where there is an angle (θ) between the transducer and flow direction, the frequency shift can be written as

$$\Delta f = 2 \cdot f_0 \cdot v_R \cdot \cos \theta / c \qquad (1.2)$$

In general, there are two distinct types of Doppler ultrasound, continuous wave (CW) and pulsed-Doppler ultrasound [3].

1.1.1 The continuous-wave Doppler ultrasound

The CW device, which was used for the first time by

Satomura (1957) in an attempt to monitor blood velocity non-invasively, is the simplest Doppler device. A block diagram of a CW device is illustrated in Figure 1.1. The master oscillator produces a waveform which is amplified by a transmitting amplifier and then drives the transmitting transducer at its resonant frequency. An ultrasonic beam is then created and targets within this beam reflect and backscatter echoes, some of which are captured by the receiving transducer. The receiving preamplifier is a low-noise device which amplifies the weak returning echoes before they are detected in the demodulator. The demodulator compares the frequency of the received waveform with the transmitted waveform, which is derived from the master oscillator. The output from the demodulator is indeed the Doppler-shifted waveform with a frequency of Δf.

A major disadvantage of the continuous-wave is its inability to discriminate in range. The continuous-wave transmission creates an ultrasonic beam which occupies the complete diffraction pattern of the transducer. Any target moving within this beam will contribute to the final Doppler output. In clinical applications, this problem makes it impossible to isolate flow in adjoining blood vessels.

1.1.2 The Pulsed-Doppler Ultrasound

Pulsed-Doppler ultrasound combines the range discriminating capabilities of a pulsed-echo system with the

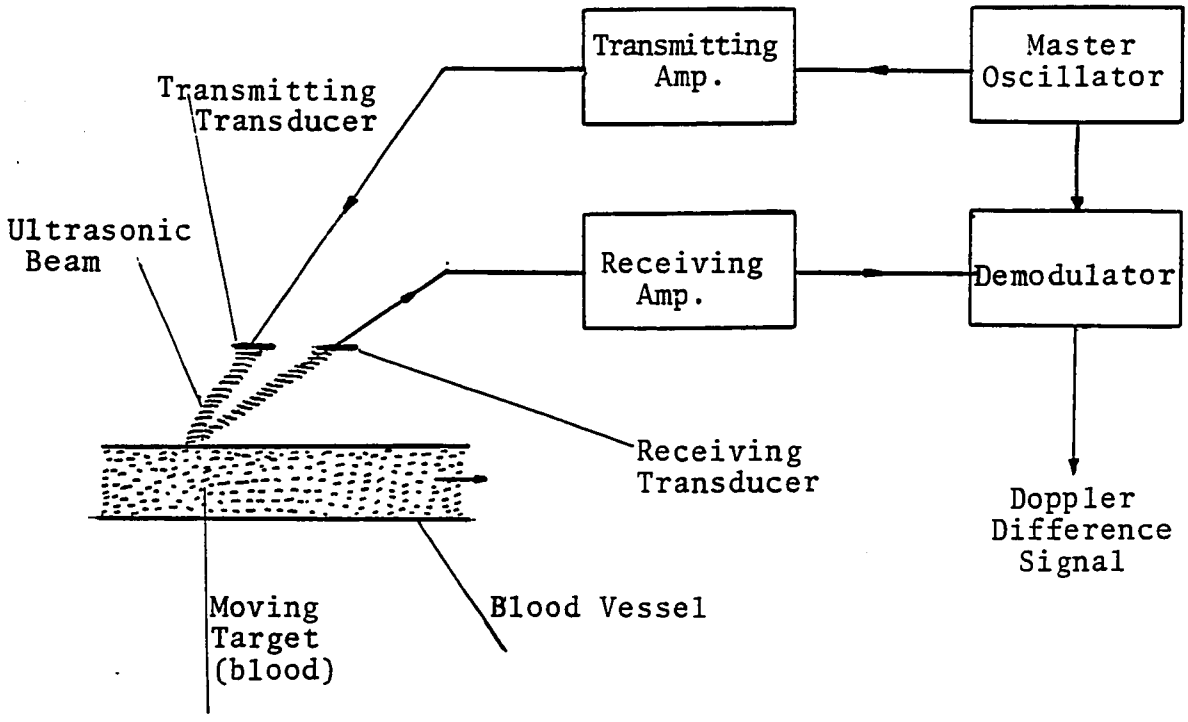

Figure 1.1 A continuous-wave Doppler ultrasound.

velocity detection capabilities of a Doppler device. As in any pulse-echo system, the principle of operation is to transmit a short burst of waves towards the target and then wait for the echoes to return. Because the sound waves travel at an essentially constant velocity through human tissue, the time delay between transmission of the pulse and reception of the echoes depends upon the range of the target. When the echoes are sampled for Doppler shifts at a fixed time after transmission, the resulting Doppler signal can originate only from those targets moving within the sample-volume corresponding to the selected delay time.

The sample volume is that region in front of the

transducer from which all returning echoes have originated. The dimensions of the sample volume are defined axially by the pulse length and laterally by the beamwidth of the combined transmitter-receiver system. By choosing to sample only those Doppler components which return after a preset constant delay from transmission, it is possible to define the position of a fixed sample volume and thus interrogate only those targets moving at a particular range from the transducer.

Figure 1.2 shows a pulsed-Doppler ultrasound system. The master oscillator generates a waveform at the resonant frequency of the transducer. Once every pulse repetition period, a few cycles of the master oscillation are passed via the transmission gate and amplified to excite the transducer. The delay gate generates a time delay which allows the transmitted ultrasonic burst to travel to and from the selected range of interest. Returning echoes are then sampled by opening the range gate and fed to the coherent demodulator, which is driven by the master oscillator. Each gated return echo produces a short output pulse from the device. If required, these samples can be stored (for example, on a capacitor plate) before being updated by the return of the next reset transmission pulse. This so-called "sample-and-hold" technique tends to produce a smoother output wave form which can then be low-pass filtered to remove

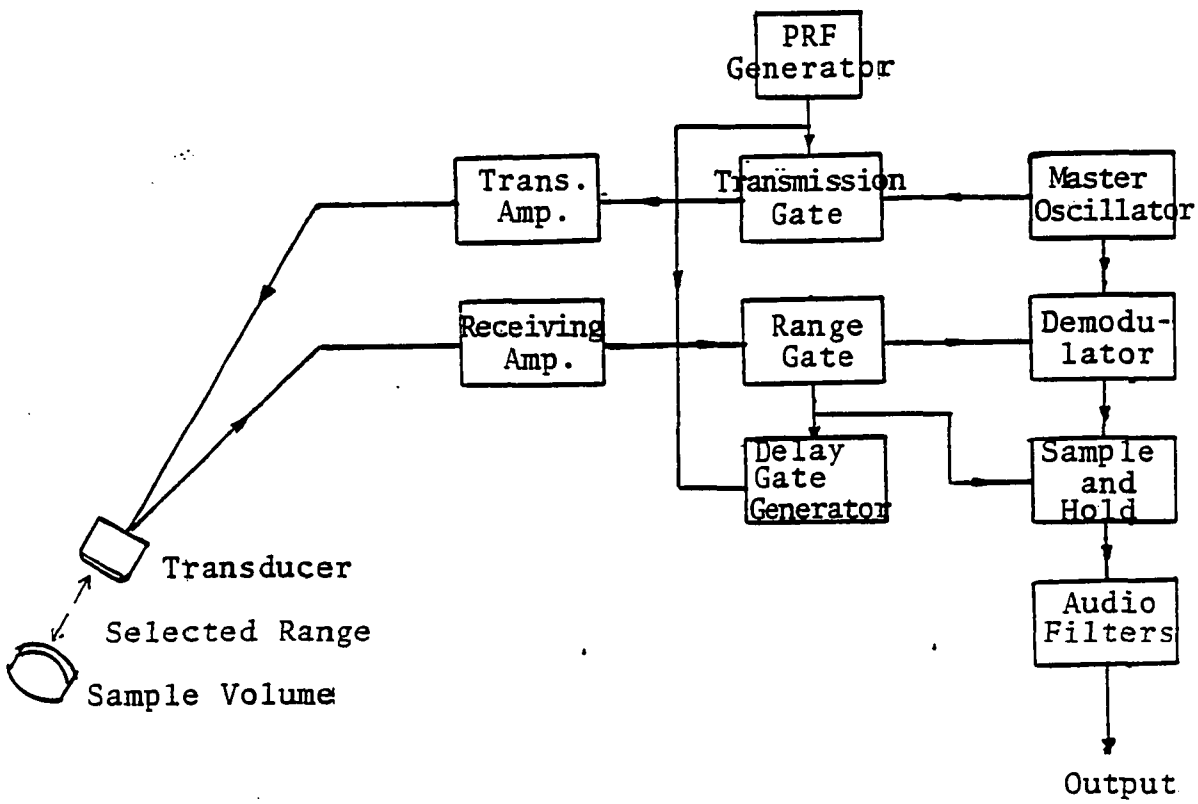

Figure 1.2 A pulsed-Doppler ultrasound system

any remaining components at the pulse repetition frequency and also high-pass filtered to remove low frequency clutter.

1.1.2.1 Pulsed-Doppler Ultrasound Limitations

Mathematically, the Doppler frequency limit f_{max} is Nyquist-related to one-half the pulse repetion frequency f_p by

$$f_{max} = \frac{f_p}{2} \qquad (1.3)$$

Substituting f_{max} for Δf in the basic Doppler expression (1.2) gives

$$v_{max} = \frac{c \cdot f_{max}}{2 \cdot f_0}$$

since

$$\lambda_0 = \frac{c}{f_0}$$

then

$$v_{max} = \frac{\lambda_0}{2} \cdot f_{max} \qquad (1.4)$$

Substituting f_{max} from (1.3) into (1.4) gives

$$v_{max} = \frac{\lambda_0}{2} \cdot \frac{f_p}{2}$$

Since

$$f_p = \frac{1}{T_p}$$

where T_p is period of pulse repetition,

then

$$v_{max} = \frac{\lambda_0/4}{T_p} \qquad (1.5)$$

indicating that the maximum velocity limit is equivalent to a $\lambda_0/4$ travel per pulse repetition period.

In addition to the velocity limitation, pulse-Doppler systems are subject to maximum range restrictions. Because it is necessary to wait for returns from the most distant target before transmitting another burst, the maximum range (z_{max}) which can be unambiguously determined is given by:

$$z_{max} = \frac{c}{2} \cdot T_p \qquad (1.6)$$

Combining Equations (1.5) and (1.6), gives the relationship

$$v_{max} \cdot z_{max} = \frac{\lambda_0 \cdot c}{8} = \frac{c^2}{8 \cdot f_0} \qquad (1.7)$$

which indicates that the product of maximum observable velocity and range is limited to a constant which is dependent upon the propagation velocity of sound within tissues and the frequency of emission.

1.2 Clinical Applications of Ultrasonic Doppler Techniques

Ultrasound, like ordinary sound, is acoustic wave, but with a frequency above the audible range (20 to 20 kHz). For diagnostic purposes, frequencies in the range of 1 to 10 MHz are used. At such high frequencies, the sound moves along straight lines like a beam of light and can be directed into the body from a handheld transducer.

The diseases in which the velocity detector has been found mostly useful can be generally outlined as follows [39]:

I. Arterial Disease
   - A. Acute arterial occlusion
     - 1- Localization of occlusion
     - 2- Estimation of length of occlusion
     - 2- Evaluation of the arteries distal to the occlusion
   - B. Arteriosclerosis Obliterans
     - 1- Localization of occlusion

2- Evaluation of the "run off" vessels

3- Operative monitoring to assess the immediate results of reconstructive arterial surgery.

C. Congenital Arteriorrenous fistula

1- Differential diagnosis

2- Localization of arterial component of the fistula

D. Thoracic Outlet Syndrome

II. Venous Disease

A. Thrombophlebitis

1- Localization of occlusion

2- Evaluation of venous flow dynamics as influenced by respiratory activity

B. Monitoring of venous flow after iliofemoral thrombectomy

C. Evaluation of venous flow characteristics

D. Evaluation of the cause of edema of the arms and legs.

The technique has also been used in conjunction with an inflatable cuff to measure blood pressure [2] and is especially valuable for measurement of blood pressure in the legs. When it is used with a servo system for cuff inflation, one may even obtain noninvasive recordings of pressure wave forms [6]. The instrument, [2] and [3], also

demonstrated the possibility of measuring the blood flow velocity in the aorta.

For most of the above mentioned diseases, a continuous wave ultrasound was used. Later (1970) the pulsed-Doppler ultrasound was introduced and made it possible, for example, measurements in the heart, because velocities in the different cavities and valve areas can be studied selectively. Scanning the range cell along the ultrasonic beam allows "velocity profiles" to be obtained. Pulsed instruments developed later give a real-time presentation of time-variable velocity profile [7].

The main advantage of ultrasonic Doppler instruments is that measurements can be performed noninvasively. But, also, invasive measurements have been made with Doppler transducers mounted at the tip of a catheter, and this technique has been used in measurements of aortic, coronary, and intracardiac blood flow velocities [14],[15]. In vascular surgery, measurements have been done directly on vessels. This procedure has an advantage over other methods, such as electromagnetic measurements, which require vessel dissection [16]. It has also been used for guidance during vascular surgical procedures in the brain [17].

In noninvasive measurements in the heart and larger vessels, an ultrasonic frequency of 1 to 3 MHz can be used. For invasive measurements and for noninvasive measurements

in peripheral vessels, 5 to 10 MHz ultrasound has been used. Experiments with 20 MHz ultrasound also have been used invasively or noninvasively for studies in animals.

One disadvantage of the Doppler ultrasound technique has been the problem of quantifying results. This problem has probably precluded a wider clinical application of these methods. In early stages of the work (up to 1970) almost all use of Doppler devices was qualitative, whether the Doppler signals were recorded and processed as analog waveforms or the clinician based his conclusion on listening to the detected signal. It was concluded, that in most instances, the devices used are not flowmeters, but rather, flow detectors [2]. Imperative in obtaining an accurate measurement of the blood flow velocity is the precise calculation of the Doppler angle (θ). It was specifically mentioned in some reports that "even a simple measurement of mean flow velocity requires that the angle between the sound beam and the velocity vector be known" and "recording in the literature that is calibrated in terms of Doppler frequency shift are both misleading and frequently inaccurate. The investigators did not or could not make the angle measurements required to quantitate their data."

Even current instruments representing state-of-the-art do not have the ability to accurately calculate the

Doppler angle. The orientation of the vessel can be visualized by new imaging systems and the Doppler angle between the transducer beam and wall of the vessel (not flow) can be measured, but even these very expensive systems are sensitive to small changes in orientation of either the vessel or the transducer. Therefore, it is very important to develop a model that can calculate the Doppler angle directly and precisely. In the present study, we have developed such a model which is capable of calculating accurately the Doppler angle rather than using an approximation. The ability to properly determine the Doppler angle enables us to accurately measure the blood velocity components. Also, by scanning the diameter of the vessel, the velocity profile and therefore diameter of the vessel can be calculated and with it the blood flow volume rate. Blood flow volume rate may be one of the best indications of available oxygen. It is also an indicator of the ability of the heart to function as a pump and to maintain normal body processes.

1.3 Blood Flow Patterns

In order to understand pathological changes of the blood flow within the vessel of interest, some knowledge of fluid dynamics in relation to the blood flow is required. It has long been recognized that fluids exhibit two distinct types of flow. The first, and the simpler, is laminar flow.

This type of flow is characterized by a fluid that flows in a straight line or layer (lamine) [6]. The second type of flow is called turbulent flow and is characterized by a random motion of the individual particles (red cells in the case of blood).

One of the characteristics of the flow used to distinguish different patterns is the Reynolds number. Although the Reynolds number is not often useful in describing blood flow because of the frequent changes of the blood vessel's diameter in the arterial tree, it is a primary factor in distinguishing the previously identified patterns. Reynolds found that flow pattern in a circular pipe depends not only on the velocity of the fluid, but also on the density and viscosity of the fluid and diameter of the pipe. The threshold for Reynolds number for laminar flow is 2100. Flow with Reynolds number of less than 2100 is considered in general to be laminar. Flow with a Reynolds number of more than 3100 is considered generally to be turbulent. Although Reynolds number is an important factor in identifying the type of flow, it is more useful in characterizing laminar flow. In the turbulent region, however, the flow pattern is affected more often by wall forces than by fluid viscosity and Reynolds number.

The most important indicator which has been developed to investigate the blood circulation is the velocity

profile [2]. It was shown that flow in the laminar core has a parabolic velocity profile and the turbulent flow has a more blunt profile across the diameter of the pipe. The velocity at the wall for all real flows is, of course, equal to zero, owing to the wall friction forces.

In the area of Doppler ultrasound, attempts have been made to investigate the blood flow circulation in conjunction with the pathological changes. Because of the simplicity in calculation of the average velocity, most of the researchers in this area have used the laminar approximation. Ohmori, et al. (1977) showed that blood flow cannot be considered laminar in all of the arteries. In fact, in many of the major arteries, especially in and around the heart, blood flow patterns are found to be of turbulent nature. In addition, random motion of the individual blood particles causes disturbances that appear as fluctuations in the output signal. In approximating the blood flow as laminar, values of the fluctuation components are ignored during the process of calculation of the flow characteristics. Whereas, in the turbulent flow, those parameters perform a very important role in calculation of blood flow characteristics such as shear stress and turbulent intensity.

1.4 Goals of the Study

In this study, first, we will discuss a practical approximation for the backscattering of periodic bursts of

damped sine waves by a volume of randomly distributed scatterers. This approximation is applied to the measurement of a volumetric backscattering cross-section, taking into account tissue, acoustics, and system parameters. Second, a dual transducer pulsed-Doppler ultrasound (DTP-Du) is developed and will be used for accurate measurements of the Doppler angle which permits determination of blood flow velocities. The fluctuation components of the velocities are then going to be determined and their relationship to the pathological changes such as stenosis, will be investigated.

To verify the results of the theoretical works, various experiments will be performed. The dual transducer pulsed-Doppler ultrasound is constructed and will be used to extract information, such as velocity, volume rate and other characteristics of blood flow. Attempts will be made to classify the degree of stenosis in the arteries under investigation.

1.5 Flow Chart

The organization of this study is as follows: In the present chapter, basic definitions and notations are given. Also, a detailed discussion of Doppler principle and Doppler instruments and a brief review of the application of Doppler ultrasound in medicine is presented.

In Chapter II (Literature Review), the theoretical

investigations of the pulsed Doppler ultrasound in relation to this study is presented. Then the fluid mechanics aspect of the work is presented in more detail. Finally, in-vivo and in-intro investigations done by other researchers in this area are introduced.

In Chapter III, the theoretical investigation in Communication is presented. Then, the dual transducer model is presented and its performance is evaluated and compared with the conventional model. Finally, the fluid mechanic aspect of the work is discussed.

In Chapter IV, experimental procedure is discussed and a brief description of different devices used in experiments is demonstrated.

In Chapter V, experimental results in calculating the Doppler angle, blood flow velocity, blood flow volume rate and shear stress using theoretical investigations are presented.

In Chapter VI, we summarize the results of theoretical and experimental study and the future work of this study is outlined.

CHAPTER II

LITERATURE REVIEW

At the present time, many investigators are using ultrasonic instruments or are involved in their development. In recent years, the clinical potential of Doppler ultrasound for obtaining important hemodynamic information has been widely recognized. Growing interest in pulsed-Doppler ultrasound has stimulated attempts by clinical researchers to correlate quantitative Doppler information with circulatory disease states. Before such studies can produce meaningful quantitative data, it is essential to approach signal processing in Doppler ultrasound from the principle of conservation. Retrieval of data by accounting for transmitted signal properties, converting the Doppler signal into the form from which information concerning velocity can be revealed, analyzing acoustical parameters affecting the backscattered signal, obtaining accurate measurements of Doppler angle, will provide the refined data needed. At present, the accuracy with which quantitative Doppler information can be determined is compromised by equipment design which fails to account for these and other sources of error.

In this chapter, we discuss some of the approaches

introduced by other researchers for processing the Doppler signal. Also, in this chapter we discuss some in-vivo and in-vitro analyses for quantitative assessment of the state of the artery. These investigations can be classified in two general categories: theoretical investigations and experimental investigations.

2.1 Theoretical Investigations

2.1.1 Processing the Doppler Signal

In recent years, different research groups have tried to develop methods which use more relevant sensitive information in the Doppler signal [9], [53], [61], [72], [75], [77]. In this section, some of the theoretical studies are investigated which are conducted by other researchers closely related to our study. But, first, the relationship is discussed between the Doppler signal and blood flow particles from which the velocity profile in the artery is formed.

In order to describe the velocity profile across the vessel diameter, consider the situation illustrated in Figure 2.1, in which it is assumed that a unit length of the vessel is uniformly insonated with continuous-wave

ultrasound. Doppler signal is a time-varying wave form which usually resembles the trace shown in Figure 2.2. The Doppler signal contains information about flow velocity and its frequency spectrum is in the audio range. To extract this information, different methods of decoding, both in time and the frequency domain, are used.

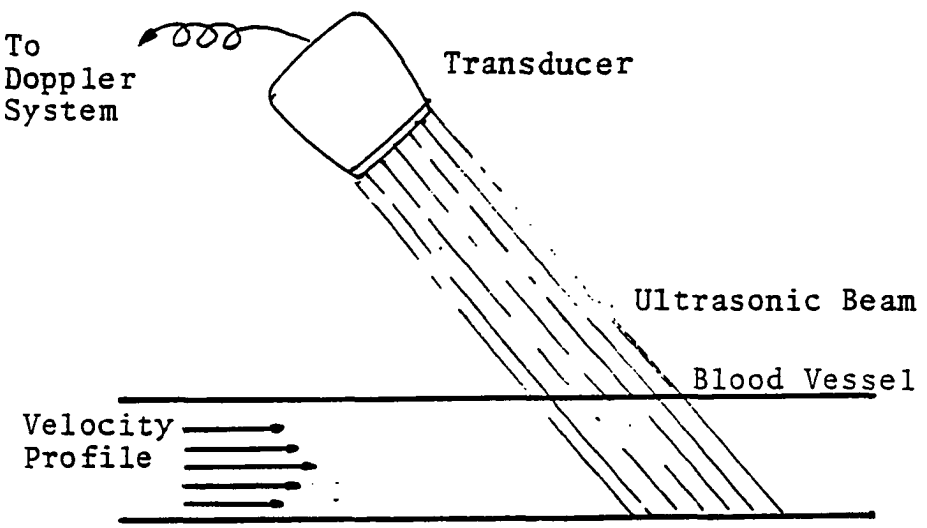

Figure 2.1 Doppler insonation of the blood.

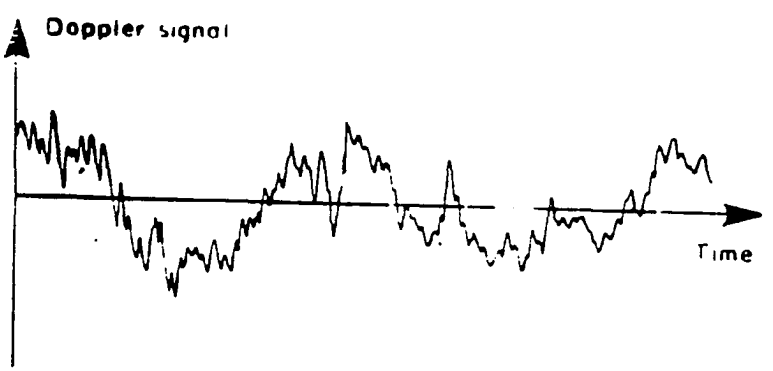

Figure 2.2 An example of a Doppler signal.

The essential problem in time domain analysis is to process the Doppler signal in some simple way such that particular parameters related to its frequency content are revealed. The first step is to examine the time domain signal to find clues to its frequency content. For the simple case of pure sinusoid, the problem is elementary: the frequency of the sine wave is equal to one-half the rate at which the wave form crosses its own mean level. However, for the case of a Doppler shift signal from a blood vessel, the problem is much less straightforward. For instance, low frequency signals originating from slow moving blood near the wall combine with higher frequency signals from the center of the vessel to produce a complicated wave form shape. Also, noise on the signal can produce unwanted zero crossings. Relating zero crossings to frequency in any particular situation is quite difficult but, nevertheless, this principle forms the basis for the most popular type of Doppler shift processor currently in use. However, it is perhaps true that this widespread popularity has been gained more from the simplicity of the device rather than from its reliable and accurate performance characteristics [7].

The theory of operation of a zero crossing detector is based on a classic theoretical analysis by Rice (1944) who analyzes the problem by predicting the expected number of zero crossings from the spectral coherent of the signal.

Atkinson, et al. (1982) and a number of other

researchers [1-6], [14], [15-16], [29], [46], [62] applied this theory to the Doppler signal. They showed the echo power backscattered from the blood in proportion to the velocity density of red cells (number of red cells in the unit volume) by the following formula:

$$P(w)\cdot dw \propto n(v)\cdot dv \tag{2.1}$$

where P(w) power spectrum and n(v) is the velocity density, and w and v are related by original Doppler equation (1.2). The number of zero-crossing proportional to the frequency is given by equation (2.2):

$$\lambda = 2\left[\frac{\int_{-\infty}^{\infty} w^2 P(w)\,dw}{\int_{-\infty}^{\infty} P(w)\,dw}\right] \tag{2.2}$$

As was mentioned earlier, the zero-crossing convertor has numerous disadvantages, especially when the frequency spectrum of the signal is broad. The continuous wave ultrasound has a broad band spectrum already, due to its covering the whole lumen size and this is depicted in Figure 2.3.

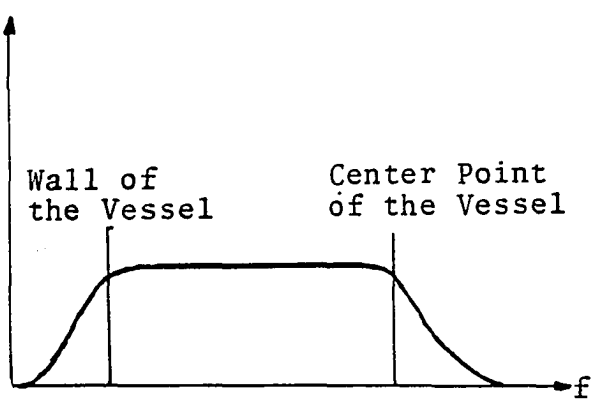

Figure 2.3 The power spectrum of a Doppler signal in CW.

In the case of pulsed Doppler ultrasound, however, the zero crossing converter is more reliable, since few bursts of pulse are transmitted to the converter during each pulse repetition period.

The second way of processing the Doppler signal is frequency analysis [7], [10], [12-13], [17-19], [44], [57], [64], [66-67], [73], [81]. As stated previously in equation 2.1, the power spectrum of the Doppler signal is proportional to its velocity density. Therefore, by determining the power spectrum of the signal, the mean frequency and consequently mean velocity of the blood flow can be obtained. However, this can be done under the following assumptions:

a) The blood particles are uniformly distributed.

b) Attenuation is negligible.

c) The medium of the blood flow is homogeneous.

The Fourier transform analysis, however, has been proven to be an effective tool in characterizing and stating the status of the blood circulation [74], [80], [83-91], [94-95], [99], [103-107].

In the processing of the Doppler waveform, the effect of tissue parameters such as thickness and attenuation factors must also be considered. Holland, et al. (1984) stated that the quantitative capbility of pulsed-Doppler ultrasound in clinical practice is limited by the effect of thickness and attenuation of ultrasound in tissue as well as several other parameters which distort the Doppler spectrum of an ultrasonic echo. In that report, results are presented

of in-vitro experiments which demonstrate the magnitude of the errors expected in clinical measurements of flood flow parameters when thickness and attenuation ultrasound in biological tissue is ignored.

Kadaba (1980[, used a modified version of pulse echo technique to measure the attenuation and backscattering coefficient of ultrasound. Also in this area [35], [44], [47], [50], [63], [68], [70], [76] have investigated only the effect of attenuation and other acoustical parameters on the Doppler signal. But, the effect of other parameters such as system and tissue parameters, together with the acoustical parameters have not been investigated.

Since the current literature does not investigate the peripheral factors outlined at the beginning of this chapter, in this study, the effect of acoustics, tissue and other elements on the transmitted and backscattered signal are investigated using an alternate form for the tranmitted signal.

2.1.2 Determining the Doppler Angle (θ)

The Doppler formula as it was shown in Chapter I can be expressed as

$$\Delta f = 2 \cdot f_0 \cdot v_R \cdot \cos \theta / c \qquad (1.2)$$

As was mentioned in the previous section, through the use of various techniques of processing the Doppler signal, it is possible to determine the frequency shift imparted to the

returning signal by the flowing blood. However, the principal unknown which remains in equation (1.2) is an accurate determination of Doppler angle (θ). Baker, D.W. [4], Jorgenson, J.E. [21], Valdescruz, L.M. et al. [34] stated that it is possible to assume some orientation for the vessel of interest and then predict the Doppler angle. However, such a procedure can lead to significant errors in the calculated velocity, since the relative error in velocity is a function of changes in Doppler angle

$$\text{(i.e. } \frac{d\, v_R}{v_R} = \operatorname{tg} \theta \, d\theta\text{)}.$$

For example, if θ is actually 45° and it is estimated 50°, the relative error in velocity is 9 percent. The error in velocity estimation increases by increasing the Doppler angle. For example, if the actual value of the Doppler angle is 65° and is estimated 70°, the error in velocity is almost 19 percent. Since the velocity is the primary factor in the calculation of other characteristics such as volume rate, velocity profile, shear stress, etc. --the important role of the Doppler angle becomes more evident.

A second approach to accurately estimating the Doppler angle, is using the Doppler imaging system [2] in addition to pulsed-Doppler ultrasound. Gill, R.W. [60], Nimura, Y. [20], Brody, W.B. [28], Bournat, J.P. [31], and Nilsson, G.E. [59] studied the quantitative measurement in deep-lying vessels. In these studies, sttempts have been made for 10 cating the vessel of interest, calculating its size and

determining the orientation of the blood vessel by combining the pulsed-Doppler ultrasound with a B-scan imaging instrument. But, the problem with using this combined system is that the Doppler angle is described as the angle between ultrasonic beam and the wall of the vessel, whereas the real Doppler angle is the angle between ultrasonic beam and the blood flow, not the wall of the vessel. Therefore, the quantitative measurements, due to the described system in these studies, are not accurate enough to describe the real values of the velocity. In general, the standard system, alone, or together with the imaging system, are capable of estimating the Doppler angle in one-dimensional cases; therefore, they can be used only when flow pattern is laminar.

In this study, we developed a model that can calculate the Doppler angle more accurately and is capable of obtaining the velocity components, which is useful not only in laminar flow, but in turbulent regions, as well.

2.1.3 Blood Flow Pattern

As was mentioned earlier, it is possible to record blood velocity waveform for many of the blood vessels using a pulsed Doppler ultrasound. In addition to the method of processing and the effect of tissue parameters on the Doppler signal previously described, characterizing the waveform in terms of flow pattern is critical. Because, recognizing the flow pattern can enhance one's understanding of the flow properties, and therefore of great help for diagnostic purposes,

changes on the Doppler signal can be related to pathological parameters causing those changes. Therefore, it is of great importance to calculate characteristics of the blood flow circulation. Specific blood flow characteristics which have roles in clinical applications include: a) the distribution of velocity (velocity profile), b) the distribution of the force on the wall of the vessel (shear stress) and c) the level of intensity developed at the site of stenosis.

The velocity profile in a laminar flow can be found from the following procedure. When the flow is within laminar region, the viscous shear stress τ is

$$\tau = -\mu \frac{du}{dr} \tag{2.3}$$

where μ is viscosity, u is velocity and r is radius of the pipe. On the other hand, shear stress in the laminar region can be expressed in terms of pressure change (Δp) due to the friction and L, the length for flow, to be fully developed as:

$$\tau = \frac{r}{2L} \cdot \Delta P \tag{2.4}$$

Equating equations (2.3) and (2.4) and integrating, u can be found

$$\frac{r}{2L} \cdot \Delta p = -\mu \frac{du}{dr}$$

$$\int_{u}^{0} du = \frac{\Delta p}{2L\mu} \int_{r}^{D/2} r dr$$

or

$$u = \frac{\Delta p D^2}{16 L \mu} \left[1 - \frac{r^2}{(\frac{D}{2})^2} \right] \qquad (2.5)$$

It can be seen from equation (2.5) that the velocity distribution in laminar flow assumes a parabolic shape. The velocity is maximum at the pipe center ($r = 0$) and is zero at the walls of the pipe ($r = \frac{D}{2}$). The maximum velocity can be found from equation (2.5) as follows:

$$u_{max} = \left(\frac{\Delta p D^2}{16 L \mu} \right) \qquad (2.6)$$

It was shown that the average velocity in laminar flow is equal to one-half the maximum velocity. This is equivalent to the fact that the height of a cylinder is one-half the height of a parabolid with the same base circle and the same volume. So

$$v_{avg} = \frac{u_{max}}{2}$$

or

$$v_{avg} = \frac{\Delta p D^2}{32 L \mu} \qquad (2.7)$$

The volume rate of flow (Q) through a circular pipe is given by the expression

$$Q = v_{avg} \cdot A = \frac{\pi D^2}{4} \cdot v_{avg} \qquad (2.8)$$

Simplicity in calculations and lack of proper instruments have forced most of the researchers to investigate the development of the arterial lesion leading to stenosis and other types of diseases, based on the assumption that blood

flow pattern is laminar in most of the cases [7], [8], [31]. But, the problem is, that in laminar flow the fluid parameters such as viscous effect, is a predominating factor and structural changes such as stenosis do not have a significant effect on the flow characteristics. Therefore, if the flow pattern is originally turbulent and approximated as laminar, significant portions of the data are lost.

Moreover, it was stated earlier that the flow cannot be considered laminar in all of the arteries. In fact, in more important arteries such as the coronary artery and the carotid artery, there are indications of disturbances caused by turbulency and flow has been categorized as turbulent [8], [11], [45], [48-49], [51-52], [69].

In turbulent flow, random motion of individual blood particles causes disturbances that appear as fluctuation components on the Doppler signal. Fluctuation components of the turbulent velocity are very important factors in calculating turbulent flow characteristics. One of the advantages of being able to detect turbulency in contrast to laminar flow, is that the characteristics of blood flow are related to structural and other tissue parameters. In the proceeding part of this section, the theoretical aspects of turbulent flow were briefly discussed.

Instantaneous velocities in turbulent flow in x (parallel) and y (perpendicular) domains are shown by the expressions

$$v_x = \bar{v}_x + v'_x \tag{2.9}$$

$$v_y = \bar{v}_y + v'_y \tag{2.10}$$

where $\bar{v}$ is the average velocity and v' is the fluctuation velocity. One of the characteristics of turbulent flow is shear stress. Shear stress is shear force per unit area acting on the control volume as a result of mass transfer from one layer of the fluid to another, and it can be expressed as follows:

$$\tau = \mu \frac{dx}{dy} - \rho \overline{v'_x v'_y} \tag{2.11}$$

The first part of the right-hand side of equation (2.11) is molecular contributions and the second part is turbulent contribution (Reynolds stress) to the shear stress. It was shown [102] that in turbulent flow, the magnitude of the Reynolds stress is much greater than the molecular contribution. Therefore, Equation (2.11) can be expressed as

$$\tau = - \rho \overline{v'_x v'_y} \tag{2.12}$$

where ρ is the density of the flow and $\overline{v'_x v'_y}$ average of the product of fluctuation components.

Another important characteristic which is a function of fluctuation is the level of intensity of turbulence and is defined as

$$I = \sqrt{(\bar{v}'^2_x + \bar{v}'^2_y)/2} \tag{2.13}$$

The most important characteristic in any type of flow, however, is velocity profile. It was shown that velocity

profile in laminar flow has a parabolic shape. In turbulent flow, especially, in a small pipe such as an artery, the velocity profile doesn't have a known form and is dependent upon the value of shear stress, in addition to the location of the sample volume and pipe radius. For example, the velocity profile in smooth pipes can be expressed as:

$$v = v_{max} + k\sqrt{\frac{\tau_0}{\rho}} \ln \frac{y}{R} \qquad (2.14)$$

Also, unlike the laminar flow in which average velocity is assumed to be one-half of maximum velocity, in turbulent flow, average velocity is a function of velocity profile and can be expressed as follows:

$$v_{avg} = \int_0^R v \cdot dA$$

Another important matter to consider is the region of turbulent flow [96-98], [101-102]. In general, turbulent flow consists of three different regions [23]. In a very thin layer near the wall of the vessel, when the velocity is low and hence viscosity predominates, flow is noted to be laminar. This region is called laminar sublayer. Immediately inside the laminar sublayer is a thin region where the velocity is greater and the effect of friction and viscosity is about equal. This layer is known as the transition or buffer zone, and the flow can be laminar and/or turbulent, or both, and possibly changing with time. The third region constitutes the major portion of the pipe cross sectional area, and it is the area

where turbulence is found and where friction forces override the effect of viscosity. This region is called turbulent core. Distinguishing between these three layers can enhance the ability to calculate characteristics more effectively.

In the present study, we have developed a direct relationship between blood flow characteristics of turbulent blood flow and tissue parameters such as thickness, in an attempt to classify the degree of stenosis.

2.2 Experimental Investigation

2.2.1 In-Vitro Experimental Investigation

In this section, we discuss the in-vitro studies similar to our work conducted by other researchers. In in-vitro experiments, it is possible to generate turbulency and to investigate state of blood flow circulation. Therefore, most of the studies investigated in this section are in the turbulent region.

Stein, et al. [89] studies the contribution of erythrocytes to the intensity of turbulence in flowing blood. The intensity of turbulent flow was measured by a hot film anemometer. It was shown that the intensity of turbulence depends upon the level of hematocrit (number of erythrocytes in plasma). However, in their study, only one component of the intensity has been reviewed, due to the use of one probe, and extracting information about the second

component of the intensity is not possible. But, as was mentioned earlier, intensity of turbulence is dependent upon both components of the velocity. Moreover, the hot film anemometer disturbs the flow. Further, it must be inserted into the artery via surgery; therefore, it is of little use in real time application.

Stein et al.[90], studied the effect of complaint tubes upon turbulent intensity. Turbulence intensity was again measured with a hot film anemometer. This study indicates that the compliance of arteries may be a physiological factor that contributes to the reduction of turbulence in the cardiovascular system. Also, in this study, steps were taken to relate the intensity of turbulence with the physiological factors, but problems encountered in previous studies held for this study as well. Walbun et al. [91], investigated the effect of the branch-to-trunk area ratio on the transition to turbulent flow (implications in the cardiovascular system), using a laser Doppler anemometer in glass tubes. Observations from this study suggest that, for a branch-to-trunk ratio of 0.4 to 0.8, the critical Reynolds number was relatively constant. As the branch-to-trunk area ratio increased beyond 0.8, a decline in the Reynolds number was observed. The velocity profiles at a branch-to-trunk area ratio of 0.4 showed acceleration of velocity in the branch, while at an area ratio of 1.4, the velocity was shown to decelerate. One problem with

this study is the use of a laser Doppler anemometer which is useful only for in-vitro analysis not in real time. Moreover, a single transducer probe is used which is not satisfactory for turbulent analysis.

In another related study, Stehbens [108] showed that critical Reynolds numbers are considerably below the generally accepted value of 2000. In that study, it was suggested that turbulence of blood flow is a factor in initiating the lesions of the arteriosclerosis at the sites of branching of the cerebral arteries. One very important observation from this paper and similar papers is that calculating the Reynolds numbers only to evaluate the physiological effect of the turbulence cannot be trusted in blood flow analysis, especially in smaller arteries and other characteristics such as intensity and shear stress must also be obtained to have a cumulative result for analyzing the turbulent flow.

Khalighi et al. [96] have investigated the steady flow development in a human aorta using a laser-Doppler anemometer. The velocity profiles at several cross-sections in the ascending aorta, mid-arch and in the brachiocephalic artery are measured. The velocity profiles for most of these cases were found to be relatively flat (an indication of turbulency). This study also investigated the effects of a physiological abnormality such as thrombus formation and tissue overgrowth on the flow pattern. In addition to

this study, Saad et al. [97] investigated the velocity field in the neighborhood of axisymmetric constrictions in rigid tubes using laser Doppler anemometer, and at Reynolds numbers characteristic of large arteries. Stenosis of 25, 50 and 75 percent area reduction were studied. Velocity profiles were presented in sufficient detail to allow comparison with biofluid dynamics models. Wall shear stresses were also estimated. It was shown that for larger arteries it is possible to distinguish between different degrees of stenosis by analyzing their flow characteristics. An interesting result of this study is its laser technique. The significance of this study is that by using laser Doppler anemometer, the flow pattern could be photographed. These images clearly show the effect of turbulency and stenosis on flow pattern.

In another related investigation, Saad et al. [98] measured instantaneous velocities in the field distal to contoured axisymmetric stenoses with a laser Doppler anemometer at Reynolds numbers ranging from 500 to 2000. Autocorrelation functions and spectra of the velocity were employed to describe the nature of fluid dynamic disturbances. Degree of stenosis of 25, 50 and 75 percent were used and the results were compared. The effect of area reduction (stenosis) on the centerline disturbances level was demonstrated. Very little change is seen for the 25 percent stenosis in the intensity level, but for 50 percent

and 75 percent stenosis, there is an increase in intensity level for a fixed value of Reynolds numbers.
In the latter two investigations, a laser Doppler anemometer was used to measure velocity components and to calculate some characteristics of the flow. The major point in these studies is that they were investigating the turbulency caused by stenosis, but the initial nature of the flow field itself was not defined. Moreover, the Doppler instrument is capable of measuring only one component of the velocity which is insufficient for turbulent regions.

Chandran et al. [99] studied the physiological pulsatile flow of past aortic valve protheses. The measurements of velocity profiles and turbulent normal stresses during several times in a cardiac cycle were obtained using laser-Doppler anemometery. The turbulent normal stresses measured downstream to the tilting disc were compared with caged ball valves. The turbulent shear stress and velocity profile for different angles of valve openings and for pulsatile and steady flow were generated. Again, in this study, single transducer laser Doppler was used which doesn't have any application in in-vivo analysis and is not an accurate device for turbulent regions.

2.2.2 In-Vivo Experimental Investigations

In this section, we discuss the in-vivo investigations which have been conducted by other researchers [22-27],

[30], [36-42], [55-56], [65], [71], [78-79], [92-93], [100]. One important difference between in-vivo and in-vitro studies should be noted. Unlike in-vitro investigations, in most of the work in this area, researchers assumed that blood flow is laminar using Doppler ultrasound. Even if the investigators conclude that blood flow is turbulent, they use hot-film anemometers as single transducer Doppler ultrasound.

Strandness et al. [39] studied ultrasonic flow detection as a useful technique in the evaluation of peripheral vascular diseases. In their study, detail evaluation of both arterial disease (84 cases) and venous disease (17 cases) is presented. The main goal of this study was to show in general, the ability of ultrasonic flowmeter in detecting the severity of the above-mentioned diseases, particularly in post operative evaluation. One problem with this study was the use of continuous wave Doppler ultrasound which is not capable of discriminationg the range in which a particular artery is located.

Now some of the other works will be introduced, aiming for quantitatively assessing the state of different types of diseases.

Brown et al [36] described a method for processing input/output blood velocity wave form for femoral arteries obtained with ultrasonic Doppler flowmeters in order to investigate the state of stenosis. In their study, the

blood velocity/time waveforms were recorded from the common femoral and popliteal arteries (see Figure 2.4), using ultrasonic Doppler shift flow velocity meter, and transfer-function modeling of the femoral artery. Maximum value of blood flow velocity for normal and deseased femoral arteries, along with the pole positions for case studies under transfer-function modeling were presented. All the normal poles were very lightly damped and are close to the imaginary axis of S-plane. The poles corresponding to the known diseased cases all lie on the negative real axis, indicating a damping ratio greater than unity and representing the considerable resistance to blood flow of the collateral circulation. The poles of the early cases occupy the regions between the normal and diseased poles.

The results of this study are interesting, but they are actually qualitative and can be applied only to an occluded femoral artery. Moreover, two separated synchronized systems applying in two different locations of the artery must be available to obtain input/output waveform simultaneously.

Skidmore et al [38] have done a similar study to the one done by Brown et al. In their study, physiological interpretation of Doppler-shifted waveforms were done for the femoral artery. A third order mathematical model was developed which described those waveforms in patients with occlusive arterial disease and in normal volunteers. In

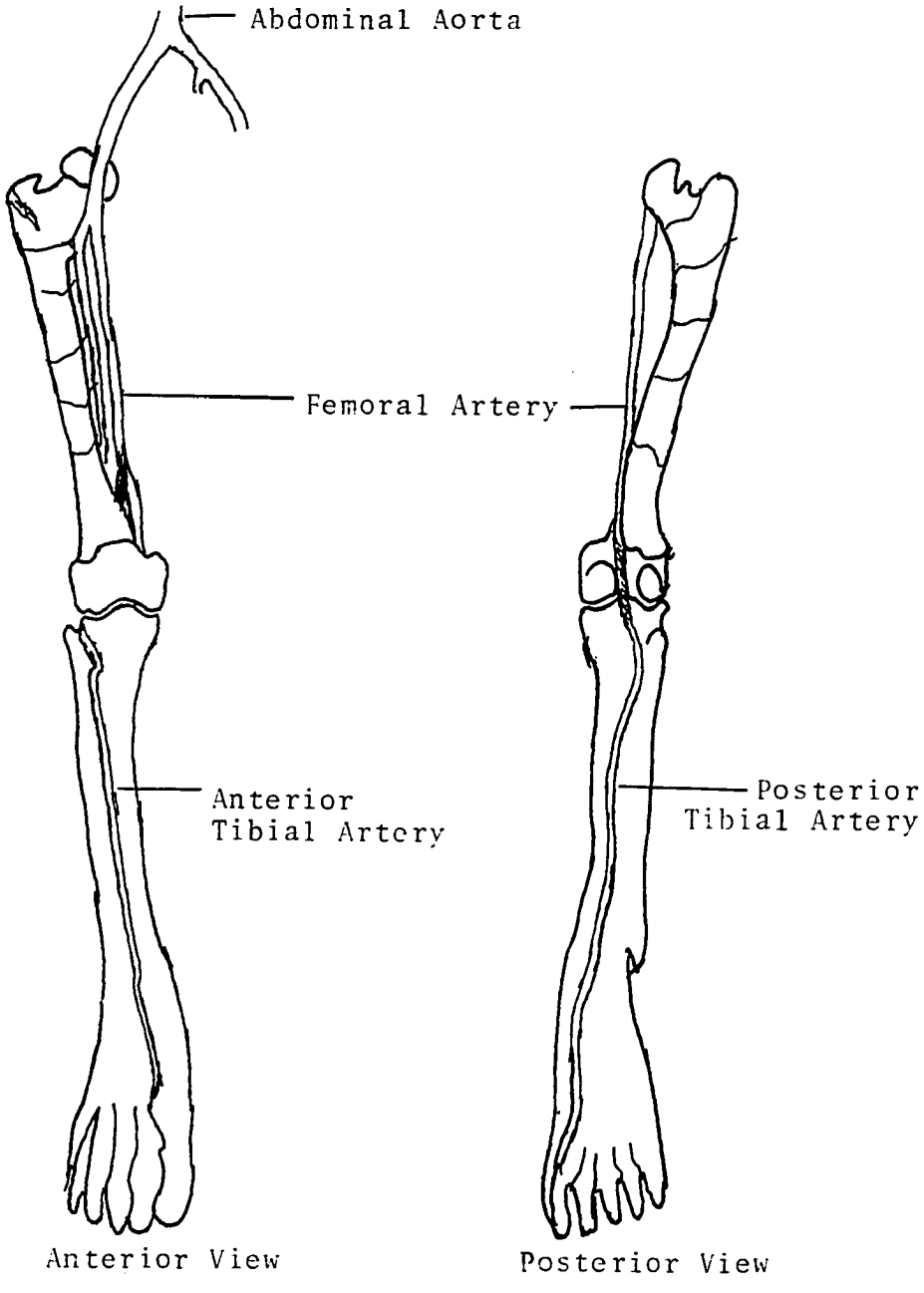

Figure 2.4 The common femoral artery.

normal subjects, the model has two complex and one real pole, and in occluded arteries with collateral circulation, all the poles are real. The complex poles are shown to be related to the elastic modulus of the artery and also to the lumen size. The real poles are shown to be related to the degree of vasoconstriction of the peripheral circulation. This study is again limited to the femoral artery, and the accuracy of determining Doppler angle is not discussed.

Stevenson et al [85] studied the diagnosis of ventricular sepatal defect (VSD) using pulsed-Doppler ultrasound by following the turbulent jet through the septum. It was shown that measuring turbulency can allow specific detection of the jet of the VSD, and detection of associated defects. It also allows the researcher to assess the magnitude of the shunt at the ventricular level. This study indicates the important role of the Doppler ultrasound machine and also the relationships between fluid dynamic characteristics of flow with a particular disease. But, again, single transducer pulsed Doppler ultrasound was used, which has been shown to be inaccurate in turbulent flow areas.

In view of the variety of effects of turbulent flow upon the circulatory system, Sabbah et al [86] have studied the effect of erythrocytic deformability. The random fluctuations of velocity indicative of turbulent flow were

measured with a hot-film probe. They showed that turbulent blood flow occurs in ascending aorta of normal subjects with a high cardiac output and it occurs routinely in the presence of aortic valvular disease. They quoted studies in dogs which suggested that turbulent blood flow may even contribute to thrombus formation. They claimed that turbulent blood flow and its associated high shear stresses can damage even normal erythrocytes. This study is another indication of the relationship between flow characteristics and physiological changes. The weakness of this study is, first, in the use of hot-film anemometer, second, only a single component of the velocity is measured which is not satisfactory in turbulent regions.

In another related study, Stein et al [87] have investigated the role of microthrombi and turbulent flow in continuing disease process of calcific aortic stenosis. They suggested that repetitive deposits of microthrombi, followed by calcification, would explain the continuous process of stenosis in previously deformed aortic valves. The formation of such thrombi may be initiated by turbulent flow and other fluid dynamic factors. Although, in this study, an attempt was made to relate stenosis to the turbulency, a single hot-film anemometer was used. As we have often noted, this procedure interferes with the blood flow

in an unknown manner. Since the actual preinvasive flow is still unknown, the entire experiment is based on data which has been altered by the investigator's surgical procedure.

Goldberg et al [88] have studied the turbulence mapping in patients with valvular aortic stenosis using pulsed-Doppler ultrasound. In their study, they presented four well-known major flow areas that occur distal to a stenotic aortic valve. These include a jet, an area alongside the jet (the parajet), an area of flow disturbance, and an area in which disturbed flow again becomes laminar downstream. Of these, the flow disturbance area has markedly turbulent flow, although some turbulence can be at time detected in the area beside the jet. The purpose of this study was to test a technique of patient examination that might allow a pulsed-Doppler ultrasound to detect each of the known areas in the aorta of valvular stenotic aorta patients. The problem encountered in this investigation was in the machine limitation which didn't allow a proper interpretation of flow dynamics from recorded information, because of its inability to measure accurate blood flow valocity.

Hwang et al [8] have done the most comprehensive study in turbulent blood flow. In their study, turbulent characteristics of pulsatile flow through a natural human mitral valve opening were measured with a pair of hot-film

anemometers. Mean velocity, distribution of turbulent intensities, and Reynolds stresses were calculated from the recorded information. It was shown that the phase average of the longitudinal velocity component increases nearly exponentially with time from the beginning of the diastolic phase, and then reaches a maximum and starts dropping, afterwards. Somewhere in the middle of the systolic phase, the velocity reaches the minimum value and stays constant at that value until the end of that phase. The maximum velocity was almost eleven times the minimum. Also, in their work, the phase average of longitudinal and transcerse components of turbulent intensities during the cardiac cycle were presented. It can be seen that the turbulent fluctuations increase dramatically just before maximum velocity is reached. Thereafter, the turbulent fluctuations reach a plateau level through the mid-diastolic phase. The intensity decreases near the end of the diastolic phase. The maximum turbulent intensity is 6 times the minimum value during the cardiac cycle. The transverse turbulent intensity varies in a qualitatively similar manner except that the minimum value and the maximum value of transverse are somewhat lower than the longitudinal.

The phase average Reynolds stress is nearly zero during the systolic phase, but is quite large during the diastolic phase. The Reynolds stress during the diastolic phase has two peaks: one during the phase when the flow

through the mitral valve is maximum and the other during the phase when the flow through the mitral valve is decelerated.

The only weakness of this study is the use of a hot-film anemometer which must be inserted by surgery inside the artery and it can affect the flow field.

In contrast to most of the work in this area, our study will introduce a transducer model which, rather than using an estimate, is capable of actually calculating the Doppler angle. This technique will allow a proper interpretation of flow dynamics from the recording Doppler signal by accurate determination of the velocities both in laminar and turbulent regions. In calculating the velocity components of the flow field, the following points must be considered:

1) Number of periods in which phase average of any variable is going to be calculated must be as large as possible.
2) In calculation of volume rate in addition to the Doppler signal at the centerline, the velocity profile and measurement of the range must be conducted.
3) For in-vitro studies, the pump speed must be kept constant throughout the procedure and for in-vivo

experiments, the heart beat of the subject must be carefully monitored while recording data in a particular experiment.

CHAPTER III

THE THEORETICAL INVESTIGATIONS

In this chapter, first, a damped sine wave is used as the transmitted pulse and the Doppler signal is derived from the power backscattered ultrasound signal from the blood. Second, a new transducer model for a more accurate determination of Doppler angle and blood flow velocity is discussed, and theoretical comparison between conventional and developed ultrasound models is presented. Finally, the fluid dynamic aspect of the work is investigated and the relationship between blood flow characteristics and stenosis is derived.

3.1 Scattering of Ultrasound by Blood

In this section, first, we develop a practical approximation for the backscattering of a transmitted signal by a volume of randomly distributed scatterers (red cells). Then, utilizing pulsed-Doppler ultrasound system (Figure 1.2), the received backscattered signal is demodulated and filtered to obtain the Doppler signal. The mathematical formulation is taking into account the transmitted pulse parameters, tissue parameters, acoustical parameters, and system parameters. Therefore, a comprehensive analysis of

the Doppler signal is presented.

Human blood is composed of a liquid called plasma in which are suspended red blood cells, white blood cells, and platelets [46]. The red blood cell is a nonnucleated biconcane disk with an average diameter of 7 μm and average thickness of 2 μm, with a mean volume of 87 μm^3. There are about $5 \times 10^9/cm^3$ of red blood cells (RBC's), $7.5 \times 10^6/cm^3$ white blood cells and $3.5 \times 10^8/cm^3$ of platelets in an adult [47]. The number of red blood cells (RBC's) is much larger than that of the white cells and the volume of red cells is much larger than that of the platelets. Thus, the scattering of ultrasound by blood, presumably, is due to the RBC's. In this study, we derive the received power backscattered signal from the scatters excited by damped-sine bursts, rather than conventional sine wave. The analysis is begun by presenting the damped-sine wave burst which can be expressed as

$$y(t) = A\, e^{-(t-t_0)^2/\tau_1} \cos w_0(t-t_0') \qquad (3.1)$$

where A is the amplitude, τ_1 is the dying rate, t_0 and t_0' are positions of highest central peaks and w_0 is the angular frequency of ultrasound beam. A plot for y(t) is shown in Figure 3.1.

The transmitted signal propagating through different tissues will be attenuated in amplitude by the different

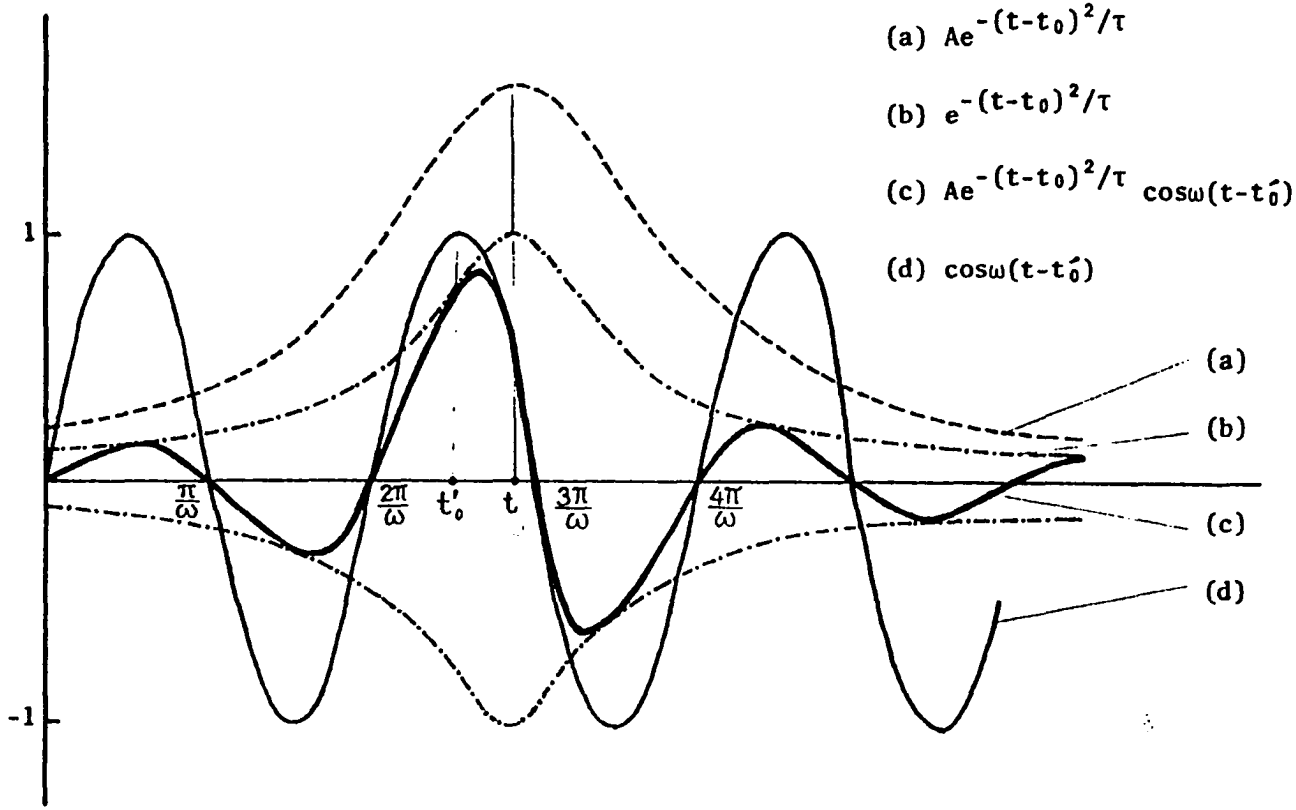

Figure 3.1 A two-sidedly damped sinusoidal wave form, curve (c).

acoustical parameters, and its phase will be changed by the effect of blood motion, and because of the structure of the blood, it will be scattered back by a random motion of small particles (red cells). Figure 3.2 can be used to describe this phenomena.

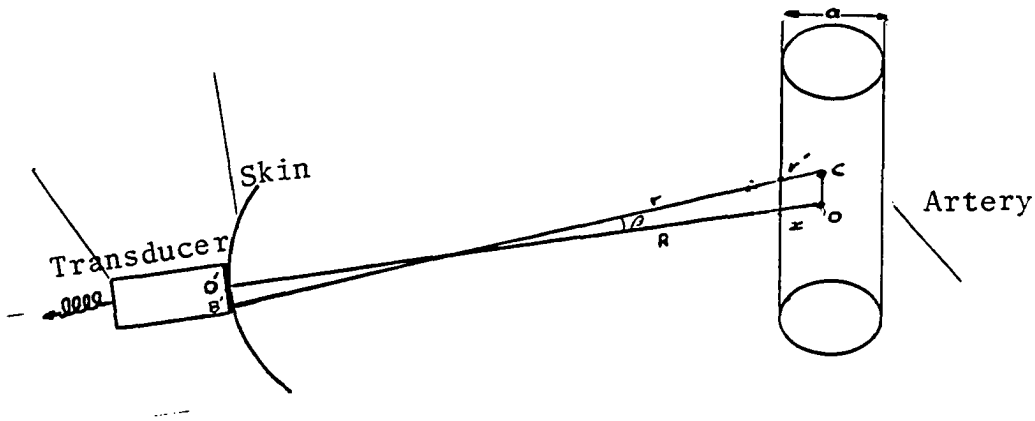

Figure 3.2 Scattering of the ultrasound signal by red cell.

The incident pressure wave inside the vessel at the point c(x,y,z) can be expressed as

$$P_i(t) = \frac{H(t)}{R+x}\, e^{-\alpha_m R}\, e^{-\alpha x}\, e^{-(t-t_0-\frac{R+x}{c})^2/\tau_1} \cdot \cos w_0(t-t_0'-\frac{R+x}{c}) \qquad (3.2)$$

where $\frac{H(t)}{R+x}$ is the amplitude of the pressure wave and α_m and α are attenuation factors in medium I and II, respectively.

The reradiated scattered pressure volume at the receiving transducer and at point B'(0,y',z') can be expressed by the following:

$$P_r(t)=\int_0\int_s^a \frac{H(t-\frac{R+x}{c})}{R+x}\cdot\frac{A_2}{r+r'}\cdot e^{-\alpha_m(R+r)}\cdot e^{-\alpha(r'+x)}$$

$$\cdot e^{-(t-t_0-\frac{R+x}{c}-\frac{r+r'}{c})^2/\tau_1}$$

$$\cdot\cos[w_0(t-t_0'-\frac{R+x}{c}-\frac{r+r'}{c})+\phi(t)]dxds \quad (3.3)$$

Suppose β is a very small angle, then the following can be defined

$$R \triangleq r \quad \text{and} \quad x \triangleq r' \quad , \quad \text{also } R >> x.$$

Since the beam cross section is constant (i.e., $S = \frac{\pi a^2}{4}$) then

$$P_r(t) = A_2 \cdot S\cdot\int_0^a \frac{H(t-\frac{R+x}{c})}{R^2}\cdot e^{-2\alpha_m R}\cdot e^{-2\alpha x}$$

$$\cdot e^{-[t-t_0-\frac{2(R+x)}{c}]^2/\tau_1}$$

$$\cdot\cos[w_0(t-t_0'-\frac{2(R+x)}{c}+\phi(t)]dx \quad (3.4)$$

Defining

$$Q = t - \frac{t_0'}{2} - \frac{R+x}{c}$$

Multiplying both sides by 2:

$$2Q = 2t - t_0' - \frac{2(R+x)}{c}$$

so

$$2Q - t = t - t_0' - \frac{2(R+x)}{c} \quad (3.5)$$

Substituting in equation (3.4)

$$P_r(t) = \frac{A_2 \cdot S}{R^2} e^{-2\alpha_m R} \int H(t - \frac{R+x}{c}) \cdot e^{-2\alpha x} \cdot e^{-[t-t_0 - \frac{2(R+x)}{c}]^2/\tau_1} \cdot \cos[w_0 \cdot (2Q-t) + \phi(t)]dx \qquad (3.6)$$

In order to calculate H(t) the relationship between the intensity, power and the pressure in acoustic medium have to be derived.

The amplitude intensity in the far field due to a radiator at range $X = R + x$ is defined as:

$$I_a = P_t G_t e^{-2\alpha_m R} e^{-2\alpha x}/4\pi(R+x)^2 \qquad (3.7)$$

where G_t is a correction factor and it is defined as gain over an isotropic radiator of the transmitting radiator and it can be expressed as

$$G_t = 4\pi A_r/\lambda^2 \qquad (3.8)$$

where A_r is the effective transducer aperture and λ is the wave length. Substituting 3.8 into 3.7:

$$I_a = P_t \cdot \frac{4\pi A_r e^{-2\alpha_m R} e^{-2\alpha x}}{\lambda^2 \cdot 4\pi (R+x)^2}$$

or

$$I_a = P_t \cdot \frac{A_r e^{-2\alpha_m R} e^{-2\alpha x}}{\lambda^2 (R+x)^2} \qquad (3.9)$$

On the other hand, from equation 3.2, one can find the

expression for the amplitude of the incident pressure wave at point $X = R + x$ as:

$$P_{ia} = \frac{H(t)}{R+x} e^{-\alpha_m R} e^{-\alpha x} e^{-(t-t_0-\frac{R+x}{c})^2/\tau_1} \qquad (3.10)$$

From the relationship between intensity and pressure, we have

$$I_a = \frac{p_{ia}^2}{2z}$$

or

$$I_a = \frac{p_{ia}^2}{2\rho c} \qquad (3.11)$$

where ρ is the density of the particles. Substituting (3.10) into (3.11) the amplitude intensity can be expressed as

$$I_a = \frac{H^2(t)\, e^{-2\alpha_m R} e^{-2\alpha x} e^{-2(t-t_0-\frac{R+x}{c})^2/\tau_1}}{2\rho c (R+x)^2} \qquad (3.12)$$

Therefore $H^2(t)$ can be expressed as

$$H^2(t) = P_t \frac{2\rho c\, A_r\, e^{2(t-t_0-\frac{R+x}{c})^2/\tau_1}}{\lambda^2} \qquad (3.13)$$

At the receiving transducer $t = t - \frac{R+x}{c}$, so

$$H^2(t-\frac{R+x}{c}) = P_t \cdot \frac{2\rho c\, A_r\, e^{2[t-t_0-\frac{2(R+x)}{c}]^2/\tau_1}}{\lambda^2} \qquad (3.14)$$

In order to have complete value of $H^2(t)$, the average transmitted power (P_t) must be calculated. Rewriting the transmitted pulse from equation 3.1,

$$y(t) = A\, e^{-(t-t_0)^2/\tau_1} \cos w_0(t-t_0') \qquad (3.1)$$

and average power transmitted is

$$P_t = \frac{kA^2}{2}\Big[\underbrace{\int_{-\infty}^{\infty} e^{-2(t-t_0)^2/\tau_1} \cos 2w_0(t-t_0')dt}_{A} + \underbrace{\int_{-\infty}^{\infty} e^{-2(t-t_0)^2/\tau_1}\, dt}_{B}\Big] \qquad (3.15)$$

To calculate P_t, A and B in equation 3.15 the following has to be calculated

$$\underline{A} = \int_{-\infty}^{\infty} e^{-2(t-t_0)^2/\tau_1} \cos 2\, w_0(t-t_0')\, dt \qquad (3.16)$$

Defining

$u = t-t_0$

$du = dt$

$d = t_0-t_0'$

$m = 2w_0$

$a^2 = \frac{2}{\tau_1} \qquad (a > 0)$

And substituting the above values into 3.16

$$\underline{A} = \int_{-\infty}^{+\infty} e^{-a^2u^2} \cos m(u+d)\,du =$$

$$\int_{-\infty}^{+\infty} e^{-a^2u^2} (\cos md \cos mu - \sin md \sin mu)\,du$$

or

$$\underline{A} = \cos md \int_{-\infty}^{\infty} \frac{e^{-a^2u^2} \cos mu\,du}{A_1^2} - \sin md \int_{-\infty}^{\infty} \frac{e^{-a^2u^2} \sin mu\,du}{A_2^2} \tag{3.17}$$

Calculating A_1^2 and A_2^2 in equation 3.17:

$$A_1^2 = \cos md \cdot 2 \cdot \int_{-\infty}^{\infty} e^{-a^2u^2} \cos mu\,du$$

or

$$A_1^2 = \sqrt{\frac{\pi\tau_1}{2}}\, e^{-w_0^2 \tau_1/2} \cos 2w_0(t-t_0') = ct \tag{3.18}$$

and

$$A_2^2 = \sin md \int_{-\infty}^{\infty} e^{-a^2u^2} \sin mu\,du = 0 \tag{3.19}$$

Substituting 3.18 and 3.19 into 3.17

$$\underline{A} = A_1^2 \tag{3.20}$$

Now, the second part of equation 3.15 (B) must be calculated.

$$\underline{B} = \int_{-\infty}^{\infty} e^{-2(t-t_0)^2/\tau_1}\,dt$$

Defining

$$u = t - t_0 \quad , \quad t = \pm\infty \text{ then } u = \pm\infty$$

$$du = dt$$

$$r^2 = \frac{2}{\tau_1} \quad \text{or} \quad r = \sqrt{\frac{2}{\tau_1}}$$

then

$$\underline{B} = \int_{-\infty}^{\infty} e^{-r^2u^2} du = 2\int_{0}^{\infty} e^{-r^2u^2} du = 2\cdot\sqrt{\frac{\pi}{2r}} = \sqrt{\frac{\pi\tau_1}{2}} = B_1^2 \quad (3.21)$$

Substituting 3.20 and 3.21 into 3.15

$$P_t = \frac{k}{2} A^2(A_1^2 + B_1^2) = c_k^2 \quad (3.22)$$

Substituting equation 3.22 into equation 3.14

$$H^2\left(t - \frac{R+x}{c}\right) = \frac{2c_k^2\ \rho c A_r}{\lambda^2} \cdot \frac{1}{e^{-2\left[t-t_0-\frac{2(R+x)}{c}\right]^2/\tau_1}} \quad (3.23)$$

Defining

$$k_1^2(\tau_1) = \frac{2c_k^2\ \rho c\ A_r}{\lambda^2}$$

and substituting into equation 3.23,

$$H^2\left(t - \frac{R+x}{c}\right) = -\frac{k_1^2(\tau_1)}{e^{-2\left[t-t_0-\frac{2(R+x)}{c}\right]^2/\tau_1}} \quad (3.24)$$

Substituting 3.24 into 3.4, the reradiated scattered pressure volume can be expressed as

$$P_r(t) = \frac{A_2 k_1(\tau_1) S\, e^{-2\alpha m R}}{R^2} \int e^{-2\alpha x} \cdot \cos[w_0(2Q-t) + \phi(t)]\, dx \qquad (3.25)$$

The pressure signal after k^{th} burst can be obtained by letting $t = kT + t_0$ where T is the period of the transmitted pulses and t_e is the time elapsed between transmitted and scattered burst (see Figure 3.3). So

$$Q = t - \frac{R}{c} - \frac{x}{c} - \frac{t_0'}{2}$$

Substituting for t

$$Q_e = kT + t_e - \frac{R}{c} - \frac{x}{c} - \frac{t_0'}{2}$$

or

$$2Q_e - t = kT + t_e - \frac{2R}{c} - t_0' - \frac{2x}{c}$$

Defining

$$t_k = kT + t_e - \frac{2R}{c} - t_0'$$

then

$$2Q_e - t = t_k - \frac{2x}{c} \qquad (3.26)$$

Substituting equation 3.26 into 3.25

$$P_k(t_e) = \frac{k_1(\tau_1) A_2\, e^{-2\alpha_m R} \cdot s}{R^2} \int_x \cos[(2Q_e - t)w_0 + \phi(t)] e^{-2\alpha x} dx$$

or

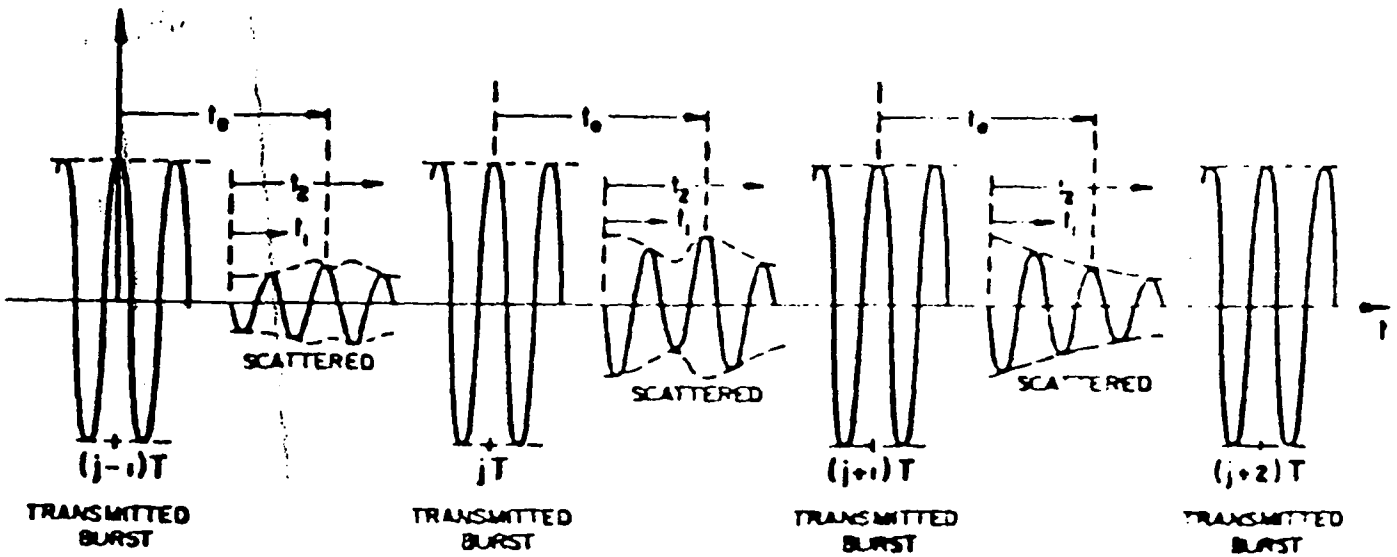

Figure 3.3 Illustration of the ensemble $P_k(t_e)$.

$$P_k(t_e) = \frac{k_1(\tau_1)A_2 e^{-2\alpha_m R} S}{R^2} \Big[\cos w_0 t_k \underbrace{\int \cos[-\frac{2w_0 x}{c} + \phi(t)]e^{-2\alpha x}dx}_{1} - \sin w_0 t_k \underbrace{\int \sin[-\frac{2w_0 x}{c} + \phi(t)]e^{-2\alpha x}dx}_{2}\Big]$$

(3.27)

Defining

$$a = -2\alpha$$

$$b = -\frac{2w_0}{c_1}$$

$$\phi(t) = c$$

And calculating each part of equation 3.27 separately

$$\underline{1} = \int e^{ax} \cos(bx + c)dx$$

$$\underline{1} = \int e^{ax} \cos bx \cos c\, dx - \int e^{ax} \sin bx \sin c\, dx$$

$$\underline{1} = [\frac{e^{ax}}{a^2+b^2}] a \cos(bx+c) + b \sin(bx+c)]$$

and

$$\underline{W} = \frac{e^{ax}}{a^2+b^2} [a \cos w_0 t_k \cos(bx+c) + b \cos w_0 t_k \sin(bx+c)]$$

(3.28)

Now, calculating the second part of equation 3.27,

$$\underline{2} = \int e^{ax} \sin(bx+c)dx$$

$$\underline{2} = \cos c \int e^{ax} \sin bx + \sin c \int e^{ax} \cos bx \, dx$$

$$\underline{2} = \frac{e^{ax}}{a^2 + b^2} [a \sin(bx+c) - b \cos(bx+c)]$$

and

$$\underline{Z} = \frac{e^{ax}}{a^2 + b^2} [a \sin w_0 t_k \sin(bx+c) - b \sin w_0 t_k \cos(bx+c)] \tag{3.29}$$

Substituting 3.28 and 3.29 into 3.27

$$P_k(t_e) = \frac{A_2 \cdot k_1(\tau_1) \cdot S \cdot c^2 \cdot e^{-2\alpha_m R} \cdot e^{-2\alpha x}}{4R^2(\alpha^2 c^2 + w_0^2)}$$

$$\left[-2\alpha \cos[w_0 t_k - \frac{2w_0 x}{c} + \phi(t)]\right.$$

$$\left. - \frac{2w_0}{c} \sin[w_0 t_k - \frac{2w_0 x}{c} + \phi(t)]\right] \tag{3.30}$$

Pressure signal $P_k(t_e)$ is converted to electrical signal $f_r(t_e)$ by passing through the receiver transducer. The received signal can be expressed as:

$$f_r(t_e) = k_2(A) \; P_k(t_e) \tag{3.31}$$

where $k_2(A)$ is a constant depends on the cross-sectional area of the transducer and varies with such a factor as

transducer material and method of processing.

The Doppler signal can be extracted by demodulating the received signal and passing the result through a low-pass filter to eliminate the components of the carrier (transmitted) signal, according to Figure 1.4. The conventional coherent demodulation technique is used to achieve the above goal. First, we multiply the received signal by transmitted signal considering the time delay as follows,

$$D_r(t_e) = f_r(t_e) \cdot y(t_e)$$

where $t_e = t - t_0 - \frac{2(R+x)}{c}$

$$y(t_e) = A\, e^{-[t-t_0 - \frac{2(R+x)}{c}]^2/\tau_1} \cos w_0[t-t_0' - \frac{2(R+x)}{c}]$$

so

$$D_r(t_e) = k\,\{-2\alpha\cos[w_0(t-t_0'-\frac{2(R+x)}{c} + \phi(t)] - \frac{2w_0}{c}$$

$$\cdot \sin[w_0(t-t_0' - \frac{2(R+x)}{c} + \phi(t)]\, Ae^{-[t-t_0-\frac{2(R+x)}{c}]^2/\tau_1}$$

$$\cdot \cos w_0[t-t_0' - \frac{2(R+x)}{c}]\}$$

where

$$k = \frac{A_2 k_1(\tau_1) k_2(A) S\, c^2 e^{-2\alpha_m R}\, e^{-2\alpha x_A}}{4R^2(\alpha^2 c^2 + w_0^2)}$$

Defining

$$a = -2\alpha$$

$$b = -\frac{2w_0}{c}$$

Equation 3.32 can be written as

$$D_r(t_e) = k\{a\cos[w_0t - w_0t_0' + bR + bx + \phi(t)]e^{-[t-t_0-\frac{2(R+x)}{c}]^2/\tau_1}$$

$$\cdot\cos(w_0t - w_0t_0' + bR + bx) + b\sin[w_0t - w_0t_0' + bR + bx + \phi(t)]$$

$$\cdot e^{-[t-t_0-\frac{2(R+x)}{c}]^2/\tau_1}\cos(w_0t - w_0t_0' + bR + bx)\} \quad (3.32)$$

The demodulated signal after passing through a low-pass filter with cut-off frequency of f_0 (i.e., $f_0 = \frac{w_o}{2\pi}$) can be expressed as

$$f_d(t_e) = \frac{1}{2}k\,e^{-[t-t_0-\frac{2(R+x)}{c}]^2/\tau_1}[a\cos\phi(t) + b\sin\phi(t)]$$

or

$$f_d(t_e) = \frac{1}{2}k\,e^{-[t-t_0-\frac{2(R+x)}{c}]^2/\tau_1}\{r\cos[\phi(t) - \phi_1]\}$$

where

$$r = \sqrt{a^2+b^2} = \sqrt{4\alpha^2 + \frac{4w_0^2}{c^2}} = \frac{2}{c}\sqrt{c^2\alpha^2 + w_0^2}$$

and

$$\phi_1 = \tan^{-1}\frac{b}{a} = \tan^{-1}\frac{\frac{-2w_0}{c}}{-2\alpha} = \tan^{-1}\frac{w_0}{c\alpha}$$

so

$$f_d(t_e) = \frac{k}{2}\cdot\frac{2}{c}\sqrt{c^2\alpha^2+w_0^2}\,e^{-[t-t_0-\frac{2(R+x)}{c}]^2/\tau_1}\cdot\cos[\phi(t) - \tan^{-1}\frac{w_0}{c\alpha}]$$

or finally, the instantaneous Doppler signal can be expressed as

$$f_d(t_e) = \frac{k\sqrt{c^2\alpha^2+w_0^2}}{c} e^{-[t-t_0-\frac{2(R+x)}{c}]^2/\tau_1} \cdot \cos[\phi(t)-\tan^{-1}\frac{w_0}{c\alpha}] \qquad (3.33)$$

Equation 3.33 is a comprehensive form of the Doppler signal, and as can be seen, it is a function of acoustics, tissue, and system parameters such as: attenuation factors in different mediums, wave length of the transmitted burst, effective transducer aperture, density of the blood, etc.

The main assumptions in deriving the Doppler signal in this section are:

1- the red cells are uniformly distributed in the blood stream,

2- the red cells behave like point scatterers (i.e., $\lambda >> D$)

3- the sound beam illuminates the entire cross-section of the vessel, with uniform intensity, and the sensitivity of the receiver is also uniform over the whole vessel cross-section, and

4- the frequency shift is only caused by red cells.

3.2 Transducer Modeling

The application of continuous wave or pulsed Doppler ultrasonics to the measurement of flowing liquids or ultrasonic imaging has been widespread. Doppler principles utilized for the specific measurements of flowing blood in

clinical or research application have been known and used for approximately twenty years. The most desirable aspect for improvement in blood flowmeters is accuracy of the velocity measurement.

The velocities of the blood cells (mainly red cells) in the bloodstream are given by the basic Doppler formula, as it was shown in equation (1.2):

$$\Delta f = 2 \cdot f_0 \cdot v_R \cdot \cos\theta / c \qquad (1.2)$$

Frequency shift (Δf) in the above equation is related to the Doppler output signal by the mean of frequency to voltage convertor described in Chapter II. In order to calculate velocity from equation (1.2), the Doppler angle, θ, has to be precisely known.

Commercially available Doppler blood flowmeters (both inplantable and externally applied) are based upon the performance of a single transducer or multiple transducers without any specific orientation to each other in an attempt to extract greater information from which the researcher can make better estimation of the Doppler angle. This prediction of the Doppler angle has a direct relationship on the calculation of blood flow characteristics. The accuracy of measuring the Doppler angle may be changed by multiple trials, but, since it is still an assumption, one cannot be certain about its percentage of accuracy. Relative error in

velocity is a function of the Doppler angle alone, and the error increases when the Doppler angle increases. Thus, we have developed a hardware and software Doppler model to more accurately determine blood flow velocity, which eliminates the assumption of the Doppler angle.

The developed model (Dual Transducer Pulsed Doppler Ultrasound - DTP-DU) has the ability to actually calculate the true Doppler angle. Therefore, it increases the accuracy in measuring the blood flow velocity, which is the primary factor in determining the blood flow volume rate and any related characteristics. In this section, is presented theoretical investigation of the developed model and also error analysis is presented for both the conventional and developed model.

3.2.1 Theoretical Investigation

In a conventional single transducer pulsed-Doppler ultrasound (STP-DU), the relationship between the received Doppler signal and the directional velocity of the blood flow can be obtained by the expression shown in the following equation:

$$\hat{v}_R = k \cdot F_1 \cos\theta \tag{3.34}$$

Equation (3.34) is another version of the Doppler equation (1.2), except for the fact that Δf is converted into F_1. Because of this change, the constant k not only

depends upon the constant parameters mentioned in equation (1.2), but also on the fluid dynamic parameters such as the resistivity factor (i.e., $R = \frac{\Delta p}{Q}$) of the blood and the area and length in which the test is conducted. Another factor is related to the method of processing, which depends upon the type of device used for converting acoustical signal to electrical signal. As can be seen from equation (3.34), there is one equation and two unknowns, θ and v_R. The only solution for this function is still a careful assumption of the angle θ.

To overcome this "assumption" problem, we have developed the DTP-DU model, in which there is a known angle between two transducers. A typical configuration for a dual transducer system is shown in Figure 3.4. To implement the developed model, a pulsed-Doppler instrument with at least two channels is required. Using both channels and this model equation (3.34) can be written in the following forms:

$$\hat{v}_R = k \cdot F_1/\cos\theta \tag{3.35}$$

$$\hat{v}_R = k \cdot F_2/\cos(\alpha-\theta) \tag{3.36}$$

where F_1 and F_2 are Doppler output signals from channel 1 and channel 2, respectively.

Note that there are three unknowns: $\hat{v}_R$, α and θ and two measurable quantities f_1 and f_2 in equations (3.35) and (3.36). The angle between the transducer, α, is fixed at

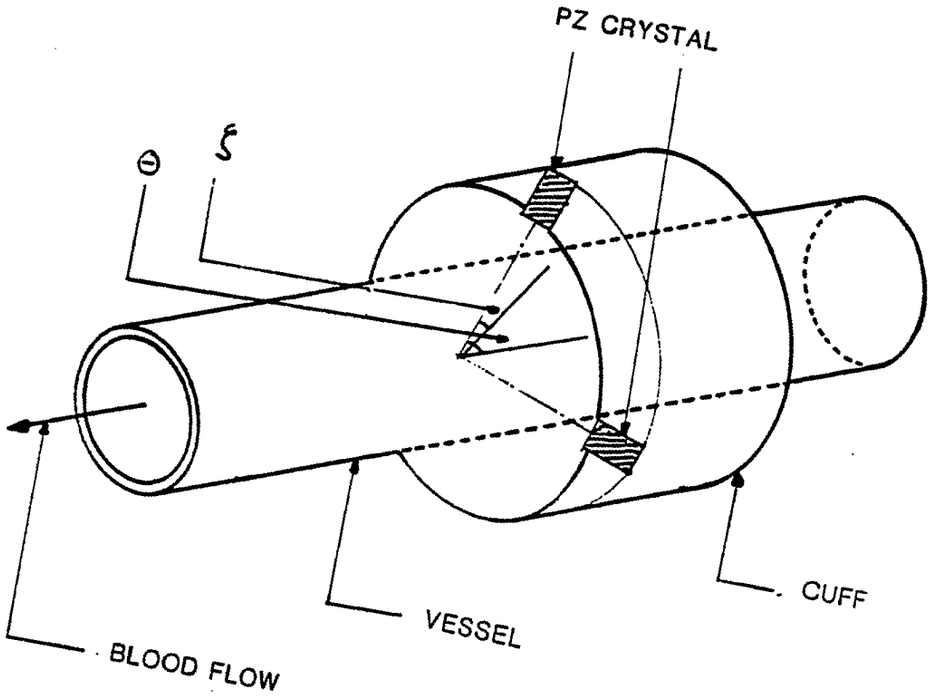

Figure 3.4 A typical configuration for a dual transducer model.

the time when the probe is built for flow measurements. If α is known by the process of manufacturing or by calibration, then there are two equations and two unknowns. This indicates that both $\hat{v}_R$ and θ can be calculated directly. Starting with equation (3.37) and (3.38), we can derive the following:

$$F_1 = \frac{\hat{v}_R}{k} \cos\theta \tag{3.37}$$

$$F_2 = \frac{\hat{v}_R}{k} \cos(\alpha-\theta) = \frac{v}{k} (\cos\alpha \cos\theta + \sin\alpha \sin\theta) \tag{3.38}$$

so

$$\begin{cases} \cos\theta = k \dfrac{F_1}{v_R} \\ \sin\theta = \sqrt{1-k^2 \dfrac{F_1^2}{v_R^2}} \\ \sin\theta \cos\theta = k \dfrac{F_1}{v_R} \sqrt{1 - k^2 \dfrac{F_1^2}{v_R^2}} \end{cases}$$

Squaring equations (3.37) and (3.38) and substituting for $\cos\theta$, $\sin\theta$, and $\sin\theta \cos\theta$ we have

$$F_1^2 = \frac{\hat{v}_R^2}{k^2} \cos^2\theta$$

$$F_2^2 = \frac{\hat{v}_R^2}{k^2} (\cos^2\alpha\cos^2\theta + \sin^2\alpha\sin^2\theta + \sin2\alpha \sin\theta \cos\theta)$$

so

$$F_1^2 + F_2^2 = \frac{\hat{v}_R^2}{k^2} (\cos^2\theta + \cos^2\alpha\cos^2\theta + \sin^2\alpha\sin^2\theta + \sin2\alpha\sin\theta\cos\theta)$$

$$\hat{v}_R^2 = \frac{k^2(F_1^2 + F_2^2)}{\frac{k^2F_1^2}{\hat{v}_R^2} + \frac{k^2F_1^2}{\hat{v}_R^2}\cos^2\alpha + \frac{\hat{v}_R^2 - k^2F_1^2}{\hat{v}_R^2}\sin^2\alpha + \frac{2F_1}{\hat{v}_R^2}\sqrt{k^2(v_R^2 - k^2F_1^2)}\ \sin\alpha\cos\alpha}$$

or

$$k^2(F_1^2+F_2^2) = k^2F_1^2+k^2F_1^2\cos^2\alpha+\hat{v}_R^2\sin^2\alpha-k^2F_1^2\sin^2\alpha+2F_1\sqrt{k^2(v_R^2-k^2F_1} \cdot \sin\alpha\ \cos\alpha$$

or

$$v_R^2\sin^2\alpha = -k^2F_1^2\cos^2\alpha+k^2F_2^2+k^2F_1^2\sin^2\alpha-2F_1\sqrt{k^2(v^2-k^2F_1^2)}\sin\alpha\cos\alpha \qquad (3.39)$$

But

$$\cos\alpha\ \cos\theta + \sin\alpha\ \sin\theta = \frac{k\ F_2}{v_R}$$

or

$$\cos\alpha\ \frac{kF_1}{v_R} + \sin\alpha\ \ \frac{\sqrt{v_R^2-k^2F_1^{\ 2}}}{v_R} = k\ \frac{F_2}{v_R}$$

and

$$\sqrt{\hat{v}_R^2\ -\ k^2F_1^2} = \frac{kF_2\ -\ kF_1\ \cos\alpha}{\sin\alpha} \qquad (3.40)$$

Substituting equation (3.40) into equation (3.39)

$$\hat{v}_R^2\sin^2\alpha = -k^2F_1^2\cos^2\alpha+k^2F_2^2 + k^2F_1^2\ \sin^2\alpha\ -2kF_1\cos\alpha(kF_2-kF_1\cos^2\alpha)$$

or

$$\hat{v}_R^2\ \sin^2\alpha = k^2F_2^2(1-2\cos\alpha)\ -\ k^2F_1^2\ \cos2\alpha$$

and velocity can be found by the following equation:

$$\hat{v}_R = \sqrt{\frac{k^2F_2^2(1-2\cos\alpha) - k^2F_1^2\cos 2\alpha}{\sin^2\alpha}} \qquad (3.41)$$

Equating equations (3.37) and (3.38)

$$\frac{kF_1}{\cos\theta} = \frac{kF_2}{\cos\alpha\cos\theta + \sin\alpha\sin\theta}$$

Dividing by $\cos\theta$

$$kF_1\cos\alpha + kF_1 \operatorname{tg}\theta \sin\alpha = kF_2$$

or

$$\theta = \operatorname{tg}^{-1}\left(\frac{F_2 - F_1\cos\alpha}{F_1\sin\alpha}\right) \qquad (3.42)$$

Notice that the Doppler angle (θ) can be directly calculated from F_1 and F_2, and, notice that the blood velocity ($\hat{v}_R$) can also be calculated from F_1 and F_2 without explicit measurement or calculation of the Doppler angle. As long as α is known accurately, the flow can be in any direction and the equation (3.41) can be used to determine $\hat{v}_R$ accurately. This is the primary advantage of dual transducer over a single transducer system.

Comparing equation (3.42) and equation (3.36), it seems that additional computations are required to find $\hat{v}_R$. But, since α is either known or is calibrated, $\cos\alpha$ and $\sin\alpha$ are fixed. Thus, equation (3.42) becomes a simple function of two variables, F_1 and F_2.

3.2.2 Theoretical Comparison of Doppler Models

3.2.2.1 One Dimensional Analysis

The Doppler shifted frequency can be measured, but the angle is estimated either by prior calibration or by assumption. In most cases, the angle is assumed to be 45°. Let θ be the assumed angle, then equation (3.34) immediately relates the measured Doppler shifted frequency to the flow velocity:

$$\hat{v}_R = \left(\frac{k}{\cos\theta}\right)\cdot F_1$$

Note that the estimated velocity is $\hat{v}_R$ and differs from the true flow velocity, v_R. The actual velocity (v_R) will be described by the following equation

$$v_R = k\cdot F_1/\cos(\theta + \xi) \tag{3.43}$$

The ratio of measured ($\hat{v}_R$) to calculated (v_R) velocity is then

$$\frac{\hat{v}_R}{v_R} = \frac{\cos(\theta + \xi)}{\cos(\theta)} \tag{3.44}$$

and the normalized velocity error (E_1) can be shown in the following equation

$$E_1 = 1 - \frac{\hat{v}_R}{v_R} = \frac{\cos\theta - \cos(\theta + \xi)}{\cos\theta} \tag{3.45}$$

The error presented in equation (3.43) is in terms of ξ, the discrepancy between the actual and assumed Doppler angle.

The ratio of changes in the velocity measurement can therefore be expressed by the following equation:

$$\frac{d}{d\xi}\left(\frac{\hat{v}_R}{v_R}\right) = \frac{-\sin(\theta + \xi)}{\cos\theta} \tag{3.46}$$

The percentage of normalized velocity error is calculated from equation (3.45). Results are obtained by using different values of the Doppler angle (in this case 0° to 75°). A plot is generated for percentage of normalized error when the uncertainty in the Doppler angle (ξ) is varied from -45° to 45° and is shown in Figure 3.5. Also, the rate of change in velocity is calculated from equation (3.46). A plot is generated for discrepancy between actual and measured flow when the uncertainty in the Doppler angle (ξ) is varied from -45° to 45° and for different Doppler angles, in this case, 30°, 45° and 60° (shown in Figure 3.6).

3.2.2.2 Two Dimensional Analysis

It has been seen that the velocity estimation in the single transducer case in equation (3.34) largely depends on how well the flow direction aligns with the assumed flow direction. In many applications, the probe cannot be changed, adjusted, or tuned instantaneously, which results in large errors as shown in Figure 3.5. For the dual transducer, however, no requirements are placed on the flow direction. In fact, the use of two transducers makes possible the measurement of the flow direction directly, hence

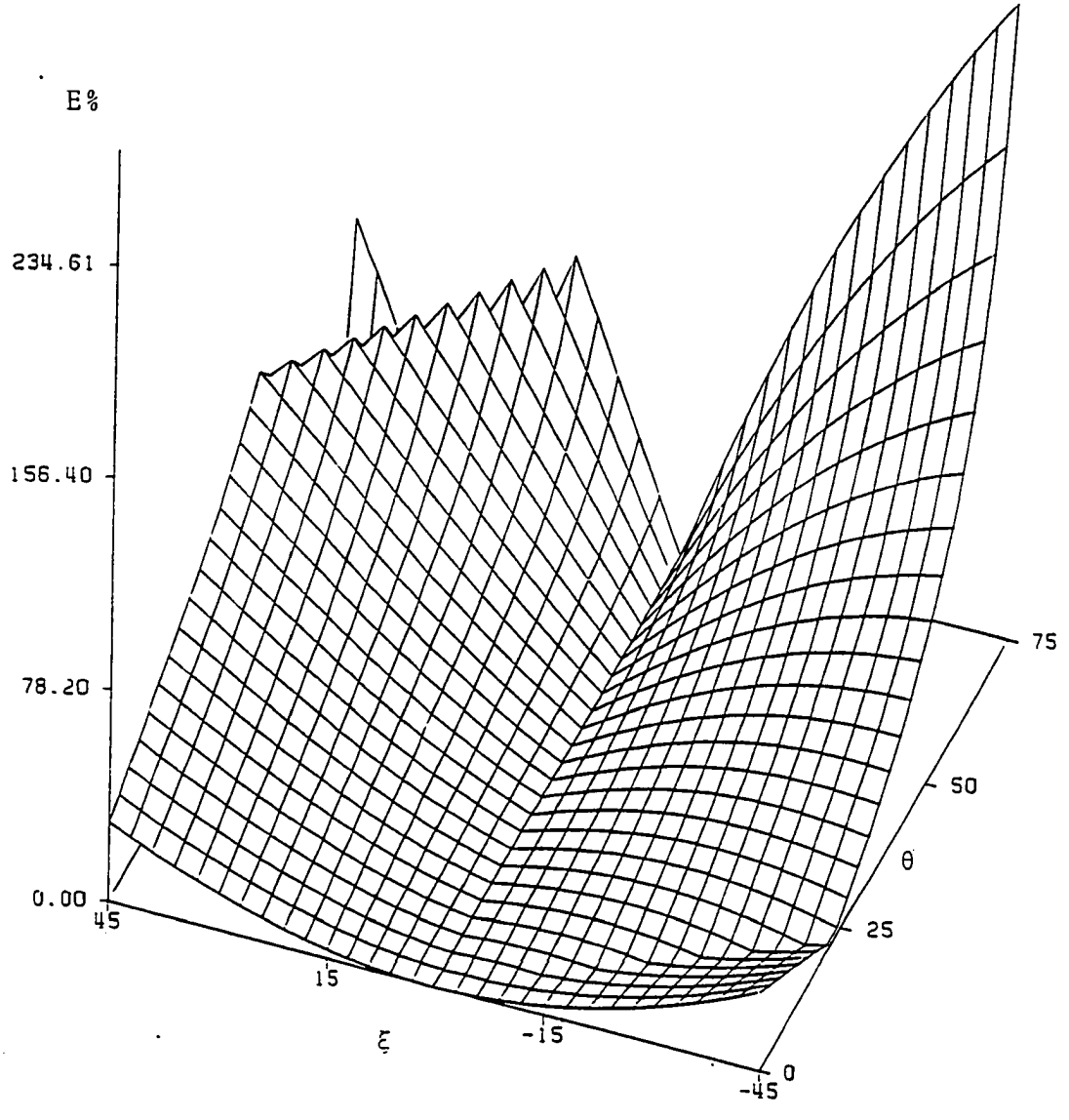

Figure 3.5 The percentage of normalized velocity error for single transducer pulsed Doppler ultrasound model.

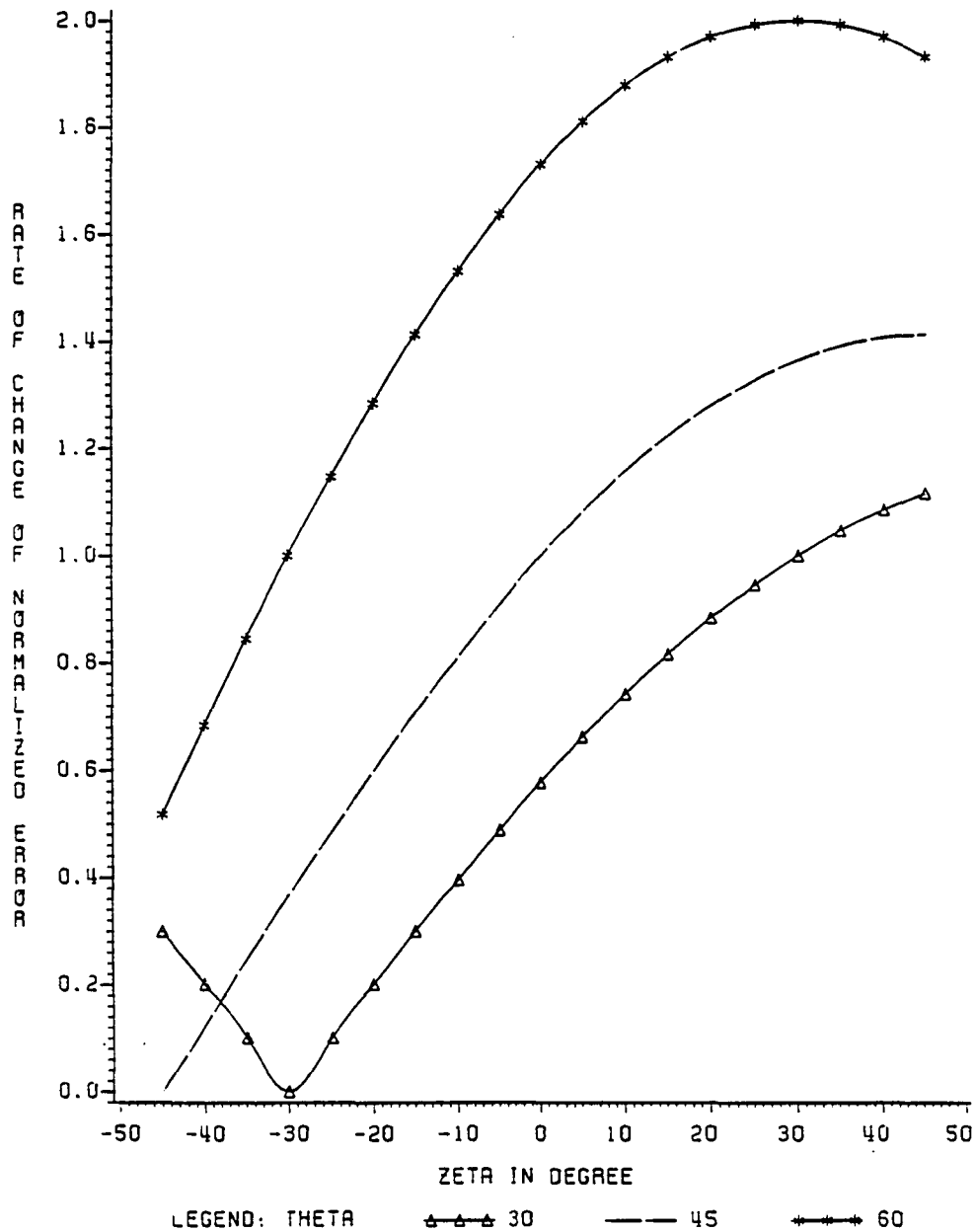

Figure 3.6 Discrepancy between actual and measured flow for single transducer pulsed Doppler ultrasound model.

providing accurate estimation of the flow velocity.

Though the velocity estimation is exact, errors may be introduced through inaccurate calibration of α. Such errors are correctible and can be made as accurate as the calibration process allows. If there is an error made in calibrating α, then the velocity estimate $\hat{v}_R$ will be as follows:

$$\hat{v}_R = \sqrt{\frac{k^2 F_2(1-2\cos\alpha) - k^2 F_1^2 \cos\alpha}{\sin^2\alpha}} \tag{3.47}$$

where $\hat{v}_R$ is the velocity estimated based on α. When α is in error, there are two places where calibration affects the velocity estimation. First, the correction factor on F_1 and F_2 in the numerator under the radical sign is modified. Secondly, the scaling in the denominator is not exact. The normalized velocity error (E_2) for the two dimensional case can now be found by rearranging the terms as follows:

The actual Doppler signals can be written as

$$F_1 = \frac{v_R}{k} \cos\theta \tag{3.48}$$

$$F_2 = \frac{v_R}{k} \cos(\alpha - \theta - \xi) \tag{3.49}$$

where v_R is the actual value of the velocity and ξ is the difference between assumed and actual value of α. Substituting equations (3.48) and (3.49) into (3.47) one obtains,

$$\hat{v}_R = \frac{k}{\sin\alpha} \cdot \frac{v_R}{k} \sqrt{\cos^2(\alpha-\theta-\xi)(1-2\cos\alpha)-\cos^2\theta\cos2\alpha}$$

or

$$\frac{\hat{v}_R}{v_R} = \frac{\sqrt{[\cos^2(\alpha-\theta-\xi)](1-2\cos\alpha)-\cos^2\theta\cos2\alpha}}{\sin\alpha} \qquad (3.50)$$

Since the normalized velocity error is

$$E_2 = \frac{v_R - \hat{v}_R}{v_R}$$

So

$$E_2 = 1 - \sqrt{\frac{[\cos^2(\alpha-\theta-\xi)](1-2\cos\alpha)-\cos^2\theta\cos2\alpha}{\sin^2\alpha}} \qquad (3.51)$$

The error E_2 shown in equation (3.51) is applicable for any value of α. It will be illustrated how the dual transducer model performs in:

A Special Case

One obvious configuration is to make the two transducers orthogonal to one another. If this is the case, the velocity estimation can be greatly simplified. Equation (3.41) can be rewritten as follows:

$$v_R = k\sqrt{F_1^2 + F_2^2} \qquad (3.52)$$

Equation (3.52) indicates that the velocity estimation is simply the vector sum of F_1 and F_2. This is reasonable because F_1 and F_2 are orthogonal to one another. Hence, the velocity estimation is simply computed by the Euclidean

distance formula.

The normalized velocity error for this orthogonal arrangement is also neatly simplified and can be computed by substituting $\alpha = 90°$ into equation (3.51), then obtaining the following:

$$E_2\Big|_{\alpha=90°} = 1 - \sqrt{\cos^2\theta + \sin^2(\theta+\xi)} \qquad (3.53)$$

A plot is generated for percentage of normalized error for a different value of θ, in this case from $0°$ to $360°$, while ξ varies between $-45°$ and $45°$ and is shown in Figure 3.7. Also, in Figure 3.8, a plot for fixed values of ξ while θ varies from $-180°$ to $180°$ is presented.

The rate of change for the normalized velocity error can be computed directly by differentiating equation 3.50:

$$\frac{\hat{v}_R}{v_R}\Bigg|_{\alpha=90°} = \sqrt{\cos^2\theta + \sin^2(\theta+\xi)}$$

but

$$\frac{d}{d\xi}\left(\sqrt{u}\right) = \frac{1}{2\sqrt{u}}\ \frac{du}{d\xi}$$

so

$$\frac{d}{d\xi}\left(\frac{\hat{v}_R}{v_R}\right) = \frac{\cos(\theta+\xi)\ \sin(\theta+\xi)}{\sqrt{\cos^2\theta+\sin^2(\theta+\xi)}} \qquad (3.54)$$

A plot is generated for discrepancy between actual and measured flow when θ varies between $0°$ to $360°$ and ξ between

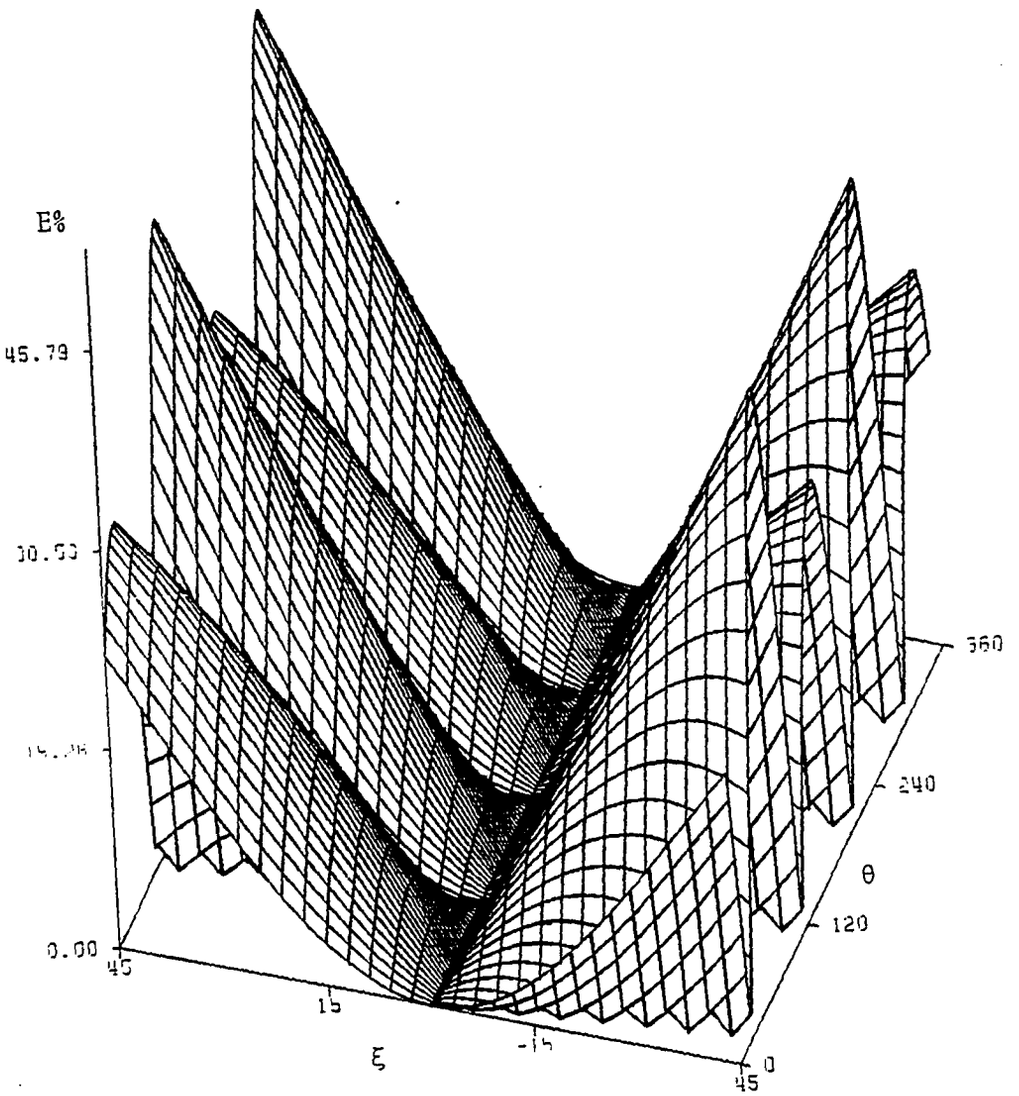

Figure 3.7 The percentage of normalized velocity error for dual transducer pulsed Doppler ultrasound model.

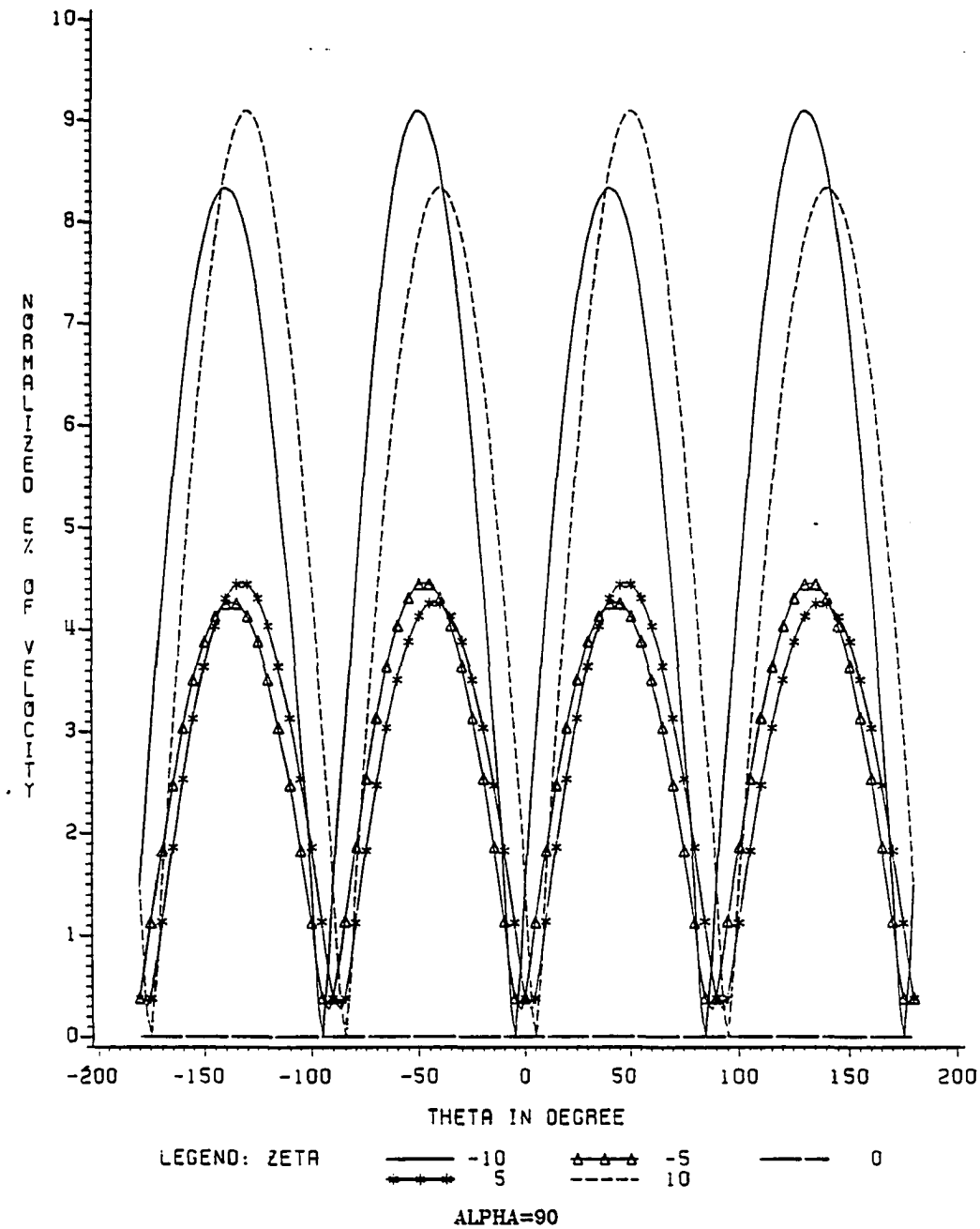

Figure 3.8 The percentage of normalized velocity error for dual transducer pulsed Doppler ultrasound model for fixed values of ξ.

-45° and 45°, and is shown in Figure (3.9). Also, in Figure (3.10) a plot is presented for fixed values of θ in this case 30°, 45°, and 60°, when ξ varies between -45° and 45°.

Although the error in the dual model is controllable by careful calibration of the angle between the 2 tranducers, the error in the single model which is caused by assumption, is not controllable. A comparison between the two models indicates dramatic improvement in the calculation of blood flow velocity by the dual model over the single transducer. As an example for $\theta = 45°$, $\alpha = 90°$, a false estimation of θ by 5° causes 9 percent and 4.25 percent changes in velocity estimation for STP-DU and DTP-DU models, respectively. For a false estimation of θ by 10°, these values are 18.08 percent for the STP-DU model and 8.213 percent for the DTP-DU model. Also, a false estimation of 5° causes the rate of change in velocity to be 1.083 for the STP-DU model and 0.49 for the DTP-DU model. For a 10° error in estimation, the rate of change is 1.158 for the STP-DU and 0.43 for the DTP-DU model, respectively. Some numerical values for error in velocity and rate of change in velocity for $\alpha = 90°$ and $\theta = 45°$ are shown in Table 3.1. Also, in Figures 3.11, 3.12, 3.13 and 3.14, plots are presented for both models for normalized error and rate of change in velocity and for $\theta = 45°$ and $\theta = 55°$ and $\alpha = 90°$. Figures 3.15 and 3.16

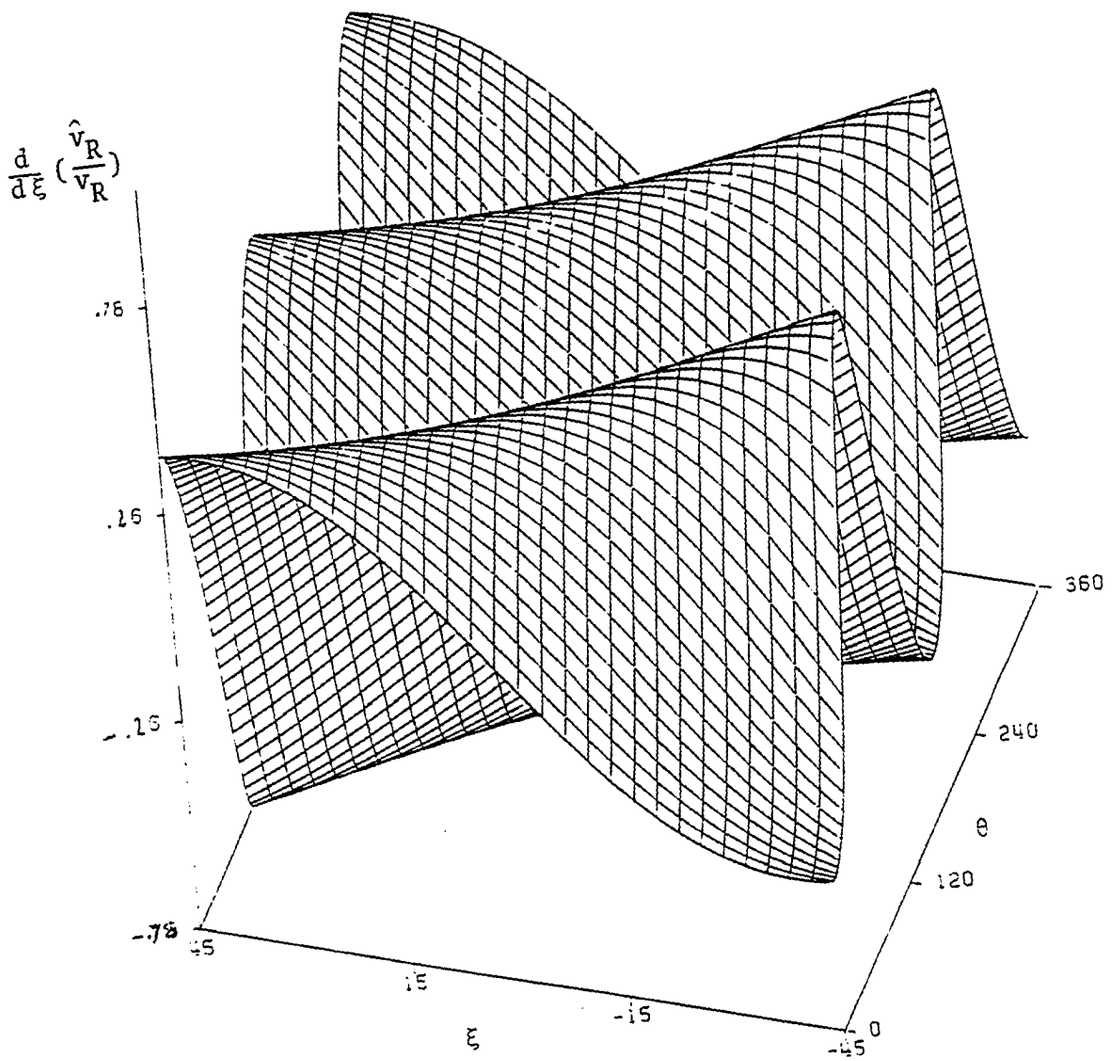

Figure 3.9 Discrepancy between actual and measured flow for dual transducer pulsed-Doppler ultrasound model.

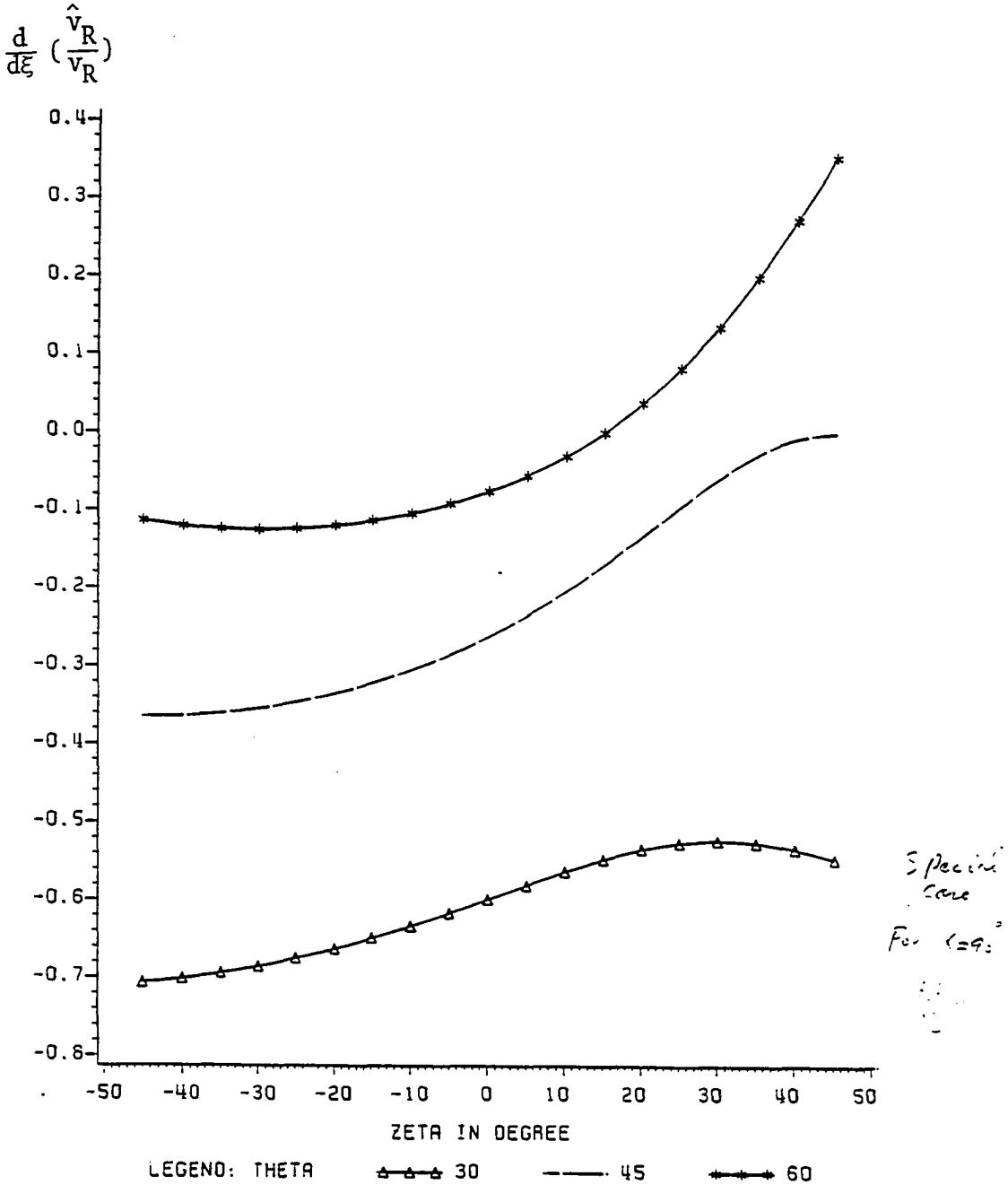

Figure 3.10 Discrepancy between actual and measured flow for dual transducer pulsed-Doppler ultrasound model for fixed values of θ.

Table 3.1 Numerical Values for Normalized Percentage of Error and Rate of Change in the Velocity for both STP-DU and DTP-DU Models.

STP-DU

Doppler Angle (θ)	% of Normalized Velocity Error	Rate of Change in the Velocity
-45	41.4194031	0.000000000E+00
-44	41.3979492	0.246806256E-01
-43	41.3332825	0.493538156E-01
-42	41.2256165	0.740118623E-01
-41	41.0749359	0.986474752E-01
-40	40.8813477	0.123252928
-39	40.6447296	0.147820950
-38	40.3654022	0.172344029
-37	40.0432587	0.196814597
-36	39.6783752	0.221224964
-35	39.2710571	0.245568216
-34	38.8212128	0.269836545
-33	38.3292084	0.294022739
-32	37.7949677	0.318119287
-31	37.2188568	0.342118979
-30	36.6008759	0.366014481
-29	35.9413147	0.389798522
-28	35.2402649	0.413463712
-27	34.4981079	0.437003076
-26	33.7149506	0.460409284
-25	32.8910828	0.483675301
-24	32.0267639	0.506793916
-23	31.1222076	0.529758155
-22	30.1776886	0.552561104
-21	29.1934967	0.575195730
-20	28.1700134	0.597655058
-19	27.1074219	0.619932532
-18	26.0061188	0.642021060
-17	24.8664856	0.663914025
-16	23.6887817	0.685604632
-15	22.4734192	0.707086563
-14	21.2207794	0.728353083
-13	19.9312134	0.749397874
-12	18.6050415	0.770214140
-11	17.2428131	0.790795982
-10	15.8448219	0.811136961
-9	14.4116402	0.831230760
-8	12.9435539	0.851071417
-7	11.4410400	0.870652795
-6	9.90457535	0.889969051
-5	8.33463669	0.909014225

Cont'd to next page

Table 3.1 (cont'd)

STP-DU

Doppler Angle (ξ)	% of Normalized Velocity Error	Rate of Change in the Velocity
-4	6.73170090	0.927782476
-3	5.09634018	0.946268082
-2	3.42884064	0.964465559
-1	1.72986984	0.982369184
0	0.000000000E+00	0.999973595
1	1.76038742	1.01727295
2	3.55070782	1.03426266
3	5.37040806	1.05093765
4	7.21892071	1.06729317
5	9.09570980	1.08332253
6	11.0001917	1.09902191
7	12.9317579	1.11438751
8	14.8898773	1.12941265
9	16.8738861	1.14409447
10	18.8832397	1.15842724
11	20.9172821	1.17240715
12	22.9754486	1.18603039
13	25.0570221	1.19929218
14	27.1613770	1.21218777
15	29.2880096	1.22471523
16	31.4361877	1.23686981
17	33.6052551	1.24864769
18	35.7945557	1.26004410
19	38.0032806	1.27105713
20	40.2310028	1.28168392
21	42.4769440	1.29191971
22	44.7404022	1.30176163
23	47.0206909	1.31120777
24	49.3170013	1.32025337
25	51.6288757	1.32889748
26	53.9554596	1.33713722
27	56.2960968	1.34496975
28	58.6500244	1.35239220
29	61.0164337	1.35940266
30	63.3948517	1.36599922
31	65.7844086	1.37217903
32	68.1843872	1.37794209
33	70.5940552	1.38328457
34	73.0125580	1.38820553
35	75.4394073	1.39270401
36	77.8737335	1.39677811
37	80.3146041	1.40042686
38	82.7618713	1.40364933

Cont'd to next page

Table 3.1 (cont'd)

DTP-DU

Doppler Angle (ξ)	% of Normalized Velocity Error	Rate of Change in the Velocity
-45	29.2883911	0.000000000E+00
-44	29.2668610	0.246693529E-01
-43	29.2023163	0.492637902E-01
-42	29.0949860	0.737088323E-01
-41	28.9451599	0.979318619E-01
-40	28.7533112	0.121861815
-39	28.5200043	0.145430803
-38	28.2459259	0.168574154
-37	27.9318542	0.191230595
-36	27.5787354	0.213343203
-35	27.1875153	0.234859824
-34	26.7592926	0.255732477
-33	26.2952423	0.275918484
-32	25.7966003	0.295380056
-31	25.2646332	0.314084351
-30	24.7007141	0.332003295
-29	24.1062164	0.349113703
-28	23.4825745	0.365396793
-27	22.8312531	0.380838513
-26	22.1537170	0.395428360
-25	21.4514771	0.409160137
-24	20.7260132	0.422030747
-23	19.9788361	0.434040725
-22	19.2114410	0.445193172
-21	18.4253387	0.455493867
-20	17.6219940	0.464951038
-19	16.8028564	0.473574758
-18	15.9694071	0.481376767
-17	15.1230392	0.488370597
-16	14.2651672	0.494570732
-15	13.3971453	0.499992967
-14	12.5203304	0.504653692
-13	11.6360302	0.508570194
-12	10.7455425	0.511760056
-11	9.85010242	0.514241397
-10	8.95093060	0.516032398
-9	8.04922581	0.517151594
-8	7.14614391	0.517617464
-7	6.24279976	0.517448306
-6	5.34029579	0.516662657
-5	4.43968773	0.515278518

Cont'd to next page

Table 3.1 (cont'd)

DTP-DU

Doppler Angle (ξ)	% of Normalized Velocity Error	Rate of Change in the Velocity
-4	3.54199982	0.513313890
-3	2.64824009	0.510786414
-2	1.75936222	0.507713675
-1	0.876319408	0.504112542
0	0.119209290E-04	0.500000000
1	0.868606567	0.495392799
2	1.72891617	0.490305901
3	2.57987976	0.484756172
4	3.42073441	0.478758991
5	4.25081253	0.472328544
6	5.06925583	0.465480447
7	5.87539673	0.458228827
8	6.66847229	0.450587749
9	7.44791031	0.442570746
10	8.21304321	0.434191346
11	8.96329880	0.425462544
12	9.69800949	0.416397154
13	10.4166031	0.407007992
14	11.1185074	0.397307515
15	11.8032455	0.387306989
16	12.4702454	0.377018511
17	13.1191254	0.366453528
18	13.7493134	0.355623543
19	14.3603325	0.344540238
20	14.9518013	0.333213449
21	15.5233383	0.321654141
22	16.0744629	0.309873223
23	16.6047974	0.297880943
24	17.1140594	0.285688043
25	17.6019592	0.273303151
26	18.0680237	0.260737360
27	18.5119629	0.248000145
28	18.9335785	0.235101104
29	19.3325043	0.222050726
30	19.7085266	0.208856881
31	20.0614929	0.195529580
32	20.3909760	0.182078421
33	20.6970215	0.168512166
34	20.9791107	0.154841185
35	21.2373657	0.141072512
36	21.4714966	0.127216160
37	21.6813965	0.113281012
38	21.8668823	0.992759466E-01

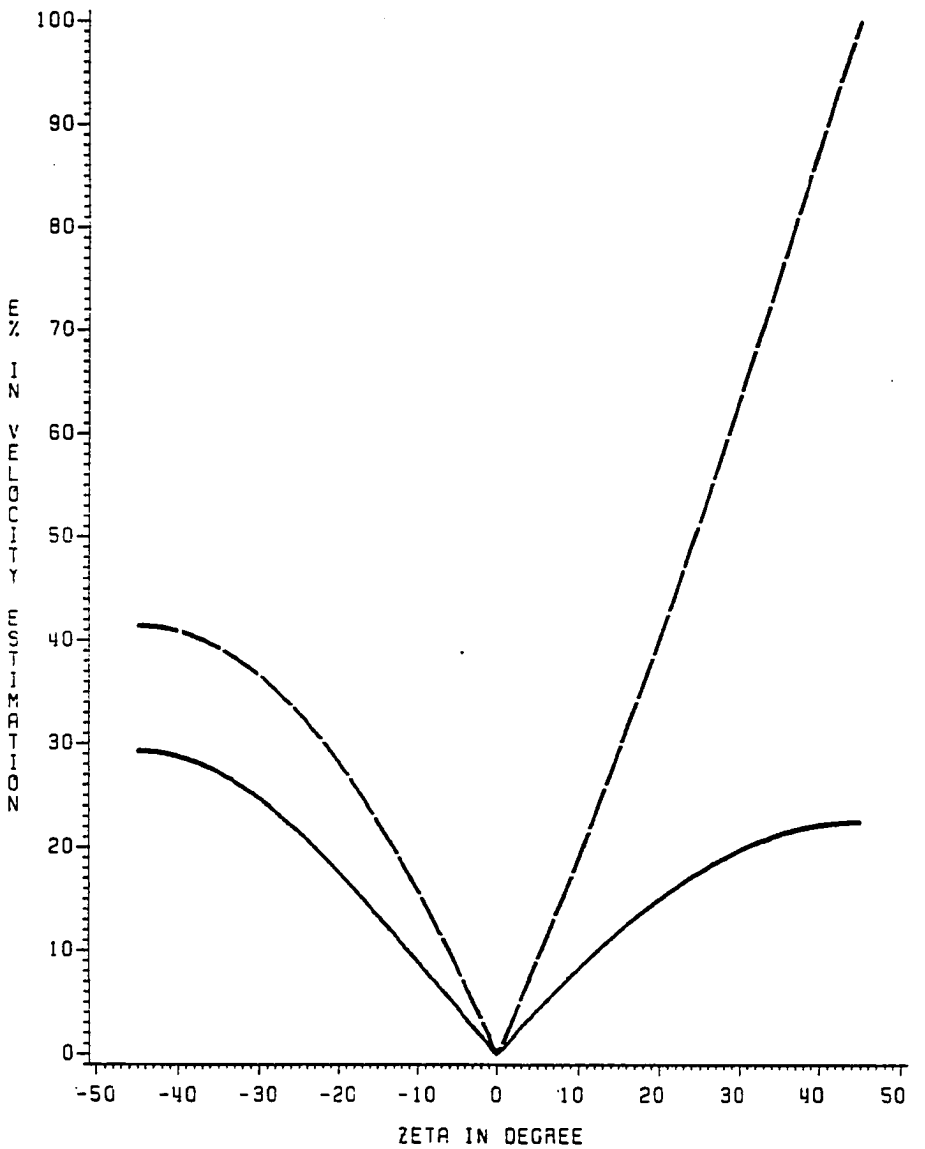

Figure 3.11 The percentage of velocity error for STP-DU and DTP-DU models (special case $\alpha = 90°$, $\theta = 45°$).

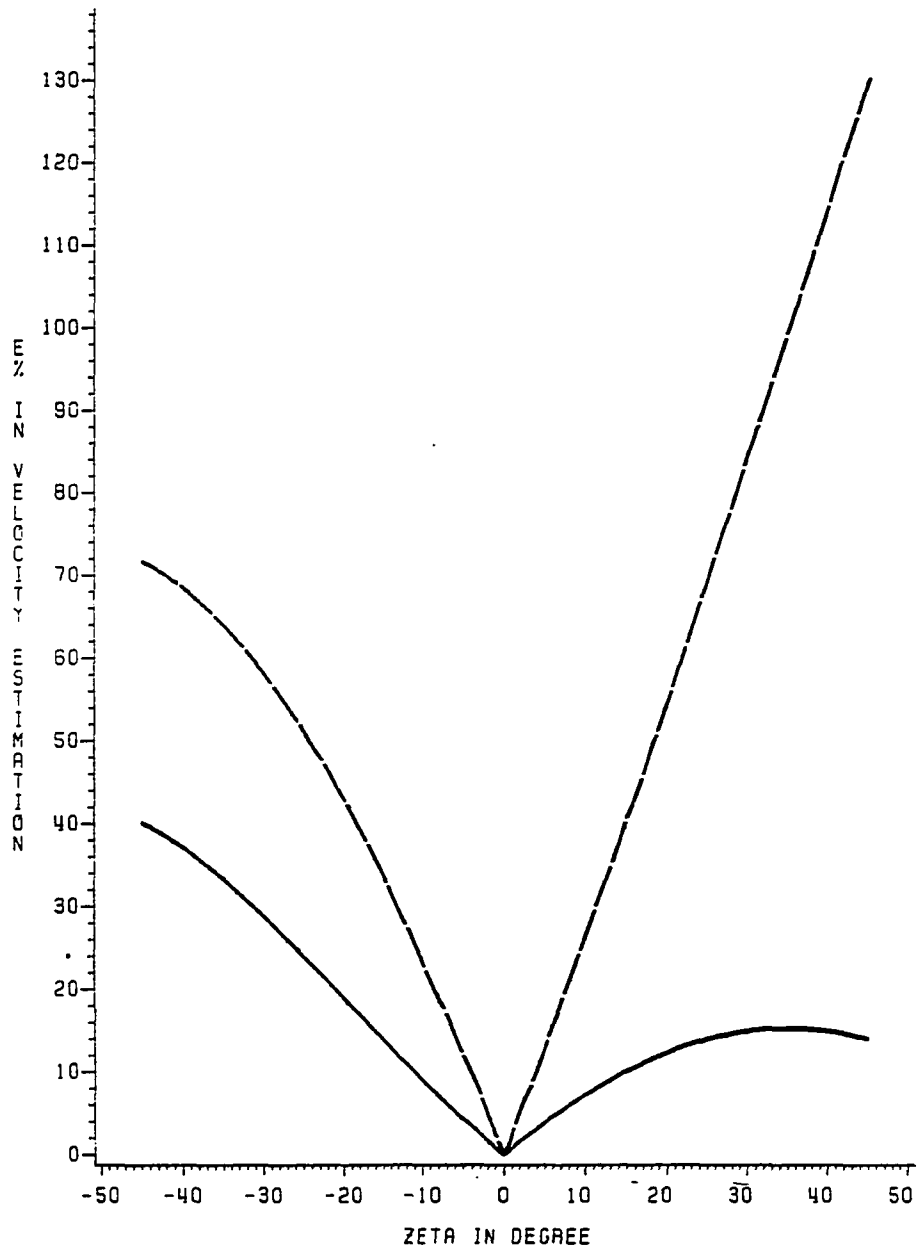

Figure 3.12 Percentage of velocity error for STP-DU and DTP-DU models (special case $\alpha = 90°$, $\theta = 55°$).

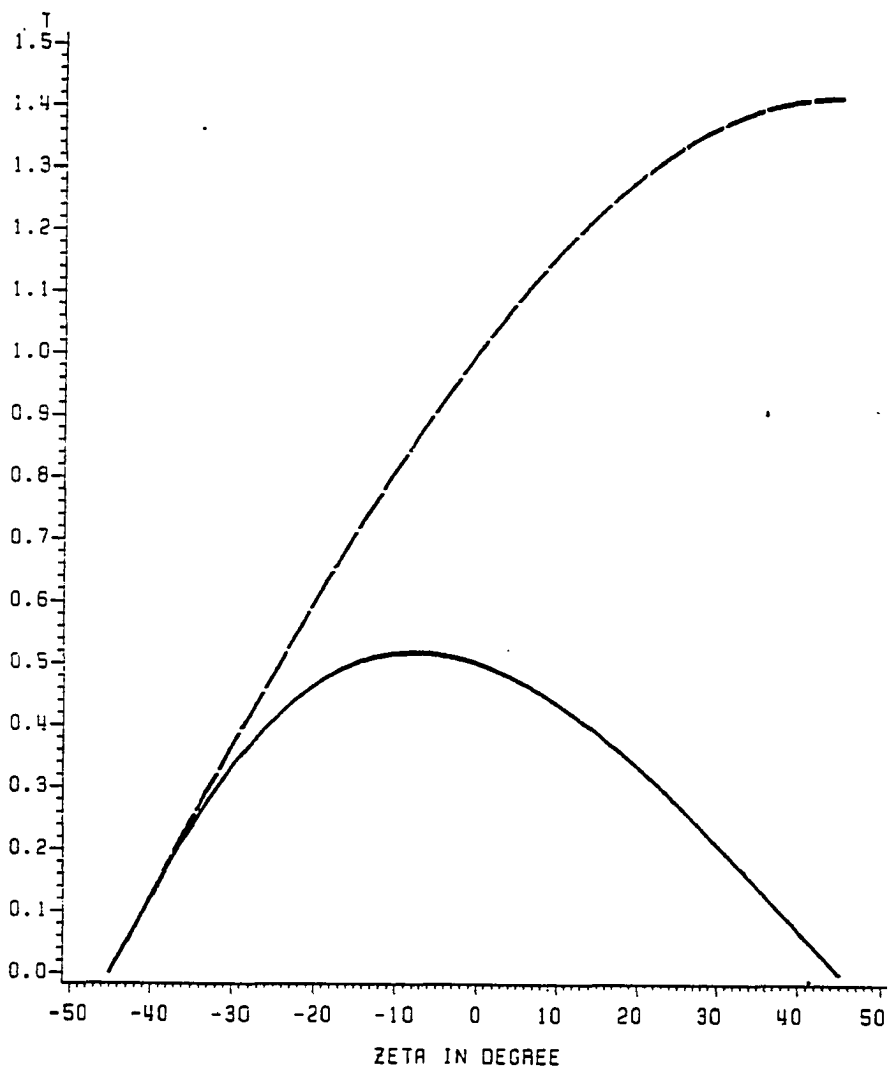

Figure 3.13 Discrepancy between actual and measured flow for STP-DU and DTP-DU models (special case $\alpha = 90°$, $\theta = 45°$).

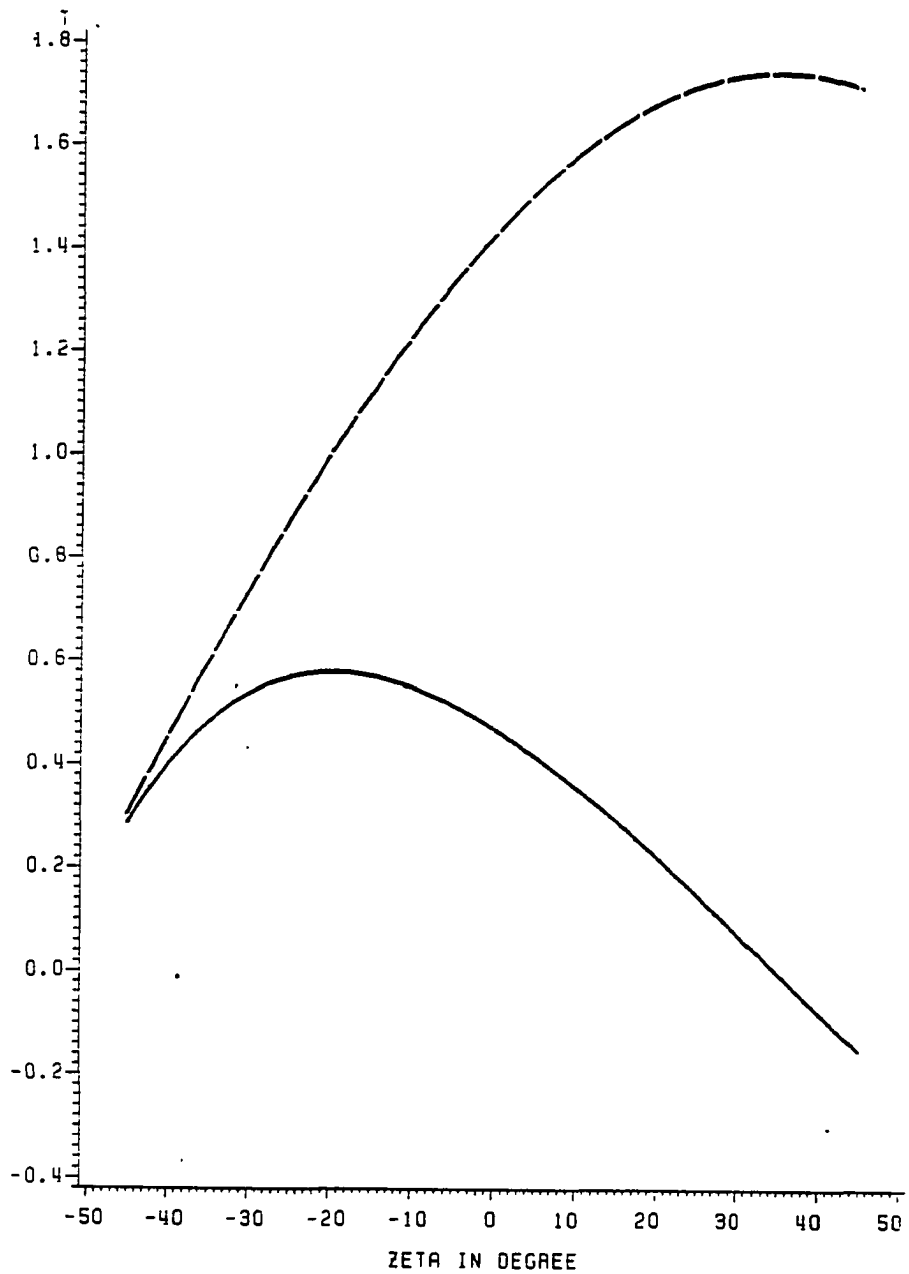

Figure 3.14 Discrepancy between actual and measured flow for STP-DU and DTP-DU models (special case $\alpha = 90°$, $\theta = 55°$).

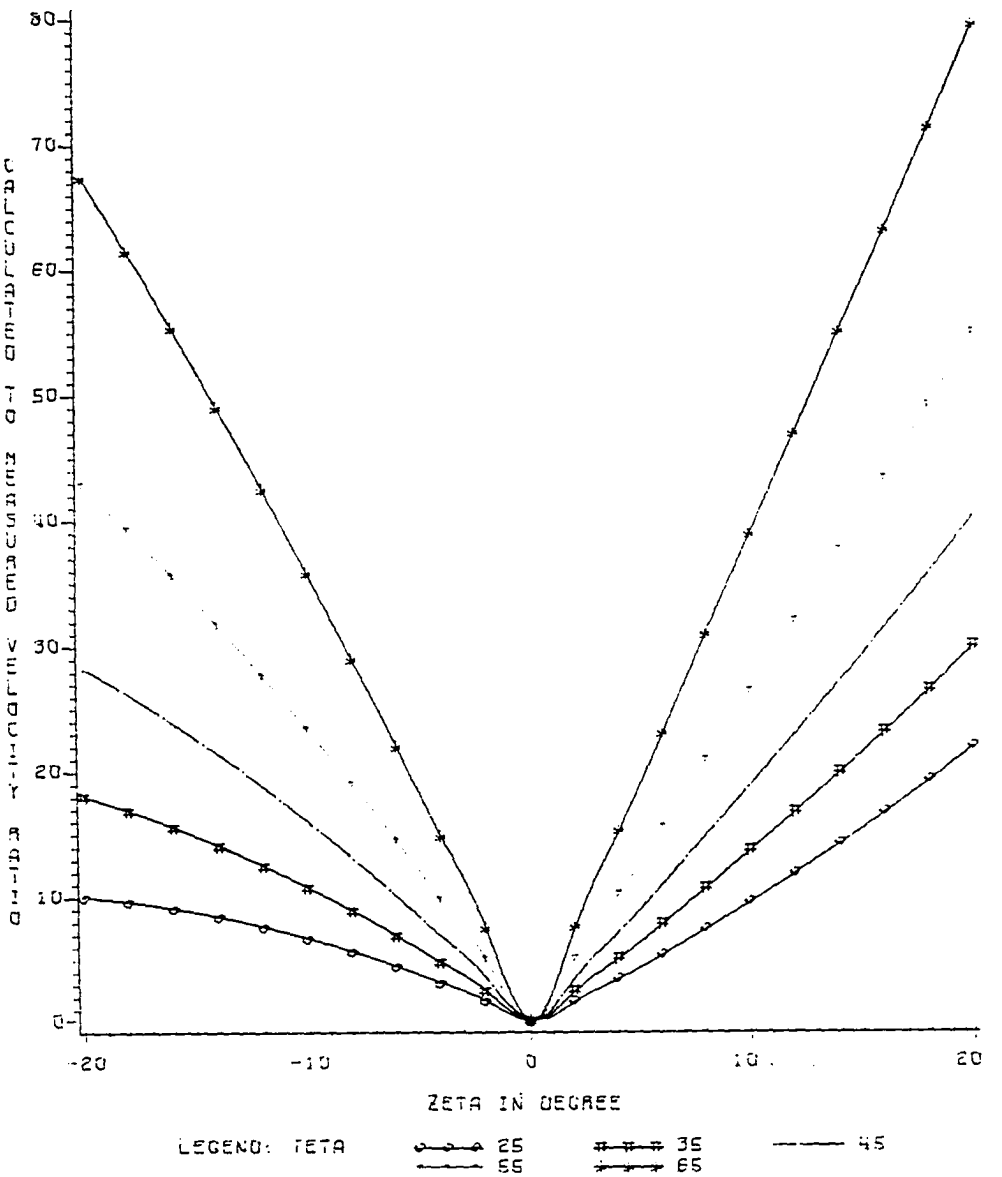

Figure 3.15 Percentage of velocity error for STP-DU model for different values of α and for $\theta = 90°$.

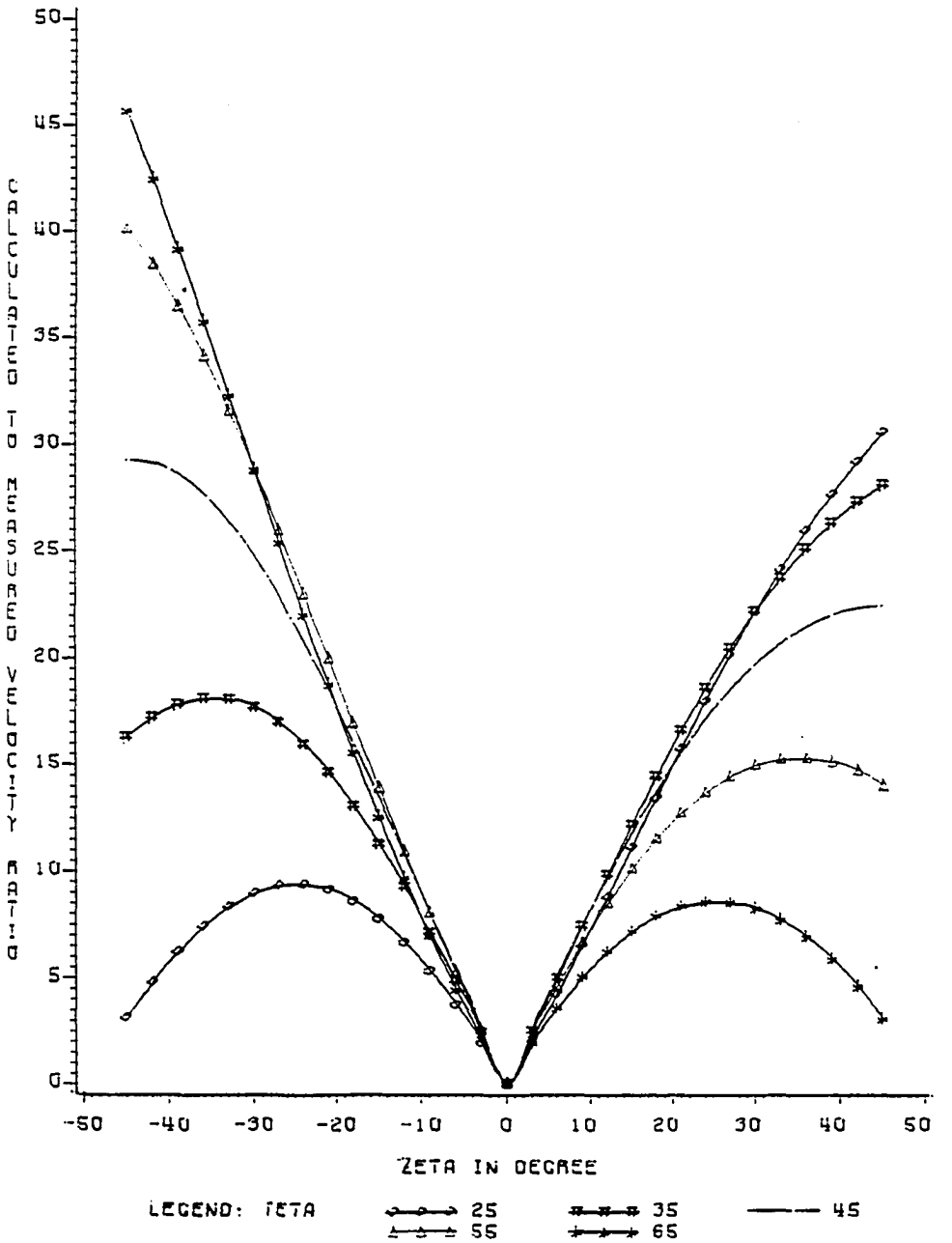

Figure 3.16 Percentage of velocity error for DTP-DU model for different values of α and for $\theta = 90°$.

illustrate the percentage of error for both the STP-DU and DTP-DU models for $\alpha = 90°$ and θ varies from 25° to 65°.

3.3 Relationship Between Velocity Components and Turbulent Blood Flow Characteristics

In section 3.2, a new transducer model (DTP-DU) was presented that enabled to estimate accurately the Doppler angle and to calculate directly the components of the flow velocity. One obvious advantage of the developed model is its ability to obtain transverse and longitudinal components of the velocity, something that is not possible with conventional (STP-DU) systems. One important application of the developed model is in calculating turbulent flow characteristics which are related to physiological changes inside the vessel, such as stenosis or occlusion. In this section, first, we discuss the use of the developed model in calculation of fluctuation components of the velocity. Then, we show the relationship between fluctuation components of the velocity and turbulent flow characteristics. Finally, the relationship between turbulent flow characteristics is presented with the vessel's parameters, such as diameter of the vessel in relation to stenosis.

The flow in a turbulent region is moving in a direction parallel and also in a direction perpendicular to the axis of the pipe. Therefore, there are two components of the velocity v_x and v_y. The instantaneous velocities are

given in the x (parallel) and y (perpendicular) by the following expressions:

$$\hat{v} = \bar{v} + v' \tag{3.55}$$

$$\hat{u} = \bar{u} + u' \tag{3.56}$$

where $\hat{v}$ and $\hat{u}$ are instantaneous velocities, $\bar{v}$ and $\bar{u}$ are average velocities, and v' and u' are fluctuation components of the velocity. One important point here, is how to calculate average value of the velocity that subtraction (derivation) of this average value from instantaneous value can represent true value of fluctuation velocity. It is clear that the ordinary time average and its subtraction from instantantaneous velocity is not a true representative of fluctuation and it is true only for stationary flow where supply pressure is constant and time independent. But, because of the cardiac cycle, blood flow is a pulsatile flow for which supply pressure is time dependent and flow velocity at any specific time in the field, no longer remains at a steady level. Hossien et al [45] introduced the use of phase average (average value at any point in space) for calculating fluctuation components of the velocity. The phase average of the velocity (in x-direction) can be calculated from the following expression:

$$\langle v_x(t) \rangle = \frac{1}{N} \sum_{n=1}^{V} \tilde{v}(x, t + nT) \tag{3.57}$$

where $\tilde{v}(x,t)$ is any instantaneous flow variable at location x and at any time t, and T is the period of the repeated phenomenon. While ideally, an infinite ensemble size is required, in reality, a finite number of periods of the data is available. If N is sufficiently high, the values obtained differ negligibly from the true phase average [7]. One then gets the instantaneous turbulent signal $v'(x,t)$ (fluctuation) as

$$v'(x,t) = \tilde{v}(x,t) - \langle v_x(t) \rangle \tag{3.58}$$

As an example, a pulsatile turbulent signal with the period T is shown in Figure 3.18. Let the period be well defined to start at "a" when the signal exceeds a fixed threshold value. Now, if we sample the signal at interval t, from the beginning of the signal and then wait and sample the signal at time, t_1, in the next cycle and in successive cycles and then take the average, we get the phase average at that particular time t_1 in the cycle. If we then repeat this operation for all t_1 in the range $0 \leq t_1 \leq T_1$, what is obtained is the phase average $\langle v_x(t) \rangle$ shown in Figure 3.18 (a). The difference between the phase average and the instantaneous signal shown in Figure 3.18(b) is thus the turbulent fluctuation $v'_x(t)$ and it is characteristic of $v'_x(t)$ which determines the nature of turbulence in the flow.

The same procedure can be applied for the transverse component of the velocity to find $u'(t)$. Now that we have

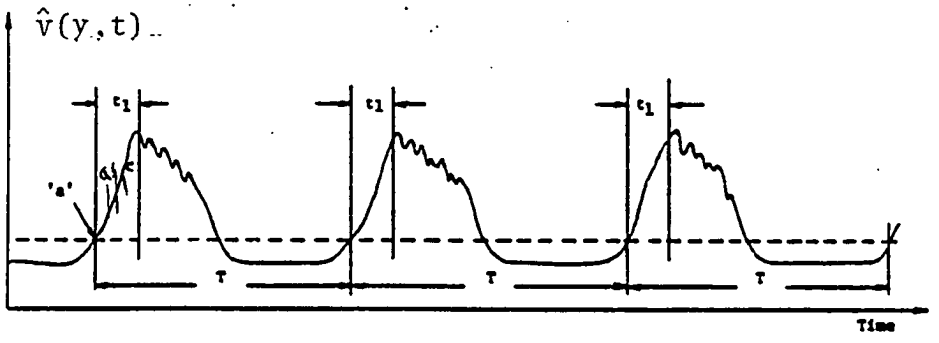

Figure 3.17. An example of pulsatile turbulent flow.

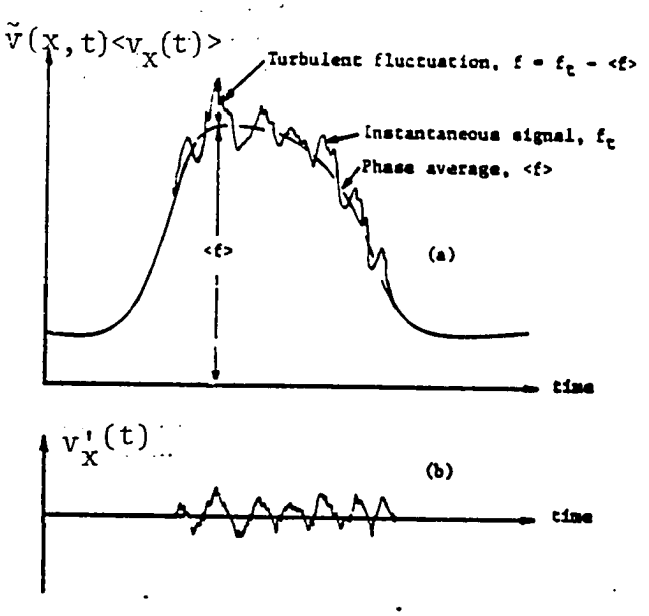

Figure 3.18 Turbulent velocity components. a) Phase average of the velocity, b) Fluctuation velocity.

discussed the procedure to calculate fluctuation velocities, we are able to calculate some characteristics of the flow.

The most important characteristic of a turbulent flow which is also a function of different flow parameters and the vessel structure's parameter is shear stress. The shear stress in turbulent regions can be obtained by the following expression,

$$\tau_0 = -\rho\langle u'v'\rangle \tag{3.59}$$

where $\langle u'v'\rangle$ is the phase average of the product of fluctuation velocities and ρ is the density of the flow. Furthermore, Prandtl [101] derived the expression for velocity in turbulent case as a function of τ_0 and radius of the pipe in the following form:

$$v = c_1 \sqrt{\frac{\tau_0}{\rho}} \ \ell n\ y + c_2 \tag{3.60}$$

where c_1 is an arbitrary constant and c_2 is constant of integration and y varies from r (the border of transition core and turbulent core) to the center of the pipe R_0. To calculate c_2, a point at the center (R_0) is considered, where the velocity is maximum.

$$v\Big|_{y = R_0} = V_{max} = c_1\sqrt{\frac{\tau_0}{\rho}} \ \ell n\ R_0 + c_2$$

or

$$c_2 = V_{max} - c_1\sqrt{\frac{\tau_0}{\rho}} \ \ell n\ R_0$$

Therefore

$$v = c_1\sqrt{\frac{\tau_0}{\rho}}\,\ell n\, y + v_{max} - c_1\sqrt{\frac{\tau_0}{\rho}}\,\ell n\, R_0 \qquad (3.61)$$

The part $\sqrt{\frac{\tau_0}{\rho}}$ is defined as friction velocity

$$v^* = \sqrt{\frac{\tau_0}{\rho}}$$

with the unit of $\frac{L}{T}$. Dividing both sides by v^*

$$\frac{v}{v^*} = c_1 \ell n\, y + \frac{v_{max}}{\sqrt{\tau_0/\rho}} - c_1 \ell n\, R_0$$

or

$$\frac{v}{v^*} = c_1 \ell n\, y + k_1 \qquad (3.62)$$

Since the left side of equation (3.62) is dimensionless, the right side should also be dimensionless. On the other hand, stenosis as narrowing (δ) is a change in the value of y. Therefore, here the height of stenosis (δ) is considered as making the right side dimensionless.

$$\frac{v}{v^*} = c_1 \ell n\, y + c_2 \ell n\, \delta - c_2 \ell n\, \delta + k_1$$

or

$$\frac{v}{v^*} = c_1 \ell n\, \frac{y}{\delta} + k_2$$

or

$$v = c_1\sqrt{\frac{\tau_0}{\rho}}\,\ell n\, \frac{y}{\delta} + \sqrt{\frac{\tau_0}{\rho}}\, k_2 \qquad (3.63)$$

Equation (3.63) is a relation between velocity, shear stress and stenosis.

Another characteristic which can also be related to the

diameter and stenosis, is friction factor. Friction factor is related to the shear stress by the following expression

$$f_f = \frac{2\tau_0}{\rho v_{avg}^2}$$

or

$$\sqrt{\frac{\tau_0}{\rho}} = \sqrt{\frac{f_f}{2}}\ v_{avg} \qquad (3.64)$$

To find a relationship between f_f and δ, v_{avg} has to be calculated.

Rewriting equation (3.61) in the following form,

$$v = v_{max} + c_1 \sqrt{\frac{\tau_0}{\rho}}\ \ell n\ \frac{y}{R_0} \qquad (3.65)$$

The v_{avg} can be calculated as

$$v_{avg} = \frac{\int_0^{R_0} v\,da}{\pi R_0^2} = \frac{\int_0^{R_0} \sqrt{(2\pi r dr)}}{\pi R_0^2} \qquad (3.66)$$

Defining $y = R_0 - v$

$$v_{avg} = \frac{\int_0^{R_0} v_{max}(2\pi r dr) + c_1\sqrt{\frac{\tau_0}{\rho}}\int_0^{R_0} \ell n\left(\frac{R_0 - r}{R_0}\right) 2\pi r dr}{\pi R_0^2}$$

or

$$v_{avg} = \frac{\pi R_0^2 v_{max} + c_1\sqrt{\frac{\tau_0}{\rho}}\int_0^{R_0} \ell n\ (R_0 - r)\,2\pi r dr - c_1\sqrt{\frac{\tau_0}{\rho}}\int_0^{R_0} \ell n R_0\,(2\pi r dr)}{\pi R_0^2} \qquad (3.67)$$

Defining

$$R_0 - r = u$$

$$dr = -du$$

$$r = R_0 - u$$

At $r=0$, $u=R_0$ and at $r=R_0$, $u=0$ and calculating integral part by part

$$\int_0^{R_0} \ell n(R_0-r)\ 2\pi r dr = \int_{R_0}^{0} \ell nu[2\pi(R_0-u)(-du)]$$

or

$$= 2\pi\int_0^{R_0} \ell n\ u(R_0-u)du$$

$$= 2\pi R_0\int_0^{R_0} \ell n\ udu - 2\pi\int_0^{R_0} u\ \ell n\ u\ du$$

$$= 2\pi R_0\ [u\ \ell n\ u-u\Big|_0^{R_0}\ ] -2\pi[\frac{u^2}{2}\ \ell n\ u - \frac{u^2}{4}\ \Big|_0^{R_0}]$$

$$= 2\pi R_0[R_0\ \ell n\ R_0-R_0] -2\pi[\frac{R_0^2}{2}\ \ell n\ R_0 - \frac{R_0^2}{4}]$$

$$= 2\pi R_0^2\ \ell n\ R_0 - 2\pi R_0^2 - \pi R_0^2\ \ell n\ R_0 - \pi\frac{R_0^2}{2}$$

$$= \pi R_0^2\ \ell n\ R_0 - \frac{3}{2}\pi R_0^2 \qquad (3.68)$$

and

$$2\pi\int_0^{R_0} \ell n\ R_0(rdr) = 2\pi\ \ell n\ R_0\ (\frac{R_0^2}{4}) = \pi R_0^2\ \ell n\ R_0 \qquad (3.69)$$

Substituting (3.68) and (3.39) into (3.67)

$$v_{avg} = v_{max} - 1.5\ c_1\sqrt{\frac{\tau_0}{\rho}} \qquad (3.70)$$

Substituting (3.64) into (3.70),

$$v_{avg} = v_{max} - 1.5\ c_1 \sqrt{\frac{f_f}{2}}\ v_{avg}$$

or

$$v_{avg} = v_{max} - 1.06\ c_1 \sqrt{f_f}\ v_{avg}$$

or

$$v_{max} = (1 + 1.06\ c_1\ \sqrt{f_f}\ )\ v_{avg} \qquad (3.71)$$

From equation (3.63) at $y = R_0$, $v = v_{max}$ (in turbulent core), so

$$v_{max} = c_1 \sqrt{\frac{\tau_0}{\rho}}\ \ln \frac{R_0}{\delta} + k_2 \sqrt{\frac{\tau_0}{\rho}}$$

or

$$\frac{v_{max}}{\sqrt{\tau_0/\rho}} = c_1\ \ln \frac{R_0}{\delta} + k_2 \qquad (3.72)$$

Substituting (3.64) and (3.71) into (3.72)

$$\frac{1 + 1.06\ c_1\ \sqrt{f_f}}{\sqrt{\frac{f_f}{2}}} = c_1\ \ln \frac{R_0}{\delta} + k_2$$

or

$$1 + 1.06\ c_1\ \sqrt{f_f} = 0.707\ c_1\ \sqrt{f_f}\ \ln \frac{R_0}{\delta} + 0.707\ k_2 \sqrt{f_f}$$

or

$$1 = \sqrt{f_f}(0.707\ c_1\ \ln \frac{R_o}{\delta} + 0.707\ k_2 - 1.06\ c_1)$$

or

$$\frac{1}{\sqrt{f_f}} = 0.707\ c_1\ \ln \frac{R_0}{\delta} + 0.707\ k_2 - 1.06\ c_1 \qquad (3.73)$$

Equation (3.73) is another indication that characteristics of the turbulent flow are a function of the structural

changes inside the vessel. Constants c_1 and k_2 can be found experimentally. For special cases in a turbulent case, c_1 and k_2 are found to be 2.5 and 8.4, respectively.

The second approach to determine the stenosis from shear stress is by using geometrical analysis presented by Young [49] and is shown in Figure 3.19.

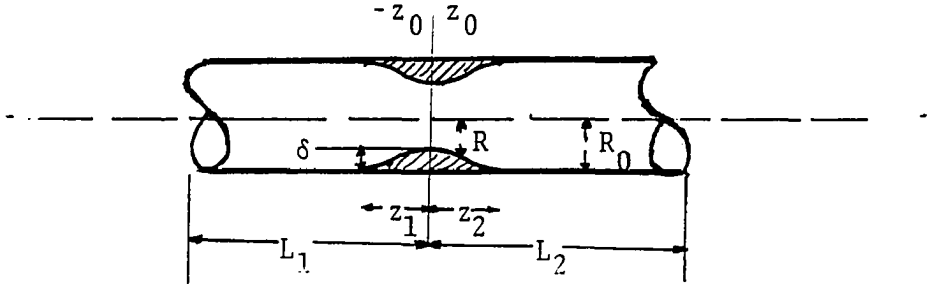

Figure 3.19. A geometric presentation of stenosis in the artery.

In general, it is assumed that the rate of change in the radius of the vessel (R) is given by

$$\begin{cases} \frac{\partial R}{\partial t} = -\alpha_0\left(1+\cos\pi\frac{z}{z_0}\right)e^{-t/\tau}, & -z_0 < z < z_0 \\ 0 \qquad \text{otherwise} \end{cases} \tag{3.74}$$

where α_0 is a constant and τ is a time constant for stenotic growth. Integrating equation (3.74)

$$R = R_0 - \tau\alpha_0(1-e^{-t/\tau})\left(1+\cos\pi\frac{z}{z_0}\right) \tag{3.75}$$

At $t = 0$ (no stenosis) $R = R_0$

As $t \to \infty$ and at $z = 0$, δ is maximum

and $R-R_0 = 2\,\tau\alpha_0 = \delta_m$

so

$$R = R_0 - \frac{\delta m}{2}(1-e^{-t/\tau})(1 + \cos\frac{\pi z}{z_0})$$

Defining $\delta = \delta_m(1-e^{-t/\tau})$

$$R = R_0 - \frac{\delta}{2}(1 + \cos\pi\frac{z}{z_0}) \qquad (3.76)$$

Since we are interested only in the maximum height of stenosis where the stenosis is stabilized and doesn't change appreciatly with time (at $z = 0$), then

$$R = R_0 - \frac{\delta}{2}(1+1)$$

or

$$\delta = R_0 - R \qquad (3.77)$$

Alternatively, shear stress is defined in another form as a function of pressure drop across the stenosis ($\frac{\Delta P}{\Delta z}$), where $z = \pm\frac{L}{2}$

$$\tau = \frac{r}{2}\,\frac{\Delta P}{\Delta z}$$

where

$$\frac{\Delta P}{\Delta z} = -\frac{8\mu}{\pi}\,\frac{Q}{r^4}$$

so

$$\tau = -\frac{4\mu}{\pi}\,\frac{Q}{r^3} \qquad (3.78)$$

where μ is viscosity of the flow. In normal cases when there is no occlusion ($r = R_0$), equation (3.78) can be rewritten as

$$\tau_n = \frac{4\mu}{\pi} \frac{Q}{R_0^3} \tag{3.79}$$

For stenosis where r = R, the shear stress can be expressed as

$$\tau_0 = - \frac{4\mu}{\pi} \frac{Q}{R^3} \tag{3.80}$$

But from equation (3.77)

$$\frac{\delta}{R_0} = 1 - \frac{R}{R^0}$$

or

$$\frac{R}{R_0} = 1 - \frac{\delta}{R_0} \tag{3.81}$$

Dividing (3.80) by (3.79) and substituting (3.81),

$$\frac{\tau_0}{\tau_n} = (1 - \frac{\delta}{R_0})^{-3} = \frac{1}{(1 - \frac{\delta}{R_0})^3}$$

or

$$\frac{\tau_0}{\tau_n} = \frac{1}{1-3\frac{\delta}{R_0} + 3(\frac{\delta}{R_0})^2 - (\frac{\delta}{R_0})^3} \tag{3.82}$$

τ_n can be calculated by having fluctuation velocities and τ_n can easily be calculated from equation (3.79) by calculating volume rate (Q) and by precisely calculating the diameter of the vessel through scanning by a range gated device. Therefore, Stenosis (δ) can be calculated.

CHAPTER IV

EXPERIMENTAL PROCEDURE

Experimental study of blood flow fields have been augmented by theoretical models using computational fluid dynamics. In order to verify the theoretical model, the calculation of such parameters and flow characteristics as Doppler angle, blood flow velocity, volume rate, velocity profile, shear stress, etc. are essential. In order to calculate these parameters, the Doppler signals must be captured, digitized, stored, processed, and then analyzed. The data are collected from various arteries of donor dogs and rabbits.

In this chapter, first, is presented an overall block diagram of experimental model and each part of the model is discussed. Then, the procedure and methods to calculate flow parameters and characteristics will be discussed.

4.1 Experimental Model

The main purpose of our hardware system is to record the Doppler signals from an ultrasound machine, display on the chart recorder, transfer it to analog-to-digital converter for digitization, select the appropriate periods of the signals and store them on the file.

An overall block diagram of the system is depicted in

Figure 4.1, and consists of the following units:

1. The variable pulsatile pump,
2. the developed dual transducer model,
3. the bidirectional pulsed Doppler ultrasound unit with two channels,
4. the chart recorder to display analog signal,
5. the communication system,
6. the analog-to-digital convertor, and
7. the digital computer.

In the following pages, each unit will be discussed separately.

4.1.1 The Variable Pulsatile Pump

To evaluate the performance of the DTP-DU model for the in-vitro experiment, a variable pulsatile pump model (Bel O Just single 1½", GRI) is used to produce, artificially, a pulsatile signal as the cardiac signal during in-vitro experiments. The speed of the pump can be controlled and varies at different levels. The pump perfused the circuit and a graduated cylinder collected the effluent.

4.1.2 The DTP-DU Transducer Model

The DTP-DU model was constructed using 20 MHz piezoelectric ceramic and a periarterial cuff to orthogonally place the crystals (Figure 3.4) was implanted in the carotid artery of a dog (for in-vivo experiments).

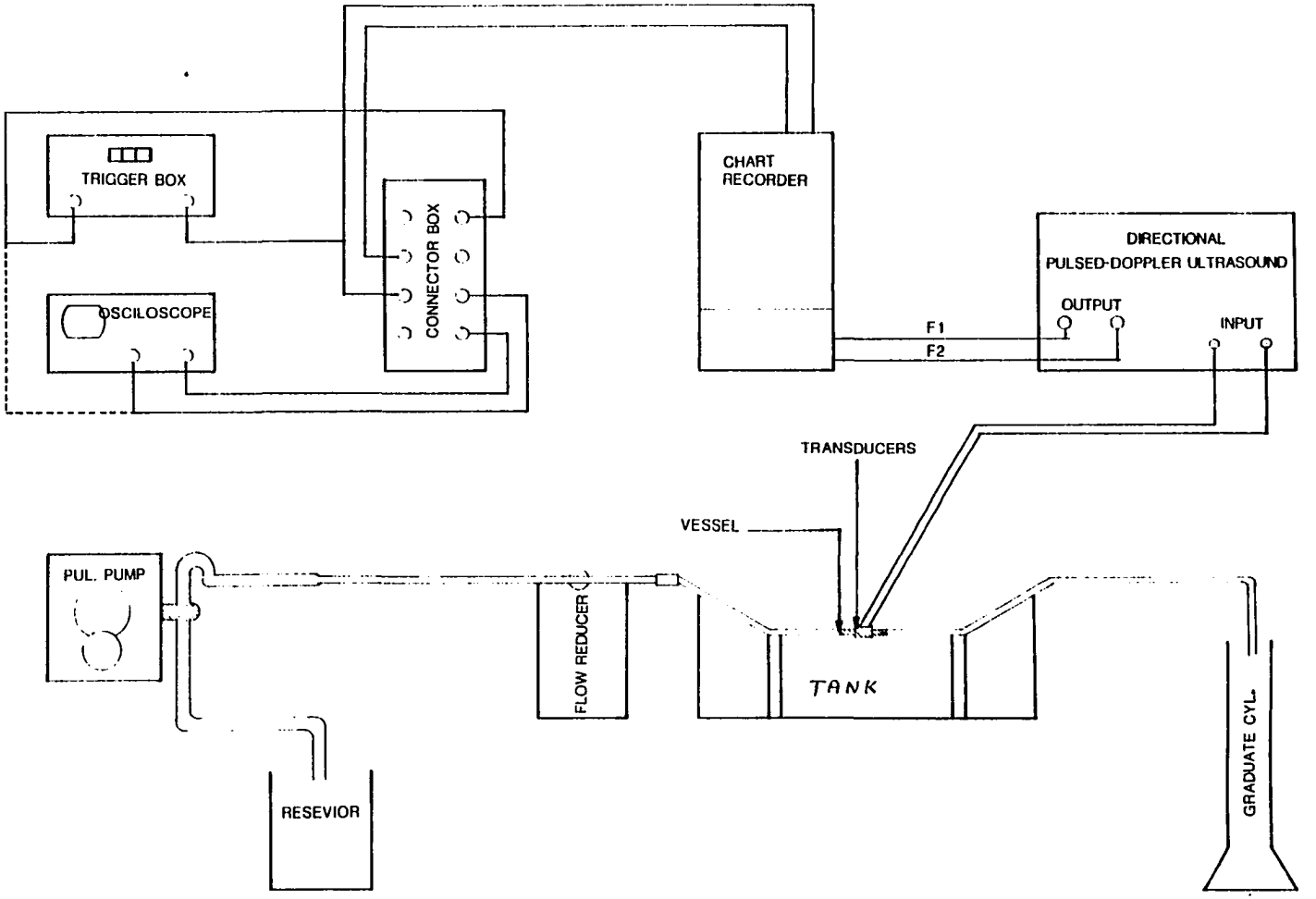

Figure 4.1 Illustration of experimental setup.

The isolated arteries from donor dogs and rabbits (for in-vitro experiment) were obtained from the femoral, carotid or terminal aortic root and perfused with an artificial blood particulate suspension in water. The DTP-DU model transmitted the ultrasound wave to the tissue and then received back the backscattered signal from the tissue and retransmitted this signal to the Doppler machine for further processing.

4.1.3 The Bidirectional Pulsed-Doppler Ultrasound Machine with Two Channels

The data used in this study are collected with the use of a bidirectional pulsed-Doppler ultrasound flowmeter (University of Iowa, model 545C-3) with an emission frequency of 20 MHz to produce the Doppler signal.

The 545C-3 unit has the ability to measure flow velocity at a specified distance from the face of the crystal probe, rather than everywhere within range of the signal. The range control adjusts this distance. The standard maximum range of this machine is 1.0 cm.

The principle behind this control is based on the fact that it is a pulsed Doppler. That is, it transmits a short burst of audio energy, then listens for an echo after some time delay. Obviously, this delay is the determining factor in the measurement of the distance that the audio signal has traveled by the pulse.

In addition to the range control, this machine also

has a sensitivity control and polarity control. The sensitivity control adjusts the level of the Doppler signal applied to the voltage-to-frequency converter stage, which provided the "phasic" and "mean" output to a recorder or oscilloscope. The polarity control determined which flow direction resulted in positive output voltage polarity, toward the crystal or away from it.

The output of the machine are range, phasic, mean and audio 1 and 2. The range is a voltage proportional to the setting of the "range" control. It may be calibrated to any convenient scale, although the standard calibration is 1.0 volt per centimeter. The phasic output is a signal related to phasic velocity information and has a normal scale factor of 0.5 volts per kilohertz of Doppler shift. The mean blood velocity is introduced/delivered at the "mean" connector with the same scale factor as the phasic output. The signals at "audio 1, 2" connectors are the actual signals and may be used for a variety of purposes, such as spectral analysis or external audio amplification. A complete description of the 545C-3 machine functions is presented in Appendix B.

4.1.4 The Chart Recorder

A Gould-2800 chart recorder (Figure 4.1) is used to display the analog signals. This machine is also capable of amplifying the signal to be transferred to the computer.

The output of the amplifier is compared with the analog signal to calculate the calibration factor.

4.1.5 The Communication Unit

The communication unit consists mainly of input/output ports. Four input ports and four output ports are built in this unit. These ports are the communication link between the pulsed-Doppler ultrasound machine and the analog-to-digital converter. In addition to the communication unit (connection box), there is a trigger unit that can synchronize the Doppler signal with the computer. The circuit is initialized by one of the Doppler signal outputs form the ultrasound machine.

4.1.6 The Analog-to-Digital Converter

The analog-to-digital converter enables the lab peripheral system user to sample analog data at specific rates and to store the equivalent digital value for subsequent processing. The system consists of an 8-channel multiplexer (eight single ended ±5 inputs), sample and hold circuitry, a 12-bit A/D converter, and six programmable light emitting diode (LED) numerical readouts. Access is via the front panel, shown in Figure 4.4. All eight channels are connected to standard 1/4-inch, 3-terminal phone jacks on the front panel, permitting direct interfacing with laboratory equipment.

For the present study, two software packages (see Appendix C) are used. In the first program, "DADC" (analog to digital program), file name of each test, required sampling rate, number of beats and number of channels should be provided. After selecting the appropriate periods, data are recorded on the file. In the second program "DCFlow", the data are converted to decimal values, the heartbeat is calculated along with maximum, minimum and mean values in each channel, the number of data in each trigger is determined and data are recorded on the file for further processing.

4.17 The Digital Computer

A PDP 11/34 minicomputer with 112k words (224k bytes) of RAM is used to process the data in the first two stages of digitizing and recording the data. The data are transferred via modem from PDP 11/34 to a VAX 11/780 (operating system is UNIX 4.2 BSD) for further processing. The VAX system is in communication with an IBM 3081. The statistical analysis and plots are performed using SAS subroutine available in the computer.

CHAPTER V

EXPERIMENTAL RESULTS

The digitized data mentioned in Chapter IV are stored under the date in which the experiment is conducted. The number of data in each file varies dependent upon the condition of each experiment. In general, for each particular test, 8 to 10 sets of data (each containing 200 to 350 pts.) are recorded. In both in-vivo and in-vito experiments, normal and stenotic arteries are investigated and results are compared. In-vivo and in-vitro studies are divided into categories intended to evaluate the five major capabilities of the dual transducer pulsed-Doppler ultradounds: measurement of the Doppler angle, flow velocity, profile distribution, volumetric flow and shear stress. One or more of these capabilities are evaluated during any single experiment. For each experiment, a protocol is written and an experiment is conducted, which follows the procedure outlined in the protocol. In this chapter, in-vivo and in-vitro experiments that are conducted at the University of Oklahoma Health Sciences Center and the procedure to calculate different parameters are described.

5.1 Parameters Calculation

5.1.1 Doppler Angle

The Doppler angle is calculated using equation 3.42 at $\alpha = 90°$ as follows:

$$\theta = \arctan\left(\frac{F_2}{F_1}\right) \tag{5.1}$$

where F_1 and F_2 are recorded Doppler signals.

5.1.2 Velocity

The velocity of blood flow is calculated from equation (3.41) at $\alpha = 90°$ as follows:

$$v_R = k\sqrt{F_1^2 + F_2^2} \tag{5.2}$$

where k for 545C-3 machine is 78.25 and is given by the manufacturer designing the instrument. The individual velocity components can be calculated from equations (3.37) and (3.38) for $\alpha = 90°$ as follows:

$$v_1 = k\ F_1/\cos\theta \tag{5.3}$$

$$v_2 = k\ F_2/\sin\theta \tag{5.4}$$

5.1.3 Blood flow volume rate

The volume rate is calculated by the following expression:

$$Q = v_R \cdot A \cdot \left(\frac{60}{1000}\right) \tag{5.5}$$

where A is the cross-sectional area under investigation (i.e., $A = \frac{\pi D^2}{4}$, where D is the diameter of the vessel) and constant $(\frac{60}{1000})$ is a unit converting constant for Q in ml/min.

5.1.4 Shear Stress

To calculate shear stress, first the phase average of the velocity is calculated from equation (3.57) as follows:

$$\langle v_x(t) \rangle = \frac{1}{N} \sum_{n=1}^{n} \tilde{v}(x_0 t + nT) \qquad (3.57)$$

Then fluctuation components of the velocity are calculated from equation (3.58), that is

$$v'(x,t) = \tilde{v}(x,t) - \langle v_x(t) \rangle \qquad (3.58)$$

And finally, shear stress is calculated from equation (3.59) as follows:

$$\tau_0 = -\rho \langle u'v' \rangle \qquad (3.59)$$

5.2 In-Vivo Experiment

The constructed DTP-DU model is implanted on the carotid artery of a 27-pound dog. Acute surgical technique is used and under barbiturate anaesthesia, the common carotid artery is exposed.

The experiment is conducted at three different

ranges and three different heartbeats. For each test, normal stenosis (25 to 45 percent) and occluded artery (85 to 95 percent), the Doppler angle, blood flow velocity and blood flow volume rate are calculated. The ultimate goal of this experiment is evaluating the performance of DTP-DU model in measuring Doppler angle in different situations.

5.2.1 Experimental Results

5.2.1.1 Normal Heartbeats (180 bPm)

5.2.1.1.a Range a (1/6 of diameter)

In this part of the experiment, the heartbeat remains stable at normal conditions. Four different tests are conducted for normal and stenotic common carotid artery. The output Doppler signals for these tests are shown in Figures 5.1, 5.2, 5.3 and 5.4. It can be seen that by increasing the degree of stenosis, the amplitude of the Doppler signals are decreased. The Doppler angle, flow velocity and blood flow volume rate are calculated from equations (5.1), (5.2) and (5.5), respectively. The diameter of the vessel in normal condition is 3 mm. The stenosis in the diameter of the vessel are imposed using a micrometer and they are 2, 1, and 0.5 mm for three different categories of stenosis. The results are presented in Table 5.1. The mean value of the Doppler angle in this part of the experiment is 51.04°.

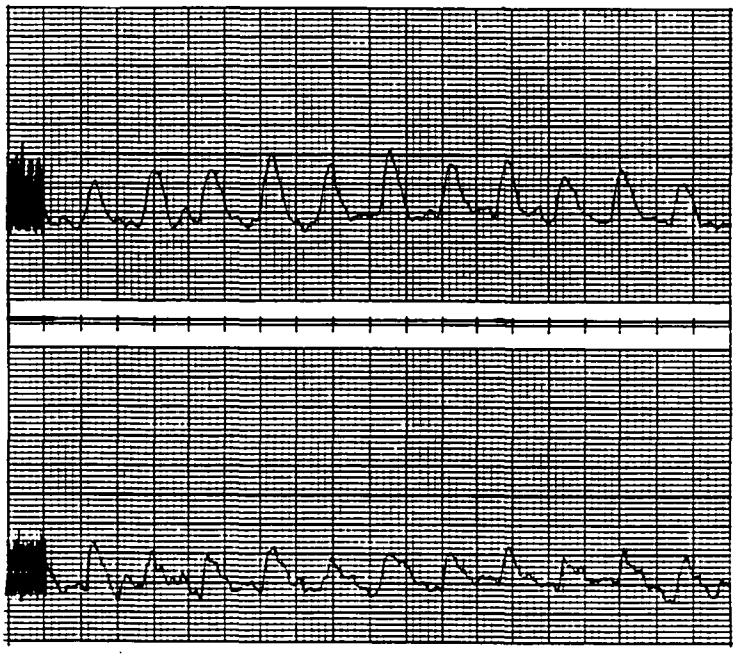

Figure 5.1 The Doppler signals recorded from normal common carotid artery at range a.

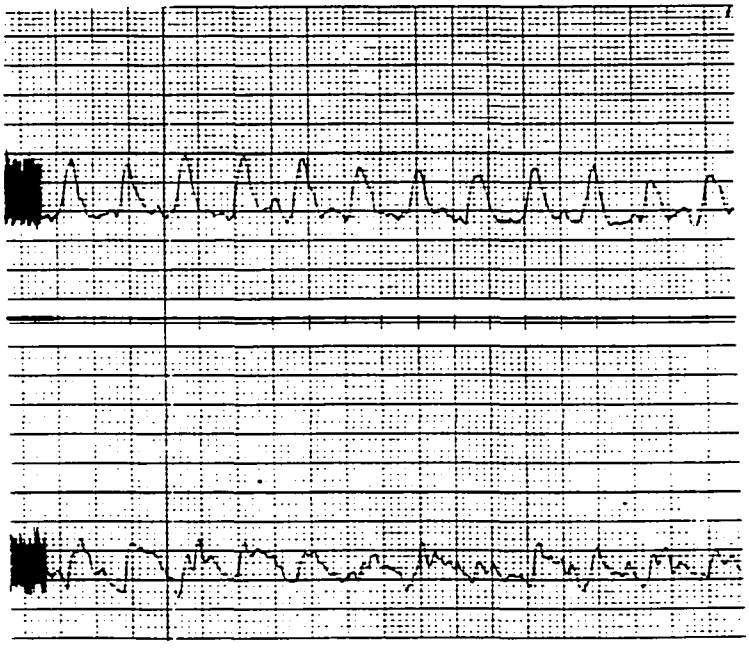

Figure 5.2 The Doppler signals recorded from stenotic (25 percent to 35 percent) common carotid artery at range a.

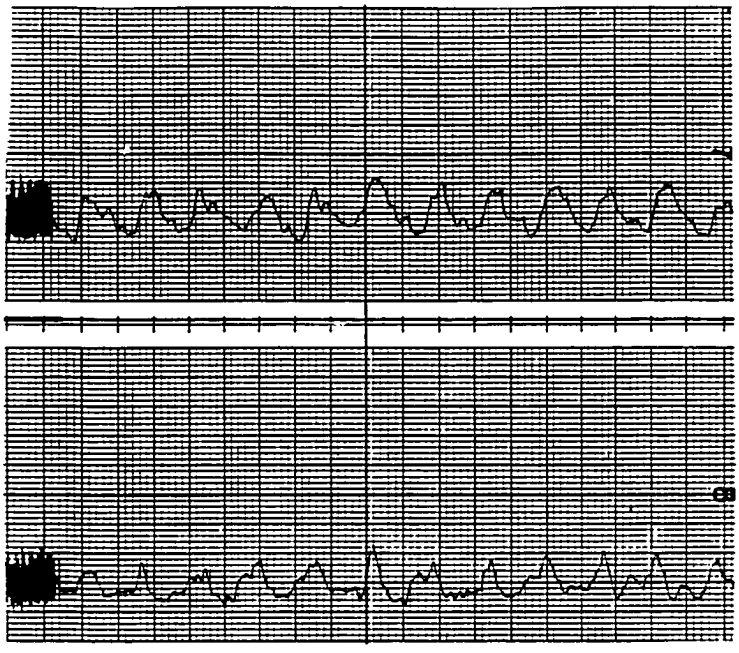

Figure 5.3 The Doppler signals recorded from stenotic (45 to 55 percent) common carotid artery at range a.

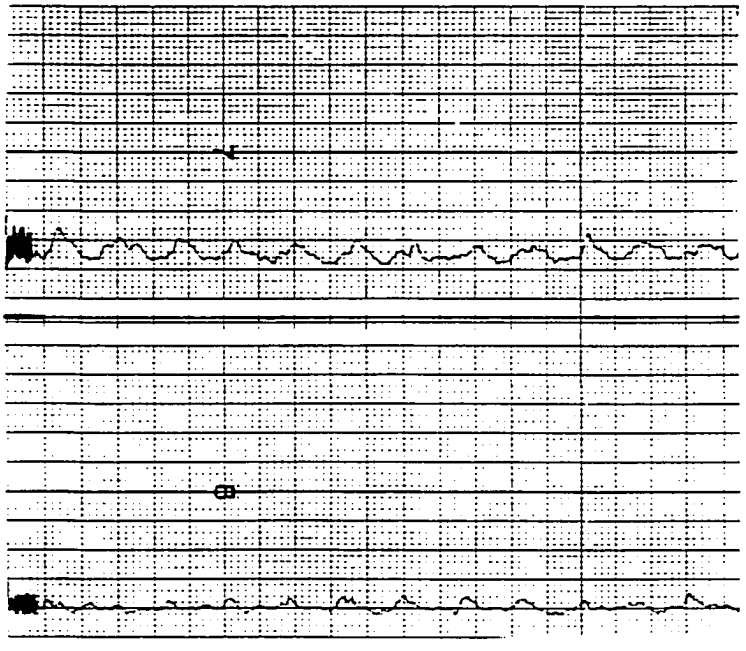

Figure 5.4 The Doppler signals recorded from occluded (85 to 95 percent) common carotid artery at range a.

Table 5.1

The Doppler Angle, Flow Velocity and Flow Volume Rate for Normal Condition of the Heart.

Range	Doppler Angle (θ) (degrees)	Velocity (mm/sec)	Diameter (mm)	Volume Rate (ml/min)
a	50.32	154.20	3	65.49
a	52.83	151.18	2	28.54
a	52.20	132.95	1	6.27
a	49.33	101.76	0.5	1.20
b	54.33	154.36	3	65.56
b	57.78	151.01	2	28.50
b	51.03	147.99	1	6.98
c	50.99	148.98	3	63.27
c	54.91	125.70	2	23.73
c	48.63	125.02	1	5.90

The normalized error in each case varies from 1.4 percent to 3.3 percent. The results indicate that a large reduction in the diameter causes a great change in the Doppler angle.

5.2.1.1.b Range b (1/3 of diameter)

In this part of the experiment, the heartbeat is still normal and is in stable condition, but the range in which the data are taken is changed from 1/6 of the diameter to 1/3 of the diameter from the near wall. Three different vessel diameters (normal, 25 to 35 percent and 45 percent to 55 percent) are tested. The output Doppler signals from each test are shown in Figures 5.5, 5.6 and 5.7. Since the range is closer to the center compared with the previous range, the signals have a higher value of amplitude. The Doppler angle, blood flow velocity and blood flow volume rate are calculated. The results are presented in Table 5.1.

The mean value of the Doppler angle in this test is 54.21°, with normalized error ranging from 2.0 percent to 5.6 percent.

5.2.1.1.c Range c (1/2 of the diameter)

In this part of the experiment, the heartbeat is again normal and in stable condition, but the range in which data are taken is changed to 1/2 of the diameter. The Doppler signals are taken from three different vessel diameters (normal, 25 percent to 35 percent and 45 percent to 55

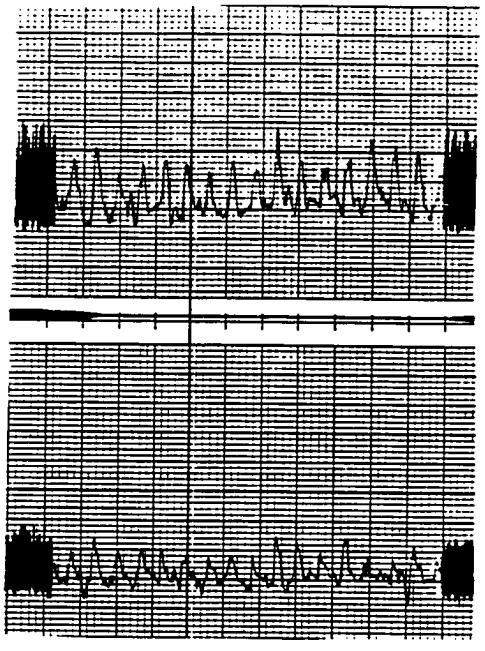

Figure 5.5 The Doppler signals recorded from normal common carotid artery at range b.

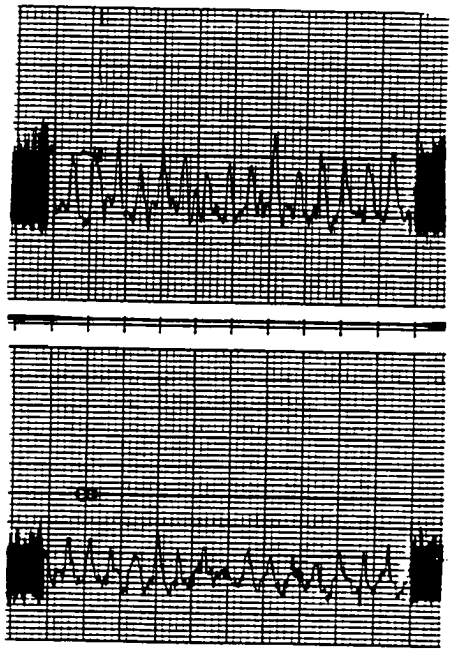

Figure 5.6 The Doppler signals recorded from stenotic (25 ro 35 percent) common carotid artery at range b.

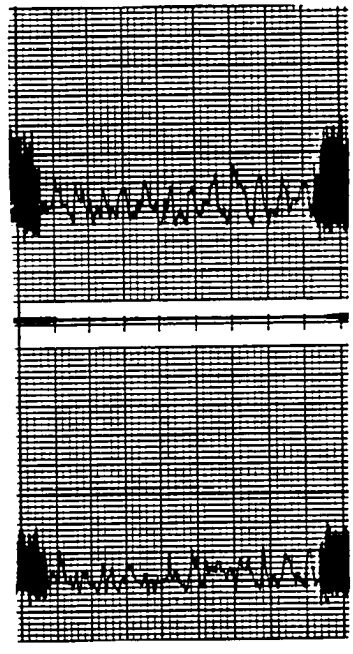

Figure 5.7 The Doppler signals recorded from stenotic (45 to 55 percent) common carotid artery at range b.

percent) and are shown in Figures 5.8, 5.9 and 5.10, respectively. Since the Doppler signals are recorded from the center point of the artery, the highest value for the amplitude can be observed. The Doppler angle, blood flow velocity and blood flow volume rate are calculated. Results are presented in Table 5.1. The mean value of the Doppler angle in this test is 51.51°. The normalized error varies from 1 percent to 5.5 percent.

The Doppler angles are found in agreement in a repetitive series of tests. The overall mean value of the Doppler angle is 52.25° with overall normalized error of 2 percent to percent.

5.2.1.2 Reduced Heartbeats (150 bpm)

To investigate the effect of reduction in heartbeats on the calculation of the Doppler angle and blood flow volume rate, Phenylephrine dyrupathonimetic was injected to increase the pressure of the blood flow. The number of heartbeats is measured from the chart recorder and is 150 bpm, a reduction of 16.67 percent. The data recorded in this experiment are taken from only one particular range (center of the artery). The output Doppler signals are shown in Figures 5.11, 5.12, 5.13 and 5.14. The figures indicate a large reduction in the amplitude of the Doppler signal due to the lower heartbeat or increase in the pressure. The Doppler angle, flow velocity and blood flow volume rate are calculated

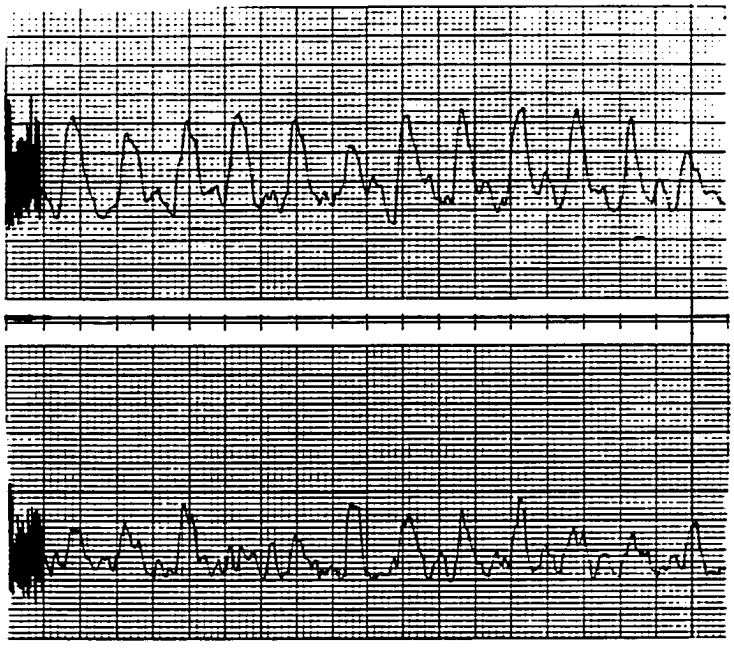

Figure 5.8 The Doppler signals recorded from normal common carotid artery at range c.

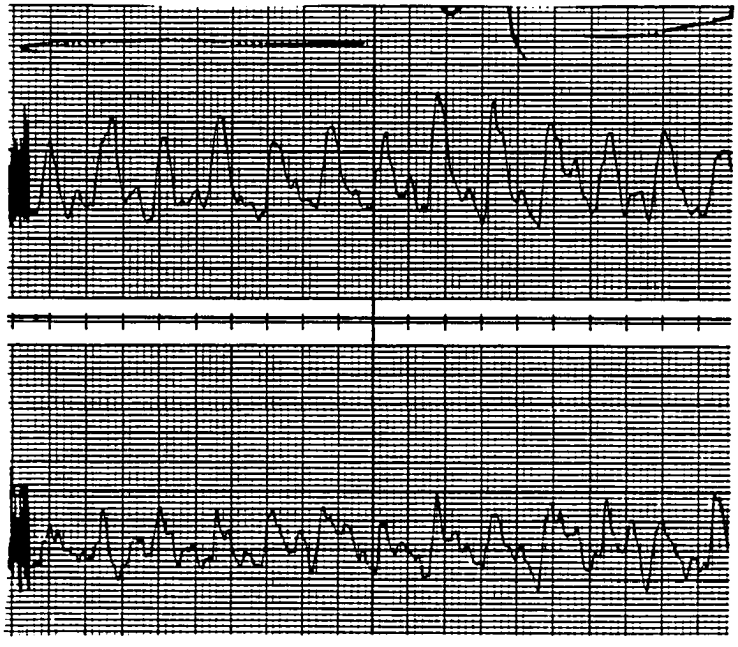

Figure 5.9 The Doppler signals recorded from stenotic (25 to 35 percent) common carotid artery at range c.

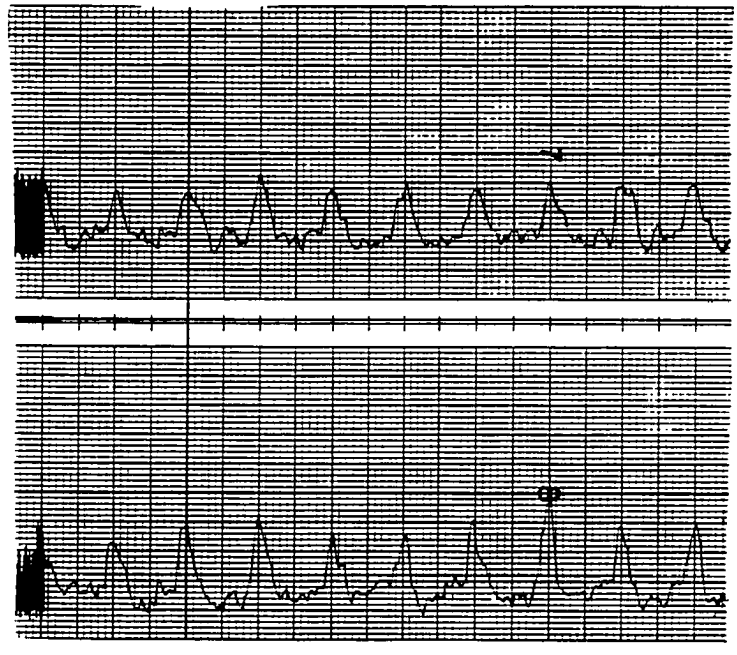

Figure 5.10 The Doppler signals recorded from stenotic (45 to 55 percent) common carotid artery at range c.

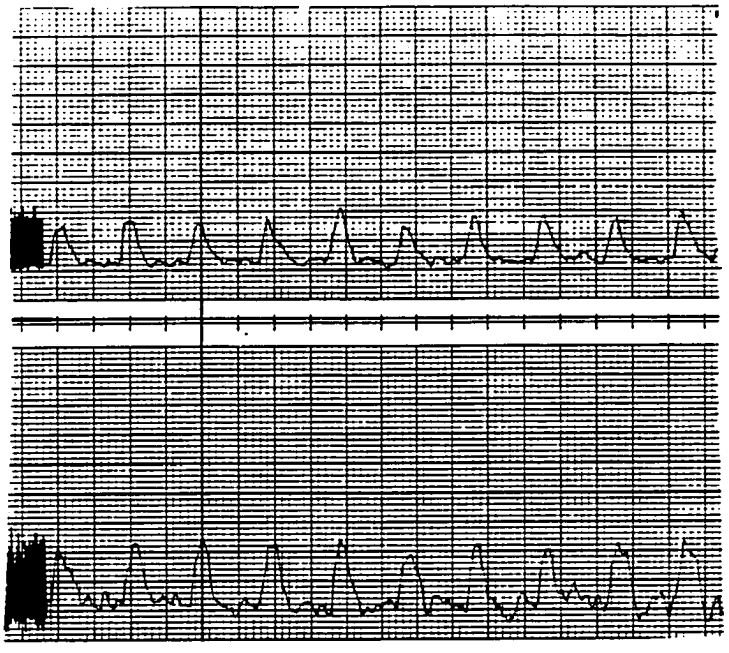

Figure 5.11 The Doppler signals recorded from normal common carotid artery at the center (heartbeats=150 bpm)

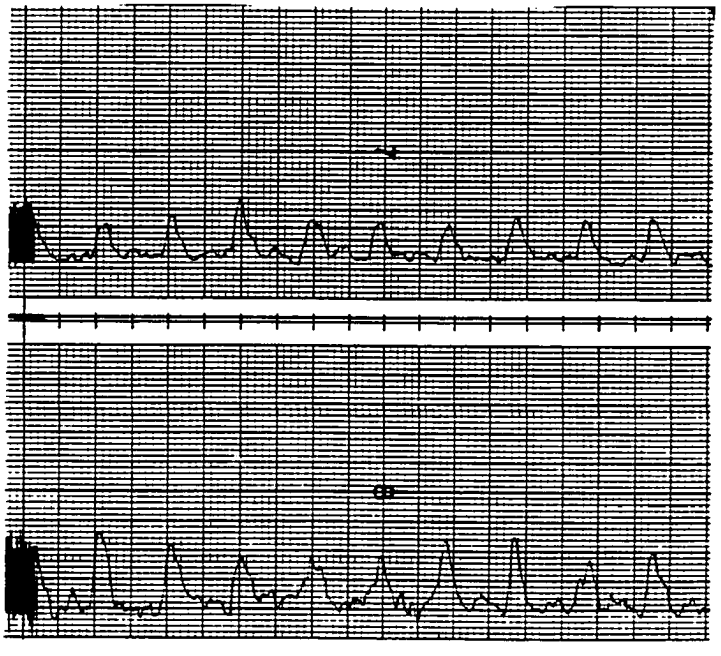

Figure 5.12 The Doppler signals recorded from stenotic (25 to 35 percent) common carotid artery at the center (heartbeats = 150 bpm).

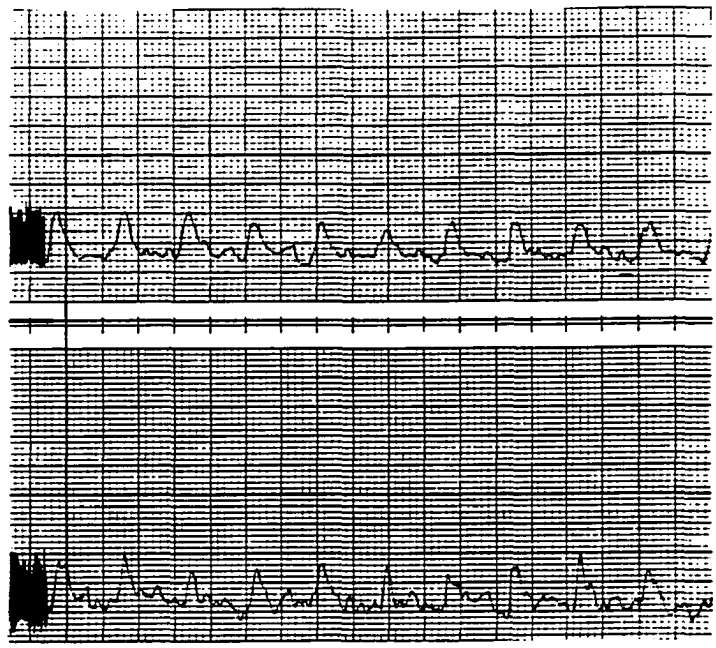

Figure 5.13 The Doppler signals recorded from stenotic (45 to 55 percent) common carotid artery at the center (heartbeats = 150 bpm).

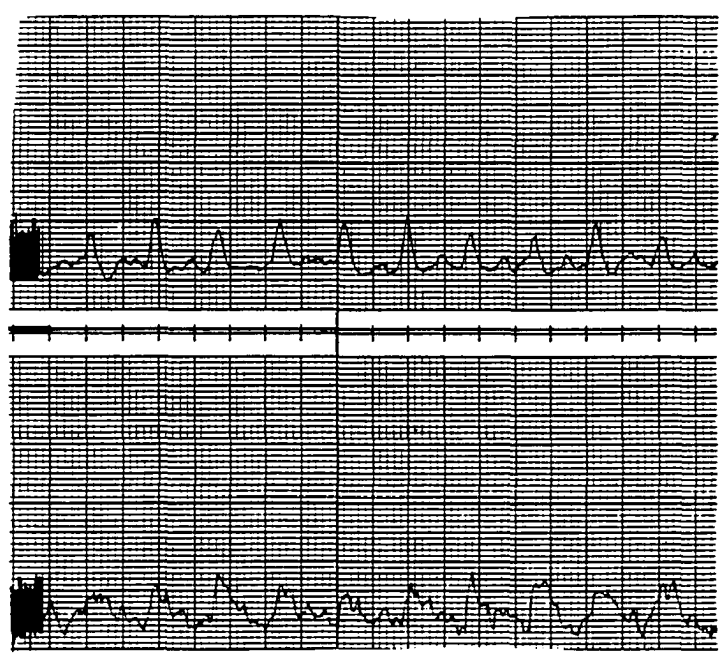

Figure 5.14 The Doppler signals recorded from stenotic (85 to 95 percent) common carotid artery at the center (heartbeats = 150 bpm).

and the results are presented in Table 5.2. The mean Doppler angle in this experiment is 49.58° with a normalized error of 2 percent to 3 percent. As expected, because of the increase in the pressure of the blood flow, the volume rate has declined by a factor of almost 3 in normal diameter of the common carotid artery compared with the normal diameter in the previous experiment (normal heartbeat).

Table 5.2

The Doppler Angle, Blood Flow Velocity, and Blood Flow Volume Rate for Reduced Heartbeats (150 bpm)

Doppler Angle (θ) (degrees)	Velocity (mm/sec)	Diameter (mm)	Volume Rate (ml/min)
47.87	94.79	3.0	40.26
49.68	88.60	2.0	16.72
50.98	90.18	1.0	4.26
49.81	67.63	0.5	0.80

5.2.1.3 Increased Heartbeats (190 bpm)

To investigate the effect of lower pressure and increase in the heartbeat on the Doppler angle and blood flow volume rate, nitroprusside was injected. The number of heartbeats from the chart recorded was measured at 190 bpm. The data taken from the center point of the artery is recorded. The output Doppler signals are shown in Figures 5.15, 5.16 and 5.17. These signals seem to be rather unstable in different periods of cardiac cycles, which is due to sudden changes in heartbeats. The Doppler angle, blood flow

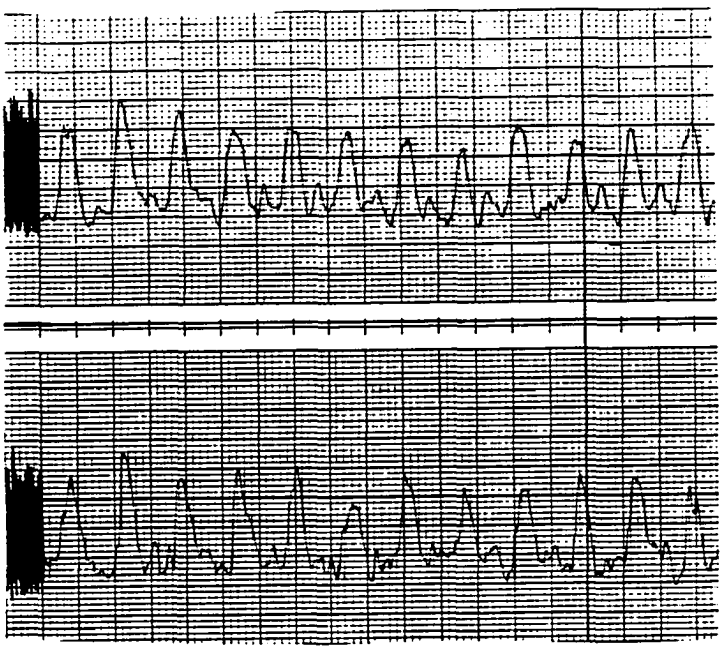

Figure 5.15 The Doppler signals recorded from normal common carotid artery at the center (heartbeats = 190 bpm).

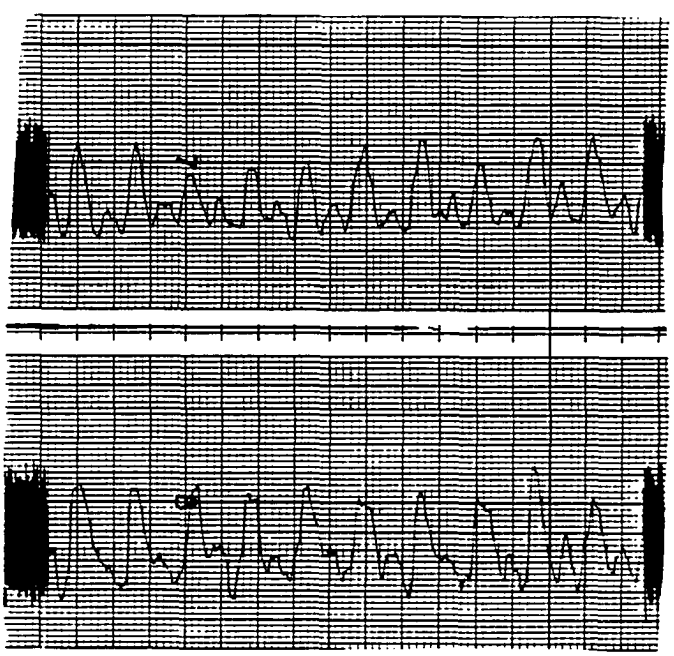

Figure 5.16 The Doppler signals recorded from stenotic (25 to 35 percent) common carotid artery at the center (heartbeats = 190 bpm).

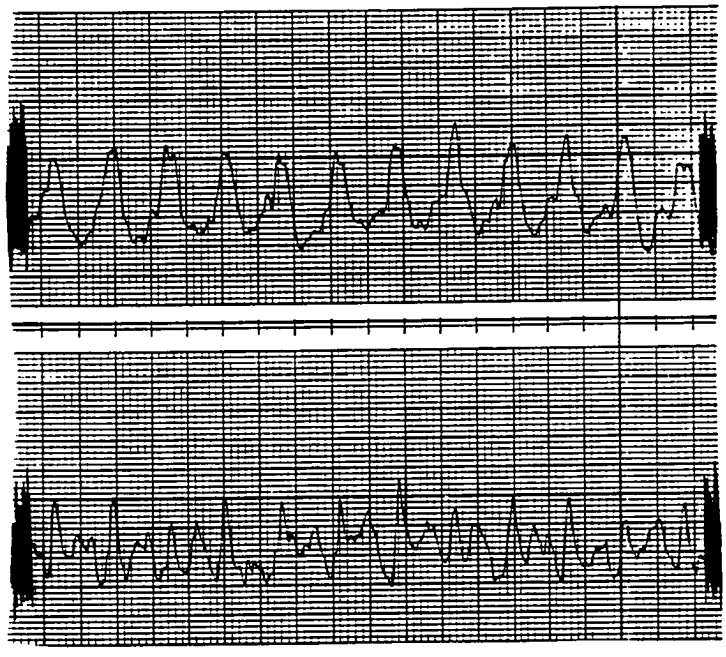

Figure 5.17 The Doppler signals recorded from stenotic (45 to 55 percent) common carotid artery at the center (heartbeats = 190 bpm).

velocity and blood flow volume rate are calculated. The results are presented in Table 5.3 The mean Doppler angle in this experiment is 48.9, with normalized error of 4 percent to 4.9 percent. As expected, because the pressure in the blood flow is lower, the volume rate has increased dramatically compared with the previous setup (from 40.26° to 62.98° in normal condition of the artery).

Table 5.3

The Doppler angle, Blood Flow Velocity, and Blood Flow Volume Rate for Higher Number of Heartbeats (190 bpm).

Doppler Angle (θ) (degrees)	Velocity (mm/sec)	Diameter (mm)	Volume Rate (ml/min)
51.32	148.30	3.0	62.98
46.83	147.59	2.0	27.86
48.57	142.31	1.0	6.72

The data presented in this experiment show that the DTP-PU model is an effective tool for analysis of the Doppler signals. Comparison among the results indicate an agreement for Doppler Angle in different conditions of a particular experiment. Overall results show the the Doppler angle is about 50° in almost all the tests conducted in this experiment. Another result is the ability of the device in detecting the blood flow under different conditions. This was demonstrated by increasing or decreasing the pressure of the blood using different drugs. It was shown that if pressure

increased, the blood flow volume rate decreased and vice versa. The Doppler angle remained mostly stable unless there was a dramatic change in the diameter of the artery.

5.3 In-Vitro Experiments

To further evaluate the performance of dual transducer pulsed-Doppler ultrasound and to verify the results of in-vivo experiments, an in-vitro perfusion bath as shown in Figure 4.1 was constructed. Isolated arteries from donor dogs and rabbits were obtained from the femoral, carotid or terminal aortic root and perfused with an artificial blood particulate suspension in water. The volumetric flow was measured by the classical "bucket and stopwatch" technique and compared with the digital calculations obtained on the PDP11/34. Three different experiments were performed using three different arteries. For each segment of each experiment, 8 to 15 sets of data were recorded and were averaged to calculate the Doppler angle, blood flow velocity and blood flow volume rate. To verify the results for each experiment, the volume rates were measured and compared with the calculated value from the experiments.

5.3.1 Calculation of the Velocity and Volume Rate (femoral artery)

In this experiment, an isolated artery from a donor dog was obtained from the femoral artery. The main goal of

this study is to verify the results obtained in in-vivo experiments for calculating the Doppler angle. The tool for verification is measured volume rate which is compared with calculated volume rate from different tests conducted in this experiment.

Figures 5.18, 5.19, 5.20, and 5.21 show the output Doppler signals recorded from a normal femoral artery for different volume rates. The change in volume rate is reflected in the amplitude of the Doppler signals. The diameter of the artery in all normal cases is 2.75 mm. The Doppler angle, blood flow velocity and blood flow volume rate are calculated. The results are presented in Table 5.4. Figures 5.22, 5.23, 5.24 and 5.25 show the output Doppler signal for the stenotic artery (33 percent and 50 percent). Again, the Doppler angle, blood flow velocity and blood flow volume rates are calculated. The results are presented in Table 5.5.

The mean value of Doppler angle for the normal femoral artery is 63.8° with normalized error ranging from 2 percent to 3.3 percent. The volume rate at each setup is different and depends on the conditions of that particular test. However, the normalized error in calculation of volume rate varies from 2.5 percent to 5.9 percent.

The mean value of the Doppler signal for stenotic (33 percent) femoral artery is 58.33, with normalized error

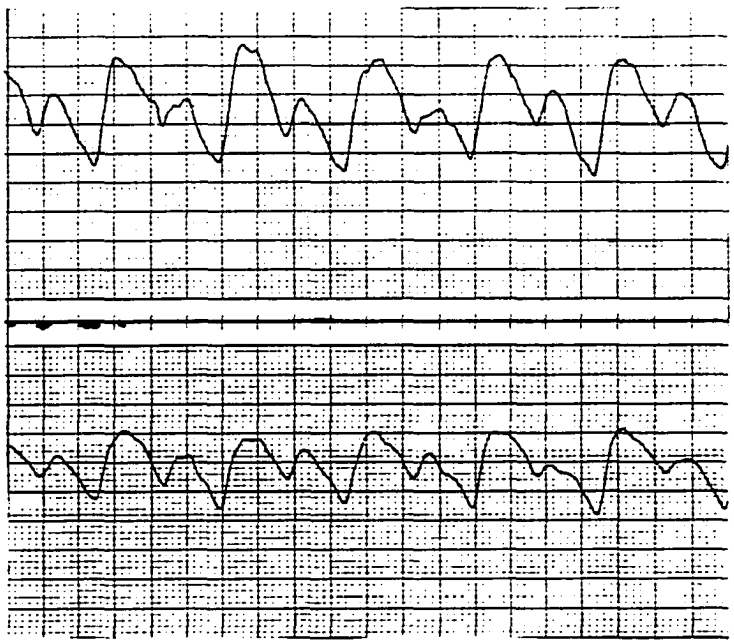

Figure 5.18 The Doppler signals recorded from normal femoral artery for Q_m = 94 ml/min.

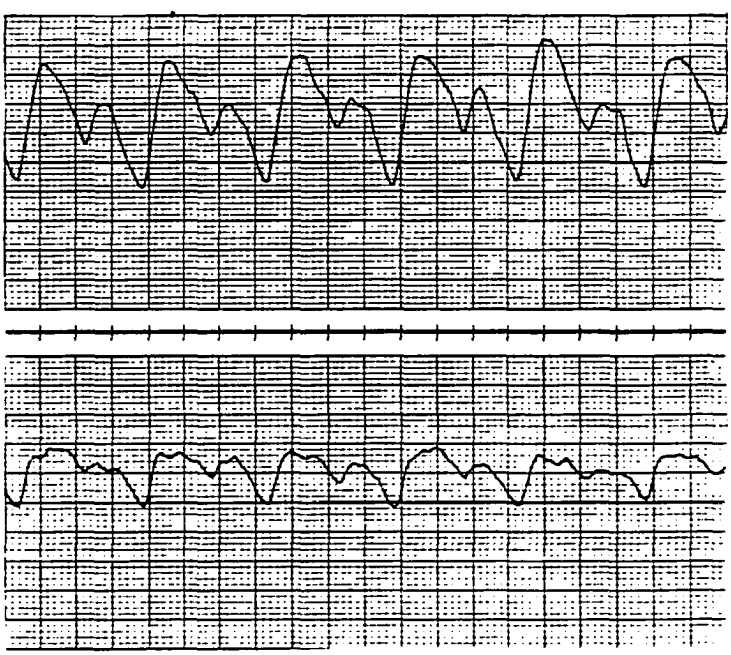

Figure 5.19 The Doppler signals recorded from normal femoral artery for Q_m = 85 ml/min.

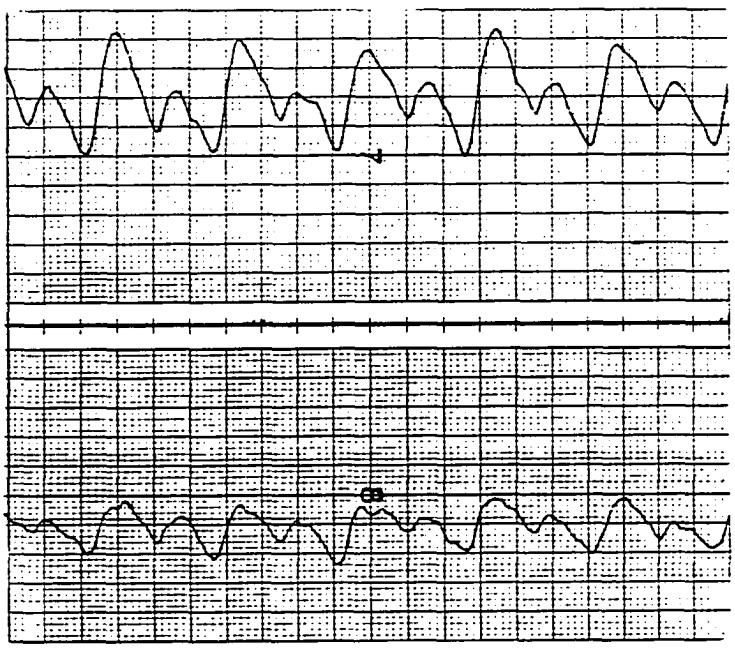

Figure 5.20 The Doppler signals recorded from normal femoral artery for Q_m = 95 ml/min.

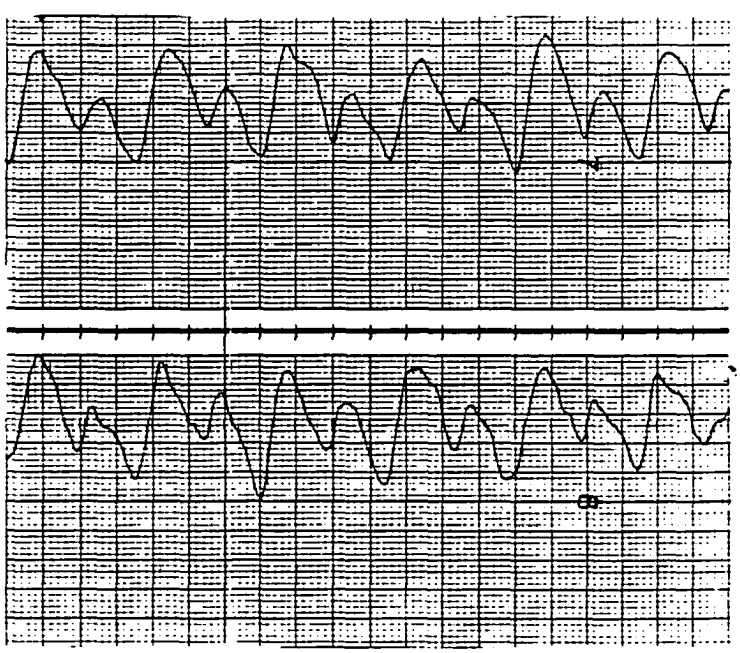

Figure 5.21 The Doppler signals recorded from normal femoral artery for Q_m = 95 ml/min.

Table 5.4

The Doppler Angle, Measured and Calculated Volume Rate at Different Ranges for Normal Femoral Artery.

Test Number	Doppler Angle (θ) (degrees)	Velocity (mm/sec)	Diameter (mm)	Q_m (ml/min)	Q_{cal} (ml/min)
1	62.23°	255.76	2.75	94	91
2	62.62°	244.986	2.75	85	87.166
3	64.43°	282.79	2.75	95	100.61
4	65.95°	319.63	2.75	108	113.22

Table 5.5

The Doppler Angle, Measured and Calculated Volume Rate at Different Ranges for Different Degrees of Stenosis for the Femoral Artery.

Test Number	Doppler Angle (θ) (degrees)	Velocity (mm/sec)	Diameter (mm)	Q_m (ml/min)	Q_{cal} (ml/min)
1 (33%)	59.3°	219.75	1.83	40	34.81
2 (33%)	57.5°	211.43	1.83	41	33.46
3 (33%)	58.19°	205.11	1.83	41	32.46
4 (50%)	64.7°	112.5	1.375	17	10.072

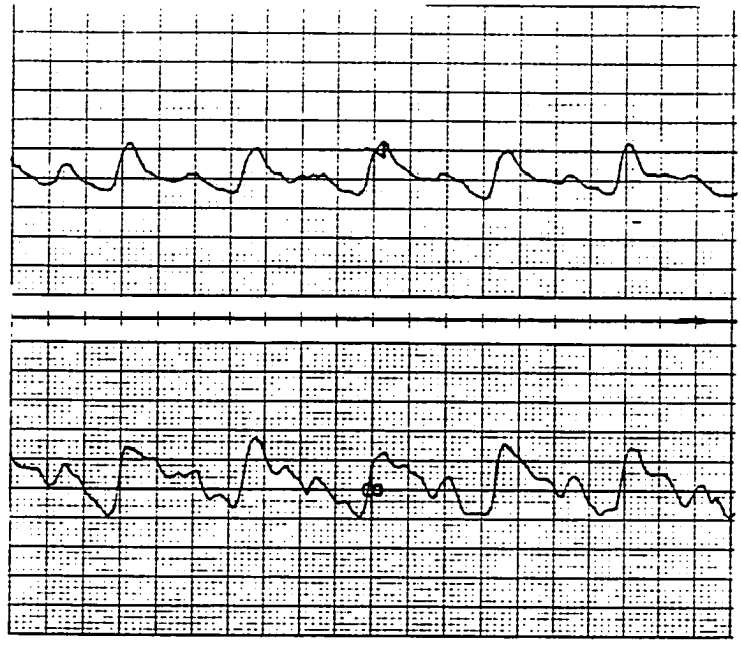

Figure 5.22 The Doppler signals recorded from stenotic (33 percent) femoral artery at 1/3 range (Q_m = 40 ml/min).

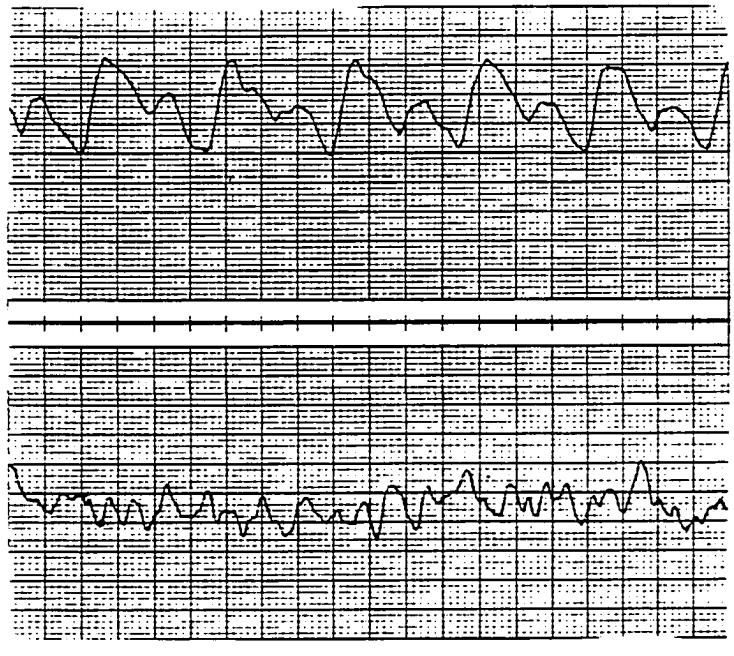

Figure 5.23 The Doppler signals recorded from stenotic (33 percent) femorai artery at 2/3 range (Q_m=41 ml/min)

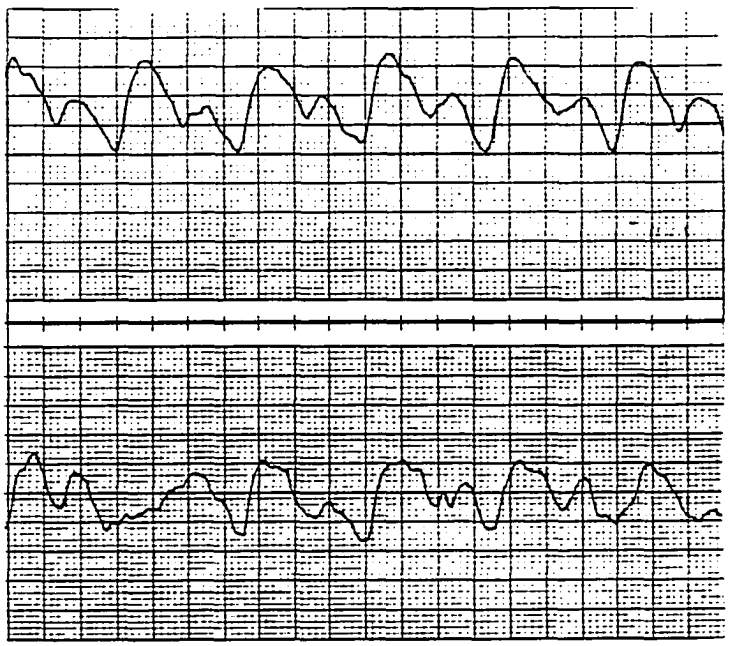

Figure 5.24 The Doppler signals recorded from stenotic (33 percent) femoral artery at 1/2 range (Q_m=41 ml/min.

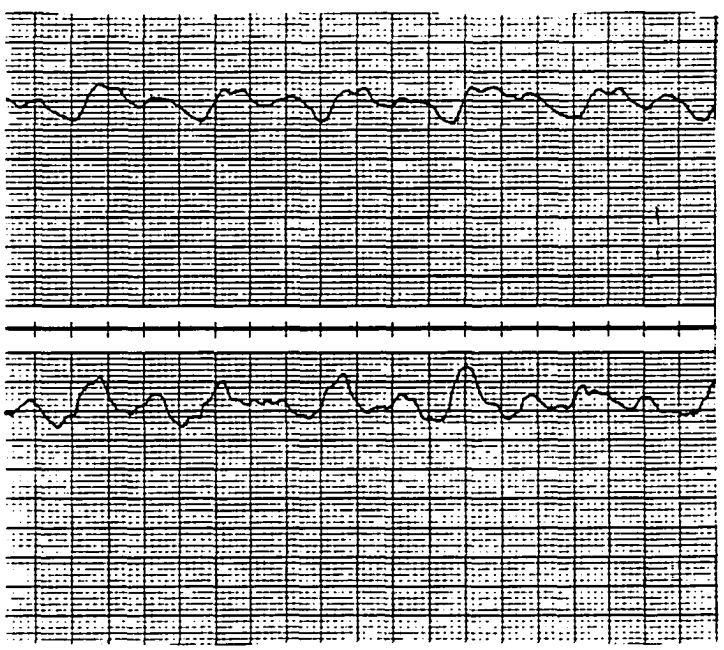

Figure 5.25 The Doppler signals recorded from stenotic (50 percent) femoral artery at 1/3 range (Q_m=17 ml/min.

ranging from 1.4 percent to 1.6 percent. for 50 percent stenosis, the Doppler angle is 64.7°. From this experiment and other similar experiments, we concluded that the DTP-DU model is a reliable device to calculate the Doppler angle. The Doppler angle was consistently very close to normal and dilated or constricted arteries under the same conditions. In calculating the blood flow volume rate, the standard formula ($Q = v \cdot A$) can be used for normal arteries. For constricted arteries, however, this method is not reliable enough and other methods, such as velocity profile (for laminar flow) and shear stress (for turbulent flow) can be used. In the next section, velocity profile method is investigated.

5.3.2 Calculation of Volume Rate from Velocity Profile (femoral artery)

As mentioned in the previous section, an alternative to calculate blood flow volume rate is using the flow velocity profile. In this experiment, the femoral artery from a donor dog is used, and by scanning through the diameter using range control, the velocity profile is produced.

The procedure to produce the velocity profile is as follows:

1) By scanning through the diameter, 3 to 10 sets of data for each range from the near wall to the far wall is recorded.

2) The Doppler angle is calculated from the center point in the artery.
3) Blood flow velocity at each particular range is calculated and is averaged to obtain the velocity value at that particular range.
4) Average blood flow velocity for the velocity profile from wall to wall is calculated.
5) Diameter of the artery is measured (either by micrometer or by using output range of the machine: in this case, 1 volt per centimeter) and along with the diameter, the area is calculated.
6) Blood flow volume rate is calculated multiplying average blood flow velocity and area.

In the above procedure, actually, area under the velocity profile is calculated. If there is more radical changes in the velocity profile, other methods of calculating integrals such as curve fitting or Simpson's role might be used.

The diameter of the femoral artery under investigation is 3 mm. Using the procedure mentioned earlier, four normal and two stenotic arteries are investigated. For each normal and stenosis case, the volume rate is measured at different ranges and then averaged to obtain a more accurate value for measured volume rate for comparison with calculated volume rate. Figures 5.26, 5,27, 5.28, 5.29, 5.30, 5.31, and 5.32 show a complete set of Doppler signals, recorded at

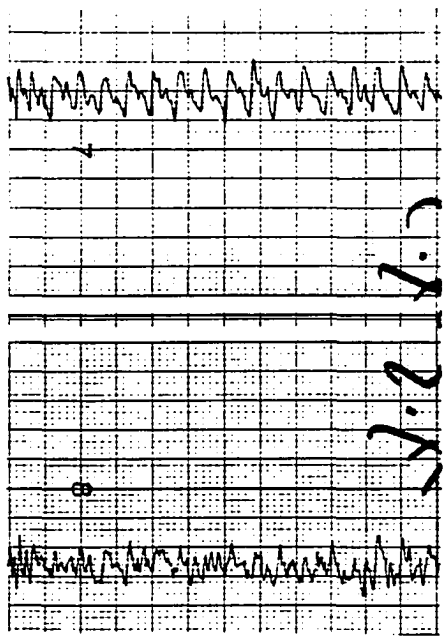

Figure 5.26 The Doppler signals recorded from normal femoral artery at a range close to the near wall (1st range).

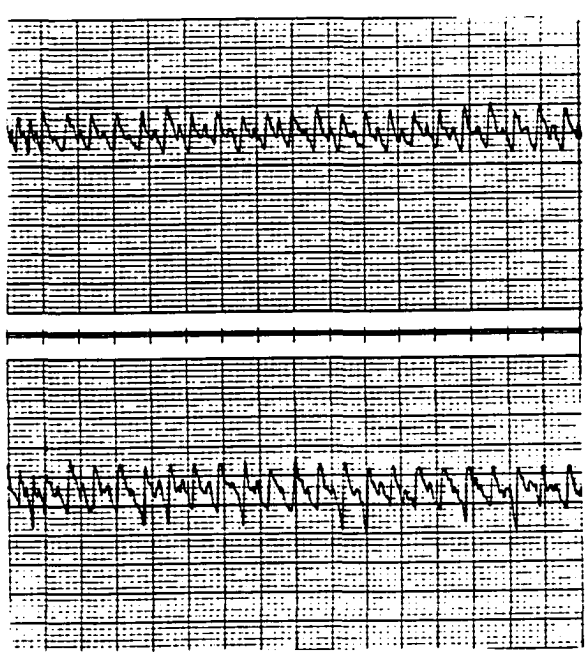

Figure 5.27 The Doppler signals recorded from normal femoral artery (2nd range).

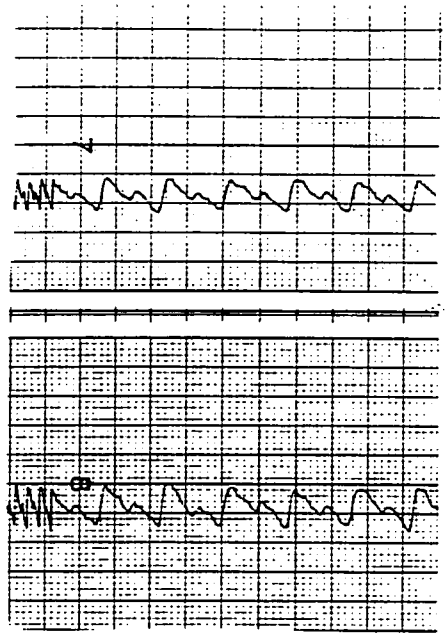

Figure 5.28 The Doppler signals recorded from normal femoral artery (3rd range).

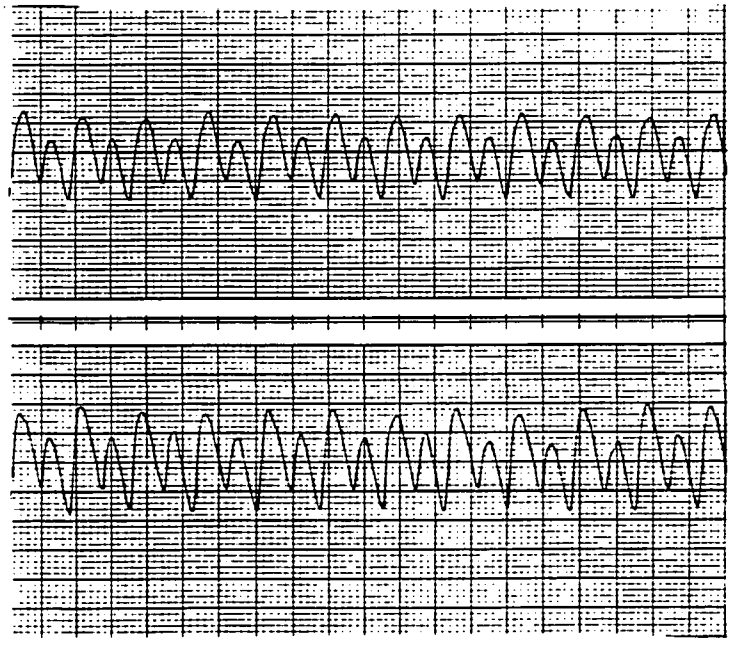

Figure 5.29 The Doppler signals recorded from normal femoral artery at the center.

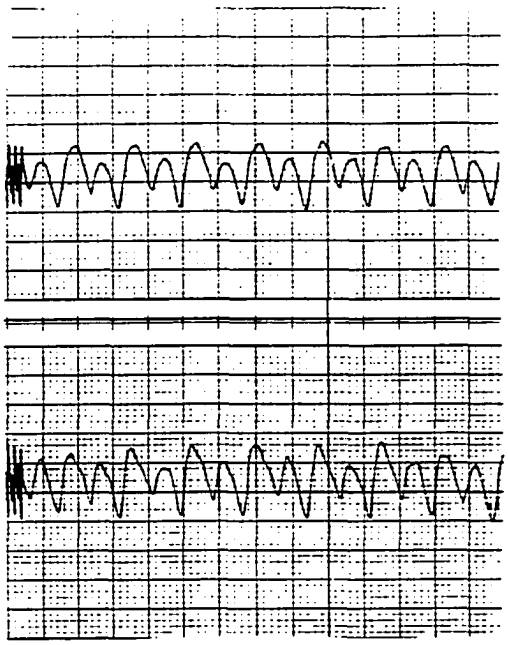

Figure 5.30 The Doppler signals recorded from normal femoral artery (6th range).

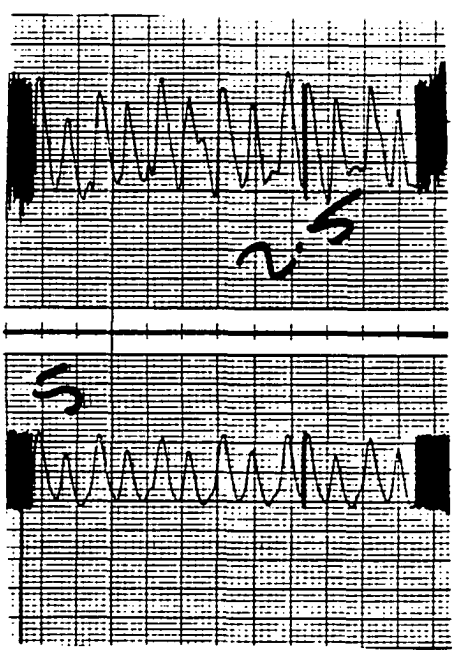

Figure 5.31 The Doppler signals recorded from normal femoral artery (7th range).

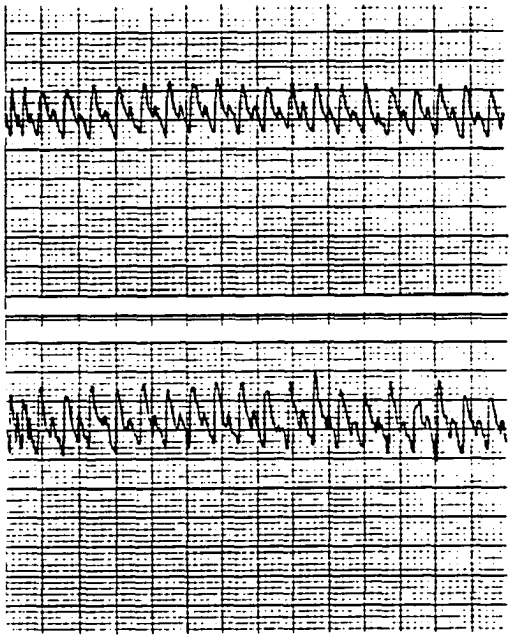

Figure 5.32 The Doppler signals recorded from normal femoral artery at a point close to far wall (8th range).

different ranges. Figure 5.33a shows the velocity profile for the normal case. The results of normal cases are presented in Table 5.6. As can be seen from the results, the normalized error is ranging from 4 percent to 5 percent comparing measured and calculated volume rate. Figure 5.33b shows the velocity profile for one of the cases of stenosis (33 percent to 35 percent). The results of stenosis cases are presented in Table 5.7. The results show a higher percentage of error compared with normal cases. The following reasons contribute to this problem:

In our experiments, we use real tissues to have more realistic results. The tissues are mostly from dogs which their femoral, carotid and aorta arteries are smaller than human arteries. The stenosis developed mostly in humans with an age of thirty years and over. In this category of human age, arteries are fully developed. The diameter of the femoral artery is between 6 to 8 mm, for the common carotid artery is between 6 to 9 mm, and for the aortic root is between 6 to 10 mm. Therefore, scanning through arteries of a human is much easier and more points for a particular velocity profile can be recorded. Therefore, more accurate results as for the normal case can be extracted. Despite this limitation, the Doppler angle is found in agreement in different tests (normal and stenosis).

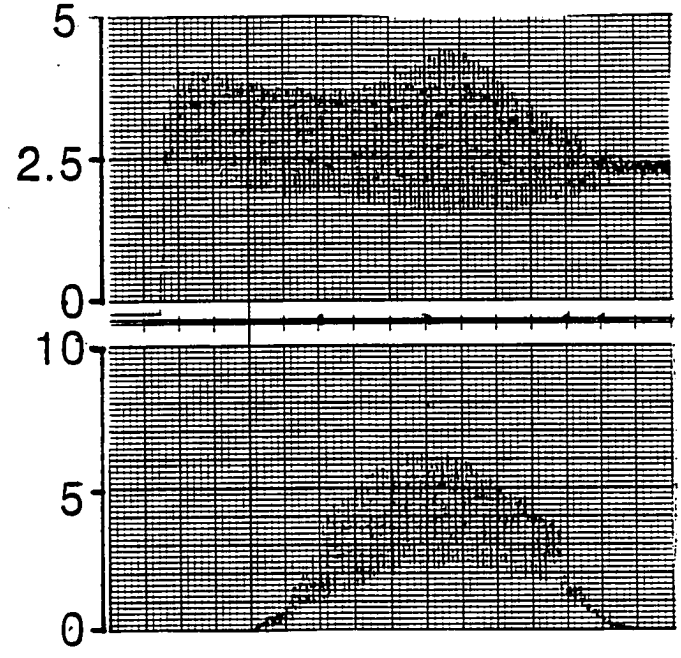

Figure 5.33a The velocity profile for normal femoral artery.

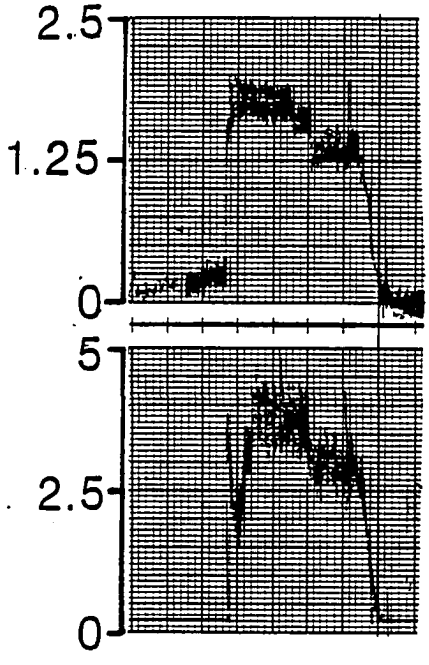

Figure 5.33b The velocity profile for stenotic (33 to 35 percent) femoral artery.

Table 5.6

The Doppler Angle, Blood Flow Volume Rate and E% for Normal Femoral Artery.

Test Number		Doppler Angle (θ) (degrees)	Measured Volume Rate(Q_m)	Calculated Volume Rate(Q_{cal})	E%
a	1	67.17°	98	101.19	4%
a	2	67.20°	96	101.26	4%
b	3	64.95°	87	90.757	5%
b	4	64.49°	83	71.71	5%

Table 5.7

The Doppler Angle, Blood Flow Volume Rate and E% for Stenotic Femoral Artery (33 percent to 35 percent).

Test Number	Doppler Angle (θ) (degrees)	Measured Volume Rate(Q_m)	Calculated Volume Rate(Q_{cal})	e%
1	63.46	34	36.96	8%
2	64.537	34	38.96	12%

5.3.3 Determination of Statistical Parameters at Flow Volume Rate (carotid artery)

In order to complete our investigations in the area of calculating Doppler angle and blood flow volume rate, the present experiment is conducted. The goals of this experiment are to calculate volume rate in various situations such as different speeds of the pulsatile pump and different sizes of tubing, and to determine statistical parameters such as mean, standard deviation and variance. The procedure to accomplish the above goals is as follows:

1) Set the pulsatile pump speed at the lowest possible rate.
2) Measure carefully the volume rate (3 to 4 times) at the start of each triggering and also at the end of each test and calculate the average value of measured volume rate.
3) Display the output Doppler signals on the chart recorder and mark carefully the range which is used for displaying the signals.
4) Trigger the pulsed-Doppler ultrasound instrument and computer.
5) Record between 8 to 10 sets of data for each triggering.
6) Change the speed of the pulsatile pump and tubing to have different volume rate and repeat points

2 to 5 of the procedure for each new setup.

7) Measure the diameter of the artery a few times throughout the experiment.

To determine the statistical parameters, the following calculations are performed:

1) Calculate the cross sectional area of the artery under investigation using the measured diameter.
2) Calculate the Doppler angle using the output Doppler signals.
3) Calculate average velocity and velocity components for each transducer using the calculated Doppler angle.
4) Calculate the volume rate from the velocity for each time that the trigger was performed.
5) Calculate average volume rate, standard deviation and variance for each setup and compare the results with the measured volume rate.

The artery used in this experiment is isolated carotid from a donor rabbit with the diameter of 2.7 mm. The Doppler signals recorded from various tests performed in this experiment, are shown in Figures 5.34, 5.35, 5.36, 5.37, 5.38, 5.39, 5.40, 5.41, 5.42 and 5.43. The effects of different volume rates caused by changes in the size of the tubing or speed of the pulsatile pump are reflected on the amplitude of the Doppler signals. The numerical results are

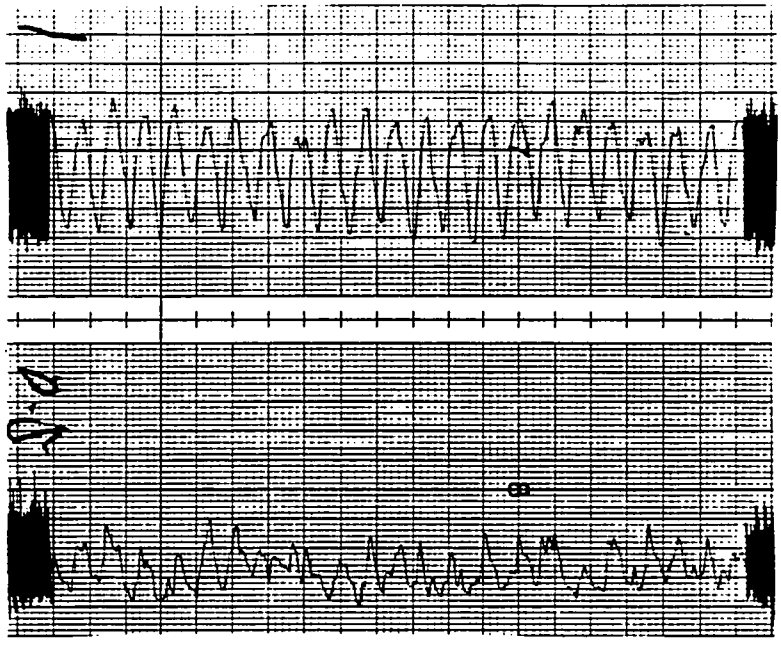

Figure 5.34 The Doppler signals recorded from normal carotid artery for Q_m = 23.5 ml/min (test C).

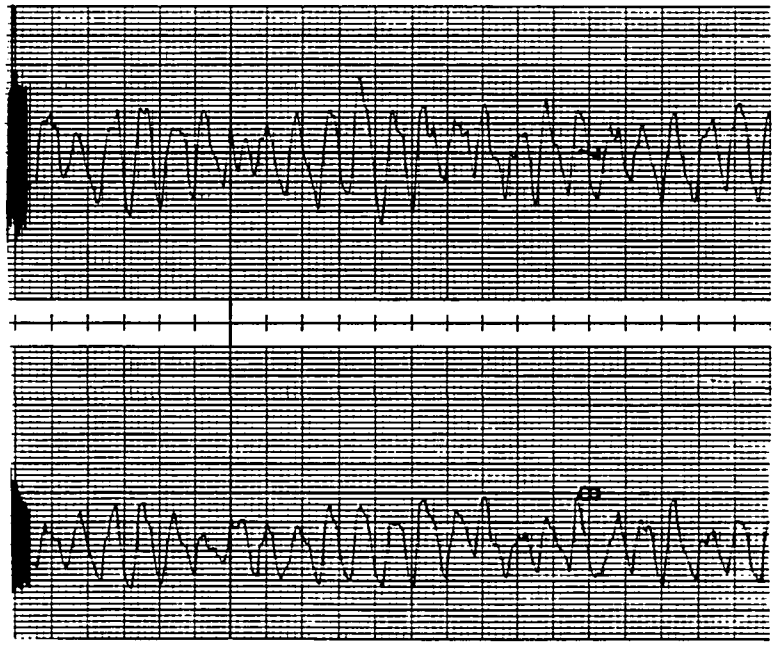

Figure 5.35 The Doppler signals recorded from normal carotid artery for Q_m = 35 ml/min (test J).

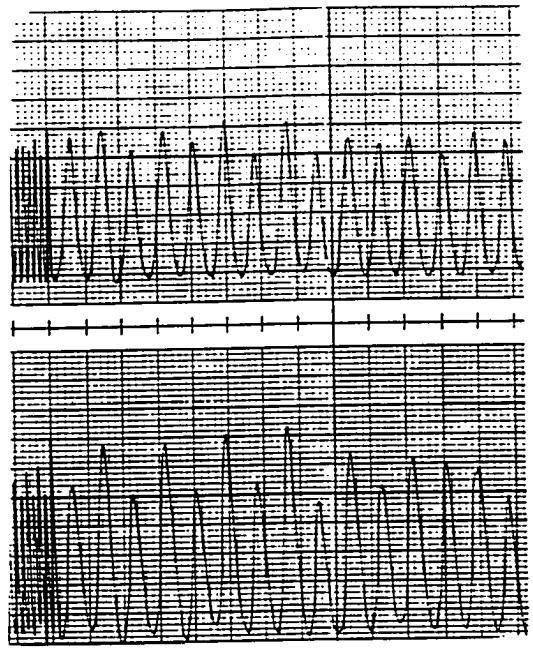

Figure 5.36 The Doppler signals recorded from normal carotid artery for Q_m = 58 ml/min (test N)

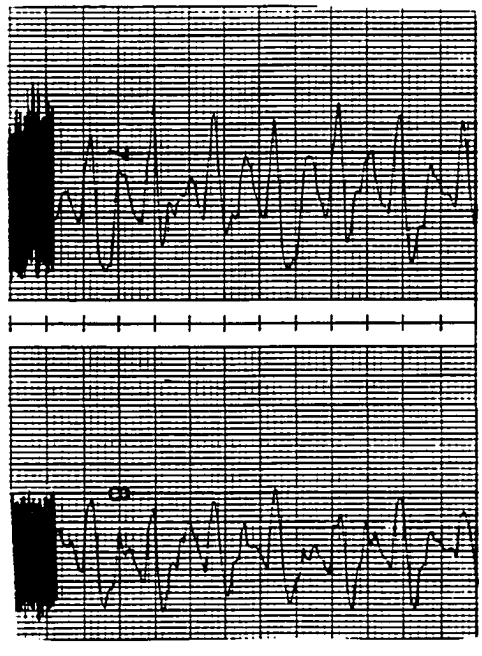

Figure 5.37 The Doppler signals recorded from normal carotid artery for Q_m = 59 ml/min (test H).

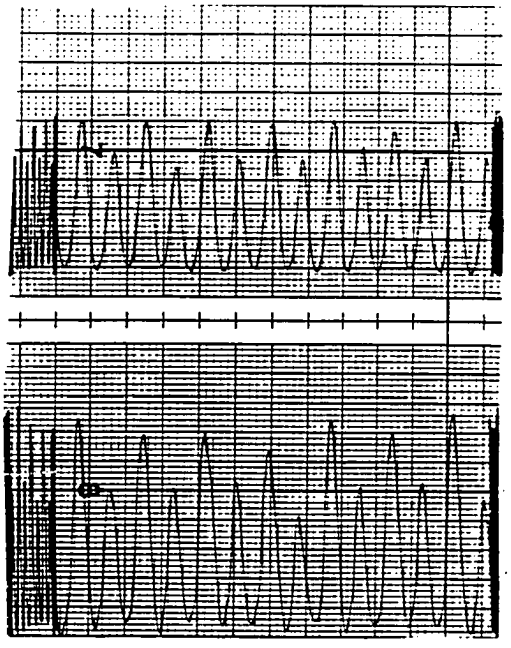

Figure 5.38 The Doppler signals recorded from normal carotid artery for Q_m= 62.5 ml/min (test P).

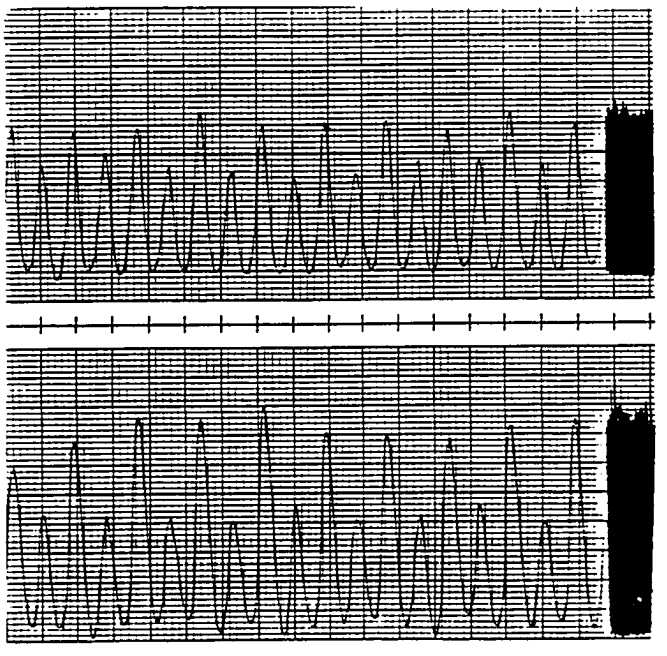

Figure 5.39 The Doppler signals recorded from normal carotid artery for Q_m= 65 ml/min (test R).

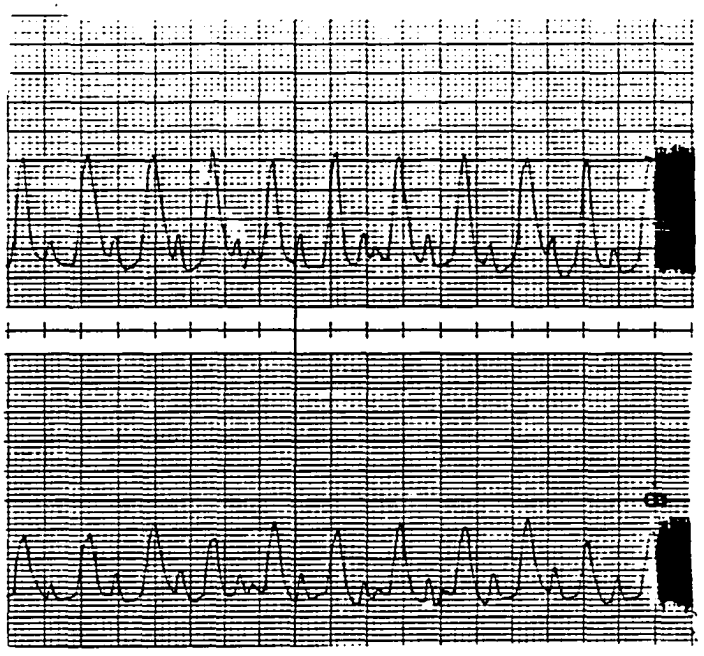

Figure 5.40 The Doppler signals recorded from normal carotid artery for Q_m= 83.75 ml/min (test E).

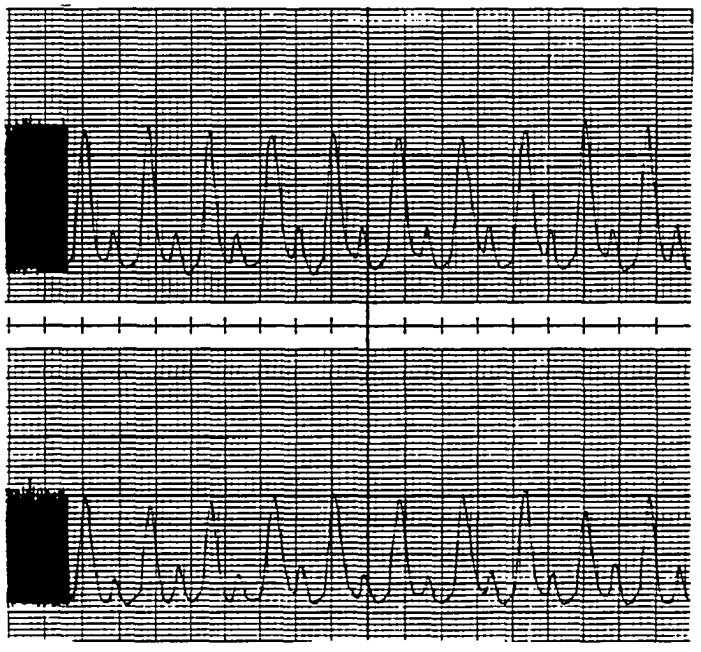

Figure 5.41 The Doppler signals recorded from normal carotid artery for Q_m= 86 ml/min (test D).

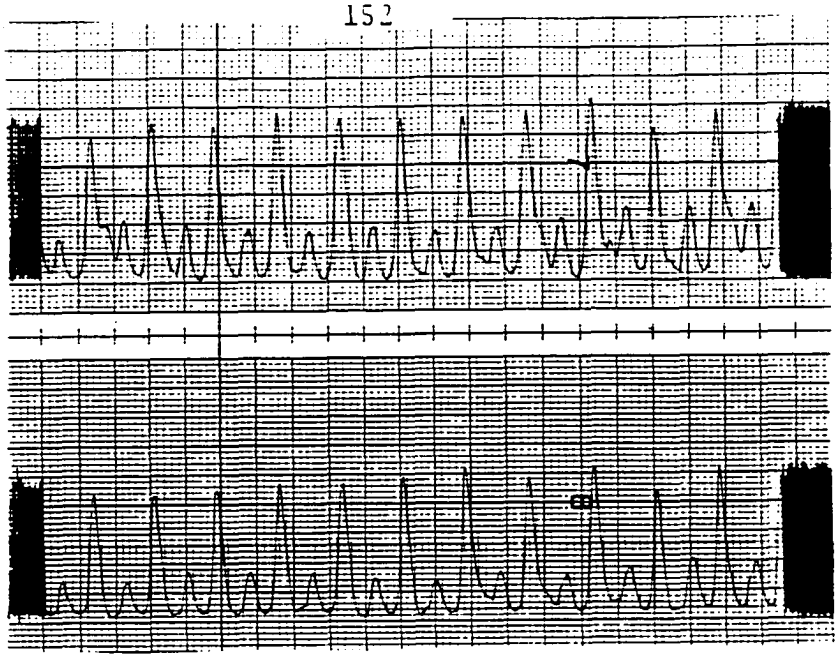

Figure 5.42 The Doppler signals recorded from normal carotid artery for Q_m= 93.75 ml/min (test C).

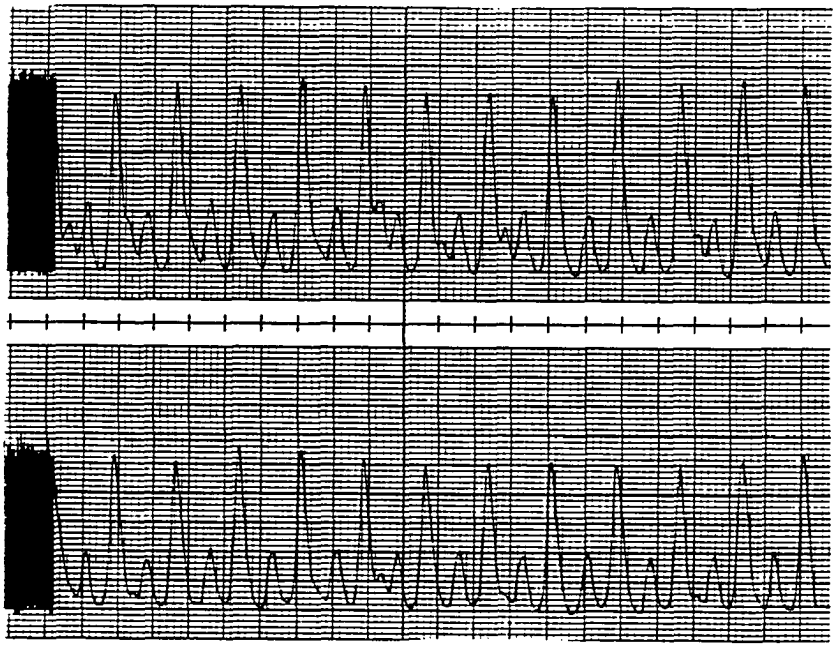

Figure 5.43 The Doppler signals recorded from normal carotid artery for Q_m= 95.5 ml/min (test I).

presented in Appendix A, where the parameters are as follows:

θ Doppler angle

Q volume rate

$\bar{v}$ averaged velocity

A_1/B_1 ratio of maximum to minimum point

bpm number of beats per minute

Pts number of points in each triggering

The overall results of the experiment are presented in Table 5.8. In this table Q_m is mean measured volume rate, Q_{cal} is mean calculated volume rate, σ, is standard deviation. A plot presenting these statistical values is depicted in Figure 5.44. The average percentage of error is 4.38 percent, ranging from 0.03 percent to 12.42 percent. Most of the results are in agreement except for two tests (H and N). These two tests are taken at the time where there is sudden change in the speed of the pulsatile pump. Since it takes a few minutes for flow to become steady and fully developed, the disagreement might be the result of unsteady flow.

Among 26 different tests which were performed for evaluation of the dual transducer pulsed-Doppler ultrasound model, only four of them gave inconsistant results and the other 22 tests were in agreement. In summarizing the results of these experiments we have found that the dual transducer (DTP-DU) system provides greater accuracy in the measurement of blood flow velocity compared with the

Table 5.8

The Doppler Angle, Measured Volume Rate, Mean Value of Calculated Volume Rate and Standard Deviation of Calculated Volume Rate.

Test Number	Measured Q (Q_m)	Calculated Q (Q_{cal})	Standard Deviation(σ)	$Q_{cal}+\sigma$	$Q_{cal}-\sigma$	Doppler Angle(θ)
F22C	94.5-93=93.75	93.783	1.858	95.641	91.927	43.81
F22D	86	90.733	0.846	91.579	89.887	45.00
F22E	83.5-84=83.75	89.005	1.176	90.181	87.829	45.55
F22H	58-60=59	53.152	1.563	54.715	51.589	42.98
F22I	95-96=95.5	94.131	1.663	45.794	92.468	44.30
F22J	35	33.772	0.987	34.759	32.785	40.90
F22K	35	34.483	1.278	35.761	33.205	43.962
F22L	23.5	23.274	1.013	24.287	22.261	15.984
F22N	58	50.793	2.05	52.843	48.743	44.69
F22P	62.5	62.726	2.474	65.2	60.252	46.013
F22R	65	60.765	2.001	62.766	58.764	46.039
F22S	65	60.765	2.001	62.766	58.764	46.039
Dec 83	70	71.247	3.682	74.929	67.565	32.55
Dec 87	83	81.709	1.299	83.008	80.410	25.44

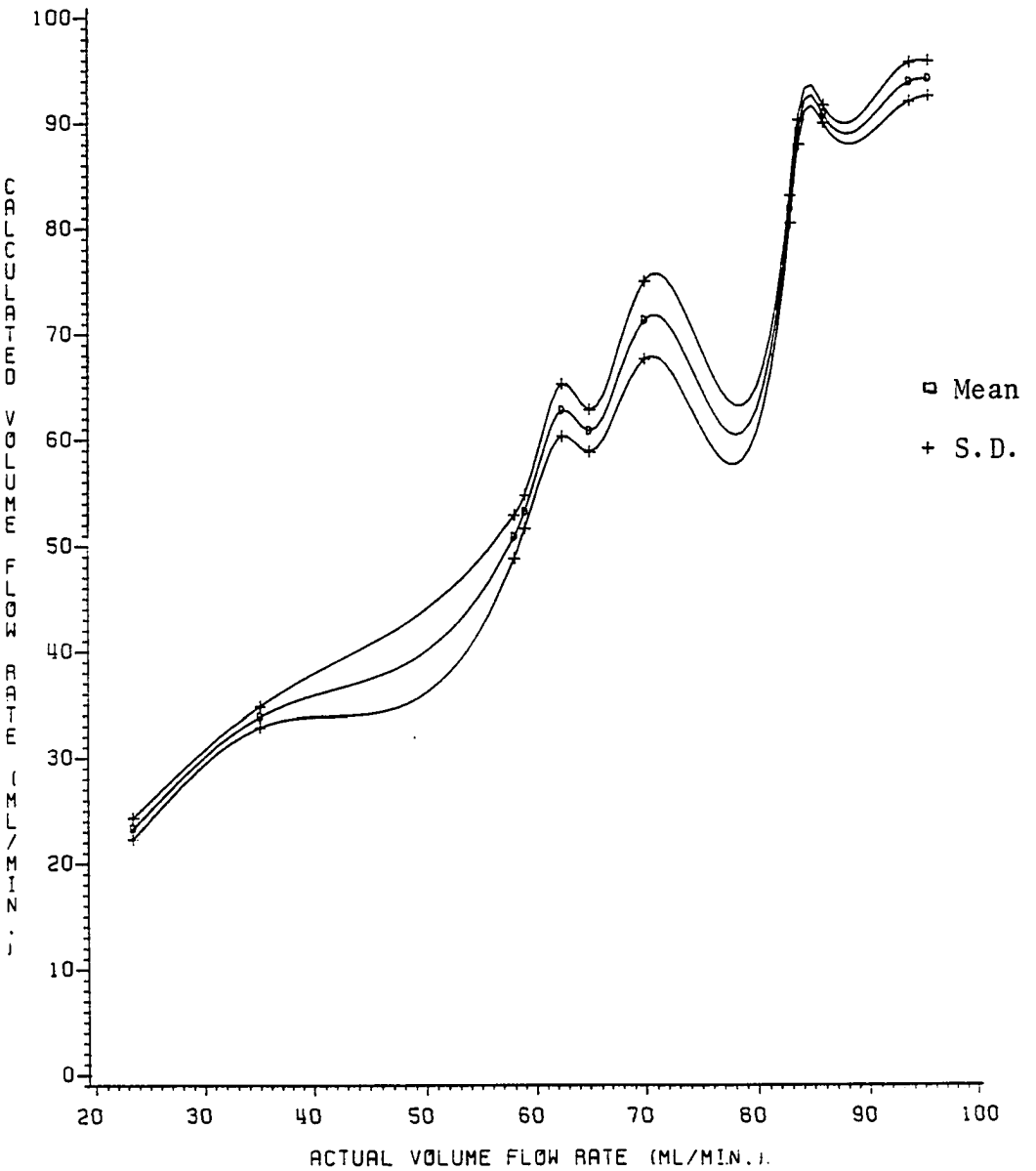

Figure 5.44 The mean and standard deviation of calculated volume rate versus measured volume rate.

conventional single transducer (STP-DU) systems.

5.3.4 Determining Turbulent Flow Characteristics (carotid artery)

The purpose of this experiment is to explore the effect of the stenosis upon the characteristics of turbulent flow. The measurement of velocity profiles and turbulent shear stresses are obtained using the dual-transducer pulsed-Doppler system. The experiment is performed using a turbulence-producing orifice 1 mm diameter and approximately 5 mm axial length, which is inserted at the distal end of the artery as illustrated in Figure 5.45. Turbulent flow

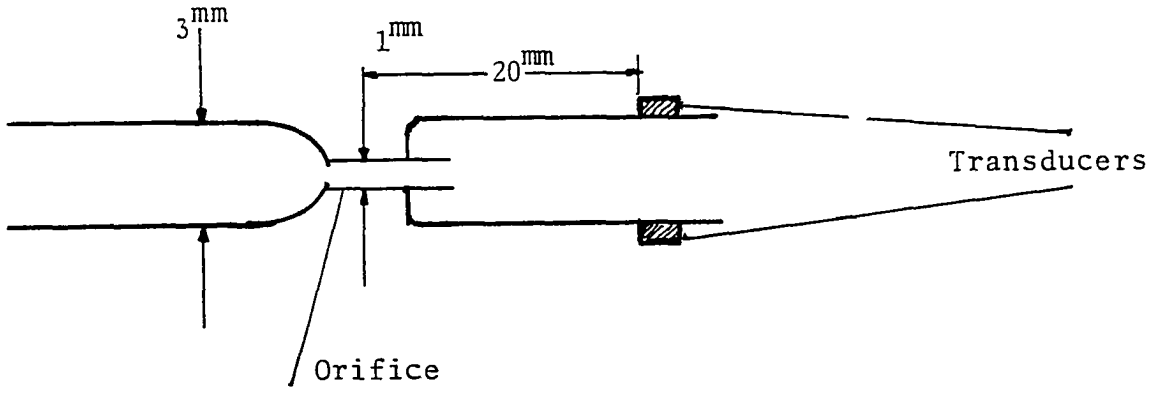

Figure 5.45 Turbulent producing orifice.

occurred downstream from the orifice. Thus, at appropriate Reynolds number, there is laminar flow upstream from the orifice, and turbulent flow downstream from the orifice. The random fluctuating velocities associated with the turbulent flow is displayed on the chart recorder and then

digitized for further analysis.

The experiment's procedure is as follows:

1) Display the velocity profile of the blood flow,
2) Obtain the center point of the artery for calculating the Doppler angle, either by scanning through the diameter or by measurement from the velocity profile,
3) Perform 2 to 3 tests for each case of normal and stenosis,
4) Trigger each test separately, and
5) Measure the diameter of the artery for each test.

The analog signal is digitized and then processed to obtain phase average of the variation of the velocity and distribution of turbulent shear stress. To calculate shear stress, first phase averages of the velocities are calculated using equation (3.57), second fluctuations are calculated using equation (3.58) and finally, shear stress is calculated from equation (3.59). Time average of shear stress is also calculated and the results of normal and stenosis artery are compared. One normal and three different degrees of stenosis (25 percent, 50 percent and 75 percent) are investigated. The artery under investigation is a specimen of the carotid of a donor dog.

Figure 5.46 and 5.47 are illustrations of velocity profile and a sample of analog Doppler signal in the normal

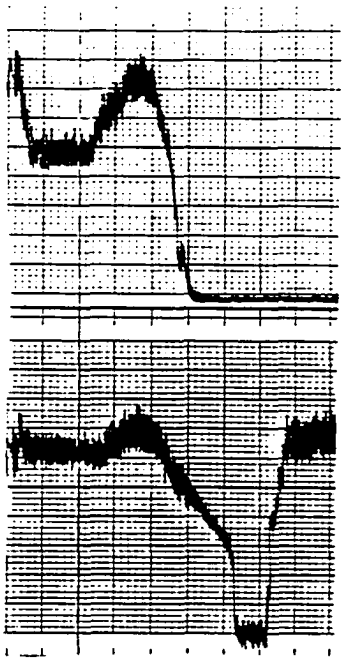

Figure 5.46 The velocity profile recorded from normal carotid artery in turbulent flow.

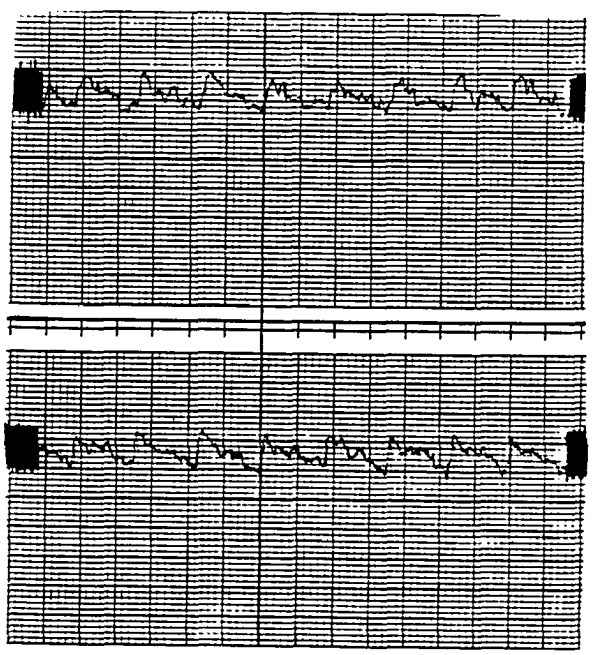

Figure 5.47 An example of Doppler signals recorded from normal carotix artery in turbulent flow.

case. Figure 5.48 and Figure 5.49 illustrate the velocity profile and Doppler signals recorded from the stenotic artery (25 percent). Figures 5.50 and 5.51 show velocity profile and an example of analog Doppler signal, recorded from the stenotic artery (50 percent). Figures 5.52 and 5.53 show the velocity profile and an example of analog signals recorded from the stenotic artery (75 percent). Figures 5.54, 5.55, 5.56 and 5.57 show velocity, phase average of the velocity and fluctuations in the normal and the stenotic artery. The effect of different degrees of stenosis are reflected in the value of the velocities in those figures. Figures 5.58, 5.59, 5.60 and 5.61 show shear stress and time average shear stress. Time average value of shear stress for normal arteries is 93; for 25 percent, stenosis is 75; for 50 percent, stenosis is 48; and for 75 percent, stenosis is 15. As we can see, the time average of the shear stress associated fairly with the degree of stenosis in most of the cases. Although the time average shear stress might show reasonable results in a particular case of turbulent flow, in general, because of the nature of turbulency, it is not a reliable approach for analysis of turbulent flow and classifying the degree of stenosis.

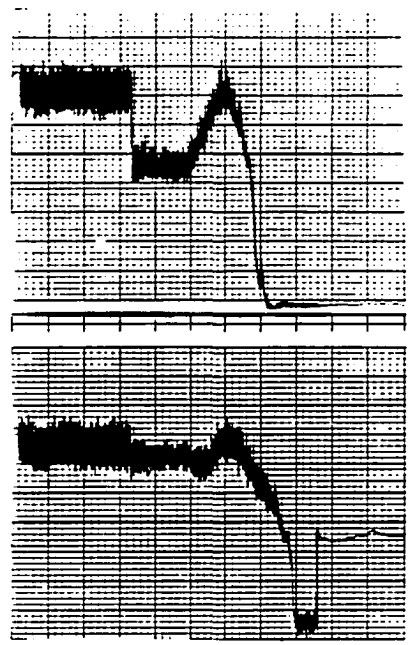

Figure 5.48 The velocity profile recorded from stenotic (25 percent) carotid artery in turbulent flow.

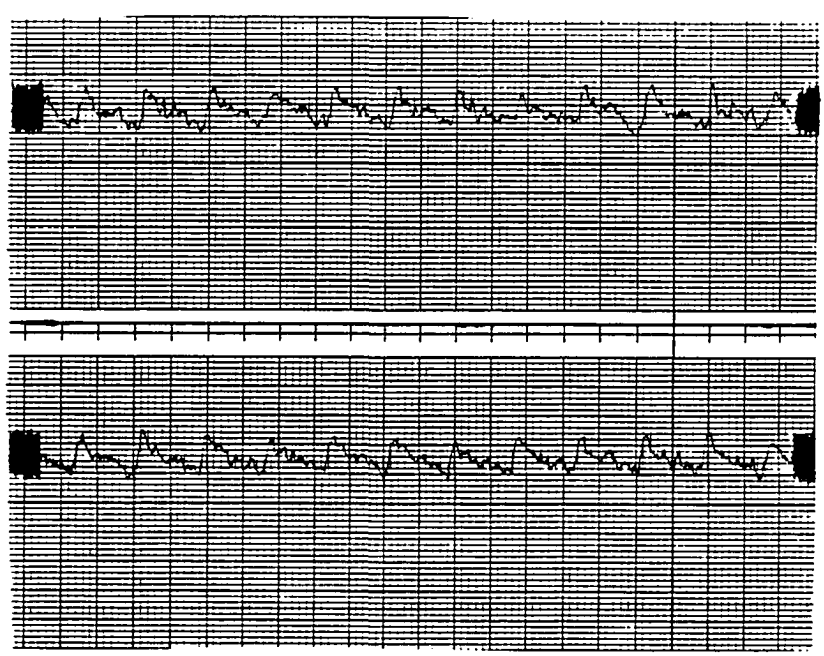

Figure 5.49 An example of Doppler signals recorded from stenotic (25 percent) carotid artery in turbulent flow.

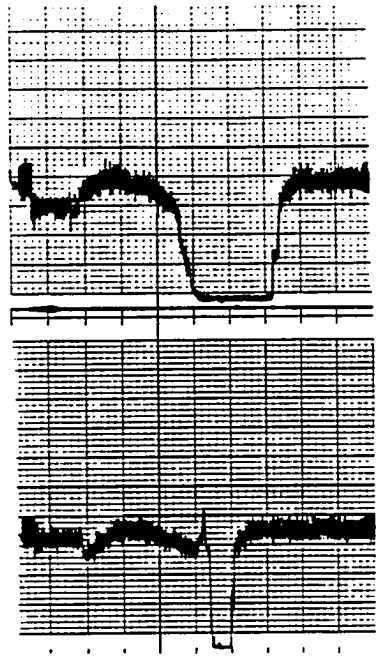

Figure 5.50 The velocity profile recorded from stenotic (50 percent) carotid artery in turbulent flow.

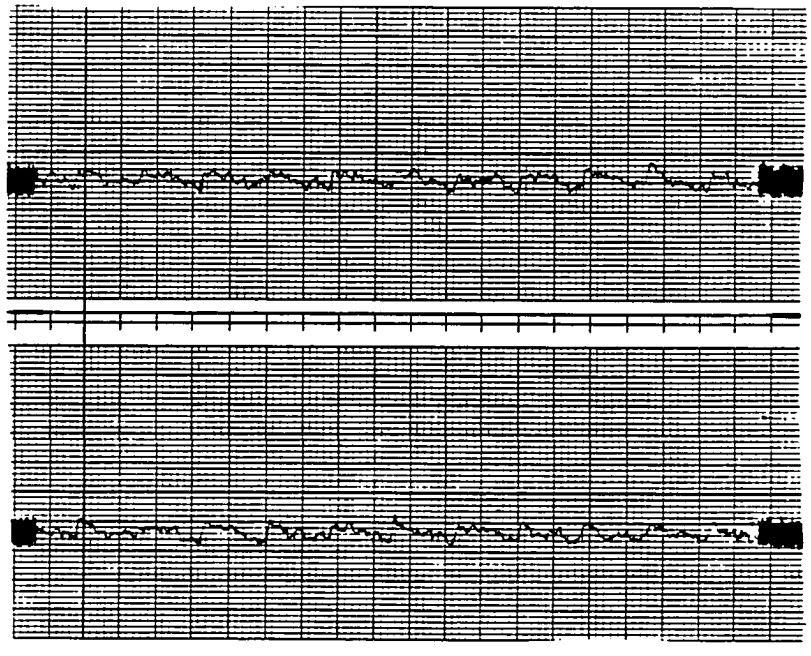

Figure 5.51 An example of Doppler signals recorded from stenotic (50 percent) common carotid artery in turbulent flow.

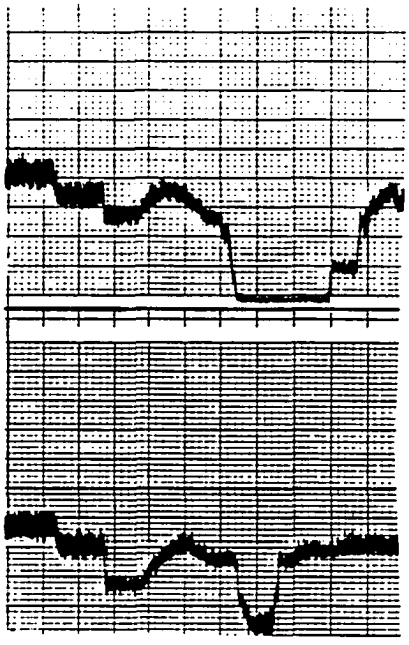

Figure 5.52 The velocity profile recorded from stenotic (75 percent) carotid artery in turbulent core.

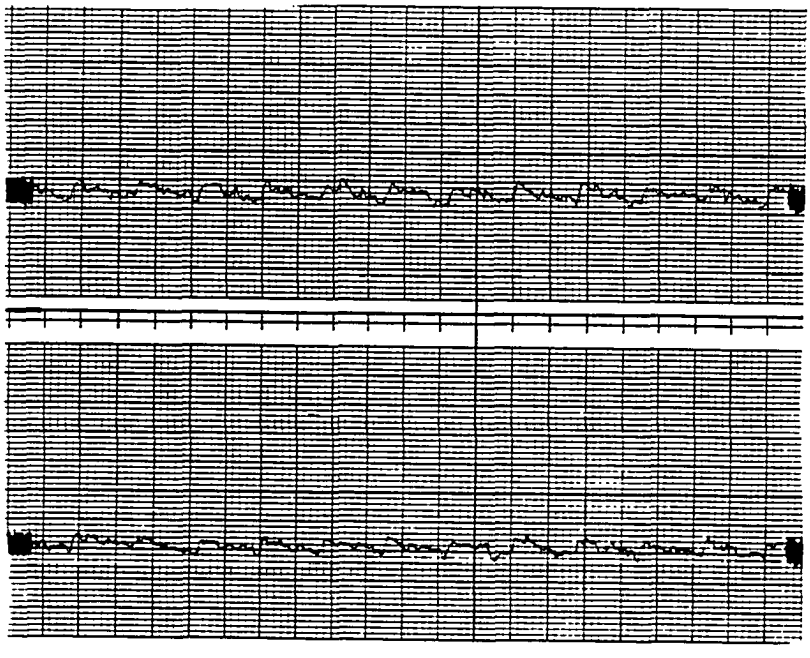

Figure 5.53 An example of Doppler signals recorded from stenotic (75 percent) artery in turbulent flow.

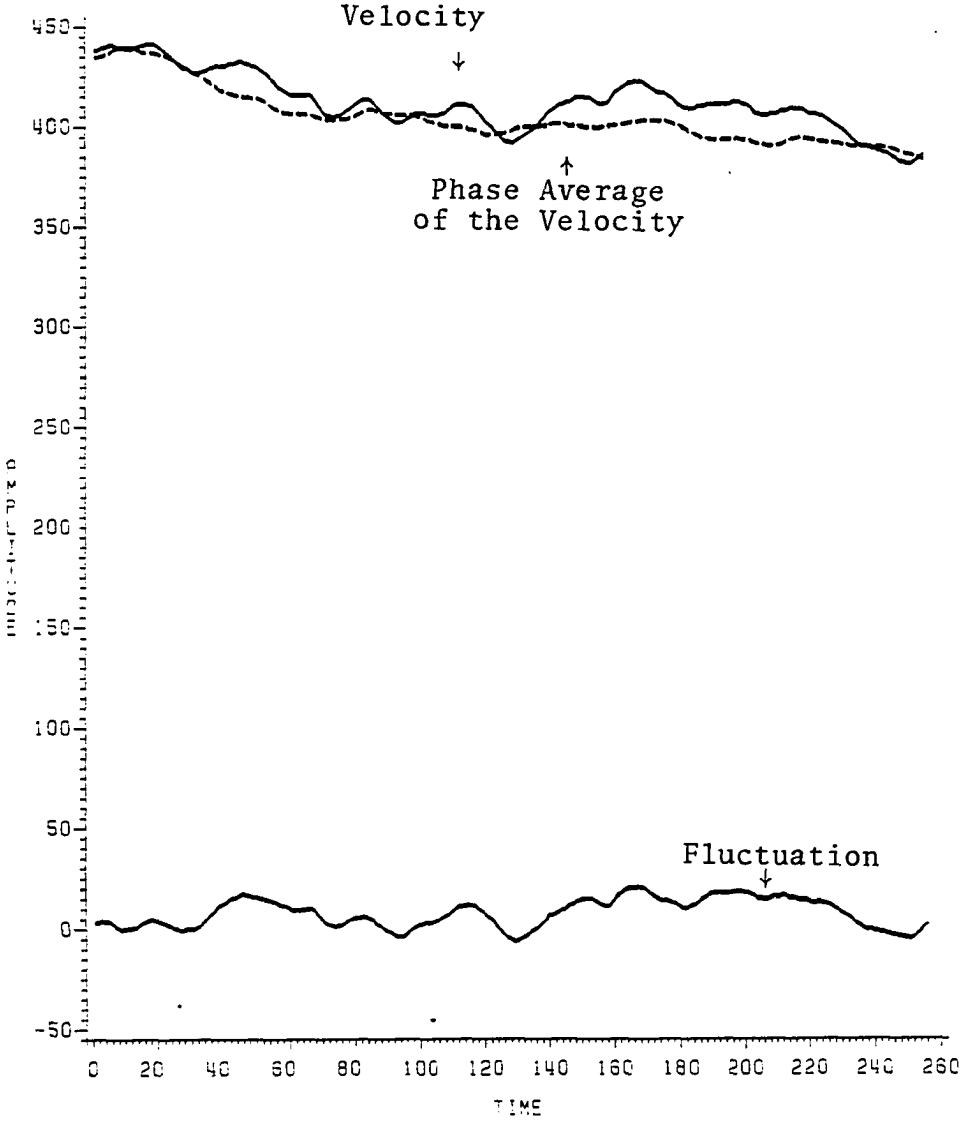

Figure 5.54 The velocity, phase average velocity and fluctuation velocity for normal carotid artery in turbulent flow.

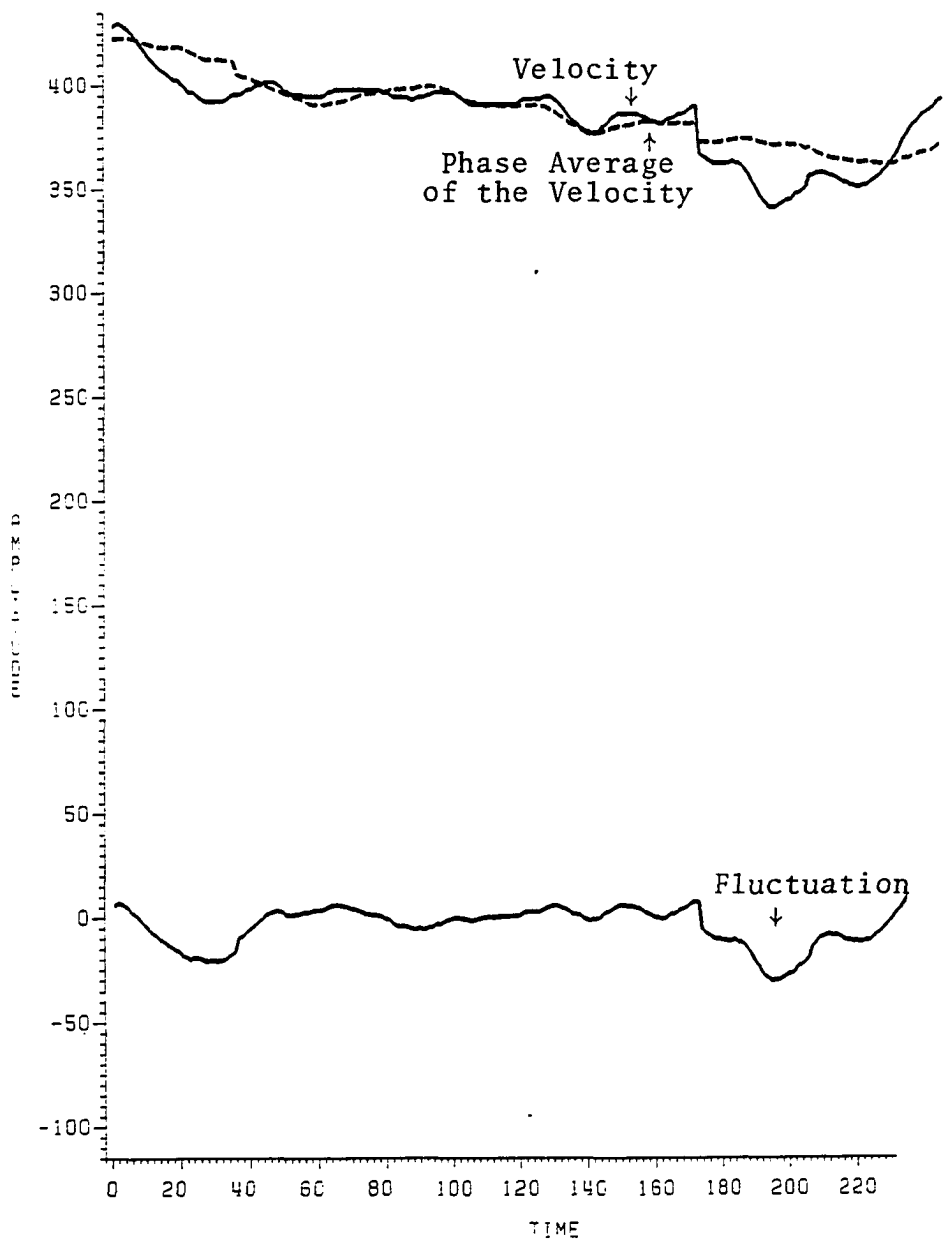

Figure 5.55 The velocity, phase average of the velocity and fluctuation velocity for stenotic (25 percent) carotid artery in turbulent flow.

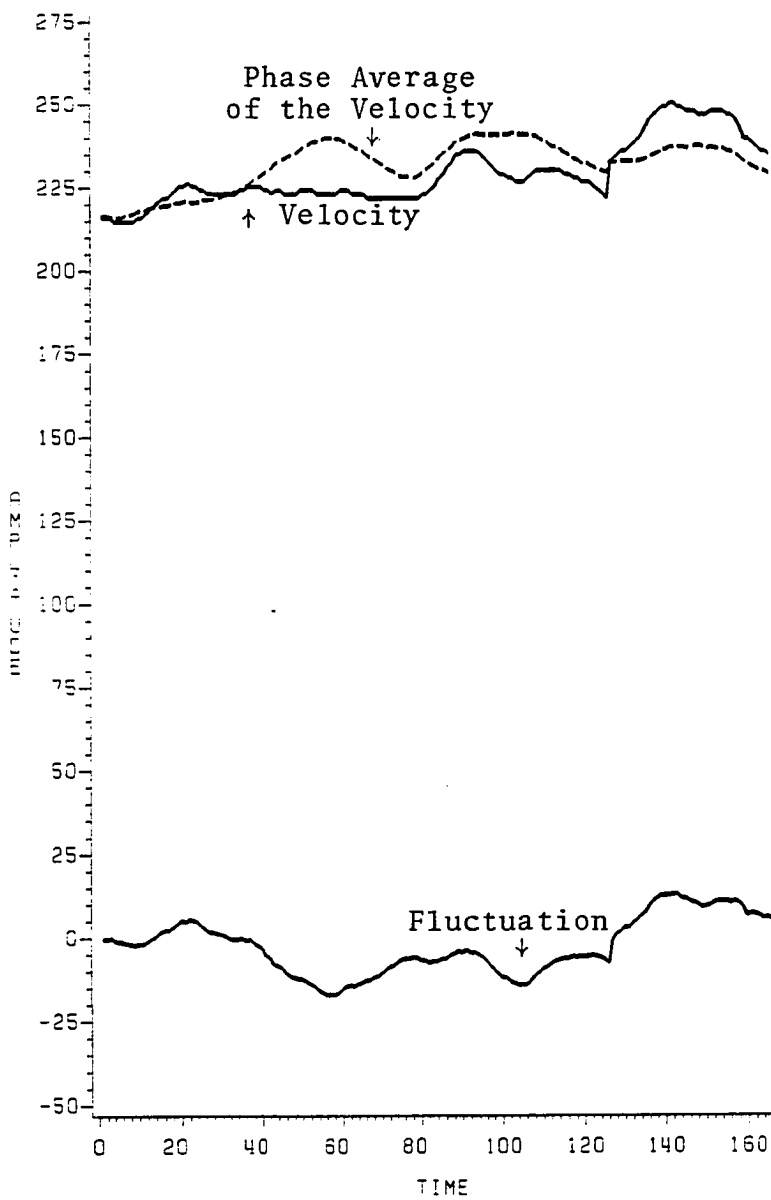

Figure 5.56 The velocity, phase average of the velocity and fluctuation velocity for stenotic (50 percent) carotid artery in turbulent flow.

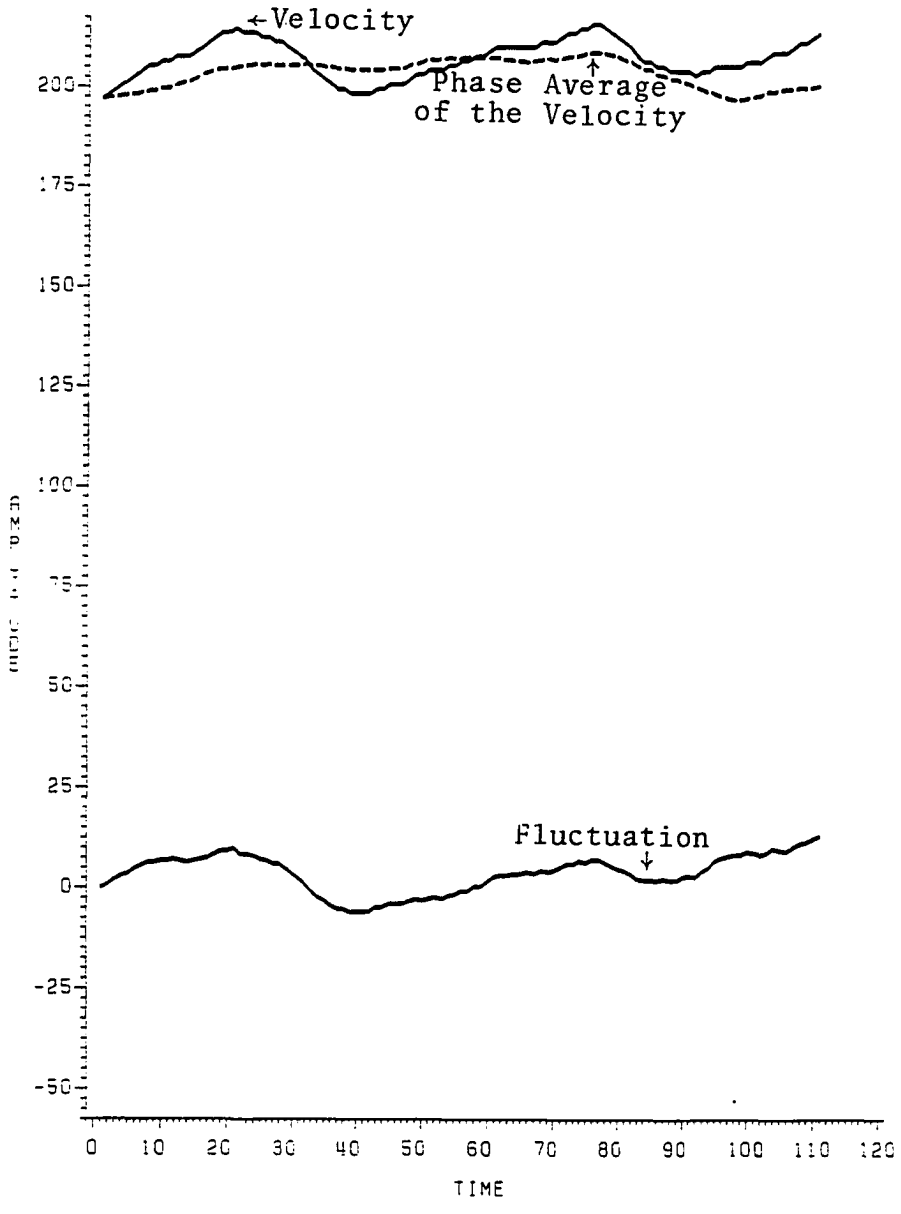

Figure 5.57 The velocity, phase average of the velocity and fluctuation velocity for stenotic (75 percent) carotid artery in turbulent flow.

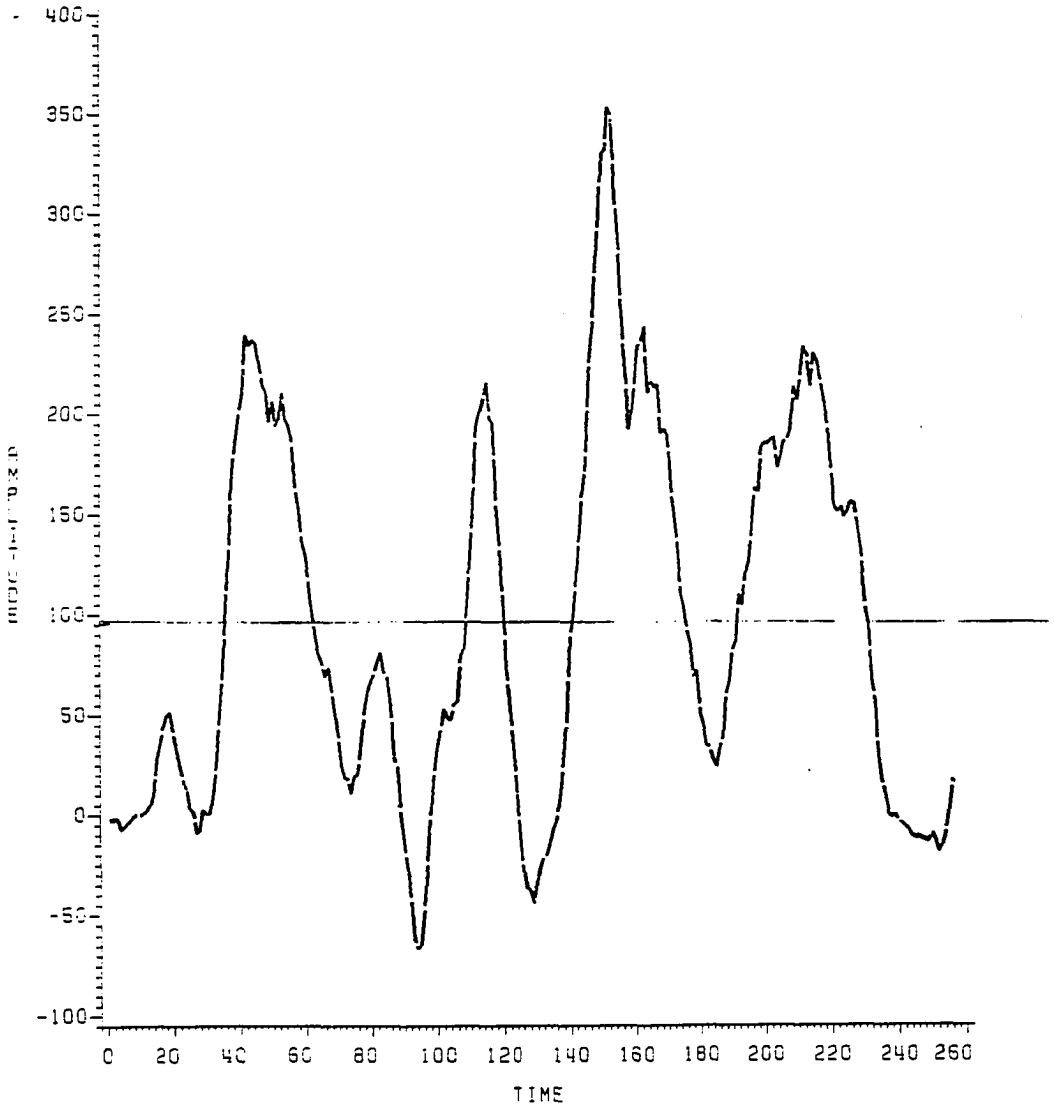

Figure 5.58 The shear stress and time average of shear stress for normal carotid artery.

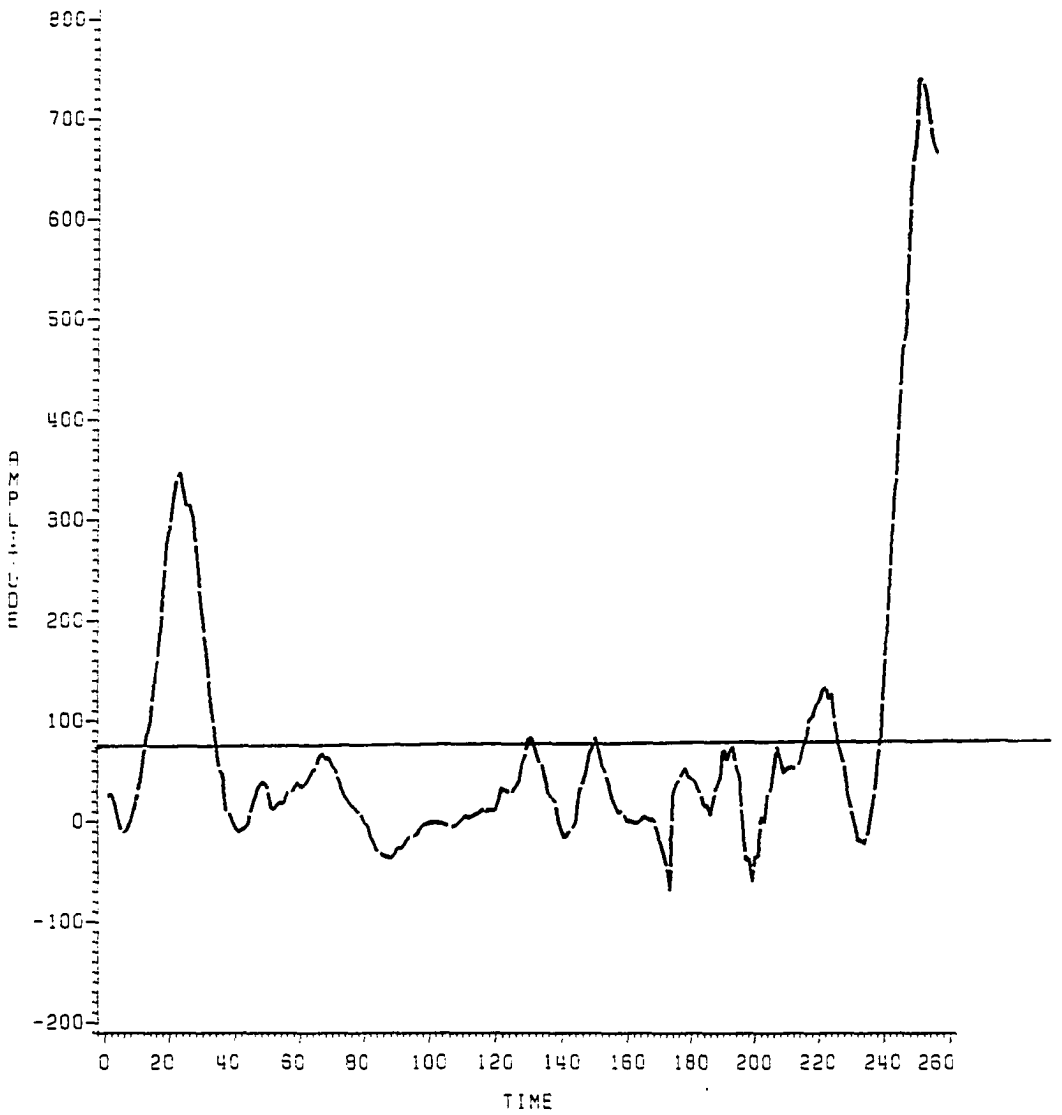

Figure 5.59 The shear stress and time average of shear stress for stenotic (25 percent) carotid artery.

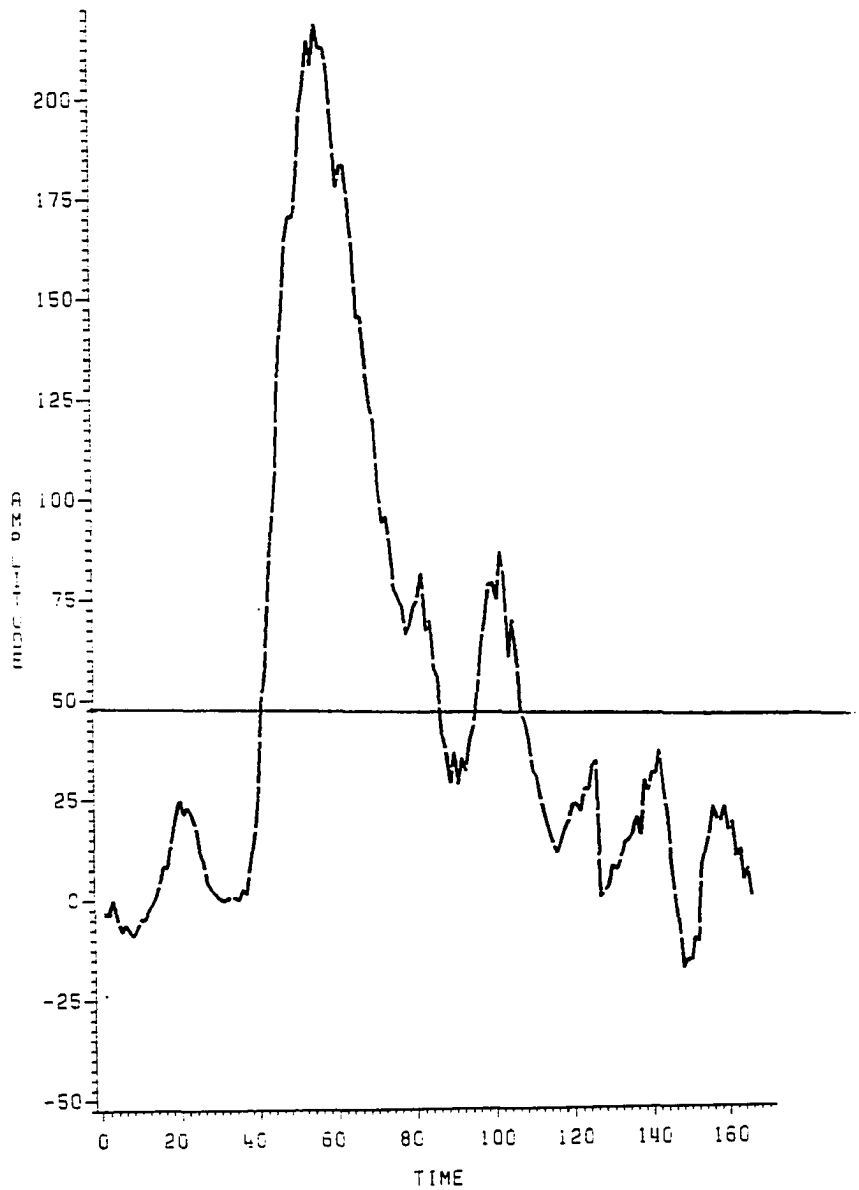

Figure 5.60 The shear stress and time average of shear stress for stenotic (50 percent) carotid artery.

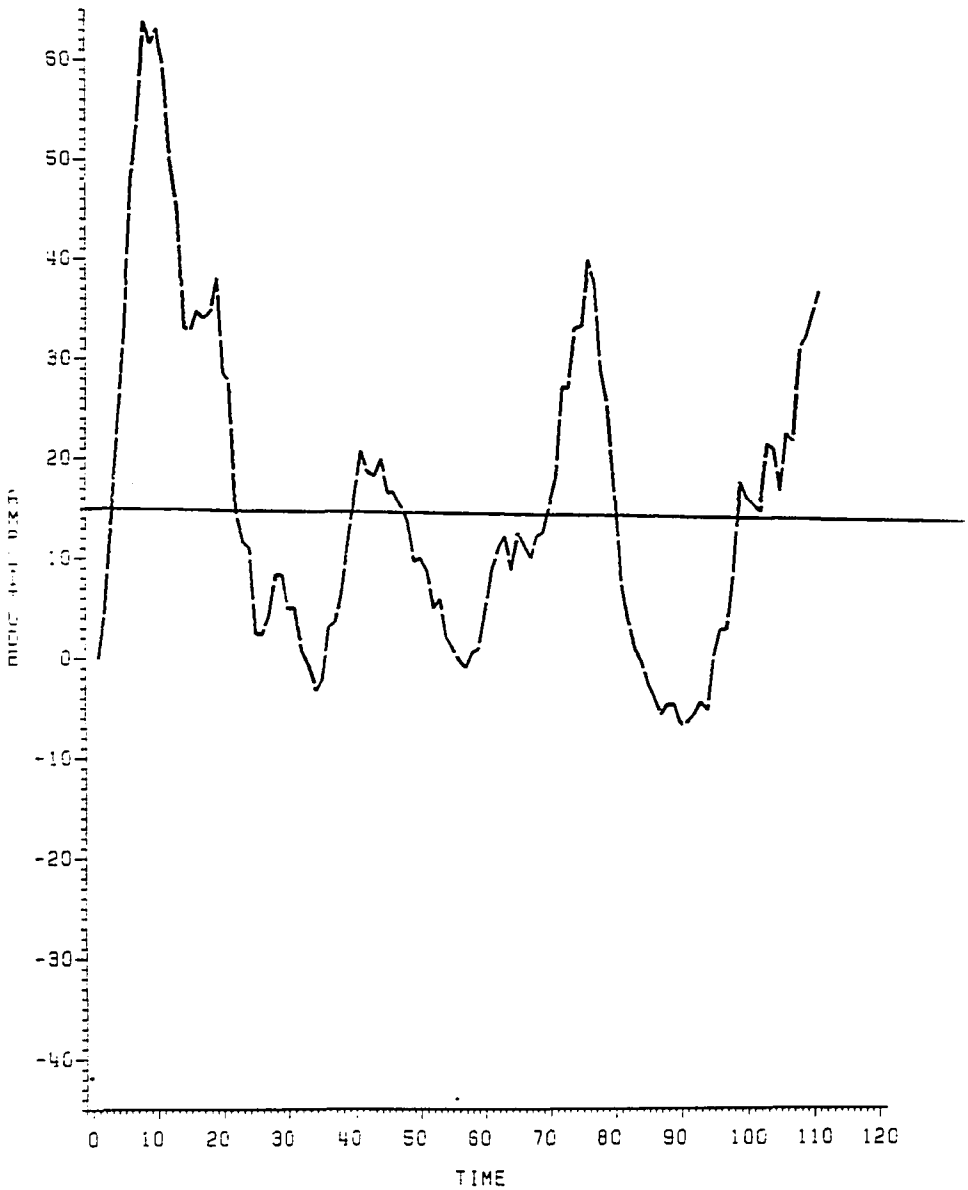

Figure 5.61 The shear stress and time average of shear stress for stenotic (75 percent) carotid artery.

5.3.5 Determining the Percentage of Stenosis Using Turbulent Flow Characteristics (carotid artery)

The purpose of this experiment is, first, to evaluate the effect of the different degrees of stenosis upon the characteristics of turbulent flow. Second, is to determine the percentage of stenosis from the characteristics of turbulent flow such as shear stress, using theoretical developments in Chapter III, section 3.3. Again, the measurements of velocity profiles and turbulent shear stress are obtained using the dual transducer pulsed-Doppler ultrasound system. The turbulency is produced as it was described in the previous experiment.

The procedure for the experiment is as follows:

1) Display the velocity profile of the blood flow.
2) Obtain the center point to calculate the Doppler angle.
3) Perform one test for each particular range in the profile for both normal and stenotic artery (8 to 10 periods).
4) Trigger each test separately.
5) Measure the diameter of the artery for each set of normal and occluded arteries.

The analog signal is digitized and then processed to obtain velocity, phase average of the velocity, fluctuations and shear stress of the turbulent flow. Three different

degrees of stenosis (25 percent, 33 percent and 50 percent) along with normal arteries are investigated. Verification has been made by comparing the measure stenosis and calculated one. The artery under investigation is a specimen of the carotid artery of a donor dog. Figures 5.62, 5.63, 5.64, and 5.65 show the velocity profile in normal, 25 percent, 33 percent and 55 percent stenosis. Notice the effect of stenosis on velocity profiles for the different cases. Figures 5.66 and 5.67 show the output Doppler signals from the near wall and the center of the carotid artery in the normal case. The difference between these two figures is a clear indication of the effect of the range in which the data are recorded. Also, a comparison between Figure 5.67 and 5.69 shows that in lower degrees of stenosis, the changes in the Doppler signals at the center are minimal. Figures 5.68, 5.69 and 5.70 show the output Doppler signals from the near wall, center point and the far wall of the stenotic artery (25 percent), respectively. Figures 5.71, 5.72 and 5.73 show the output Doppler signals from the near wall, center point and far wall of the stenotic carotid artery (33 percent) in turbulent core. Comparing Figure 5.67 with 5.72, a dramatic change in the amplitude of the Doppler signals due to an increase in the degree of the stenosis can be observed. Figures 5.74, 5.75 and 5.76 show the output Doppler signals from the near wall, center point

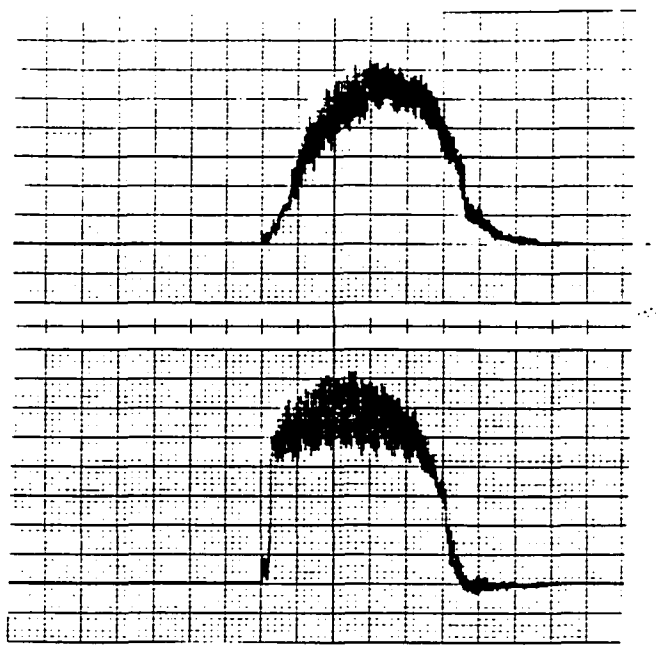

Figure 5.62 The velocity profile recorded from normal carotid artery in turbulent flow.

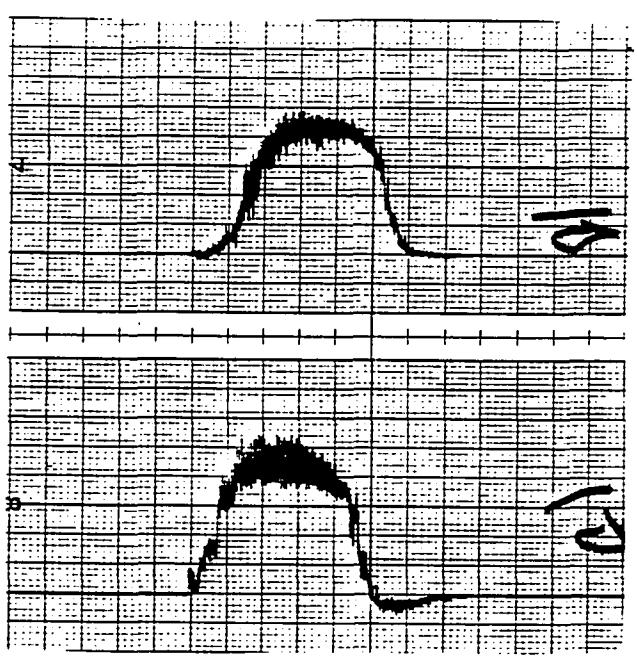

Figure 5.63 The velocity profile recorded from stenotic (25 percent) carotid artery in turbulent flow.

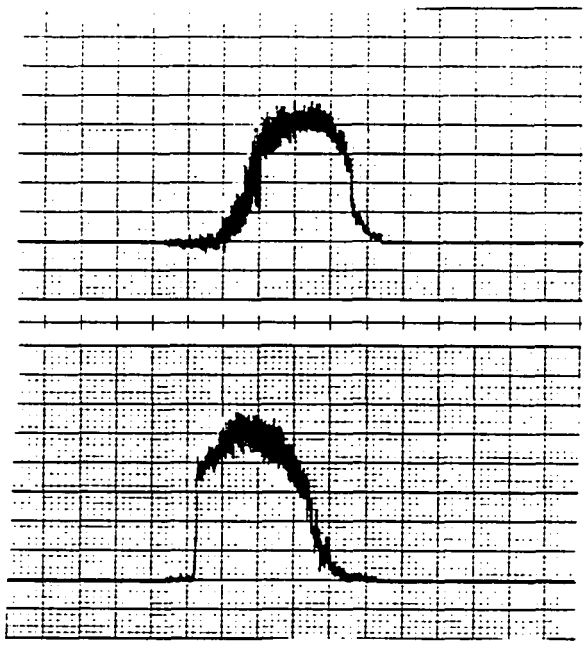

Figure 5.64 The velocity profile recorded from stenotic (33 percent) carotid artery in turbulent flow.

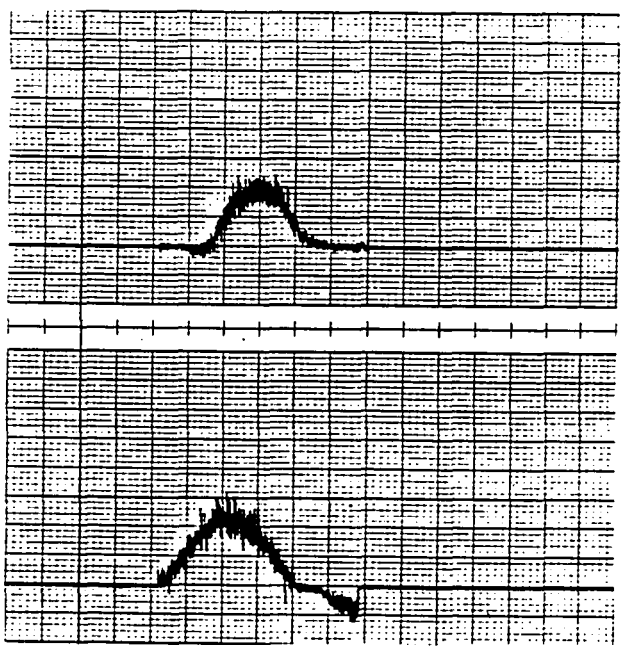

Figure 5.65 The velocity profile recorded from stenotic (50 percent) carotid artery in turbulent flow.

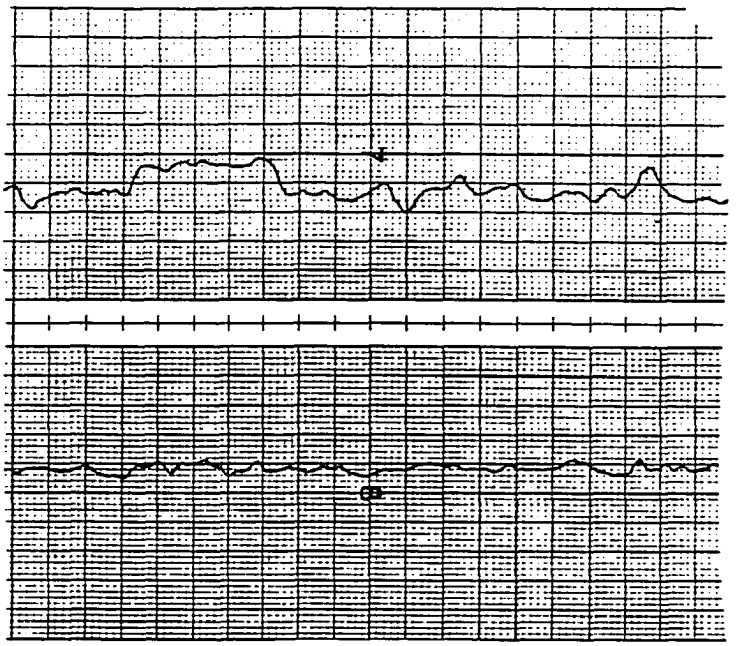

Figure 5.66 The Doppler signals recorded from the near wall of the normal carotid artery.

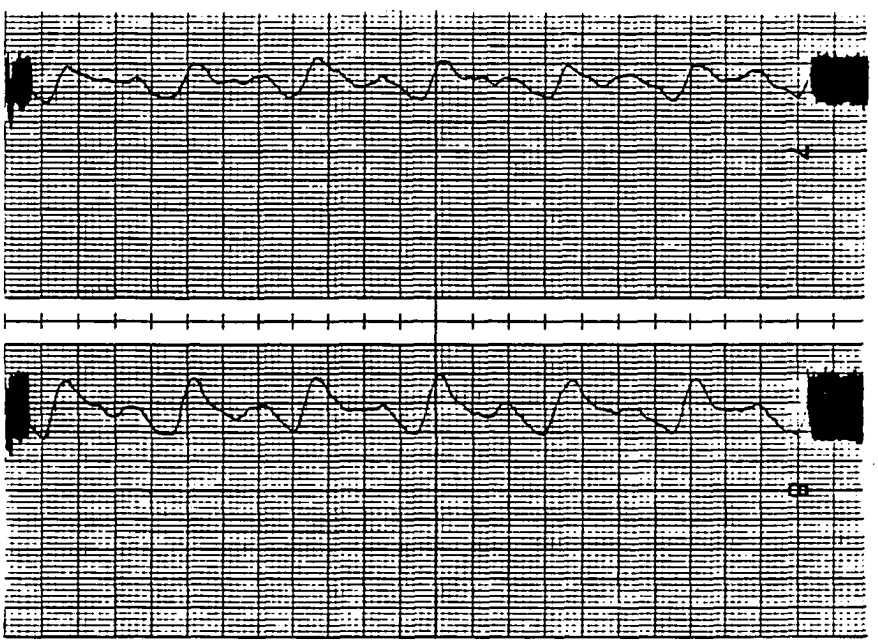

Figure 5.67 The Doppler signals recorded from the center of the normal carotid artery.

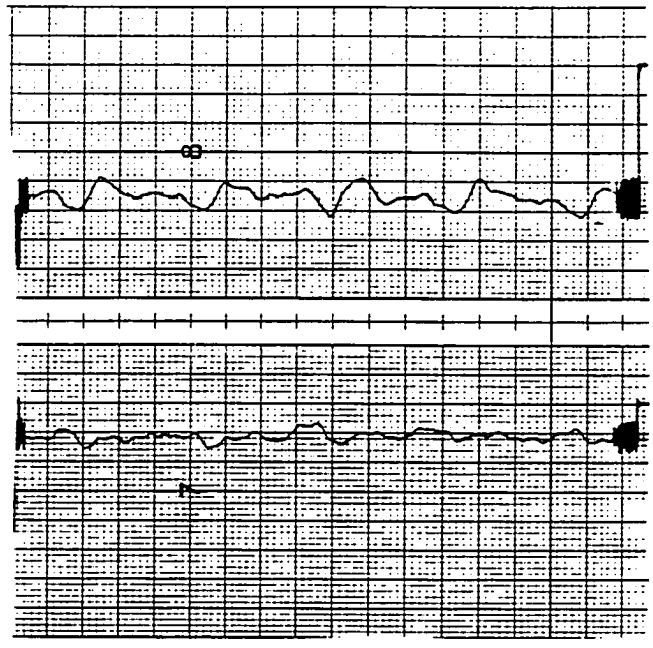

Figure 5.68 The Doppler signals recorded from the near wall of the stenotic (25 percent) carotid artery.

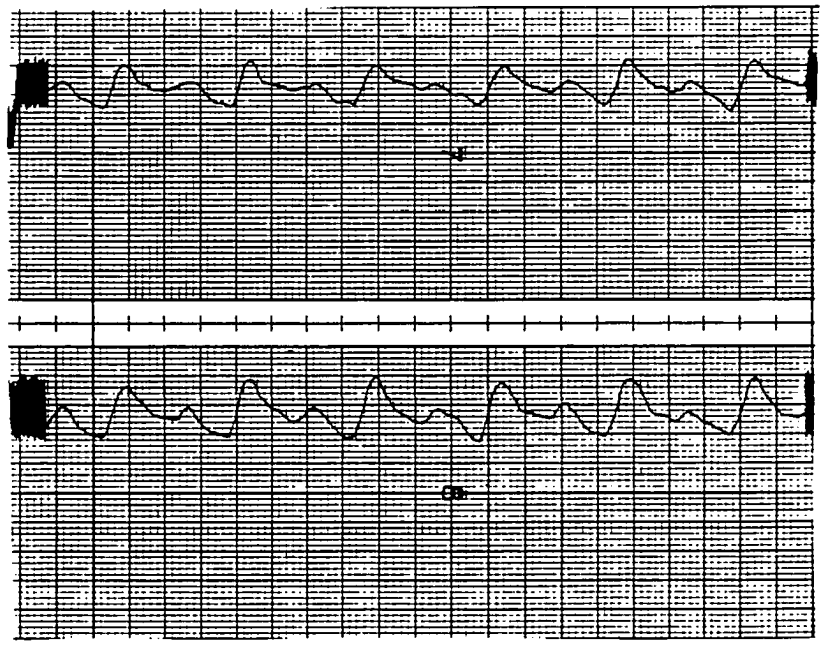

Figure 5.69 The Doppler signals recorded from the center of the stenotic (25 percent) carotid artery.

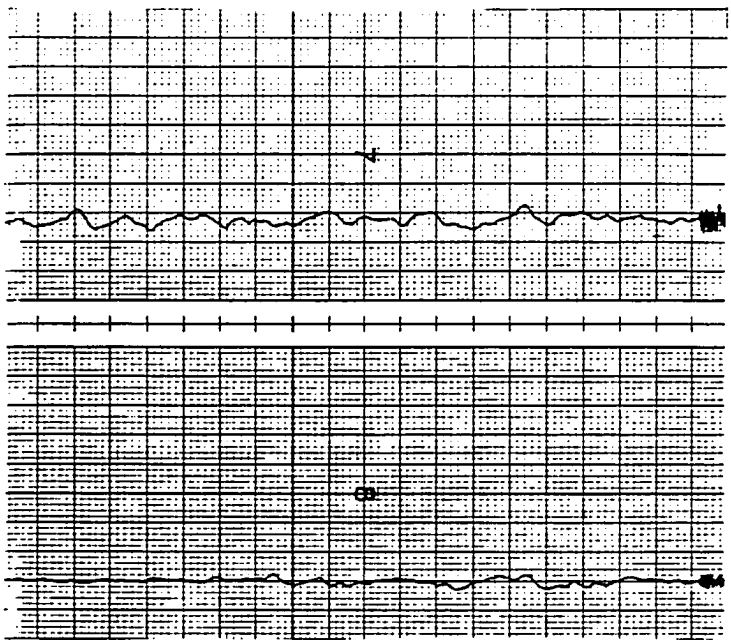

Figure 5.70 The Doppler signals recorded from the far wall of the stenotic (25 percent) carotid artery.

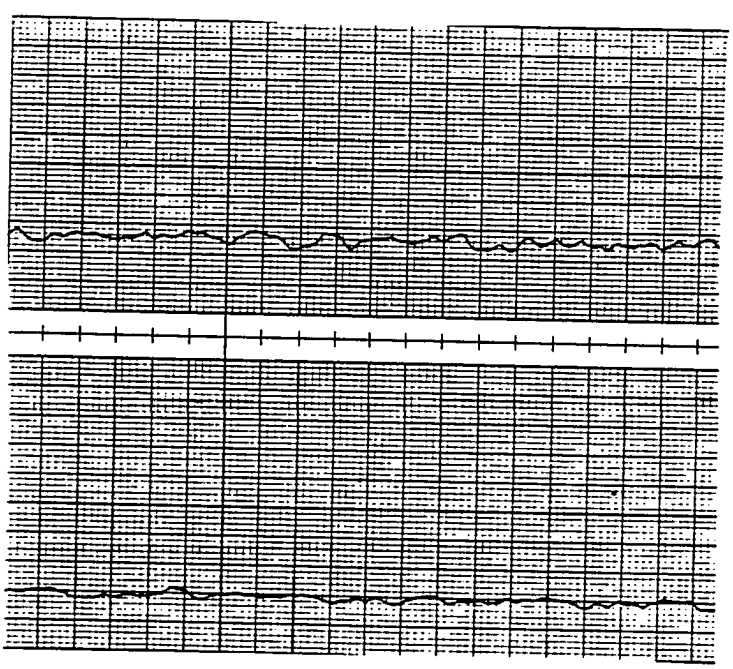

Figure 5.71 The Doppler signals recorded from the near wall of the stenotic (33 percent) carotid artery.

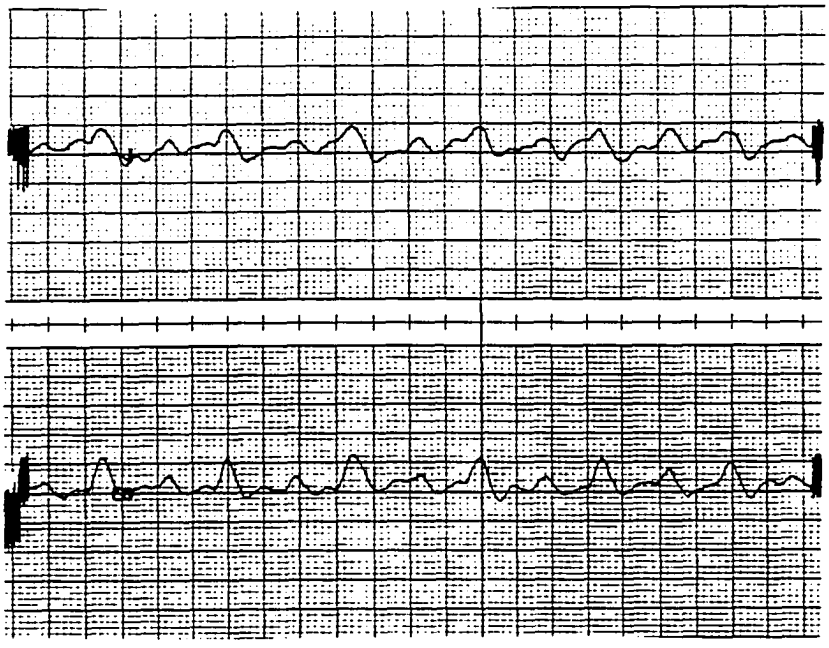

Figure 5.72 The Doppler signals recorded from the center of the stenotic (33 percent) carotid artery.

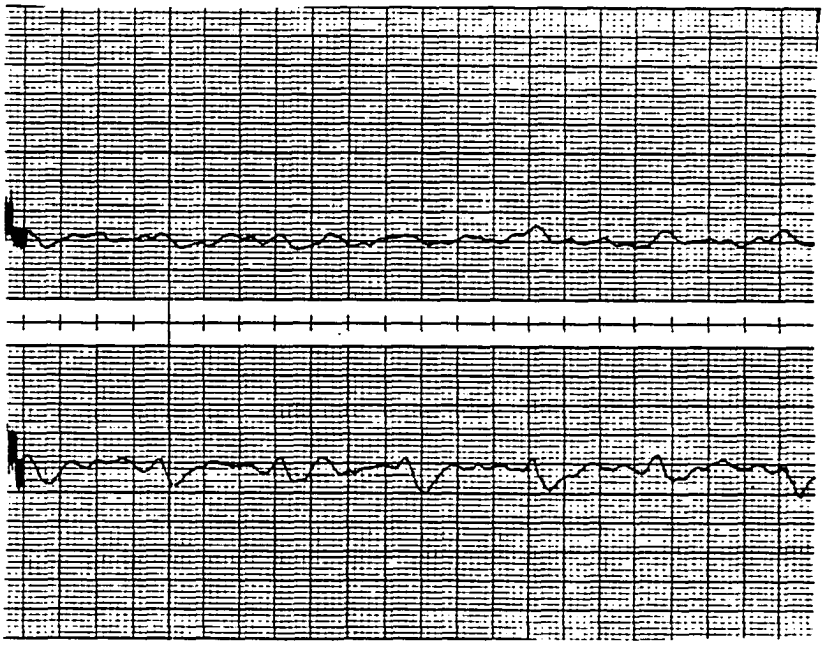

Figure 5.73 The Doppler signals recorded from the far wall of the stenotic (33 percent) carotid artery.

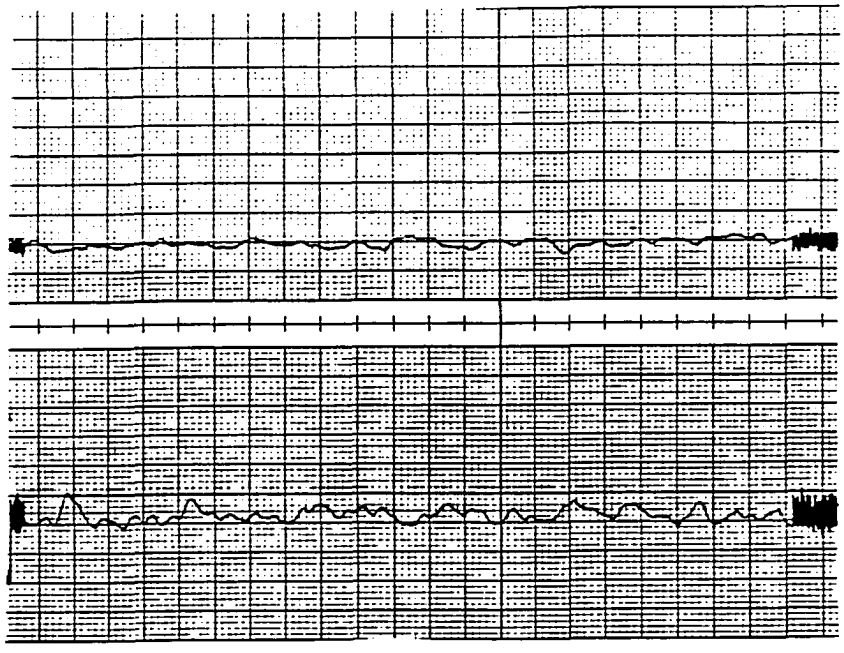

Figure 5.74 The Doppler signals recorded from the near wall of the stenotic (50 percent) carotid artery.

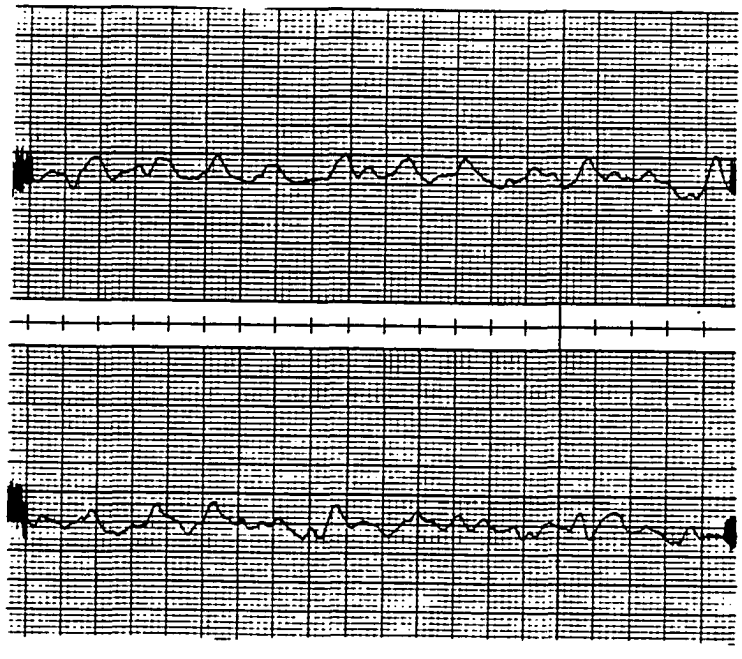

Figure 5.75 The Doppler signals recorded from the center of the stenotic (50 percent) carotid artery.

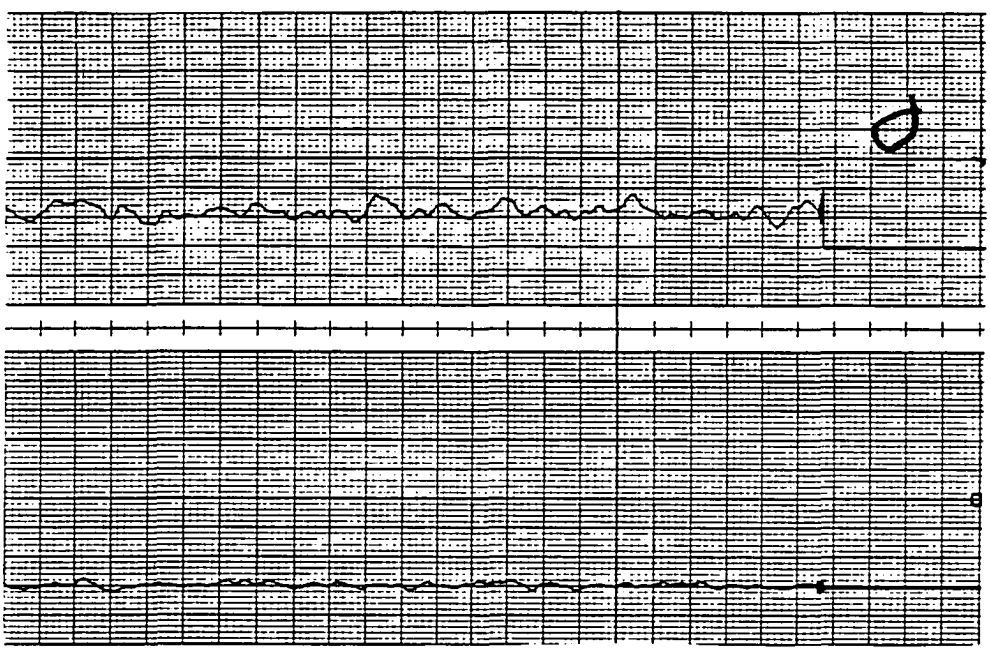

Figure 5.76 The Doppler signals recorded from the far wall of the stenotic (50 percent) carotid artery.

and far wall of the stenotic (50 percent) carotid artery in turbulent flow. The effect of further reduction in the degree of the stenosis can be seen clearly by comparing Figure 5.75 with Figures 5.72, 5.67, or 5.65. Figures 5.77 5.78, 5.79 and 5.80 show the velocity and phase average of the velocity. The effect of the changes in the degree of the stenosis is reflected on the velocity amplitude. In Figures 5.81, 5.82, 5.83 and 5.84, the fluctuations for normal, 25 percent, 33 percent and 50 percent stenosis is shown, respectively. An increase in the level of fluctuation can be observed due to the increase in the degree of stenosis. Figures 5.85, 5.86, 5.87 and 5.88 show the power spectrum of shear stress. The distinction between normal and stenosis can be made by comparing these figures. The main point in this experiment is in calculating δ (degree of stenosis) from equation (3.79) and equation (3.80). To accomplish the above goal, the following procedure has been followed:

1) The flow volume rate for each case of normal and stenosis is calculated.
2) The shear stress at the near wall (maximum variation) for each case is calculated.
3) Dividing equation (3.80 by (3.79), the following equation is obtained:

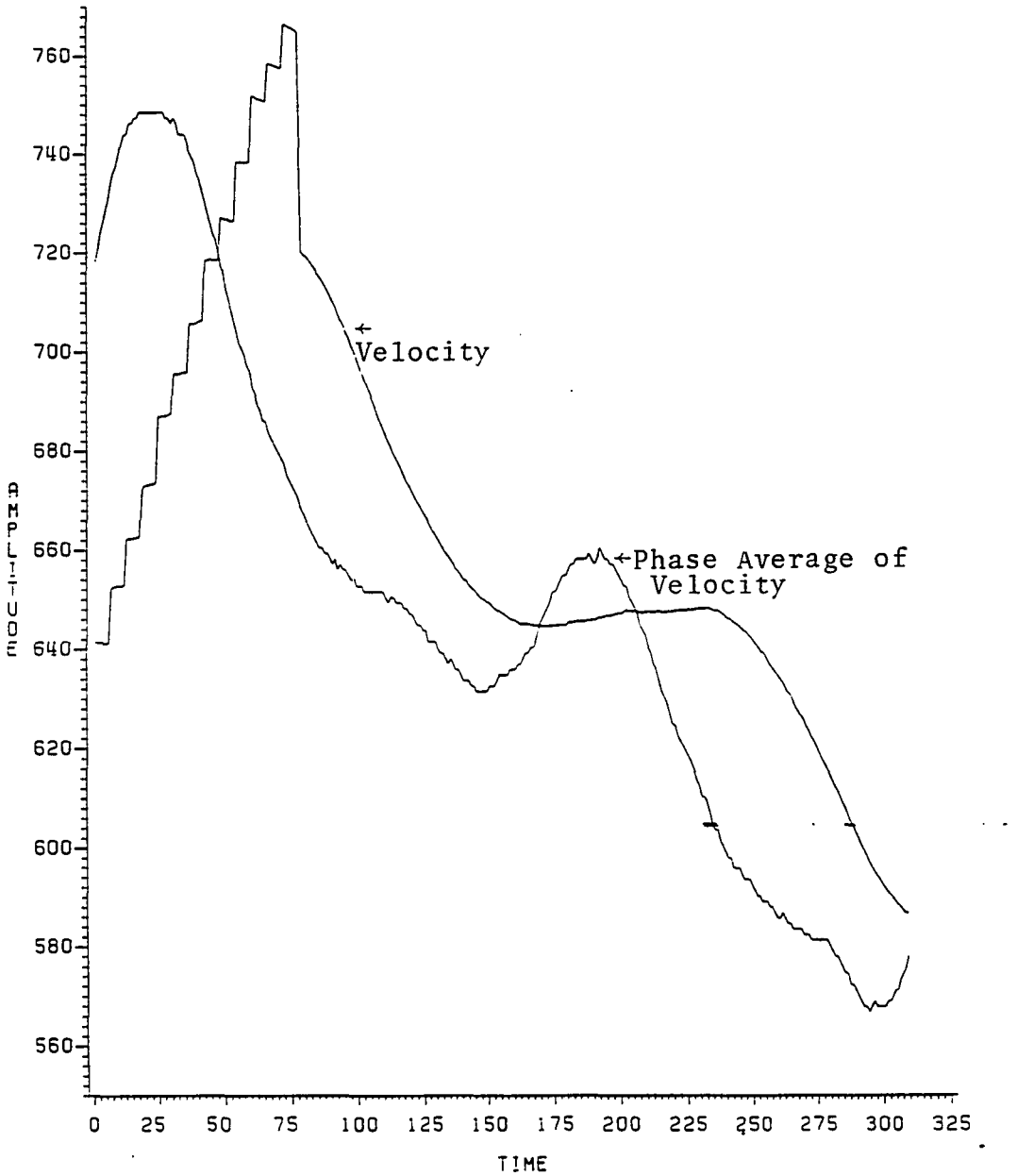

Figure 5.77 The velocity and phase average of the velocity for normal carotid artery.

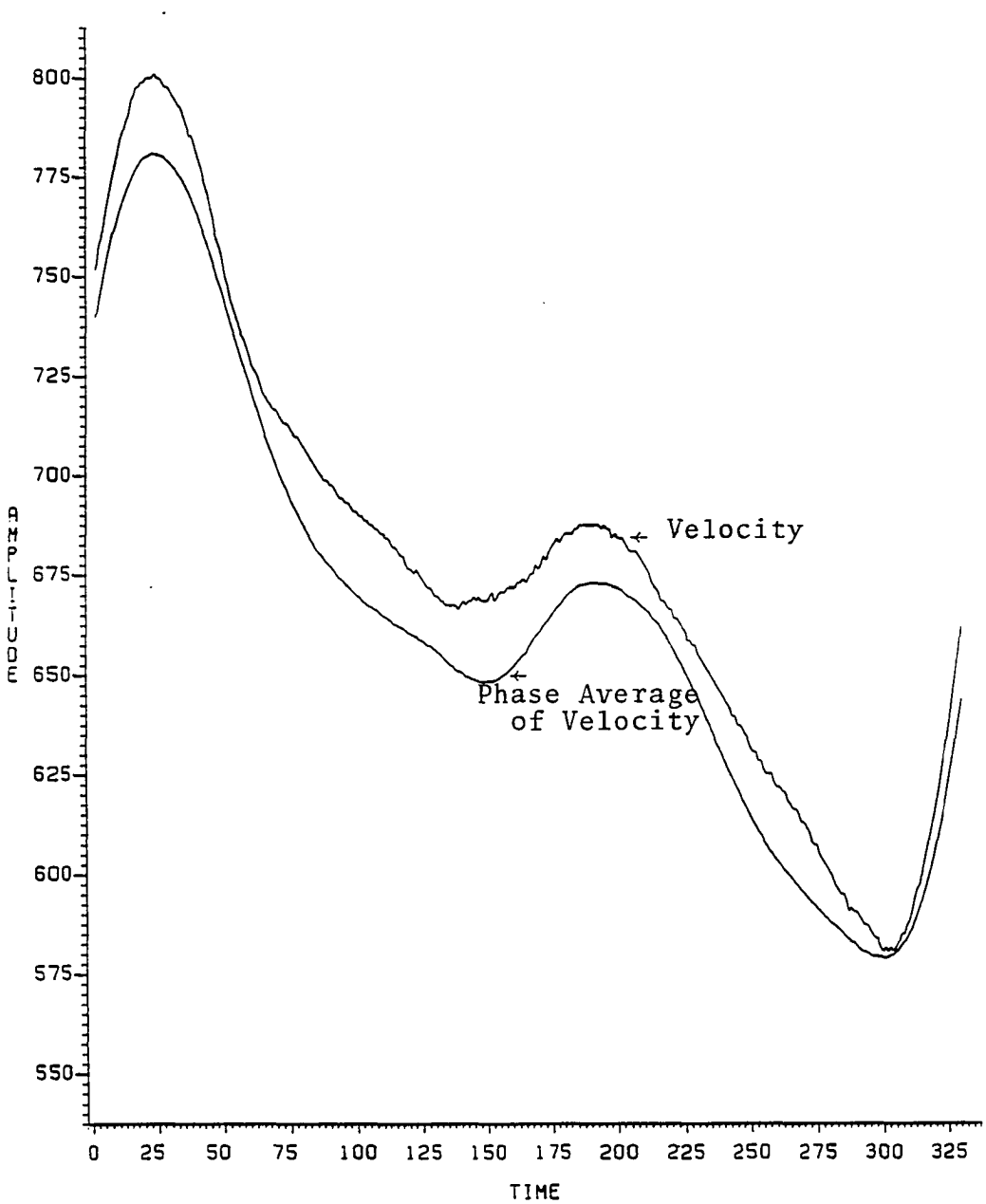

Figure 5.78 The velocity and phase average of the velocity for stenotic (25 percent) carotid artery.

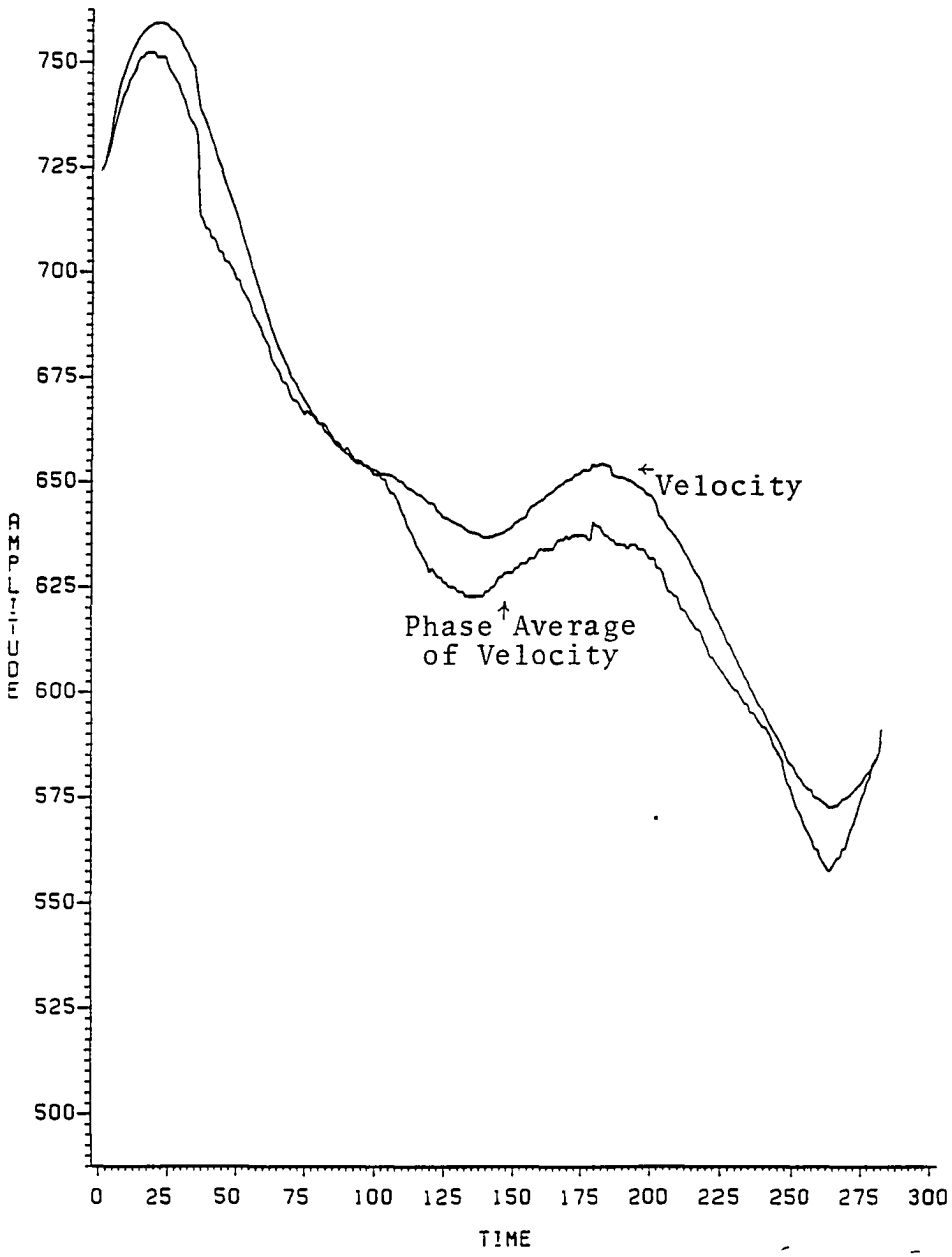

Figure 5.79 The velocity and phase average of the velocity for stenotic (33 percent) carotid artery.

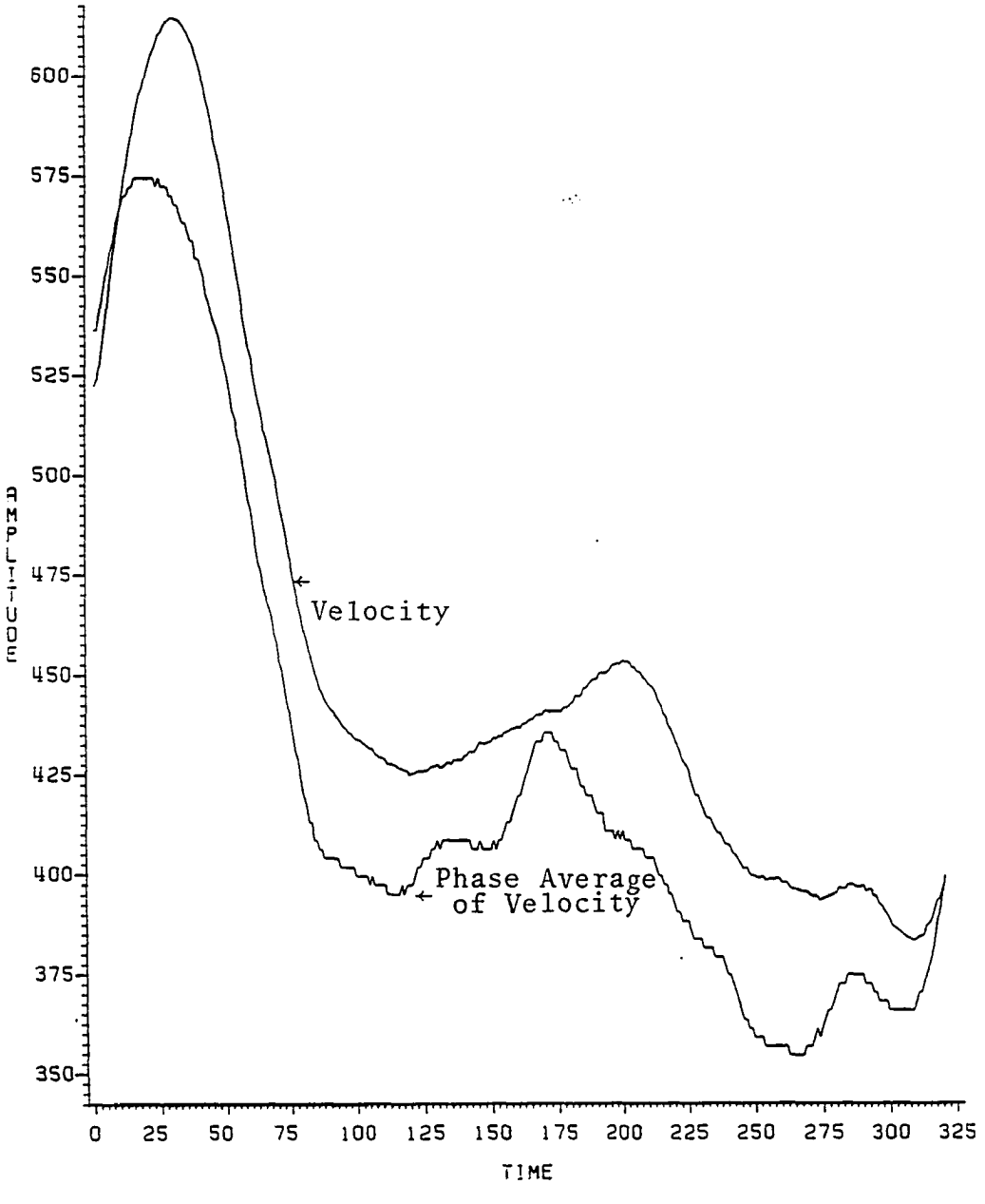

Figure 5.80 The velocity and phase average of the velocity for stenotic (50 percent) carotid artery.

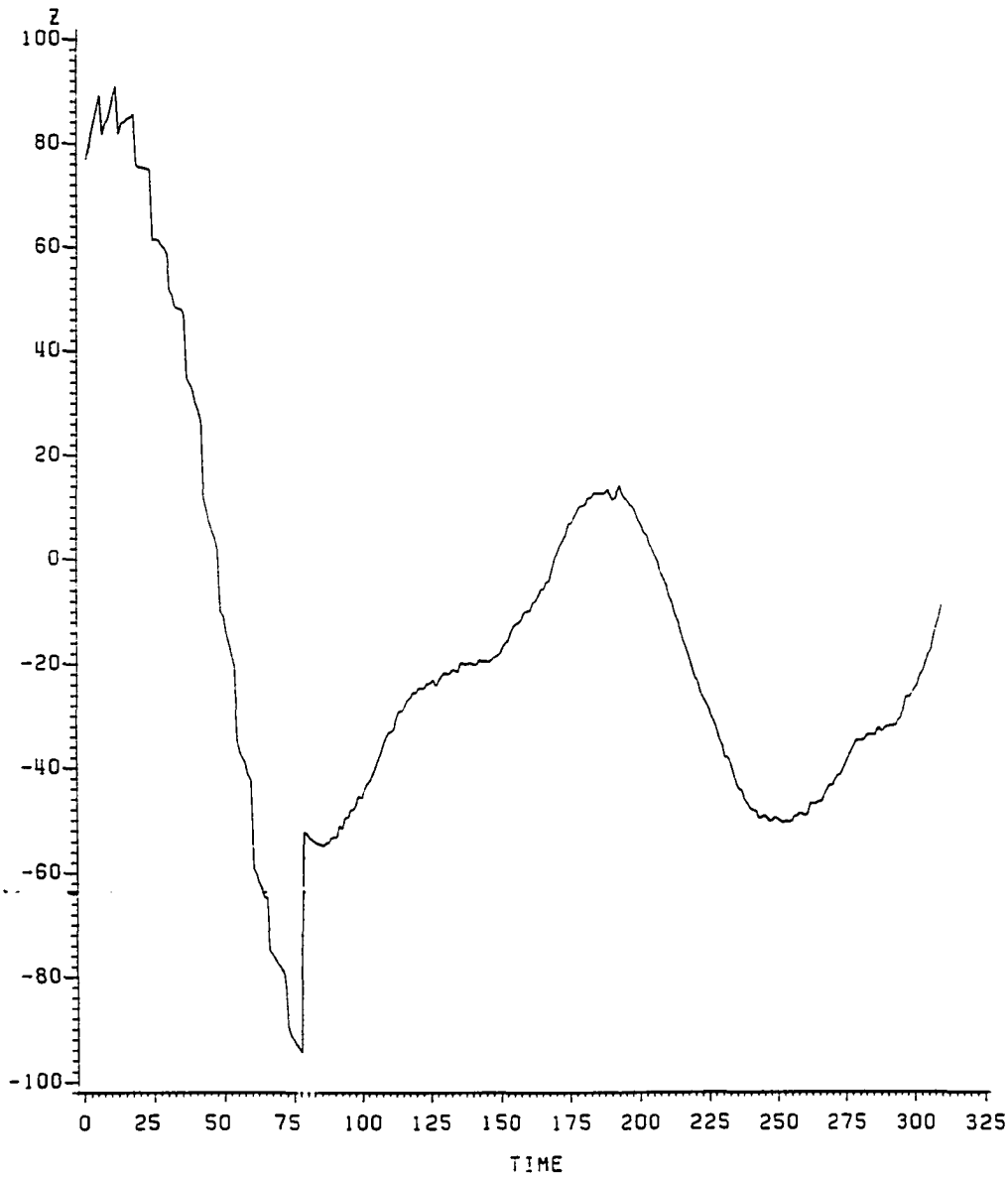

Figure 5.81 The fluctuation component of the velocity for the normal carotid artery.

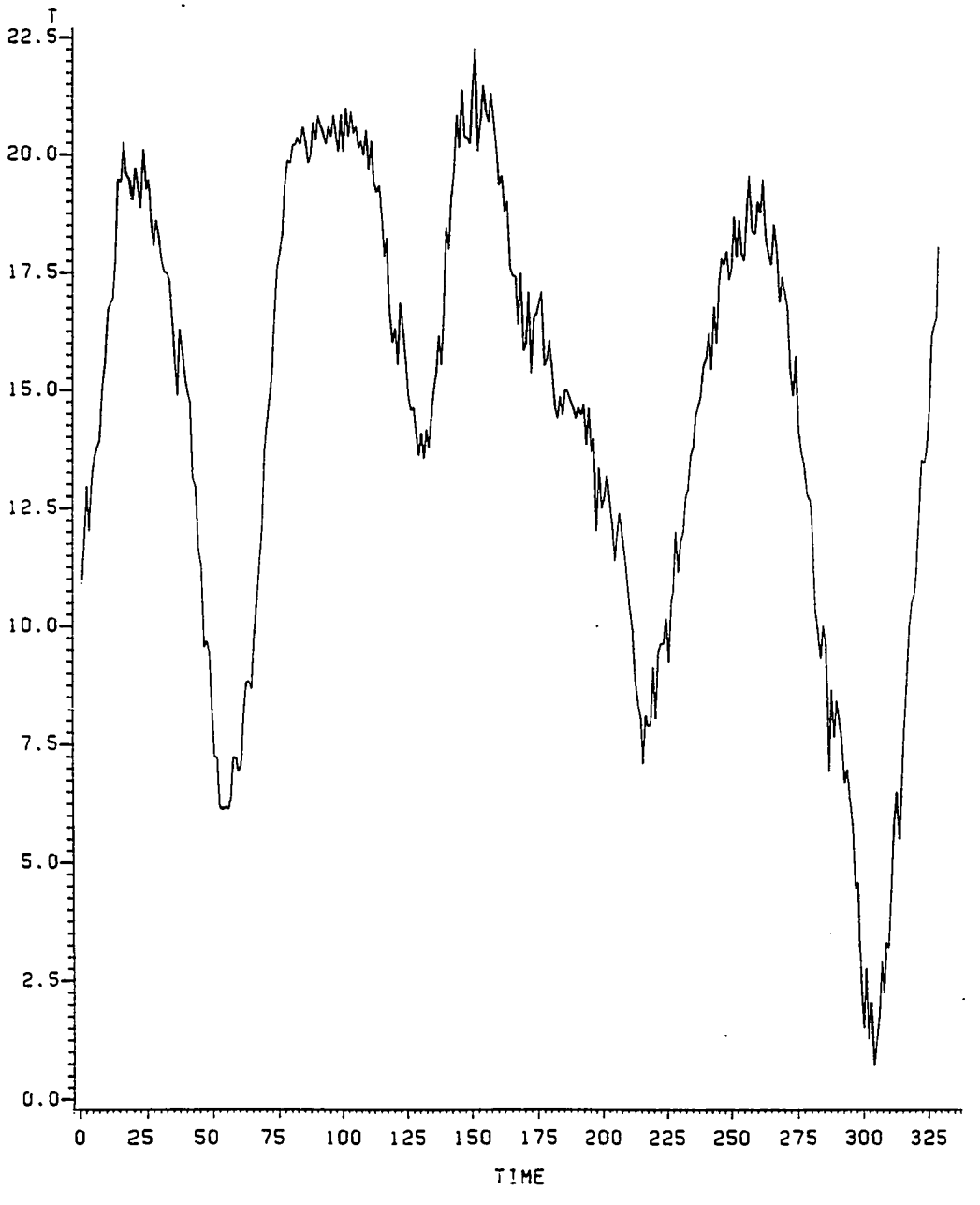

Figure 5.82 The fluctuation component of the velocity for stenotic (25 percent) carotid artery.

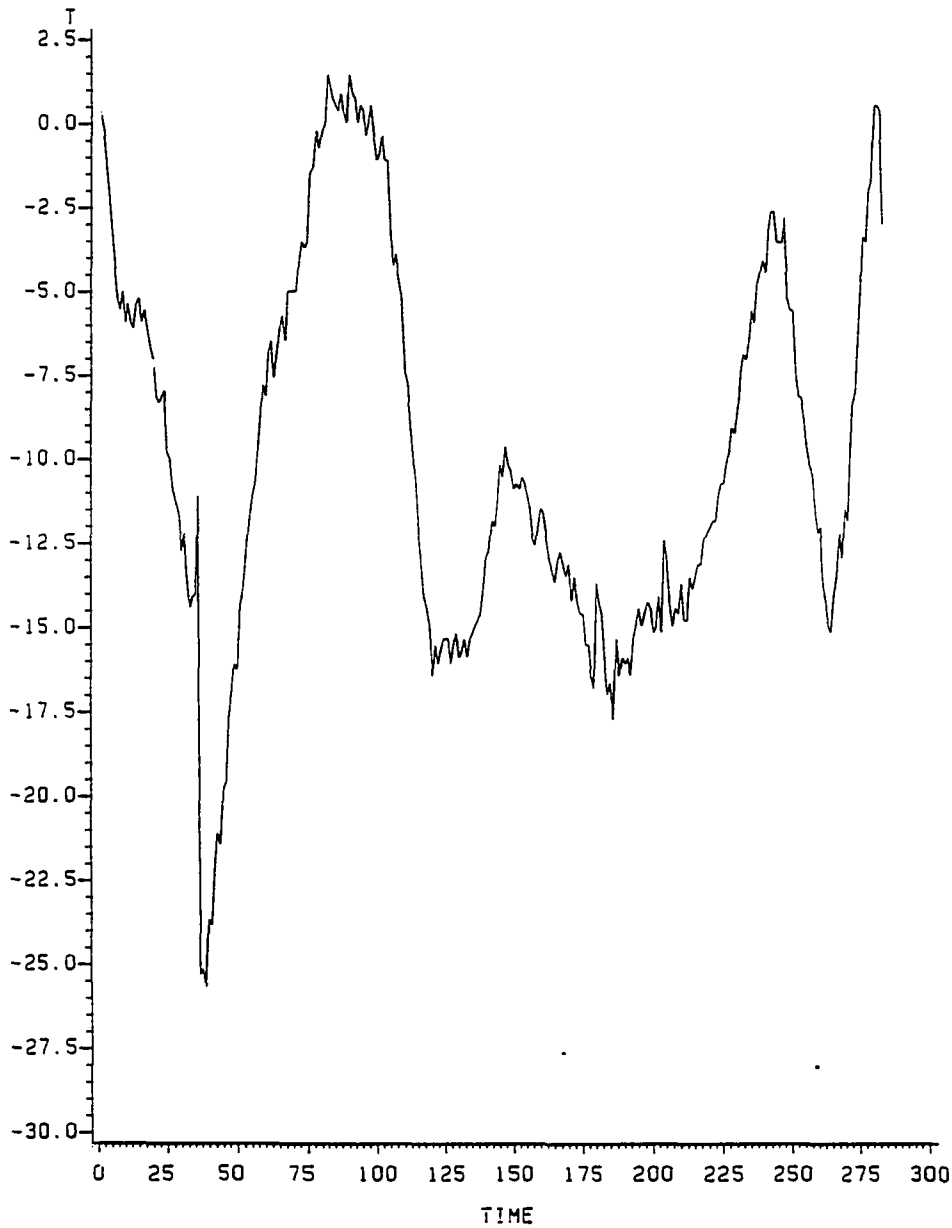

Figure 5.83 The fluctuation component of the velocity for stenotic (33 percent) carotid artery.

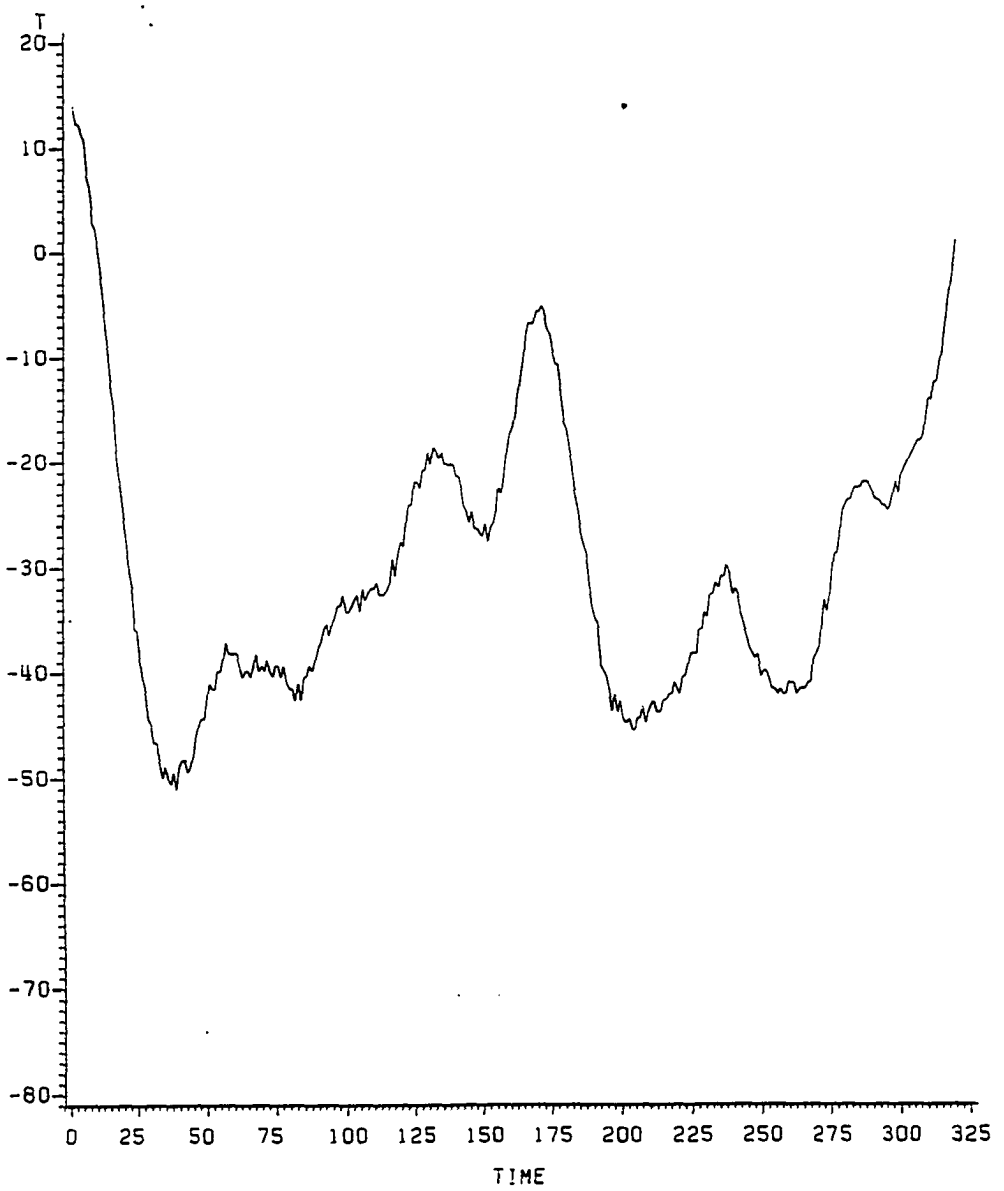

Figure 5.84 The fluctuation component of the velocity for stenotic (50 percent) carotid artery.

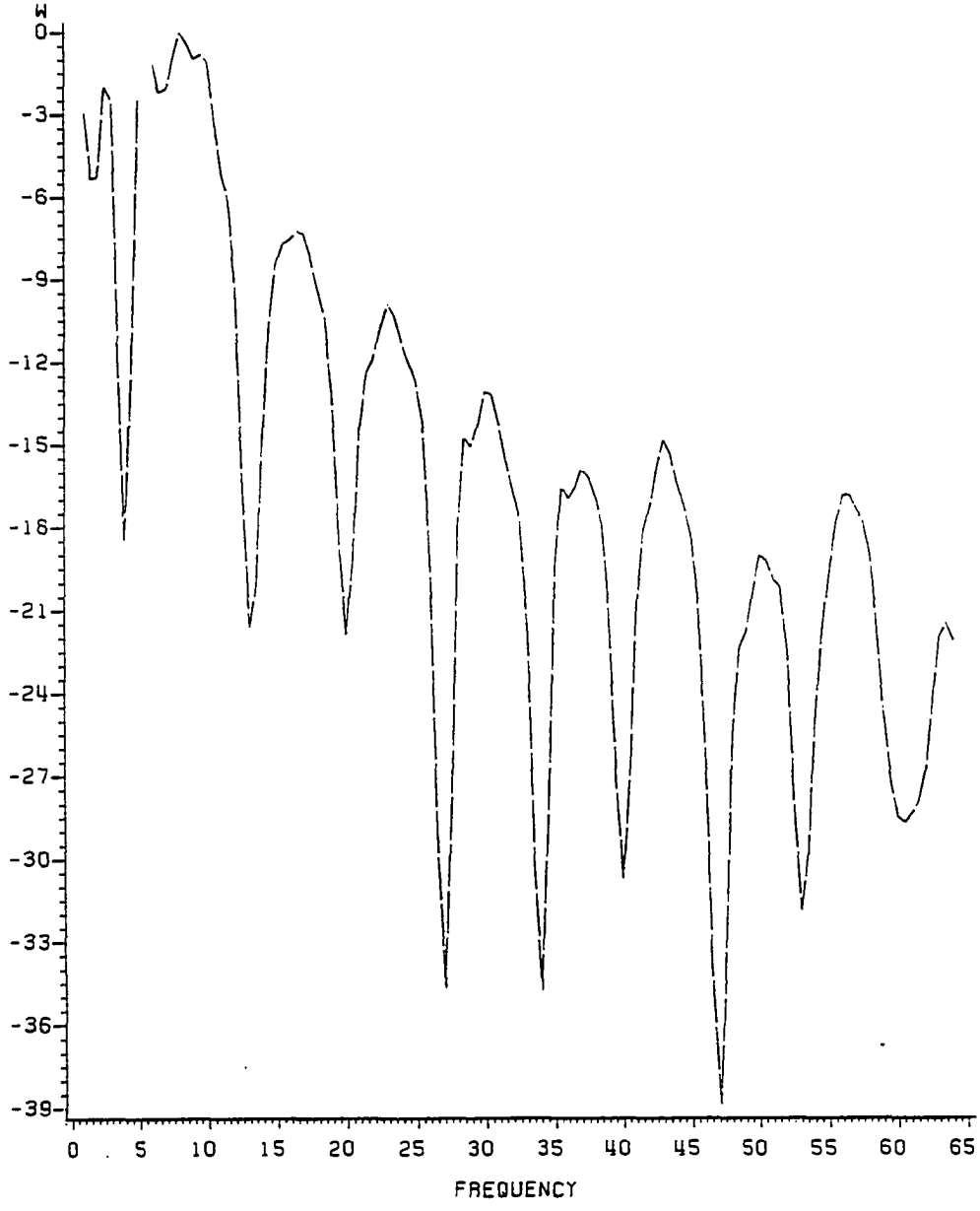

Figure 5.85 The power spectrum of the shear stress for the normal carotid artery.

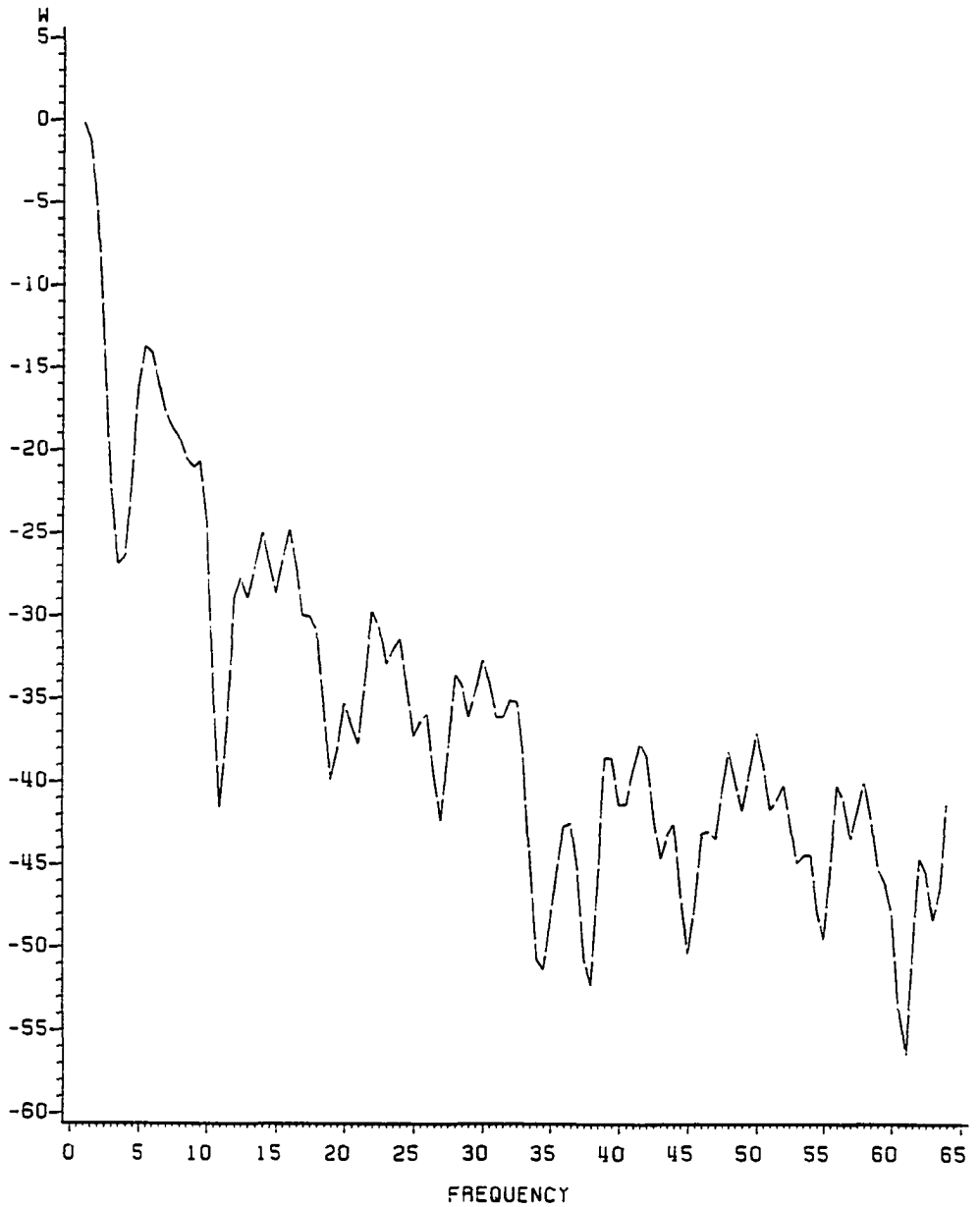

Figure 5.86 The power spectrum of the shear stress for stenotic (25 percent) carotid artery.

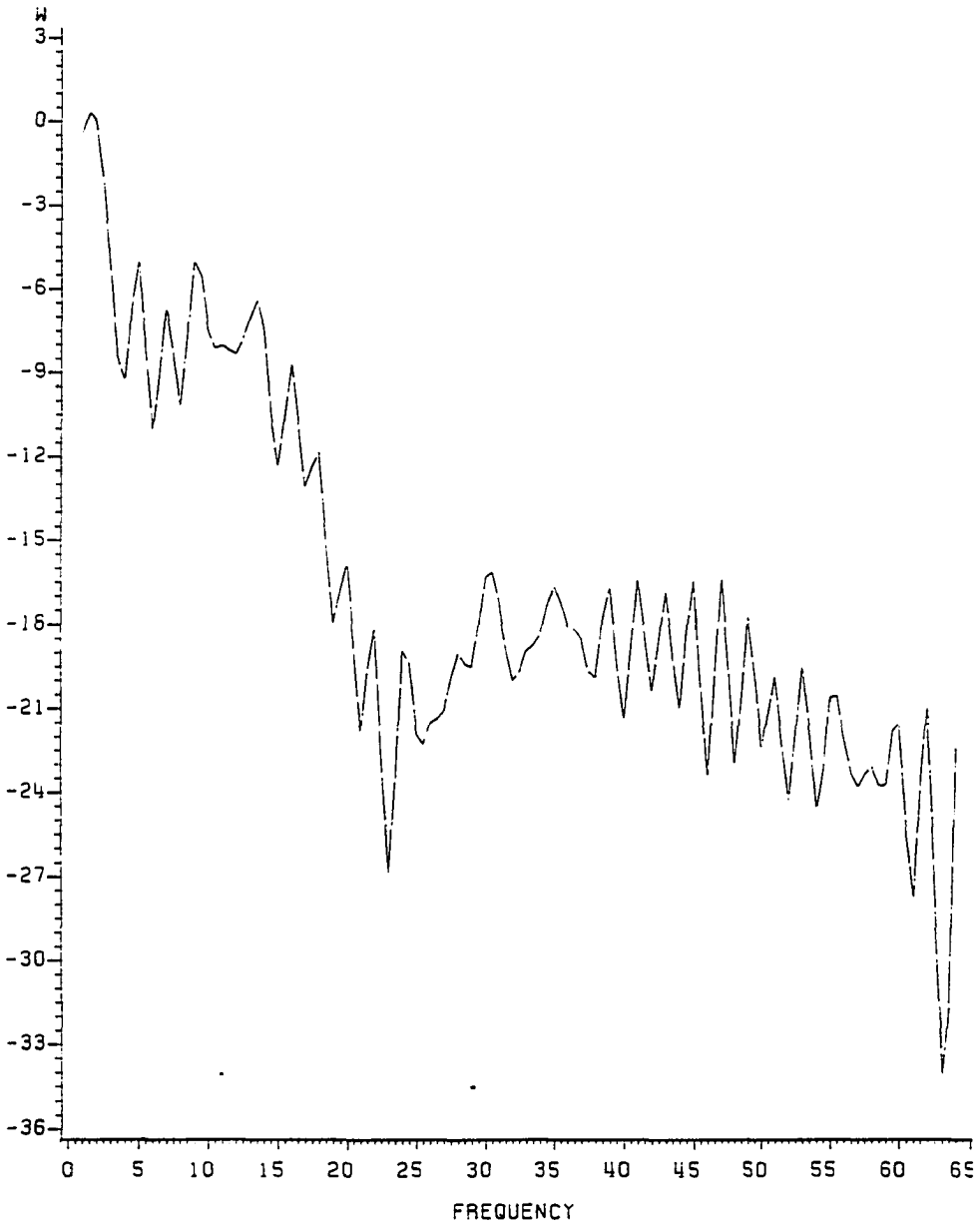

Figure 5.87 The power spectrum of the shear stress for stenotic (33 percent) carotid artery.

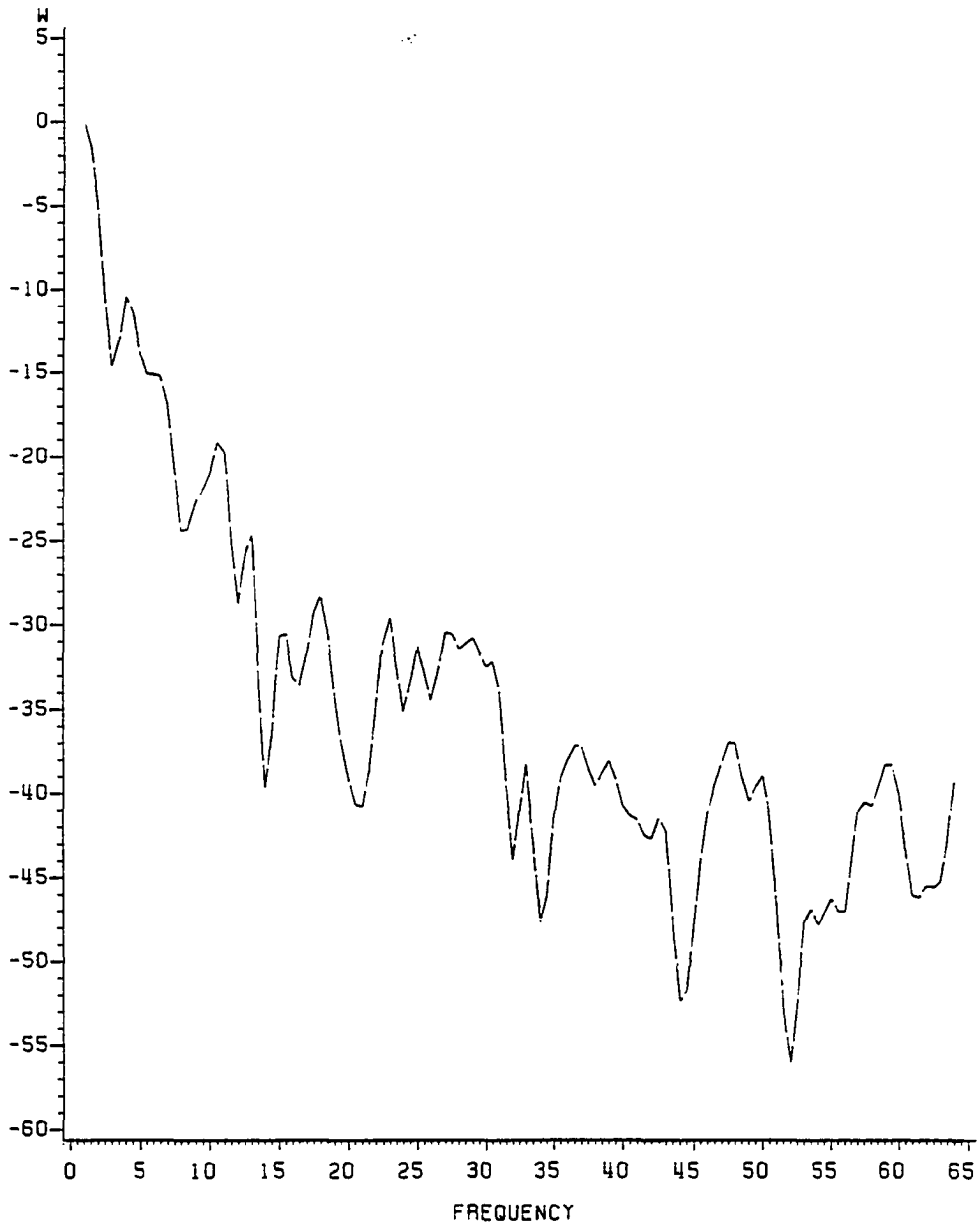

Figure 5.88 The power spectrum of the shear stress for stenotic (50 percent) carotid artery.

$$\frac{\tau_0}{\tau_n} = \frac{Q_1 R_0^3}{Q_0 R_1^3} \tag{5.6}$$

where τ_n and τ_0 are shear stresses, Q_0 and Q_1 are volume rates, and R_0 and R_1 are the radius, in the normal stenotic and stenotic artery, respectively.

From equation (3.77), the height of the stenosis (δ) at midpoint, can be calculated and from that the percentage of the stenosis (st. %) as follows:

$$\delta = R_0 - R_1$$

$$\text{st.\%} = \frac{\delta}{R_0} \cdot 100\% \tag{5.7}$$

In this experiment, the flow volume rate, along with shear stress, are calculated, using the measured diameter of the artery. The results are presented in Table 5.19. The calculated results are slightly different than measured results. Although this work is the first attempt ever to calculate directly the partial occlusion, the following problems can be recognized as contributing to this problem:

1) The diameter is measured by micrometer. The error in reading the exact value and changes in elasticity of the artery can influence the exact measurement, and contribute some error.
2) The calibration between the chart recorder and the computer also can contribute some error to

Table 5.9

Test Condition	Volume Rate	Shear Stress	Shear Stress Ratio τ_o/τ_n	Volume Rate (ratio) Q_1/Q_0	Radius R (mm)	Stenosis (mm)	Stenosis (%)
Normal	137.96	9351	1	1	1.5	-	-
25% stenosis	79.25	11597	1.236	0.574	1.16	0.338	22.56
33% stenosis	61.70	11699	1.751	0.447	1.064	0.435	29.02
50% stenosis	24.63	8354	0.893	0.1785	0.87	0.63	42

the process.

3) The frequency to voltage converter in the pulsed-Doppler instrument is also a major factor that can change the results.

Despite the difference between measured and calculated percentage of occlusion caused by the above-mentioned problems and other factors, the results of this experiment can serve as the first step in calculating the partial occlusion.

CHAPTER VI

SUMMARY

In the theoretical portion of the present study, a practical approximation for the backscattering of periodic bursts of damped sine wave was developed by a volume of randomly distributed scatterers. The approximation was applied to the measurement of a volumetric backscattering cross section, taking into account structural parameters of the tissue and acoustical properties of ultrasound scattering. This provided a means of describing the Doppler-shifted signal content which in turn was used to study the theoretical behavior of blood flow. The Doppler-shifted signal was presented following the theoretical procedure to obtain such a signal by pulsed-Doppler ultrasound instruments.

The relationship between Doppler-shifted frequency and velocity of the blood was described, and a dual-transducer model was developed to calculate the most important parameter (Doppler angle) in that relationship. The calculation of Doppler angle allowed the accurate measurement of the blood flow velocities. The superiority of the developed model in obtaining the flow velocity was verified by

theoretically comparing it with the conventional single transducer model. The application of the developed model in both laminar and turbulent blood flow pattern was outlined and it was shown that in fact the new model is the only effective tool to obtain turbulent blood flow characteristics such as turbulent intensity and shear stress, since two or more components of the velocities are required to obtain such characteristics. Also, in the theoretical development of this study, a direct relationship between turbulent blood flow characteristics and structural changes of the artery was presented, which is of great importance in medical applications.

The theoretical analyses were verified by experimental analysis and were found to be in general agreement. In acute animal experiments (in-vivo), instantaneous flow tracings of the carotid artery were obtained with a directional pulsed-Doppler ultrasound at rest and under anesthesia. Results of in-vivo experiments in obtaining the Doppler angle and blood flow velocities were verified by an in-vitro experimental model using a pulsatile pump as the source of producing the blood flow. In addition to the above in-vitro experiment, other in-vitro experiments were conducted to evaluate the performance of the developed transducer model in this study by presenting the results for blood flow velocities, blood flow velocity profile,

volume flow rate and shear stress. Since the most important objective of the pulsed-Doppler ultrasound instrument is quantitative assessment of the state of peripheral arterial diseases, attemps have been made to relate the blood flow characteristics with the degree of stenosis.

The developed model in this study was implemented internally in in-vivo experiments. However, the noninvasive application of a dual model is foreseeable for future work, using the aid of microprocessor control systems. For accomplishing this goal, the basic design considerations of a dual-transducer model has been outlined in the hope of acquainting the potential user with both the possibilities and the limitations inherent in such a model. In addition to this, the most important recommendation for future studies is the design of a more comprehensive device or development of a different procedure to be utilized for converting the Doppler shifted signal to instantaneous velocity waveform, which can eliminate many errors inherent with the use of zero-crossing converters.

REFERENCES

1. Powis, R. L., "Ultrasound Physics.... For the Fun of It," Unirad Corporation,, 1978.

2. Wells, P.N.T. and Ziskin, M.C., New Techniques and Instrumentation in Ultrasonography, Churchill Livingstone, New York, 1980.

3. Atkinson, P. I. and Woodcock, J. P., Doppler Ultrasound and Its Use in Clinical Measurement, Academic Press, 1982.

4. Baker, D. W., "Pulsed Ultrasounic Doppler Blood-Flow Sensing," IEEE Transactions on Sonics and Ultrasounics, Vol. SU-17, No 3, July 1970.

5. Holland, S. K., "Frequency-Dependent Attenuation Effects in Pulsed Doppler Ultrasound: Experimental Results," IEEE Transactions on Biomedical-Engineering, Vol. BME-31, No. 9, Sept. 1984.

6. Caprihan, A., Davis, J., Greene, E. R., Loeppky, J.A. and Eldridge, M.W., "Waveform Analysis of Doppler Ultrasound Signals by a Microcomputer," IEEE Transactions on Biomedical Engineering, Vol. BME-29, pp. 138-146, No. 2, Feb. 1982.

7. Wille, S., "A Computer System for On-Line Decoding of Ultrasonic Doppler Signals from Blood Flow Measurement," Ultrasonics, pp. 226-230, Sept. 1977.

8. Hwang, N.H.C., Hussain, A.K.M.F., Hui, P.W., and Striplang, T., "Turbulent Flow Through a Natural Human Mitral Valve," J. Biomechanics, Vol. 19, pp. 59-67, 1977.

9. Chu, W. K. and Cheung, J. Y., "Computer Simulation of Ultrasound Propagation and Attenuation," World Congress on Medical Physics and Biomedical Engineering, Hamburg, 23.06, 1982.

10. Ringers, S. E., Putney, W. W. and Barnes, R. W., "Real-Time Spectrum Analysis and Display of Directional Doppler Ultrasound Blood Velocity Signals," IEEE Transactions on Biomedical Engineering, Vol. BME-27, No. 12, pp. 723-727, Dec. 1980.

11. Champagne, F. H., Sleicher, C. A. and Wehrmann, O.H., "Turbulent Measurements with Inclined Hot-Wires," Part I. Heat Transfer Experiments with Inclined Hot-Wire, J. Fluid Mech. (1967), Vol. 28, Part I, pp. 153-175 (1976).

12. Elias, C.M., "Ultrasonic Pseudorandom Signal-Correlation System," IEEE Transactions on Sonics and Ultrasonics, Vol. SU-27, No. 1, pp. 1-7, Jan. 1980.

13. Jethwa, C. P., and Olinger, M. D., "Blood Flow Measurement Using Random Signal Flowmeter," UIM, pp 334, 1977.

14. McLead, F. D., "Doppler Detection of Flow Distributions," UIM, pp. 351-353.

15. Daigle, R. E., Miller, C. W., Histand, M. B., McLead, F. D., and Hokanson, D. E., "Nontraumatic Measurement of Aortic Blood Velocity Fields, Flow, and Wall Properties, UIM, pp. 352.

16. Miller, G. W., McLead, F. D., and Butterfield, A. B., "Measurement of Hemodynamics in Atherogenic Swine Using Ultrasound," UIM, pp. 353, 1977.

17. Coghlan, B. A., and Taylor, M. G., "Improved Real-Time Spectrum Analyzer for Doppler-Shift Blood Velocity Waveform," Medical and Biological Engineering and Computing, Vol. 17, pp. 316-322, 1979.

18. Chow, C. K., "An Experimental Data Acquisition System for Ultrasound Imaging," IEEE Transactions on Instrumentation and Measurement, Vol. IM-28, pp. 79-83, March 1979.

19. Grezberg, L., and Meindl, J. D., "Mean Frequency Estimation With Application in Ultrasonic Doppler Flowmeter," UIM, pp. 1174-1179, 1978.

20. Nimura, Y., "Studies on the Intracardiac Blood Flow With a Combined Use of the Ultrasonic Pulsed Doppler Technique and Two-Dimensional Echocardiography From a Transcutaneous Approach," UIM, pp. 1279-1289, 1978.

21. Jorgensen, J. E. and Garbini, J. L., "An Analytical Procedure of Calibration for the Pulsed Ultrasonic Doppler Flow Meter," J. Fluids Engineering, Vol. 96, pp. 153-167, 1974.

22. Morris, S. J., Woodcock, J. P. and Wells, P. N. T., "Impulse Response of a Segment of Artery Derived from Transcutaneous Blood-Velocity Measurement," Medical and Biological Engineering, pp. 803-812, Nov. 1975.

23. Wells, P. N. T., "The Directiveties of Some Ultrasonic Doppler Probes, Hol. Engineering, Vol. 18, pp. 241-256, 1970.

24. Thomson, F. J., "Broad Pulsed Doppler Ultrasonic System for the Noninvasicer Measurement of Blood Velocity in Large Vessels," Medical and Biological Engineering and Computation, Vol. 16, pp. 135-146, 1978.

25. Franklin, D., Schlegel, W. and Rushmer, R., "Blood Flow Measurement by Doppler Frequency Shift of Back-Scattered Ultrasound," Science, Vol. 134, pp. 564-565, 1961.

26. Newhouse, V. L., "Analysis of Transit Time Effects on Doppler Flow Measurement," IEEE, BME, Vol. 120, pp. 381-387, 1976.

27. Brody, W. B., "Theoretical Analysis of the CW Doppler Ultrasonic Flowmeter," IEEE, BME, Vol. 110, pp. 183-192, 1974.

28. Barber, F. E., "Ultrasonic Duplex Echo-Doppler Scanner," IEEE, BME, Vol. 124, pp. 109-113, 1974.

29. Gore, J. C., "Echo Structure in Medical Ultrasonic Pulse-Echo Scanning," Medical Physics Dept., Royal Postgraduate Medical School, Hammersmith Hospital, London, pp. 431-443, 1979.

30. Okuda, J., Shiraishi, J., Kaneko, Z., and Iwamoto, K., "An Ultrasonic Pulsed Doppler Flowmetery Comprising with the NTSC (National Television System Committee) Television System," UIM, pp. 1237-1246, 1977.

31. Bournat, J. P., Peronneau, P., and Herment, A., "Theoretical and Experimental Evaluation of a New Ultrasonic Doppler Method for Vascular Imaging," UIM, pp. 1343-1345, 1977.

32. Ohmori, S., and Moritz, W. E., "A New Method of Quantifying Flow Using Pulsed Doppler," UIM, pp. 1247-1253, 1977.

33. Freund, W. R., and Anliker, J. E., "Matrix Analysis of Doppler Spectra," UIM, pp. 1341-1342, 1977.

34. Valdes-Cruz, L. M., and Sahn, D. J., "Two Dimensional Echo Doppler for Non-Invasive Quantization of Cardiac Flow: A Status Report," Journal of American Heart Association, Vol. 51, pp. 123-128, Oct. 1982.

35. Hughes, D. J., Geddes, L. A., Babbs, C. F., Bourland, J. D. and Newhouse, V. L., "Attenuation and Speed of 10 MHz Ultrasound in Canine Blood of Various Packed-Cell Volumes at 37 degrees Celsius," Medical and Biological Engineering, Vol. 17, pp. 619-622, Sept. 1979.

36. Brown, J. M., Nahorski, Z. T., Woodcock, J. P., and Morris, S. J., "Transfer-Function Modeling of Arteries," Medical and Biological Engineering and Computing, Vol. 16, pp. 161-184, 1978.

37. Padmanabhan, N., and Devanathan, R., "Mathematical Model of an Arterial Stenosis Allowing for Tethering," Medical and Biological Engineering and Computing, pp. 385-390, July 1981.

38. Skidmore, R. and Woodcock, J. P., "Physiological Interpretation of Doppler-Shift Waveforms-I, Theoretical Considerations," Ultrasound in Medicine and Biology, Vol. 6, pp. 7-10, 1080.

39. Strandness, D. E., Schultz, R. D., Summer, D. S., and Rushmer, R. F., "A Useful Technic in the Evaluation of Peripheral Vascular Disease," American Journal of Surgery, Vol. 1, pp. 311-320, 1967.

40. Woodcock, J. P., Morris, S. J., and Wells, P. N. T., "Significance of the Velocity Impulse Response and Cross-Correlation of the Femoral and Popliteal Blood-Velocity/Time Waveforms in Disease of the Supervicial Femoral Artery," Medical and Biological Engineering, pp. 813-818, Nov. 1975.

41. Forrester, J. N., and Young, D. F., "Flow Through Converging-Diverging Tube and Its Implications in Occlusive Vascular Disease-I," Journal of Biomechanics, Vol. 3, pp. 297-305, 1970.

42. Wells, P. N. T., "A Range-Gated Ultrasonic Doppler System," Medical and Biological Engineering, Vol. 7, pp. 641-652, 1969.

43. Angelsen, B. A., "A Theoretical Study of the Scattering of Ultrasound from Blood," IEEE Transactions on Medical Engineering, Vol. BME-27, pp. 61-67, 1980.

44. Angelsen, B. A., "Instantaneous Frequency, Mean Frequency, and Variance of Mean Frequency Estimators for Ultrasonic Blood Velocity Doppler Signals," IEEE Transactions on Biomedical Engineering, Vol. BME-28, No. 11, pp. 733-741, 1981.

45. Hussain, A. K. M. F. and Reynolds, W. C., The Mechanics of an Organized Wave in Turbulent Shear Flow," J. Fluid Mechanics, Vol. 41, Part 2, pp. 241-258, 1970.

46. Shung, K. K., Sigelmann, R. A., and Reid, J. M., "Scattering of Ultrasound by Blood," IEEE Transactionss on Biomedical Engineering, Vol. BME-23, No. 6, pp. 460-467, Nov. 1976.

47. Sigelmann, R. A., and Reid, J. M., "Analysis and Measurement of Ultrasound Backscattering from an Ensemble of Scatters Excited by Sine-Wave Bursts," The Journal of Acoustic Society of America, Vol. 53, pp. 1351-1355, 1973.

48. Stein, P. D. and Sabbah, H. M., "Contribution of Erythrocytes to Turbulent Blood Flow," Biorheology, Vol. 12, pp. 293-299, 1975.

49. Young, D. F., "Effect of a Time-Dependent Stenosis on Flow Through a Tube," Journal of Engineering for Industry, Vol. 90, pp. 248-254, 1968.

50. Cathignol, D. J., Fourcade, C., and Chapelon, J. Y., "Transcutaneous Blood Flow Measurements Using Pseudorandom Noise Doppler System," IEEE Transactions on Biomedical Engineering, Vol. BME-27, No. 1, pp. 30-36, Jan. 1980.

51. Gerrard, J. H., "The Effect of the Skin Friction on the Solution of the One-Dimensional Equations of Pulsatile Flow in Distensible Tubes," Medical and Biological Engineering and Computing, pp. 79-82, Jan. 1981.

52. Letelier, M. F. and Leutheusser, H. J., "Analytical Deduction of the Instantaneous Velocity Distribution, Wall Shear Stress and Pressure Gradient from Transcutaneous Measurements of the Time-Varying Rate of Blood Flow," Medical and Biological Engineering and Computing, pp. 433-436, July 1981.

53. Ahmed, M., "The Role of the Computer in Diagnostic Ultrasound," IEEE Transactions or Biomedical Engineering, Vol. 16, pp. 173-180, 1979.

54. Kadaba, M. P., Bhagat, P. E., and Wu, V. C., "Attenuation and Backscattering of Ultrasound on Freshly Excised Animal Tissues," IEEE Transactions on Biomedical Engineering, Vol. 27, pp. 76-83, Feb. 1980.

55. Beretsky, M. D., "Detection and Characterization of Atherosclerosis in a Human Arterial Wall by Raylographic Technique, an In-Vitrostudy," Recent Advances in Ultrasound in Biomedicine, Vol. 1, pp. 1592-1612, 1977.

56. Ghista, D. N., "Analysis for the Non-Invasive Determination of Arterial Properties and for the Transcutaneous Continuous Monitoring of Arterial Blood Pressure," IEEE, BME, pp. 715-726, 1978.

57. Wallace, T. P., and Wintz, P. A., "An Efficient Three-Dimensional Aircraft Recognition Algorithm Using Normalized Fourier Descriptors," IEEE, BME, Vol. 103, pp. 722-733, 1980.

58. Ramsey, S., "Composition B-Scan/Doppler Imaging of Blood Vessels in Real-Time," UIM, pp. 1347-1348, 1978.

59. Nilsson, G. E., "Evaluation of a Laser Doppler Flowmeter for Measurement of Tissue Blood Flow," IEEE, BME, Vol. 10, pp. 597-604, 1980.

60. Gill, R. V., "Quantitative Blood Flow Measurement in Deep-Laying Vessels Using Pulsed-Doppler with the Octoson," UIM, Vol. 4, pp. 341-347, 1978.

61. Duerinckx, A., "Modeling Wavefronts from Acoustic Phased Arrays by Computer," IEEE, BME, pp. 221-234, 1981.

62. Moulinier, H. and Marsural, G., "Detection of Bubbles in Blood Vessels and the Evaluation of their Flow," Med. & Biol. & Comp., pp. 585-588, 1978.

63. Greenleaf, J. F., Johnson, S. A., Lee, S. L., Herman, G. T., and Wood, E. H., "Algebraic Reconstruction of Spatial Distribution of Acoustic Absorption within Tissue from their Two-Dimensional Acoustic Projections," Acoustic Holography, Vol. 5, pp. 591-603.

64. DeLavault, E., "Fourier Analysis of Nonlinear Fluid System," IEEE, BME, pp. 215-219, 1982.

65. Learoyd, B. M., and Taylor, M. G., "Alterations with Age in the Viscoelastic Properties of Human Arterial Wells, "Circulation Research, Vol. 5.

66. Klepper, J. R., "Application of Phase-Insensitive Detection and Frequency-Dependent Measurements to Computed Ultrasonic Attenuation Tomography," IEEE, BME, pp. 186-201, 1981.

67. Sainz, A., Roberts, V. C. and Pinardi, G., "Phase-Locked Loop Technique Applied to Ultrasonic Doppler Signal Processing," Ultrasonic, pp. 127-132, 1976.

68. Klee, G., Ackerman, E. and Leonard, A., "Computer Detection of Distortion in Arterial Pressure Signals, IEEE, Biomed, Engr., pp. 73-75.

69. Stewart, W., Wilson, J. R. and Burling, R. W., "Some Statistical Properties of Small Scale Turbulence in an Atmospheric Boundary Layer," J. of Biomechanics, Vol. 41, pp. 141-152, 1970.

70. Glover, G. H., "Reconstruction of Ultrasound Propagation Speed Distribution in Soft Tissue: Time-of-Flight, Tomography," IEEE, Sonics and Ultrasonics, pp. 229-234, 1977.

71. Laxminarayan, S., Laxminarayan, R., Langewerters, G.J. and Vos, A. B., "Computing Total Arterial Compliance of the Arterial System from its Input Impedance, "Medical & Biological Engineering & Computer, Vol. 17, pp. 623-628, 1979.

72. Norton, S., "Ultrasonic Reflectivity Imaging in Three Dimensions: Exact Inverse Scattering Solutions for Plane, Cylindrical, and Spherical Apertures," IEEE, BME, pp. 202-220, 1981.

73. Chowdhury, S., "Digital Spectrum Analysis of Respiratory Sound," IEEE, BME, pp. 784-793, 1981.

74. Lin, J. C., "A Note on the Optical Scattering Characteristics of Whole Blood," IEEE, BME, pp. 43-45, 1974.

75. Moritz, W. and Shreve, P., "A Microprocessor-Based Spatial-Locating System for Use with Diagnostic Ultrasound," IEEE, BME, pp. 966-974, 1976.

76. Bedini, L., and Bramanti, M., "Analysis of the Electromagnetic Interaction Between a Resonator and a Lossy Dielectric Body as a first theoretical Approach to Noninvasive Heart Movement Detection," IEEE, BME, pp. 623-630, 1980.

77. Greenleaf, J. F., "Clinical Imaging with Transmissive Ultrasonic Computerized Tomography," IEEE, BME, pp. 177-185, 1981.

78. Cook, L. T., "Assessment of Scoliosis Using Three-Dimensional Analysis," IEEE, BME, pp. 366-371, 1981.

79. Garrett, W. J., "The Octoson in Use," UIM, pp. 341-349, 1976.

80. Beaver, W. L., "Ultrasonic Imaging with an Acoustic Lens," IEEE, BME, pp. 235-242, 1977.

81. Angelsen, B. A., "Spectral Estimation of a Narrow-band Guassian Process from the Distribution of the Distance between Adjacent Zeros," IEEE, BME, pp. 108-112, 1980.

82. Hagfors, T., "Mapping of Planetary Surfaces by Radar," IEEE, BME, pp. 1219-1225, 1973.

83. Stein, P. D., Parsons, E. D., and Blick, E. F., "Modification of Dynamic Flow Properties of Turbulency Flowing Human Blood by Long Chain Polymers," Medical Research Engineering, pp. 6-10, 1972.

84. Blick, E. F., and Stein, P. D., "Work of the Heart: A General Thermodynamics Analysis," Journal of Biomech., Vol. 10, pp. 589-595, 1977.

85. Stevenson, J. G., Kawabor, I., Dooley, T., and Guntheroth, W. G., "Diagnosis of Ventricular Septal Defect by Pulsed-Doppler Echocardiolography," Advanced Technology Lab., pp. 322-326, 1978.

86. Sabbah, H. N., and Stein, P. D., "Effect of Erythrocytic Deformability upon Turbulent Blood Flow," Biorheology, pp. 309-314, 1976.

87. Stein, P. D., Sabbah, H. N. and Pitha, J. K., "Continuous Disease Process of Calcific Aortic Stenosis (Role of Microthrombi and Turbulent Flows)," The American Journal of Cardiology, Vol. 39, pp. 159-163, 1977.

88. Goldberg, S. J., Kececieglu-Draelos, Z., Shan, D. J., Valdes-Crus, L. M. and Allen, H. D., "Range Gated Echo-Doppler Velocity and Turbulence Mapping in Patients with Vascular Aortic Stenosis," The C.V. Mosby Co., pp. 858-863, 1981.

89. Stein, P. D., Sabbah, H. N., and Blick, E. F., "Contribution of Erythrocytes to Turbulent Blood Flow," Biorheology, pp. 293-299, 1975.

90. Stein, P. D., Walburn, F. J. and Blick, E. F., "Damping Effect of Distensible Tube on Turbulent Flow Implications in the Cardiovascular System," Biorheology, pp. 275-281, 1980.

91. Walburn, F. J., Blick, E. F. and Stein, P. D., "Effect of the Branch-to-Trunk Area Ratio on the Transition to Turbulent Flow: Implications in the Cardiovascular System," Pergamon Press, Ltd., p. 411-417, 1979.

92. Carter, J., Reynoldson, J. A., Thorburn, G. D. and Bates, W. A., "Blood Flow Measurement During Exercise in Sheep Using Doppler Ultrasounic Method," Medical & Biological Engineering and Computer, pp. 373-376, 1981.

93. Wells, P. N. T., Halliwel, M., Skidmore, R., Webb, A.J., and Woodcock, J. P., "Tumor Detection by Ultrasound Doppler Blood Flow Signals," Ultrasounics, pp. 231-232, 1977.

94. Khalilollahi, A. and Sharma, M. C., "Numerical Analysis of Blood Flow Through Stensed Arteries," Proc. of IASTED International Conference, ACTA Press, pp. 167-169, 1984.

95. Hatle, L., and Angelsen, B., Doppler Ultrasound in Cardiology, 2d Edition, Lea & Febiger, PA, 1985.

96. Khaligh, B., Chandram, K. B., and Chen, C. J., "Steady Flow Development Past Valve Prostheses in a Model Human Aorta I. Centrally Occluding Valves," J. Biomechanics, Vol. 16, No. 12, pp. 1003-1011, 1983.

97. Saad, A. A., and Giddens, D. P., Velocity Measurements in Steady Flow Through Axisymmetric Stenoses at Moderate Reynolds Number," Jour. of Biomechanics, Vol. 16, No. 12, pp. 955-963, 1983.

98. Saad, A. A., and Giddens, D. P., "Flow Disturbance Measurement Through a Constricted Tube at Moderate Reynolds Number," J. Biomechanics, Vol. 16, No. 12, pp 955-963, 1983.

99. Chandran, K. B., Cabell, G. N. and Khalighi, B., "Laser Anemometry Measurements of Pulsatile Flow Past Aortic Valve Prostheses," Jour. of Biomechinics, Vol. 16, No. 10, pp. 865-873, 1983.

100. Gibbons, D. T., Evans, D. H., Barrie, W. W. and Gosgriff, P. S., "Real-Time Calculation of Ultrasounic Pulsatility Index," Medical & Biological Engineering & Computer, pp. 28-34, 1981.

101. Kenyon, R. A., Principles of Fluid Mechanics, The Ronald Press Co., 1960.

102. Welty, J. R., Wicks, C. E., and Wilson, R. E., Fundamentals of Momentum-Heat, and Mass Transfer, 2d Ed., John Wiley & Sons, Inc., 1976.

103. Mates, R. E., Nerem, R. M. and Stein, P. D., "Mechanics of the Coronary Circulation," The Applied Mechanics, Bioengineering and Fluids Engineering Conference, Houston, TX, 1983.

104. Michel, R., Cousteix, J. and Houdeville, R., "Unsteady Turbulent Shear Flows," International Union of Theoretical and Applied Mechanics, Symposium, Toulouse, France, 1981.

105. Hinze, J. O., Turbulence, McGraw Hill, 1959.

106. Yamaguchi, T. and Kikkawa, S., "Measurement of Turbulence Intensity in the Center of the Canine Ascending Aorta with a Hot-Film Anemometer," Jour. of Biomech. Engineering, pp. 177-187, 1983.

107. Stehbens, W. E., "Turbulence of Blood Flow," UIM, pp. 110-117, 1978.

APPENDIX A

SOME OF THE NUMERICAL RESULTS OF EXPERIMENT 5.3.3

Table A.1

Test Number	Doppler Angle (θ)	Volume Rate	Average Velocity	Peak to Peak Ratio (A_1/B_1)	Number of Points
F22C1	43.40	93.148	271.148	2.393	346
F22C2	44.712	92.475	269.190	2.540	344
F22C3	44.131	91.319	265.824	2.486	328
F22C4	44.195	94.382	274.73	2.517	343
F22C5	44.029	94.110	273.949	2.472	344
F22C6	42.568	97.305	283.25	2.353	344
F22C7	44.279	93.184	271.254	2.593	341
F22C8	43.938	96.692	281.454	2.613	343
F22C9	43.554	94.769	275.866	2.518	340
F22C10	43.756	92.37074	268.884	2.509	344
F22C11	43.485	92.262	268.569	2.572	327
F22D1	45.084	89.850	261.548	2.452	334
F22D2	45.154	91.864	267.410	2.386	343
F22D3	44.580	91.164	265.374	2.372	345
F22D4	44.819	91.437	266.169	2.453	340
F22D5	45.125	89.236	259.761	2.331	343
F22D6	45.183	89.384	260.193	2.398	337
F22D7	44.663	91.167	265.382	2.433	340

(cont'd to next page)

Table A.1 (cont'd)

Test Number	Doppler Angle (θ)	Volume Rate	Average Velocity	Peak to Peak Ratio (A_1/B_1)	Number of Points
F22D8	45.082	90.293	262.838	2.464	342
F22D9	44.912	91.612	266.678	2.398	345
F22D10	45.344	90.679	263.961	2.274	343
F22D11	44.765	91.323	265.837	2.301	342
F22D12	45.111	90.381	263.096	2.250	342
F22D13	45.272	91.144	265.315	2.270	345
F22E2	45.233	89.511	260.560	1.924	341
F22E3	46.106	86.625	252.161	2.152	338
F22E4	45.173	90.94377	264.729	1.984	341
F22E5	46.215	89.599	260.817	1.967	339
F22E6	45.384	87.539	254.822	2.050	338
F22E7	45.577	89.741	261.230	2.073	340
F22E8	45.762	89.841	261.52	2.016	332
F22E9	45.185	88.581	257.855	2.	341
F22E10	45.237	88.605	257.924	2.085	338
F22E11	45.157	89.951	261.841	1.947	336
F22E12	45.287	88.877	258.716	2.006	337
F22E13	46.311	88.254	256.903	2.045	340
F22H1	43.139	52.213	151.988	2.346	340
F22H2	42.275	54.855	159.580	2.005	340

(cont'd to next page)

Table A.1 (cont'd)

Test Number	Doppler Angle (θ)	Volume Rate	Average Velocity	Peak to Peak Ratio (A_1/B_1)	Number of Points
F22H3	43.243	53.175	154.789	2.020	338
F22H4	42.269	54.446	158.490	1.947	326
F22H5	43.994	51.073	148.670	2.634	341
F22I1	44.370	93.077	270.943	2.884	328
F22I2	43.747	94.456	274.954	2.910	343
F22I3	44.311	94.124	273.990	2.772	343
F22I4	44.041	92.823	270.203	2.837	339
F22I5	44.841	92.989	270.865	2.786	339
F22I6	44.666	92.514	269.514	2.886	345
F22I7	44.440	92.612	269.587	3.012	345
F22I8	43.960	95.939	279.271	3.006	342
F22I10	44.826	94.817	276.008	2.916	344
F22I11	44.744	92.688	269.809	2.775	343
F22I12	44.050	96.822	281.844	2.886	338
F22I13	43.689	97.710	284.4294	2.868	331
F22I14	43.786	94.115	273.953	2.741	341
F22I15	44.757	93.151	271.157	2.680	340
F22J1	40.269	33.639	97.920	1.416	163
F22J2	41.661	34.824	101.370	1.310	166
F22J3	40.577	34.237	99.662	1.385	169

(cont'd to next page)

Table A.1 (cont'd)

Test Number	Doppler Angle (θ)	Volume Rate	Average Velocity	Peak to Peak Ratio (A_1/B_1)	Number of Points
F22J4	40.967	33.697	98.089	1.282	155
F22J5	40.709	34.848	101.441	1.331	158
F22J6	40.403	33.145	96.484	1.390	159
F22J7	41.435	33.986	98.932	1.236	165
F22J8	41.193	31.800	92.530	1.391	161
F22L1	15.763	25.759	74.985	1.845	166
F22L2	15.231	23.921	69.632	1.713	158
F22L3	16.281	23.342	67.949	1.860	159
F22L4	15.857	23.387	68.050	1.798	164
F22L5	16.398	23.366	68.017	1.578	165
F22L6	15.242	23.054	67.106	1.971	153
F22L7	16.907	22.270	64.829	1.739	165
F22L8	14.546	23.253	67.689	1.667	164
F22L9	16.296	23.383	68.067	1.797	153
F22L10	16.573	22.171	64.539	1.693	170
F22L11	16.731	22.109	64.359	1.749	166
F22L13	16.146	21.697	63.159	1.792	162
F22N1	44.641	52.301	152.246	2.167	157
F22N4	45.409	52.706	153.423	2.687	166
F22N5	43.601	50.604	147.306	2.353	162

(cont'd to next page)

Table A.1 (cont'd)

Test Number	Doppler Angle (θ)	Volume Rate	Average Velocity	Peak to Peak Ratio (A_1/B_1)	Number of Points
F22N7	46.050	52.952	154.141	2.688	163
F22N10	45.451	47.767	139.047	2.375	162
F22N11	44.400	48.967	142.540	2.500	164
F22N13	43.252	48.734	141.862	2.437	166
F22N15	44.740	52.319	152.298	2.471	163
F22P1	47.299	65.948	191.971	5.125	336
F22P2	46.070	65.699	191.245	4.500	344
F22P3	46.016	62.677	182.449	4.789	341
F22P4	44.735	59.345	169.840	4.706	341
F22P5	45.351	62.824	182.878	5.015	342
F22P6	47.447	61.991	180.45291	4.472	333
F22P8	45.798	60.887	177.24	4.288	341
F22P9	45.394	63.443	184.678	4.351	350
F22R1	45.757	60.639	176.518	4.413	343
F22R2	46.449	64.338	187.286	4.408	341
F22R3	46.980	62.074	180.893	4.452	341
F22R4	45.148	59.795	174.059	4.211	342
F22R5	45.746	60.153	175.103	4.288	346
F22R6	45.743	62.445	181.775	4.351	342

(cont'd to next page)

Table A.1 (cont'd)

Test Number	Doppler Angle (θ)	Volume Rate	Average Velocity	Peak to Peak Ratio (A_1/B_1)	Number of Points
F22R7	45.919	62.133	180.865	4.141	341
F22R8	45.408	57.366	166.990	4.227	332
F22R9	46.076	59.210	172.358	4.117	337
F22R10	47.168	59.506	173.219	3.873	341

APPENDIX B

DESCRIPTION OF THE 5453-c ULTRASOUND MACHINE

THE 5453-c ULTRASOUND MACHINE

MASTER/SLAVE

This portion of the system is provided so that two or three Dopplers may be synchronized to each other to prevent interference where more than one such unit is operated in a single lab. For normal use, the "Master/Slave" switch must be in the "Master" position, and no connections made to the "Remote" jacks. To synchronize two or three units, only one of the units must be in the "Master" mode and the other one or two units must be in the "Slave" mode. The units must be connected together with the proper cable, which is available from bioengineering. The cable connects between either of the "Remote" connectors on the several units.

AUDIO

An audio power amplifier is provided so that the Doppler signal can be aurally monitored. A small speaker is built into the unit, or an external speaker or headphones may be plugged into the "Remote Speaker" jack, which automatically disconnects the internal speaker. The remote speaker should be 4-16 ohms impedance. One channel at a time may be monitored. For units with more than one channel, a "Channel" selector switch is provided.

RANGE

A pulsed Doppler flowmeter has the ability to measure flow velocity at a specified distance from the face of the crystal probe, rather than everywhere within range of the signal. The "Range" control adjusts this distance. The standard maximum range is 1.0 cm, although this may be altered with a simple internal adjustment, up to a maximum of about 1.6 cm.

The principal behind this control is based on the fact that this is a "pulsed" Doppler, that is, it transmits a short burst of audio energy, then "listens" for an echo after some time delay. Obviously, this delay determines how far the audio signal has had a chance to travel and return. The "range" control adjusts the period of a monostable multivibrator that is triggered on the leading edge of the transmit burst. The trailing edge of this pulse triggers another monostable multivibrator which causes sampling of the received signal at that time.

SENSITIVITY

This control adjusts the level of the Doppler signal applied to the voltage-to-frequency converter stage, which provides the "phasic" and "mean" outputs to a recorder or oscilloscope. It is adjusted for optimum signal quality, with attention paid to peak velocity response and baseline

noise (baseline noise is particularly important in the case of zero flow, and the sensitivity should not be high enough to cause a large apparent flow signal in the absence of any flow). Normally, sensitivity should be set no more clockwise than is necessary for obtaining a good output signal.

POLARITY

This control determines which flow direction results in positive output voltage polarity, toward the crystal or away from it. The center "zero" position turns off the signal, both to the output stages and to the audio amplifier. It does not turn off the transmitted energy.

OUTPUT CONNECTIONS

1. Probe

The crystal probe connects here, with pin assignments on the amphenol connector as follows:

Pin B Signal

Pin D Signal

Pin A Shield

The two signal lines are interchangeable, to prevent interference from outside signal sources such as noisy electric motors or radio transmitters. A shielded twisted-pair cable should be used to connect to the crystal.

2. Range

This output is a voltage proportional to the setting of the "range" control. It may be calibrated to any convenient scale. Although the standard calibration is 1 volt per centimeter, e.g., with the range control fully clockwise, the output should be 1.00 volts.

3. Phasic

Phasic blood velocity information appears at this connector with a normal scale factor of 0.5 volts per kilohertz of Doppler shift. The velocity that this represents may be calculated from the formulas given at the beginning of this Appendix, the Master/Slave and Audio sections.

4. Mean

The mean blood velocity is presented at this connector at the same scale factor as the phasic output. The time constant of the meaning circuit is about 600 milliseconds.

5. Audio 1, 2

The signals at these connectors are the actual Doppler audio signals and may be used for a variety of purposes, such as spectral analysis or external audio amplification, which may be done in "stereo." If these signals are used externally, the audio "channel" switch should be set to

another channel, as the audio amplifier "loads" these outputs, resulting in reduced amplitude of one of the signals.

BASIC DOPPLER INFORMATION

1. Doppler Equation (for sound reflected from moving objects):

1.A $FD = 2 * F0 * V * COS\ A)/C$

or

1.B $V = (FD * C) / (2 * F0 * COS\ A)$

where:

FD = Doppler shift frequency in kilohertz

F0 = Transmitter frequency in kilohertz (20,000 KHz in 545C-3'5)

V = Velocity of blood in millimeters per second

C = Velocity of sound in blood (1,565,000 millimeters per second)

A = Angle between sound beam and blood velocity vector

Substituting the above constants for F0 and C in equation 1.B yields:

1.C $V(MM/SEC) = 39.125 * FD / COS\ A$

Finally, substituting the phasic or mean output of the 545C-3 in volts (E) for FD yields:

1.D $V(MM/SEC) = 78.25 * E / COS\ A$

INSTANTANEOUS VOLUME FLOW:

2.A Q = V * P1 * ((D/2) ** 2)

where

Q = Instantaneous volume flow in cubic millimeters per second (liters/1,000,000)

P1 = 3.14159...

D = Lumen diameter in millimeters

V = Instantaneous blood velocity in millimeters per second.

Substituting Equation (1.B) above for "Y" and simplifying yields:

2.B Q = (FD * C * PI * (D ** 2))/(8 * F0 * COS A)

Substituting constants for C, PI and F0 and converting cubic millimeters per second to liters per minute yields:

2.C Q(L/MIN) = FD * (D ** 2)/(542.4 * COS A)

Finally, substituting the phasic or mean output of the 545C-3 in volts (E) for "FD" yields:

2.D Q(L/MIN) = E * (D ** 2)/(271.2 * COS A)

NOTES:

545C-3 directional pulsed Doppler flowmeters are calibrated for 0.5 volts per kilohertz of Doppler shift.

APPENDIX C

SOME OF THE OPERATION SOFTWARE

```
c       In this program we process the data taken
c        from an experiment in hsc(normal flow1).
        dimension a(5500),b(5500),c(5500),d(5500)
        dimension e(5500),v1(2400),v2(2400)
        dimension xreal1(1500),xreal2(1500),ximag1(1500),ximag2(1500)
        dimension x1real(2500),x2real(2500),x1imag(2500),x2imag(2500)
        dimension ps1(2500),ps2(2500)
        dimension psf1(2500),psf2(2500)
        dimension cb1(2500),cb2(2500)
        dimension cbf1(2500),cbf2(2500)
        dimension s1(1500),s2(1500),av1(1500),av2(1500)
        dimension fl1(1500),fl2(1500)
        dimension z(1500)
  110   format(2x,'time= ',f6.1,3x,'channel1= ',f7.2,3x,'channel2= '
     c   ,f7.2)
  120   format(2x,'ave1= ',f10.5,3x,'ave2= ',f10.5)
  130   format(2x,'vt1= ',f12.5,3x,'tet1= ',f10.4,3x,'teta= ',f8.3)
  140   format(2x,'diameter= ',f4.2,3x,'area= ',f5.2,3x,'volume rate= '
     c   ,f10.5)
  150   format(2x,'velocity1= ',f10.5,3x,'velocity2= ',f10.5)
  160   format(2x,'xmax1= ',f10.3,3x,'xmin1= ',f10.3,3x,'xmax2= ',f10.3,
     c   3x,'xmin2= ',f10.3)
  170   format(2x,'a1/b1= ',f5.3,3x,'a2/b2= ',f5.3)
  180   format(3x,'pul1= ',f10.3,3x,'pul2= ',f10.3)
  190   format(2x,'time= ',f6.1,3x,'channel1= ',f5.2,3x,'channel2= '
     c   ,f5.2,3x,'velocity1= ',f12.5,3x,'velocity2= ',f12.5)
  210   format(20x,'period= ',i)
  220   format(2x,'av1= ',f10.5,3x,'av2= ',f10.5)
  240   format(10x,'phaseave= ',f12.5)
  250   format(5x,'timeave= ',f12.5,5x,'sheerstress= ',f12.5)
    9   format(10x,' The output data are ')
   12   format(10x,'the power spectrum is')
   13   format(10x,'power spectrum in db is')
   14   format(10x,'The power spectrum of fluctuations are')
   15   format(10x,'power in db is')
        n=1698
        nn=n+350
        nnd2=nn/2
        iper=283
        ipp=iper+229
        ippd2=ipp/2
        np=n/iper
        ro=1.
        nu=11
        nu2=9
        p=79.25
        pi=3.1415927
        dim=2.
        area=(dim**2)*pi/4.
        deg=180./pi
        read(5,*)(a(i),b(i),c(i),i=1,n)
        do 20 i=1,n
        d(i)=b(i)*(+1.)
        e(i)=c(i)*(+1.)
   20   continue
        sum1=0.0
        sum2=0.0
        do 10 i=1,n
        sum1=sum1+d(i)
        sum2=sum2+e(i)
   10   continue
        ave1=sum1/n
        ave2=sum2/n
        write(6,120) ave1,ave2
        sq1=ave1**2+ave2**2
        vt1=p*(sqrt(sq1))
        ave4=abs(ave2/ave1)
        tet1=atan(ave4)
        teta=tet1*deg
c       since this file is belong to max. point therefore
c        velocities are max. and they should be divided by 2.
        q=(vt1/2.)*area*60./1000.
        write(6,130) vt1,tet1,teta
        write(6,140) dim,area,q
        do 30 i=1,n
        v1(i)=d(i)*p/cos(tet1)
        v2(i)=e(i)*p/sin(tet1)
        write(6,150) v1(i),v2(i)
   30   continue
        do 80 j=1,per
        sum1=0.0
        sum2=0.0
        do 70 i=j,n,per
        sum1=sum1+v1(i)
        sum2=sum2+v2(i)
   70   continue
        av1(j)=sum1/np
        av2(j)=sum2/np
        write(6,220) av1(j),av2(j)
   80   continue
```

```
c       In this part we calculate mean value of smooth signal.
        mav1=0.0
        mav2=0.0
        do 501 i=1,per
        mav1=mav1+av1(i)
        mav2=mav2+av2(i)
501     continue
c       In this part we calculate pulstality factor and A/B
c        from smooth signal.
        xmax1=av1(1)
        xmax2=av2(1)
        xmin1=av1(1)
        xmin2=av2(1)
        do 40 i=2,n
        if(av1(i).gt.xmax1) xmax1=av1(i)
        if(av2(i).gt.xmax2) xmax2=av2(i)
        if(av1(i).lt.xmin1) xmin1=av1(i)
        if(av2(i).lt.xmin2) xmin2=av2(i)
  40    continue
        atb1=xmax1/xmin1
        atb2=xmax2/xmin2
        pul1=(xmax1-xmin1)/mav1
        pul2=(xmax2-xmin2)/mav2
        write(6,160) xmax1,xmin1,xmax2,xmin2
        write(6,170) atb1,atb2
        write(6,180) pul1,pul2
c        calculte fourier transform of the velocity.
c       last 128 points are zero, and poewer spectrum is calculated
c        for one half of total points.
        do 50 i=1,nn
        if(i.le.n)    xreal1(i)=v1(i)
        if(i.gt.n)    xreal1(i)=0.0
        if(i.le.n)    xreal2(i)=v2(i)
        if(i.gt.n)    xreal2(i)=0.0
        ximag1(i)=0.0
        ximag2(i)=0.0
  50    continue
        call fft(xreal1,ximag1,nn,nu)
        call fft(xreal2,ximag2,nn,nu)
        write(6,3)
        do  60 i=1,nn
        ps1(i)=xreal1(i)**2+ximag1(i)**2
        ps2(i)=xreal2(i)**2+ximag2(i)**2
  60    continue
c         calculate power spectrum in db.
        write(6,12)
        pmax1=ps1(1)
        pmax2=ps2(1)
        do 111 i=2,nn
        if(ps1(i).gt.pmax1) pmax1=ps1(i)
        if(ps2(i).gt.pmax2) pmax2=ps2(i)
 111    continue
        write(6,13)
        do 112 i=1,nnd2
        cb1(i)=10.*alog10((ps1(i)/pmax1)+0.000001)
        cb2(i)=10.*alog10((ps2(i)/pmax2)+0.000001)
        write(6,*) i,cb1(i),cb2(i)
 112    continue
        do  81 j=1,no
        write(6,140) j
        do 82 i=1,per
        ja=per*(j-1)+i
        fl1(ja)=v1(ja)-av1(i)
        fl2(ja)=v2(ja)-av2(i)
        z(ja)=fl1(ja)*fl2(ja)
        write(6,*) i,fl1(ja),fl2(ja),z(ja)
  82    continue
  81    continue
        do 83 j=1,per
        sum3=0.0
        do 84 i=j,n,per
        sum3=sum3+z(i)
  84    continue
c       At this point we calculate phase average of  fluctuation
c        components to be used in calculation of instantaneous
c        shear stress.
        s1(j)=sum3/no
        write(6,240) s1(j)
  83    continue
c       In order to calculate time average sheer stress, we can
c        either divide ave3 by per, or take average of all points
c        of z, the result is the same. Here we do the first
c        one.
        sum4=0.0
        do 85 i=1,per
        sum4=sum4+s1(i)
  85    continue
```

```
      ave4=sum4/per
      sheer=-1*rg*abs(ave4)
      write(6,250) ave4,sheer
c      In this part we calculate F.T. of the fluctuations.
      do 41 i=1,pp
      if(i.le.per) x1real(i)=fl1(i)
      if(i.gt.per) x1real(i)=0.0
      if(i.le.per) x2real(i)=fl2(i)
      if(i.gt.per) x2real(i)=0.0
      x1imag(i)=0.0
      x2imag(i)=0.0
 41   continue
      call fft(x1real,x1imag,pp,nu2)
      call fft(x2real,x2imag,pp,nu2)
      do 51 i=1,pp
      psf1(i)=x1real(i)**2+x1imag(i)**2
      psf2(i)=x2real(i)**2+x2imag(i)**2
 51   continue
      write(6,14)
      pfmax1=psf1(1)
      pfmax2=psf2(2)
      do 113 i=2,pp
      if(psf1(i).gt.pfmax1) pfmax1=psf1(i)
      if(psf2(i).gt.pfmax2) pfmax2=psf2(i)
113   continue
      write(6,15)
      do 114 i=1,ppd2
      cdf1(i)=10.*alog10((psf1(i)/pfmax1)+0.000001)
      cdf2(i)=10.*alog10((psf2(i)/pfmax2)+0.000001)
      write(6,*) i,cdf1(i),cdf2(i)
114   continue
      stop
      end
      subroutine fft(xreal,ximag,n,nu)
c     This subroutine is written for comolex values. If there is
c      no imaginary value ximag must be define as zero for all values
c      of xreal.
      dimension xreal(n),ximag(n)
      n2=n/2
      nu1=nu-1
c     nu is power of n in base 2. For n=2**3 nu=3
      k=0
      do 100 l=1,nu
102   do 101 i=1,n2
      p=ibitr(k/2**nu1,nu)
      arg=6.2831853*p/float(n)
      c=cos(arg)
      s=sin(arg)
      k1=k+1
      k1n2=k1+n2
      treal=xreal(k1n2)*c+ximag(k1n2)*s
      timag=ximag(k1n2)*c-xreal(k1n2)*s
      xreal(k1n2)=xreal(k1)-treal
      ximag(k1n2)=ximag(k1)-timag
      xreal(k1)=xreal(k1)+treal
      ximag(k1)=ximag(k1)+timag
101   k=k+1
      k=k+n2
      if(k.lt.n) go to 102
      k=0
      nu1=nu1-1
100   n2=n2/2
      do 103 k=1,n
      i=ibitr(k-1,nu)+1
      if(i.le.k) go to 103
      treal=xreal(k)
      timag=ximag(k)
      xreal(k)=xreal(i)
      ximag(k)=ximag(i)
      xreal(i)=treal
      ximag(i)=timag
103   continue
      return
      end
      function ibitr(j,nu)
      j1=j
      ibitr=0
      do 200 i=1,nu
      j2=j1/2
      ibitr=ibitr*2+(j1-2*j2)
200   j1=j2
      return
      end
```

```
c       In this program is to calculate ... of flow ...
        dimension a(5500),b(5500),c(5500),d(5500)
        dimension e(5500),v1(5400),v2(5400)
        dimension xreal1(5500),xreal2(5500),ximag1(5500),ximag2(5500)
        dimension x1real(5500),x2real(5500),x1imag(5500),x2imag(5500)
        dimension ps1(5500),ps2(5500)
        dimension psf1(5500),psf2(5500)
        dimension cb1(5500),cb2(5500)
        dimension cbf1(5500),cbf2(5500)
        dimension s1(5500),s2(5500),av1(5500),av2(5500)
        dimension fl1(5500),fl2(5500)
        dimension z(5500)
  110   format(2x,'time= ',f6.1,3x,'channel1= ',f7.2,3x,'channel2= '
     c  ,f7.2)
  120   format(2x,'ave1= ',f10.5,3x,'ave2= ',f10.5)
  130   format(2x,'vt1= ',f12.5,3x,'tet1= ',f10.6,3x,'teta= ',f8.3)
  140   format(2x,'diameter= ',f4.2,3x,'area= ',f5.2,3x,'volume rate= '
     c  ,f10.5)
  150   format(2x,'velocity1= ',f10.5,3x,'velocity2= ',f10.5)
  160   format(2x,'xmax1= ',f10.3,3x,'xmin1= ',f10.3,3x,'xmax2= ',f10.3,
     c  3x,'xmin2= ',f10.3)
  170   format(2x,'a1/b1= ',f5.3,3x,'a2/b2= ',f5.3)
  180   format(3x,'pul1= ',f10.3,3x,'pul2= ',f10.3)
  190   format(2x,'time= ',f6.1,3x,'channel1= ',f5.2,3x,'channel2= '
     c  ,f5.2,3x,'velocity1= ',f12.5,3x,'velocity2= ',f12.5)
  210   format(20x,'period= ',i3)
  220   format(2x,'av1= ',f10.5,3x,'av2= ',f10.5)
  240   format(10x,'phaseave= ',f12.5)
  250   format(5x,'timeave= ',f12.5,5x,'sheerstress= ',f12.5)
        format(10x,' The output data are ')
        format(10x,'the power spectrum is')
        format(10x,'power spectrum in db is')
        format(10x,'The power spectrum of fluctuations are')
  15    format(10x,'power in db is')
c       n is number of data in each file.
        n=1699
        nn=n*350
        nn2=nn/2
c       iper is number of data in each period.
        iper=283
        ipp=iper+229
        ipp2=ipp/2
c       np is number of periods in each file.
        np=n/iper
        ro=1.
        nu=11
        nu2=9
c       p is the constant value given by the manufactuger.
        p=78.2c
        pi=3.1415927
        dim=3.
c       calculate cross-sectional area.
        area=(dim**2)*pi/4.
        deg=180./pi
c       read transfered data to this file.
        read(5,*)(a(i),b(i),c(i),i=1,n)
c       use calibration factor to assess real values of data.
        do 20 i=1,n
        d(i)=b(i)*(+2.)
        e(i)=c(i)*(+2.)
   20   continue
c       calculate the phase average value of the data.
        do 30 j=1,np
        write(6,210) j
        sum1=0.0
        sum2=0.0
        do 10 i=1,iper
        ja=iper*(j-1)+i
        write(6,210) j
        sum1=0.0
        sum2=0.0
        do 10 i=1,iper
        ja=iper*(j-1)+i
        sum1=sum1+d(ja)
        sum2=sum2+e(ja)
   10   continue
        ave1=sum1/iper
        ave2=sum2/iper
        write(6,120) ave1,ave2
c       calculate the  blood flow velocity from doppler signal.
        sq1=ave1**2+ave2**2
        vt1=p*(sqrt(sq1))
        ave4=abs(ave2/ave1)
c       calculate the doppler angle.
        tet1=atan(ave4)
        teta=tet1*deg
c       calculate the individual values of velocities.
        do 111 i=1,iper
        ja=iper*(j-1)+i
        v1(ja)=d(ja)*p/cos(tet1)
        v2(ja)=e(ja)*p/sin(tet1)
  111   continue
```

```
c         calculate volume rate using average velocity.
          q=vt1*area*60./1000.
          write(6,130) vt1,teti,teta
          write(6,140) dim,area,q
30        continue
c         calculate phase average of the velocity.
          do 80 j=1,np
          write(6,210) j
          suma1=0.0
          suma2=0.0
          do 70 i=1,iper
          ja=iper*(j-1)+i
          suma1=suma1+v1(ja)
          suma2=suma2+v2(ja)
70        continue
          av1(j)=suma1/iper
          av2(j)=suma2/iper
          write(6,220) av1(j),av2(j)
  80      continue
c         calculate the fluctuation components of the velocity.
          do 90 j=1,np
          write(6,210) j
          suma3=0.0
          do 100 i=1,iper
          ja=iper*(j-1)+i
          fl1(ja)=v1(ja)-av1(j)
          fl2(ja)=v2(ja)-av2(j)
          z(ja)=fl1(ja)*fl2(ja)
          suma3=suma3+z(ja)
100       continue
c         calculate the time average of sheer stress.
          aveb=suma3/iper
          write(6,*) j,aveb
 90       continue
          stop
          end
```

```
CCCCCCCCCCCCCCCCCCCCCCCCCCCCCCCCCCCCCCCCCCCCCCCCCCCCCCCCCCCCCCCCCCCCCCC
C
C       PROGRAM ADC
C
C       FUNCTION-
C       This  a/d  conversion program for use with the LPS11 is
C       compatible with the CFLOW and FLOW analysis programs.
C       The rate of digitizing is variable, and can be used for
C       1 to 4 channels simulatenously. However, it must be used
C       from CH0 upwards. The input signals must be within +5.0
C       and -5.0 volts maximum.
C
C       AUTHOR-
C               KIM HANSON
C               TECH-TIME, INC.
C               RE-WRITTEN FROM CODE BY KENNY TEOH
C
C       COMMON AREAS
C
C       A. /AZ/
C               1. NCHN - number of channels (1 - 4)
C               2. NBTS - number of beats to measures
C               3. IRTE - calculated clock rate ( based on XINT )
C               4. ICNT - calculated clock counter preset (based on XINT)
C               5. IFC - number of samples for heart rate calculation
C               6. IBEAT - total number of beats counted
C               7. MHB(12) - time (in samples of up to 12 beats)
C               8. BUFF - data buffer for A/D data
C
C       B. /BZ/
C               1. XINT - sample time in sec/sample
C               2. CHNM(40) - channel name (4 * 10 characters)
C
C       C. /CZ/


C               TKB>ASG=US:1
C               TKB>//
C
C

        INTEGER MHB(12),BUFF(5000)
        LOGICAL*1 KMAN,KMV,ID(30),CHNM(40)
        BYTE FILENM(13)
        COMMON /AZ/NCHN,NBTS,IRTE,ICNT,IFC,IBEAT,MHB,BUFF
        COMMON /BZ/XINT,CHNM
        COMMON /CZ/IX,IY,IZ,LAST
C
C       TYPE HEADER
C
        WRITE(5,10)
10      FORMAT(1H1,//,T10,'** ANALOG TO DIGITAL CONVERSION PROGRAM **')
C
C       INITIALIZE  FILE AND CHANNEL NAMES
C
        DO 15 I=1,30
                CHNM(I)=0
                ID(I)=0
15      CONTINUE
C
C       ASK FOR FILENAME
C
        TYPE 20
20      FORMAT(//,3X,'GIVE FILENAME:   ',$)
        ACCEPT 25,(FILENM(I),I=1,13)
25      FORMAT(13A1)
        OPEN(UNIT=1,NAME=FILENM,TYPE='NEW',FORM='UNFORMATTED',ERR=200)
```

```
C
C       GET SUPPORTING PARAMETERS
C
30      CALL PROTO
C
C       GET MAIN AND SUB ID
C
        DO 35 I=1,20
                ID(I)=0
35      CONTINUE
        TYPE 40
40      FORMAT(3X,'MAIN ID:   ',$)
        ACCEPT 45,(ID(I),I=1,20)
45      FORMAT(20A1)
48      TYPE 50
50      FORMAT(3X,'SUB ID:     ',$)
        ACCEPT 55,(ID(I),I=21,30)
55      FORMAT(10A1)

        WRITE OUT HEADER INFORMATION TO FIRST THREE RECORDS


        IF(JTIME1 .LE. 0.)GOTO 71
        JTIME=JTIME1
  71    IFC=JTIME/XINT
C
C       GET DIGITAL DATA
C
        CALL ATOD
C
C       IF MHB(1)=999 =>RUN ABORTED - ERASE PREVIOUSLY WRITTEN HEADER
C
        IF(MHB(1) .NE. 999)GOTO 80
        DO 75 I=1,3
                BACKSPACE 1
75      CONTINUE
        GOTO 140
C
C       CALCULATE AND DISPLAY HEART RATES
C
80      CONTINUE
        LAST=MHB(NBTS)
        INO=LAST
        RATE=((NBTS-1)*60.)/(LAST*XINT)
        TYPE 85,RATE
85      FORMAT(/,3X,'HEART RATE =   ',F5.1,' BPM',//)
C
C       CHECK FOR BUFFER OVERFLW THEN WRITE OUT A/D DATA
C
90      LASTD=LAST*NCHN
        IF(LASTD .GE. 5000)GOTO 210
        WRITE(1)RATE,LASTD,(MHB(I),I=1,NBTS)
        IF(NCHN .EQ. 1)GOTO 95
        DO 92 I=1,LASTD,NCHN
                II=I-1+NCHN
                WRITE(1)(BUFF(J),J=I,II)
92      CONTINUE
        GOTO 100
95      DO 96 J=1,LASTD
                WRITE(1) BUFF(J)
96      CONTINUE
C
C       FORMAT DATA FOR DISPLAY ON OSCILLISCOPE
C
100     DO 105 I=1,LASTD
                BUFF(I)=BUFF(I)/4
```

```
105     CONTINUE
        IX=4
        IY=2*NCHN
        IF(INO .LE. 1024)GOTO 110
        IX=2
        LAST=LAST/2
        IY=IY*2
145   FORMAT(X,/,3X,'CONTINUE,RESET,OR QUIT ?[C,R,Q]:',$)
        ACCEPT 150,KMAN
150     FORMAT(A1)
        IF(KMAN .EQ. 'C')GOTO 48
        IF(KMAN .EQ. 'R')GOTO 30
        IF(KMAN .EQ. 'Q')GOTO 170
        GOTO 140
C
C       EXIT PROGRAM
C
170     CALL CLOSE(1)
        STOP
C
C       ERROR MESSAGES
C
200     TYPE 205
205     FORMAT(3X,'*** ERROR OPENING DATA FILE ***')
        STOP
C
210     TYPE 215
215     FORMAT(3X,'*** DATA OVERFLOW - SAMPLE DELETED ***')
        GOTO 140
        END
```

```
        .TITLE  ATOD
        .ENABLE AMA
        .MCALL  CINI$,DIR$,QIOW$
        ; (VERSION W/BEL)
        ;
ICH:    .BLKW   1
ITIME:  .BLKW   1
        ;
        ;
        ;COMMON AREA
        ;
        .PSECT  AZ,RW,D,GBL,REL,OVR
NCHN:   .BLKW   1
NRTS:   .BLKW   1
IRTE:   .BLKW   1
ICNT:   .BLKW   1
IEC:    .BLKW   1
IBEAT:  .BLKW   1
MHB:    .BLKW   14
BUFF:   .BLKW   5000.
BUFEND  =.
        ;
        ;
        .PSECT
COUNT:  .WORD   0
INBUF:  .BYTE   0
BEEP:   .BYTE   7
LUN.TI  =       5
RDYMSG: .ASCII  /**READY FOR DATA ACQUISITION ENTER 'R' OR 'S' **/
RDYSIZ  =       .-RDYMSG
PROMPT: .ASCII  />/
PMTSIZ  =       .-PROMPT
        ;
        ;ASSEMBLY LEVEL DIRECTIVES
```

```
        CLR     @#CKSR
        MOV     #MHB,R3         ;FRAME POINTER
        MOV     #BUFF,R2        ;DATA BUFFER POINTER
        DIR$    #RDY
        MOV     ICNT,@#CKBR     ;SET CLOCK COUNTER
        MOV     IRTE,@#CKSR     ;SET CLOCK RATE
INIT:   DIR$    #PMT
        DIR$    #TTYIN          ;ENTER S TO START
        CMPB    #122,INBUF      ;R TO REGRESS
        BEQ     ABORT
        CMPB    #123,INBUF
        BNE     INIT
        MOV     NBTS,R0         ;NUMBER OF BEATS
        BIC     #100000,@#CKSR
WAIT:   CALL    ISR             ;CHECK FOR BEAT
        CMP     NBTS,R0         ;WAIT FOR FIRST INTERRUPT
        BEQ     WAIT
        BIS     #401,@#CKSR     ;START CLOCK, REPEAT MODE
LOOP:   CALL    ISR
        TST     R0
        BEQ     LINGER
        INC     IFC             ;INCREMENT FRAME COUNT
        CMP     R2,#BUFEND
        BGE     LINGER
        MOV     NCHN,ICH
TICK:   TSTB    @#CKSR
        BPL     TICK
        BIC     #200,@#CKSR
        CLR     @#ADSR
GO:     INC     @#ADSR          ;START A/D
CHECK:  TSTB    @#ADSR
        BPL     CHECK
        MOV     @#ADBR,(R2)+
        DEC     ICH
        BEQ     AD
        INCB    @#ADSR+1        ;NEXT CHANNEL
        JMP     GO
;
;
;
LINGER: CALL    ISR
        INC     IFC
        CMP     IFC,ITIME       ;TIME UP YET?
        BGE     RETURN
TOCK:   TSTB    @#CKSR
        BPL     TOCK
        BIC     #200,@#CKSR
        JMP     LINGER
ABORT:  MOV     #999.,(R3)      ;ABORT CODE
XIT:    RETURN
RETURN: RETURN

        ;
        ;CHECK FOR NEW BEAT PULSE AND COUNT IT
        ;
ISR:
        TST     @#CKSR
        BPL     BACK
        BIC     #100000,@#CKSR
        DEC     R0
        BLT     AWHILE
        DIR$    #BEL
        MOV     @#IFC,(R3)+
        RETURN
AWHILE: INC     @#IBEAT
BACK:   RETURN
        .END
```

```
        .TITLE  SAMPLT
        .ENABL  AMA
        .MCALL  DIR$,QIOW$
        ;
        ;       COMMON AREA
        ;
        .PSECT  Z1,RW,D,GBL,REL,OVR
ICHN:   .BLKW   1
BUFF:   .BLKW   144
        ;
        ;
        .PSECT  SAMPLT
MG:     .BYTE   13.
        .ASCII  .   READY ? [Y/N]: ,
AGAIN:  .BYTE   13.
        .ASCII  .   REPEAT SAMPLE ? [Y/N]: ,
RING:   .BYTE   7                       ,
INBUF:  .BYTE
        .EVEN
TTYOUT: QIOW$   IO.WVB,5,1,,,,<MG,19.,44>
TTYCR:  QIOW$   IO.WVB,5,1,,,,<MG,1.,44>
REPEAT: QIOW$   IO.WVB,5,1,,,,<AGAIN,27.,44>
BELL:   QIOW$   IO.WVB,5,1,,,,<RING,1,0>
TTYIN:  QIOW$   IO.RVB,5,1,,,,<INBUF,1>
        ;
        ; PROGRAM ENTRY
        ;
SAMPLT::        CLR     @#ADSR
        CLR     @#CKSR
        MOVB    ICHN,@#ADSR+1
        MOV     #177777,@#CKBR
        BIS     #40,@#ADSR              ;CLOCK OVERFLOW MODE
        MOV     #BUFF,R1
        MOV     #144,R2
WAIT:   DIR$    #TTYOUT
        DIR$    #TTYIN
        CMPB    #'Y,INBUF
        BEQ     SAMPLT
        DIR$    #TTYCR
        RETURN
        .END
```